



Old Crow landscape hazards

Geoscience mapping for climate
change adaptation planning



Northern Climate ExChange
YUKON RESEARCH CENTRE • Yukon College



Indigenous and
Northern Affairs Canada

Affaires autochtones
et du Nord Canada

This publication may be obtained online at yukoncollege.yk.ca/research.

This publication may be obtained from:

Northern Climate ExChange
Yukon Research Centre, Yukon College
500 College Drive
PO Box 2799
Whitehorse, Yukon Y1A 5K4
867.668.8895 or 1.800.661.0504

Recommended citation:

Recommended citation: Benkert, B.E., Kennedy, K., Fortier, D., Lewkowicz, A., Roy, L.-P., de Grandpré, I., Grandmont, K., Drukis, S., Colpron, M., Light, E., Williams, T. 2016. Old Crow landscape hazards: Geoscience mapping for climate change adaptation planning. Northern Climate ExChange, Yukon Research Centre, Yukon College. 136 p. and 2 maps.

Front cover photograph: Aerial view of Old Crow looking north across the Porcupine River

Photo Credit: Yukon Geological Survey

Disclaimer: This report, including any associated maps, tables and figures (the “Information”), conveys general observations only. The Information is based on an interpretation and extrapolation of discrete data points and is not necessarily indicative of actual conditions at any location. The Information cannot be used or relied upon for design or construction at any location without first conducting site-specific geotechnical investigations by a qualified geotechnical engineer to determine the actual conditions at a specific location (“Site-Specific Investigations”). The Information should only be used or relied upon as a guide to compare locations under consideration for such Site-Specific Investigations. Use of or reliance upon the Information for any other purpose is solely at the user’s own risk. Yukon College and the individual authors and contributors to the Information accept no liability for any loss or damage arising from the use of the Information.

LEAD AUTHORS

Bronwyn Benkert

Kristen Kennedy

Daniel Fortier

Antoni Lewkowicz

Northern Climate ExChange, Yukon Research Centre,
Yukon College

Yukon Geological Survey, Government of Yukon

Université de Montréal

University of Ottawa

CONTRIBUTING AUTHORS

Louis-Philippe Roy

Isabelle de Grandpré

Katerine Grandmont

Shaylin Drukis

Maurice Colpron

Erin Light

Tyler Williams

Northern Climate ExChange, Yukon Research Centre,
Yukon College

Université de Montréal

Université de Montréal

Northern Climate ExChange, Yukon Research Centre,
Yukon College

Yukon Geological Survey, Government of Yukon

Water Resources Branch, Government of Yukon

Water Resources Branch, Government of Yukon

TECHNICAL ADVISOR

Jeff Bond

Richard Janowicz

Yukon Geological Survey, Government of Yukon

Water Resources Branch, Government of Yukon

TECHNICAL EDITING AND PRODUCTION

Leyla Weston, Whitehorse, Yukon

ACKNOWLEDGEMENTS

The project team would like to thank all the participants in this project for their enthusiasm and commitment. We would like to express our appreciation to the Yukon Geological Survey, Yukon Research Centre, Université de Montréal, University of Ottawa, Université Laval, Government of Yukon, and all those noted above for their support.

We would especially like to thank Vuntut Gwichin First Nation for supporting this project and welcoming us on their lands and within their Traditional Territory. We appreciate the support and cooperation of community residents, which have led to fruitful conversations that enhanced the research presented here. Thank you to Sophia Flather, our community project liaison, for her involvement in this project.

Thank you to the many field assistants involved in the project, including several of our contributing authors, as well as Erin Eady, David Silas, Fiona D'Arcy, Alison Perrin and Brian Horton. Brett Elliot from the Yukon Geological Survey contributed to the development of the final hazard risk map, and Peter von Gaza developed modelled flood extent figures. Cover design by Lalena Designs.

Funding for this project was provided by Indigenous and Northern Affairs Canada, and in-kind contributions were made by project partners. Project coordination was conducted by the Northern Climate ExChange, part of the Yukon Research Centre at Yukon College.

TABLE OF CONTENTS

| | |
|---|----|
| INTRODUCTION | 5 |
| Climate Change Adaptation Planning | 5 |
| What Are Hazards Maps? | 5 |
| Hazards Maps and Decision-Making | 5 |
| HOW HAZARDS MAPS ARE CREATED | 6 |
| Community Consultation | 6 |
| Surficial Geology Characterization | 6 |
| Permafrost Distribution and Characteristics | 7 |
| Hydrological Characterization | 7 |
| Projections of Future Environmental Conditions | 7 |
| Hazard Ranking | 8 |
| <i>Limitations and Uncertainty</i> | 8 |
| THE OLD CROW REGION | 8 |
| Physiography | 10 |
| Vegetation | 12 |
| Contemporary Climate | 12 |
| Regional Hydrology | 13 |
| <i>River Ice</i> | 16 |
| <i>Snow Water Equivalent</i> | 18 |
| <i>Groundwater</i> | 18 |
| Landscape Evolution | 19 |
| <i>The Neogene Period and Earlier</i> | 20 |
| <i>The Pleistocene Epoch</i> | 21 |
| <i>The Holocene Epoch</i> | 23 |
| Surficial Materials | 24 |
| <i>Bedrock (R) and Weathered Bedrock (D)</i> | 25 |
| <i>Fluvial Deposits (F^A, F and F>P)</i> | 25 |
| <i>Lacustrine Deposits (L<M; L>P)</i> | 28 |
| <i>Colluvial Deposits (C)</i> | 29 |
| <i>Organic Deposits (O)</i> | 30 |
| <i>Eolian Deposits (E)</i> | 31 |
| <i>Anthropogenic Deposits (A)</i> | 31 |
| Stratigraphy | 32 |
| Permafrost | 33 |
| <i>Forest Cover</i> | 33 |
| <i>Soil Texture</i> | 34 |
| <i>Contemporary Permafrost Temperature Modelling</i> | 34 |
| POTENTIAL HAZARD RISKS FOR THE OLD CROW REGION | 38 |
| Seismicity | 38 |
| Mass Wasting | 38 |
| <i>Landslides</i> | 39 |
| <i>Debris Falls</i> | 40 |
| <i>Active Layer Detachment</i> | 41 |
| <i>Slow Periglacial Wasting</i> | 43 |
| Flooding | 43 |
| Permafrost | 48 |
| <i>Permafrost Development</i> | 48 |

| | |
|--|-----|
| <i>Geotechnical Properties</i> | 48 |
| <i>Permafrost as a Hazard Risk</i> | 51 |
| ASSESSING CURRENT HAZARD RISKS FOR THE OLD CROW REGION | 52 |
| Case Study Sites..... | 52 |
| Old Crow Community Core..... | 54 |
| <i>Site 1</i> | 54 |
| <i>Site 2</i> | 56 |
| <i>Site 3</i> | 57 |
| <i>Site 4</i> | 58 |
| <i>Site 5</i> | 59 |
| <i>Site 6</i> | 60 |
| North Road and Vicinity..... | 61 |
| <i>Site 7</i> | 61 |
| <i>Site 8</i> | 63 |
| <i>Site 9</i> | 65 |
| <i>Site 10</i> | 66 |
| <i>Site 11</i> | 67 |
| Ski Lodge and Vicinity..... | 67 |
| <i>Site 12</i> | 67 |
| <i>Site 13</i> | 70 |
| Crow Mountain Road and Vicinity..... | 70 |
| <i>Site 14</i> | 70 |
| <i>Site 15</i> | 73 |
| <i>Site 16</i> | 74 |
| <i>Site 17</i> | 74 |
| Portage Trail..... | 77 |
| <i>Site 18</i> | 77 |
| HAZARD RISKS IN A CHANGING CLIMATE | 78 |
| Projected Climate Change for the Old Crow Region..... | 78 |
| <i>Global Climate Models</i> | 78 |
| <i>Climate Change Scenarios</i> | 78 |
| Implications of Climate Change for Hazards in the Old Crow Region..... | 81 |
| Integrating Risk in a Landscape Hazards Map for the Old Crow Region..... | 82 |
| <i>Input data</i> | 82 |
| <i>Modelling</i> | 85 |
| Hazard risk rankings for the Old Crow region..... | 87 |
| <i>Limitations</i> | 90 |
| GENERATING ACTION FROM SCIENCE | 90 |
| REFERENCES | 93 |
| APPENDIX A - APPROACH AND METHODS | 99 |
| APPENDIX B - BOREHOLE LOGS | 109 |
| APPENDIX C - SAFE HOME CONSTRUCTION ON PERMAFROST | 121 |

INTRODUCTION

Climate change is a significant challenge for northern communities, where the impacts of a warming climate are already having considerable effects (Huntington and Weller, 2005). Many people living in small, isolated communities in northern Yukon are concerned about climate-related risks in their regions. Because adverse impacts are a reality, it is important to implement measures to reduce or moderate the negative effects of climate change – in other words, to implement climate change adaptation strategies.

CLIMATE CHANGE ADAPTATION PLANNING

Community-based adaptation planning aims to incorporate the potential impacts of climate change into decision-making for community development. For example, the design of a new building that is resilient to permafrost thaw, or the selection of future development zones away from areas that may be prone to flooding during the spring melt, are both decisions rooted in adaptation planning. Ultimately, adaptation planning anticipates future scenarios, reduces risk, increases resilience, and may even seek to reap the benefits of certain aspects of climate change.

In order to better prepare our communities to incorporate adaptation planning in the decision-making process, we must first identify the risks of, or vulnerabilities to, climate change, and then mitigate or reduce these risks so that we may adapt in a safe, sustainable manner.

Hazards maps help identify potential future risks associated with natural phenomena such as permafrost thaw, landslides and flooding. In order to adequately measure the potential risks associated with climate change, it is critical to gather scientific baseline data. These data, in conjunction with complementary research and future climate projections, strive to reduce vulnerability by increasing our knowledge base; this in turn will increase a community's adaptive capacity to climate change.

WHAT ARE HAZARDS MAPS?

A hazards map is a map that delineates or highlights areas on the land that are affected by, or are vulnerable to, a particular hazard. For example, in northern latitudes such as Yukon, thawing permafrost can be a significant climate change-related hazard. Flooding is another common hazard faced by Yukon communities, which may or may not be directly related to thawing permafrost. Hazards maps illustrate the risk associated with these and other hazards (ranked by risk severity), and are represented graphically in stoplight colours.

Hazards maps integrate complex environmental data into an easy-to-interpret, user-friendly tool for decision-making. The maps are created on a community-by-community basis and combine information about current and future landscape and climate conditions in order to rank the risk related to environmental change. As a result, they are tailored to each community's unique environment.

HAZARDS MAPS AND DECISION-MAKING

Hazard mapping, in conjunction with risk assessment, forms the basis of the risk management decision-making process by providing a community with baseline information that is necessary to understanding what risks may exist. One of the main objectives of the risk management process is to determine "what risks potentially interfere with the community's ability to meet the goals and objectives defining the community's vision for the future" (Noson, 2002). In this case, hazards

maps help address a community's goal of incorporating climate change adaptation planning into its approaches to decision making and community development.

The series of landscape hazards maps produced by Northern Climate ExChange (NCE) and its partners are prepared as guides; that is, they act as one of the first steps in community planning and development. They identify areas where there is low risk of hazards exposure, as well as areas requiring more advanced and detailed scientific and engineering studies, should development be desired. Because hazards maps depict risk using stoplight colours, they are accessible and easy to interpret; in addition to community planning, hazards maps are useful educational tools illustrating local environmental conditions. They may also be used by scientists studying hazard phenomena (Noson, 2002), or could be revisited several years in the future to assess landscape change over time.

While hazards maps are tailored to local conditions and provide more detail than most other existing map products, it is important to note that they do not capture fine-scale variability within a site. For example, a slope underlain by permafrost may be more susceptible to thaw slumps in some areas compared to others because of small-scale variations in ice content of the soil or morphology of the slope. However, the entire slope may be classified as moderate risk to encompass the highest possible degree of vulnerability. Because of this, it is important to recognize the limitations of hazards maps – they provide an initial guide to local conditions, but detailed site studies (e.g., geotechnical or engineering studies) will still be required.

HOW HAZARDS MAPS ARE CREATED

There are many different approaches to creating hazards maps. Different mapping projects from different jurisdictions around Canada's North, and globally, will incorporate different hazards elements and types of data. For this project, we developed an approach that incorporates local community concerns and infrastructure, disturbance history, permafrost distribution and characteristics, surficial geology conditions, hydrology, and projections of future climate. Approaches for each stage are briefly described below. Detailed descriptions of each approach, including equipment used, lab analyses conducted, and data processing specifics are included in Appendix A.

COMMUNITY CONSULTATION

Support from local community governments and First Nations is sought for each hazards mapping project when project funding proposals are developed. Upon project commencement, community consultations, meetings and interviews are held with members of the public and local decision-makers to identify areas of concern and sites for potential future development. These areas of interest then become case-study sites as part of the hazards project. Where local capacity exists, a community project liaison is hired to serve as a link between the research team and the community.

SURFICIAL GEOLOGY CHARACTERIZATION

Surficial geology is the study of the unconsolidated material (i.e., the surficial material that overlies bedrock) on the Earth's surface, including all sediments and soils. Surficial geology mapping involves a combination of aerial photograph interpretation and fieldwork. Surficial geology maps provide information on the physical properties and characteristics of the surface sediments, the morphology (shape) of the landforms produced, and the genesis or origin of the landforms. In the process of mapping the surficial geology, the distribution of permafrost is also captured, making

these maps an essential part of the hazards assessment process. The surficial geology maps become the basis for the final hazards maps produced through each project.

PERMAFROST DISTRIBUTION AND CHARACTERISTICS

Permafrost is defined as ground (including rock, unconsolidated sediments and organic material) that remains at or below 0°C for a minimum of two consecutive years (Brown et al., 1997). For this project, the research team studied both the distribution and characteristics of permafrost as part of the hazards map development.

Permafrost distribution is studied via the application of two geophysical surveys: 1) ground-penetrating radar (GPR), and 2) electrical resistivity tomography (ERT). Ground-penetrating radar uses electromagnetic radiation to send a tiny pulse of energy into the ground, and then measures the speed and strength of that pulse's reflection back to the instrument. It produces an image that delineates boundaries created by changes in soil characteristics (for example, the presence of frozen ground or stratigraphic layers). Electrical resistivity tomography is another type of non-invasive geophysical survey that measures the changes in the ability of the ground to conduct electricity along a transect. ERT profiling has been used extensively to investigate mountain permafrost in Europe (e.g., Kneisel et al., 2000, 2008; Hauck et al., 2004; Hilbich et al., 2008, 2009) and is growing in importance in North America as a technique for permafrost investigations in mountains and elsewhere (e.g., Lewkowicz et al., 2012). An electrical resistivity survey produces a two-dimensional image of the subsurface which can be used to identify frozen (high resistivity) versus unfrozen (low resistivity) surface materials or soils, and can therefore be used to map permafrost distribution along a transect.

Permafrost characteristics are studied by extracting cores of permafrost from the ground and conducting a series of laboratory analyses on subsections of these cores. These analyses provide information about grain size, porosity, ice volume, and settlement potential, among other properties. These characteristics affect how different materials and soils will behave if permafrost thaws, and are also useful in verifying interpretations of the geophysical techniques described above.

HYDROLOGICAL CHARACTERIZATION

The study of the movement and distribution of water is critical in understanding responses to climate change. Having baseline knowledge of the hydrologic regime in an area is essential in defining potential future hazards that are related to climate change. To incorporate hydrological conditions and risk into hazards maps, data about river discharge, lake level and the groundwater table are gathered from monitoring stations. Flood histories are also compiled from existing records and anecdotal evidence. Historical patterns are analyzed, and current conditions are assessed on the context of projected future changes in climate.

PROJECTIONS OF FUTURE ENVIRONMENTAL CONDITIONS

An important component of the hazards mapping projects involves projections of future environmental conditions. They represent an important aspect of adaptation planning, which by definition requires a future focus; thus incorporating future-oriented data is a key element of the development of hazards maps.

The future environmental conditions modelled through this project are completed through permafrost probability projections and climate projections. Models of permafrost probability are developed using data from a series of meteorological and permafrost monitoring stations

established by research partners throughout the territory. These models build on existing knowledge of permafrost distribution to depict future changes in permafrost under different scenarios of annual air temperature increase as a result of climate change.

Climate projections for each community are developed by using a variety of Global Climate Models (GCMs) in combination with discrete scenarios, in order to make a range of projections for numerous climate variables (e.g., temperature and precipitation) on a local scale. Hazards projects typically incorporate a range of scenarios (reflecting escalating degrees of climate change) at several points in the future (e.g., 2020, 2050 and 2080).

HAZARD RANKING

Hazard mapping applies a variety of scientific data in order to arrive at a hazard risk ranking. The combination of surficial material type (glacial deposits and soils), landform shape and slope, permafrost nature and distribution, hydrological conditions, and the present climate regime are used to rank hazard risk. For easy interpretation, a stop-light colour coding system is applied to each risk ranking.

The hazards ranking is tailored to suit the conditions in each of the communities mapped. For example, in communities where permafrost presence or absence largely determines risk, three risk categories are sufficient. In environments with more complex landscape conditions (e.g., where permafrost conditions are more nuanced), a fourth risk category is introduced. Tailoring risk ranking to community conditions makes hazards maps relevant and reflective of the local landscape. The hazards risk ranking matrix used in this project is discussed in more detail in the section “Integrating risk in a landscape hazards map for the Old Crow region”, p. 82 of this report.

LIMITATIONS AND UNCERTAINTY

It is very important to note that this report is prepared as a guide for planning. It should not be used as the basis for final site selection for development, and it does not replace geotechnical and/or engineering assessments completed on a site level. Rather, it should be treated as a tool for use in identifying areas of interest with regards to future large-scale land use planning, which will then undergo subsequent site-specific investigations (which may include geotechnical or engineering assessments).

It is also important to note that the classification scheme applied here does contain a level of uncertainty. Because of the scale at which the study area was mapped, and the duration of the field program for this project, researchers were unable to visit all the areas within the map boundary. Therefore, results have been extrapolated beyond areas visited by researchers. While we have developed a model that integrates the geoscience data the research team has collected to make the most informed assessment of hazard risk for the study area, this approach does introduce some uncertainty that users of the hazard risk maps should be aware of.

Finally, it is important to note that in some cases, a polygon may contain areas of both higher and lower risk. In such cases, we have taken a precautionary approach and applied a category of higher risk where we were not confident in lower categories. This is another reason why the hazards map should serve only as an initial guide for planning purposes, and should not replace site-specific investigations – the landscape within each polygon will vary naturally.

THE OLD CROW REGION

Old Crow (67.57°N, 139.84°W) is located in Yukon’s far north, 128 km north of the Arctic Circle and approximately 800 km north of Whitehorse. It is situated at the confluence of the Crow and

Porcupine Rivers (Figure 1). It is the most northerly community in the Yukon, and the only one that is north of the Arctic Circle. As the only Yukon community that cannot be accessed by road, Old Crow has a year-round airport that allows access from other parts of the territory. During the ice-free seasons, it is also possible to access Old Crow by boating down the Porcupine River from the Eagle River located off the Dempster Highway. Occasionally, a winter road is also constructed.

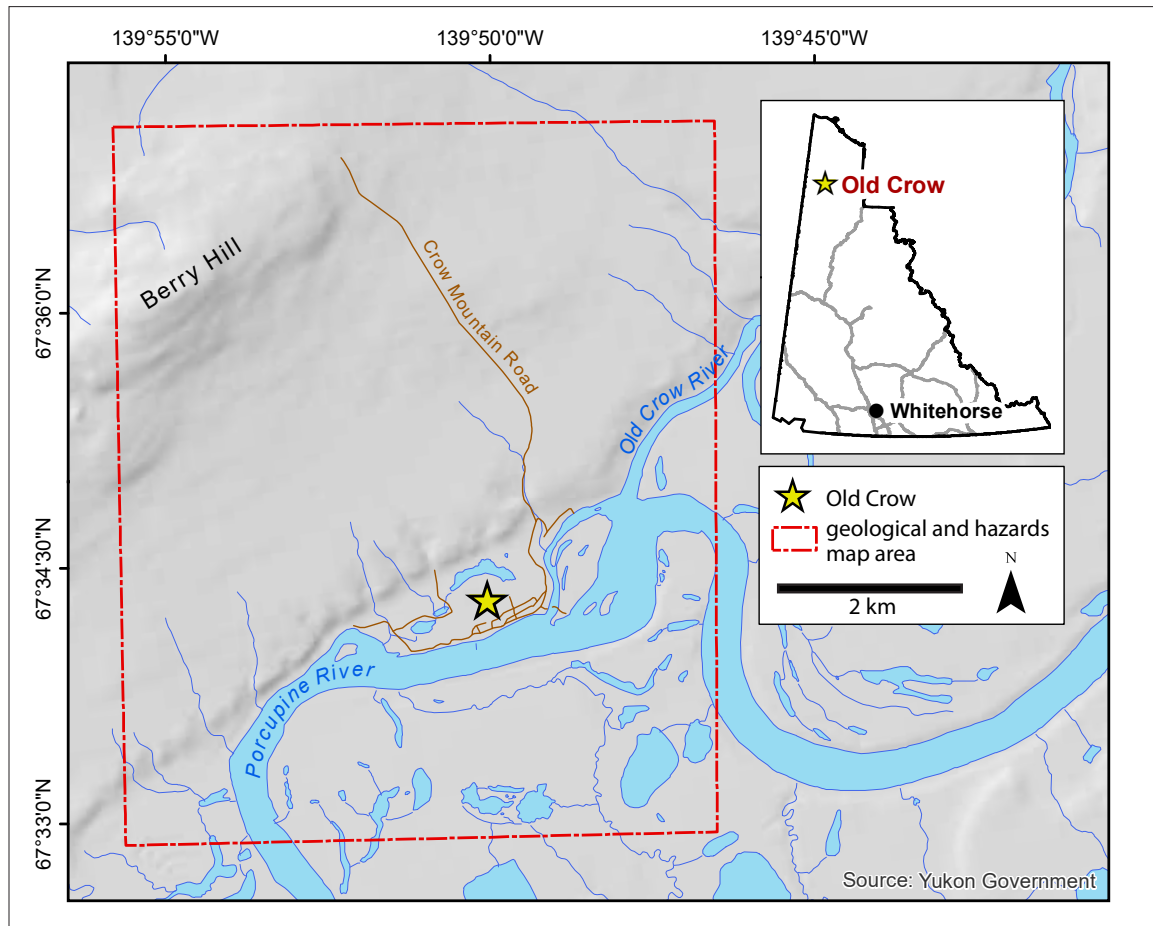


Figure 1. Location of study area, illustrating the surficial geology and hazards map footprints.

Old Crow is situated within the Traditional Territory of the Vuntut Gwitchin First Nation. Vuntut Gwitchin means the “People of the Lakes”, a name derived from their annual muskrat trapping season in the lakes just north of Old Crow. Gwich’in is the Indigenous language spoken within the community, and is taught in the local school. The Vuntut Gwitchin make up one community within the Gwich’in Nation that spans across the north (Yukon, Northwest Territories and Alaska). In 1993, the Vuntut Gwitchin became one of the first self-governing First Nations by signing land claims and self-government agreements. These agreements came into effect in 1995 (Fred, 2014).

For thousands of years, the rivers, lakes, mountains, forests and tundra of this area have sustained the ancestors of the modern Vuntut Gwitchin. They have relied on fishing, hunting and trapping as their main source of livelihood (Sherry and Myers, 2002). There is evidence of human occupation from at least 12,000 years ago when there was a Bering Strait Land Bridge connecting North America to Asia. Archeological reports indicate that along the Porcupine and Old Crow Rivers, caribou may have been hunted for around 30,000 years (Porcupine Caribou Management Board,

2002). While the Vuntut Gwitchin traditionally moved around with the natural migrations of the wildlife they depended on, the community of Old Crow was officially settled in the early 1900s. The community was named after the Gwitchin Chief, Deetru' K'avihdik, who died in 1870. His people named the mountains, river and area (Old Crow) in honour of Deetru' K'avihdik which means 'Crow May I Walk'. Each family group in Old Crow had been given their own trapping areas that have been passed down over the generations and are used today. The Porcupine Caribou herd that migrates through the area constitutes one of their most important sources of meat and clothing materials (Government of the Vuntut Gwitchin First Nation, 2015).

The Old Crow area had been a gathering spot that was used for hunting and trade along the Porcupine River. Since the early 1900s, muskrat trapping has provided an important source of income for the Vuntut Gwitchin (Yukon Bureau of Statistics, 2015). The Hudson's Bay Company established a trading post (Rampart House) in the area in 1890 and the Vuntut Gwitchin began to incorporate a stop at this post during their normal overland travel. When the fur-bearing animal populations began to collapse in the 1950s, families began to move into the Old Crow area. The community became a year-round settlement in the 1950s when amenities such as a school, store and RCMP office were built (Moses, 2015). The Canadian Government took a strong interest in assessing the hydroelectric potential of the Old Crow region in 1962, mapping out much of the region's geology with its "Operation Porcupine" initiative (Zazula and Froese, 2013).

Today, Old Crow is a 'dry' community that is less dependent on the subsistence economy, and is largely supported by government services. The Vuntut Gwitchin Government provides employment through construction, building maintenance, water and fuel delivery, education, health care, as well as support services (Carr et al., 2013). Of the 140 individuals comprising the labour force population in 2011 (age >15 years), over half were employed in the public administration sector; the remainder worked in construction, retail, trade and transportation, and educational services (Statistics Canada, 2013). In addition, the Vuntut Development Corporation plans and creates successful business ventures for the citizens of the Vuntut Gwitchin First Nation.

Old Crow has a variety of services and amenities including a post office, bank, grocery/hardware store, Yukon Electrical, high-speed satellite internet, RCMP, Chief Zzeh Gittlit Public School, community library, bed and breakfasts, and medical services (Yukon Community Profiles, 2015). Yukon College opened its Alice Frost Community Campus in Old Crow in 1987, offering skills training and upgrading courses (Yukon College, 2012). Old Crow also has an airport (operated by the Yukon Government), a community hall, arena, youth centre, playground, and ball diamond (Lorimer & Associated, 2005).

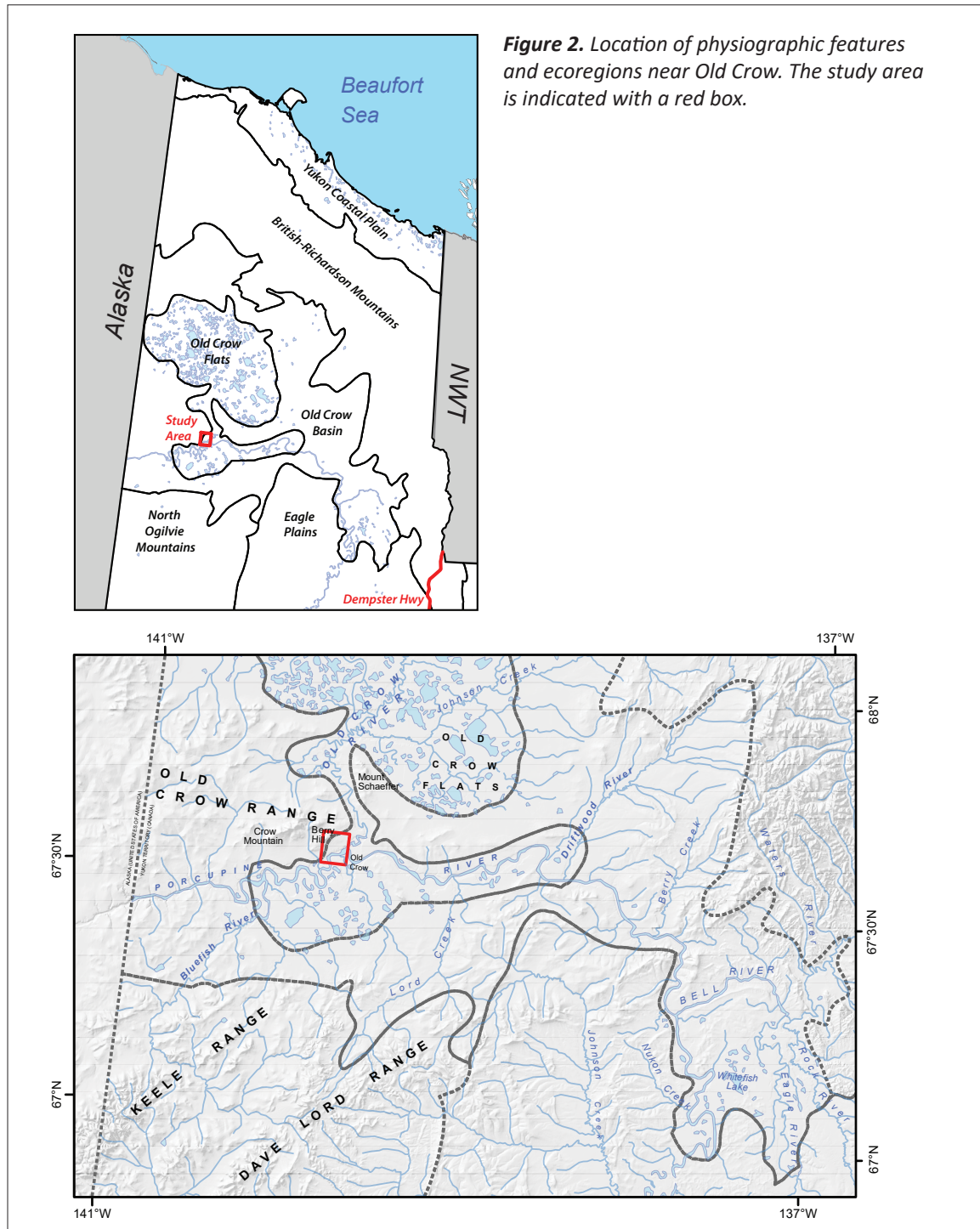
In 2015, Old Crow had a population of approximately 250 individuals, of whom 88% were identified as Aboriginal. Due to its isolated location, the population has remained quite stable from 2004-2014, with no significant increase in the summer months (Yukon Bureau of Statistics, 2015). In 2011, there were 110 occupied single private dwellings in Old Crow; the median value of a single-family dwelling was \$229,159 (Statistics Canada, 2013).

PHYSIOGRAPHY

The Old Crow study area is situated north of the Arctic Circle, within the Old Crow Basin Ecoregion (Smith et al., 2004; Figure 2). The ecoregion is comprised primarily of a physiographic basin, with pediment and upland topography surrounding the lowland plains and plateaus of the Crow and Porcupine rivers. Topographic highs are typically between 600 and 1000 m above sea level (a.s.l.) and descend to fluvial plains between 250 and 300 m a.s.l. The Old Crow Basin ecoregion includes upland areas (parts of the Keele and Dave Lord ranges to the south, and the British and Richardson Mountains to the north and east) and the low, depositional basins they surround (Old

Crow Flats, Driftwood Basin, and Bluefish Basin). Uplands are characterized by deep weathering, flat cryoplanation terraces, and gently sloped pediments (low angle erosional bedrock surfaces).

The map area for this project extends from the top of Berry Hill to the confluence of the Old Crow and Porcupine rivers (see Figure 1). It includes the town of Old Crow and extends uphill to include the pediment slopes that make up the southeastern flank of Berry Hill. The pediment is bordered on all sides in the map area by a steep fluvial escarpment separating the uplands from the floodplains and terraces of the Old Crow and Porcupine rivers below.



VEGETATION

Vegetation is determined by topography, elevation and microclimate. The vegetation of Old Crow's ecoregion (the Old Crow Basin) therefore reflects the soil in this area, which was formed under the influence of the continental subarctic climate and the slightly sloping topography. The dominating unglaciated pediment surfaces primarily consist of open spruce-lichen-heath vegetation communities, with cottongrass, sedge and tussocks dominating slopes that have grades less than 5%. Also present are other tundra species, such as low and dwarf shrubs (willows and shrub birch), ericaceous shrubs (such as blueberry and Labrador tea), lichens, mosses, and black spruce. The treeline is situated at 600 m a.s.l., and below this elevation, trees exhibit a stunted growth. Because of underlying permafrost, the trees in this region average around 4 m in height. Vegetation communities of black spruce, lichen and heath dominate lower elevations; floating mats of mosses and sedges are also present. Higher elevations with colluvial and residual slopes contain moss, lichen, willow and birch (both dwarf and low shrub), while steep, east-facing slopes also support alder and paper birch.

In the Old Crow Flats Ecoregion, lakes are the dominant feature. The majority of the vegetative communities in this area are shallow aquatic wetland species. Sedge fens surround these lakes, consisting of emergent vegetation – usually horsetail, yellow pond lily, buckbean and bur-reed. Additionally, this location hosts a variety of other vegetative communities such as graminoid meadows, treed heath and tussock tundra, as well as sphagnum blankets. Since much of the upland area is also a wetland, there are a number of frozen peat plateau bogs that overlie thick glaciolacustrine sediments, which are dominated by lichen heath. Low shrubs and sparse black spruce can also be found here, underlain by reindeer lichen in drier locations, and sphagnum moss in moister areas.

Successional vegetative communities are a prominent feature in this region. Within the riparian zones, where flooding is a common disturbance, the vegetation reflects the complex thaw-lake cycle of the formation and draining of lakes. Flood-tolerant species, such as sedges, grasses, forbs, alder and willow initially colonize the floodplain, and then are taken over by birch and white spruce once the permafrost table re-establishes itself within the rooting zone. Past fire disturbance has also enabled the growth of numerous vegetative communities that represent various intermediate stages of succession (Smith et al., 2004).

CONTEMPORARY CLIMATE

Old Crow is situated within the Old Crow Basin, and latitudinal and solar radiation influences largely control local climate conditions in the region. Situated above the Arctic Circle, the sun remains above the horizon for around two weeks every summer. Summers are often short, mild and moist because of weak low-pressure systems, whereas the winters can be long and cold from the prolonged low angle of the sun above the horizon. Compared to other areas in southern Yukon, spring and summer are often delayed about a month and winter is generally extended from October to mid-May. The growing season is short, but intense because of the amount of daylight in the summer. The transition between summer and winter can occur rapidly, since frost is able to develop at any time of the year. During the winter, there are approximately two weeks where the sun does not rise above the horizon, creating more stable winter climate patterns. Winter is usually dominated by arctic high-pressure systems; however brief, windy mild spells do occasionally occur from low-pressure systems that move over from the Beaufort Sea (Smith et al., 2004).

Based on 30-year (1981-2010) climate normal data collected from the Environment Canada meteorological monitoring station at the Old Crow airport (67°34'14 N, 139°50'21 W), temperatures in Old Crow can be highly variable. Regardless, mean annual air temperature is -8.2°C (one of the

lowest in Yukon). The average January and July temperatures are -29.2°C and 14.6°C , respectively. Average annual precipitation is 278 mm, with about half falling as snow during the winter months (Environment Canada, 2014a). Month-by-month climate normal temperature and precipitation data are summarized in Figure 3.

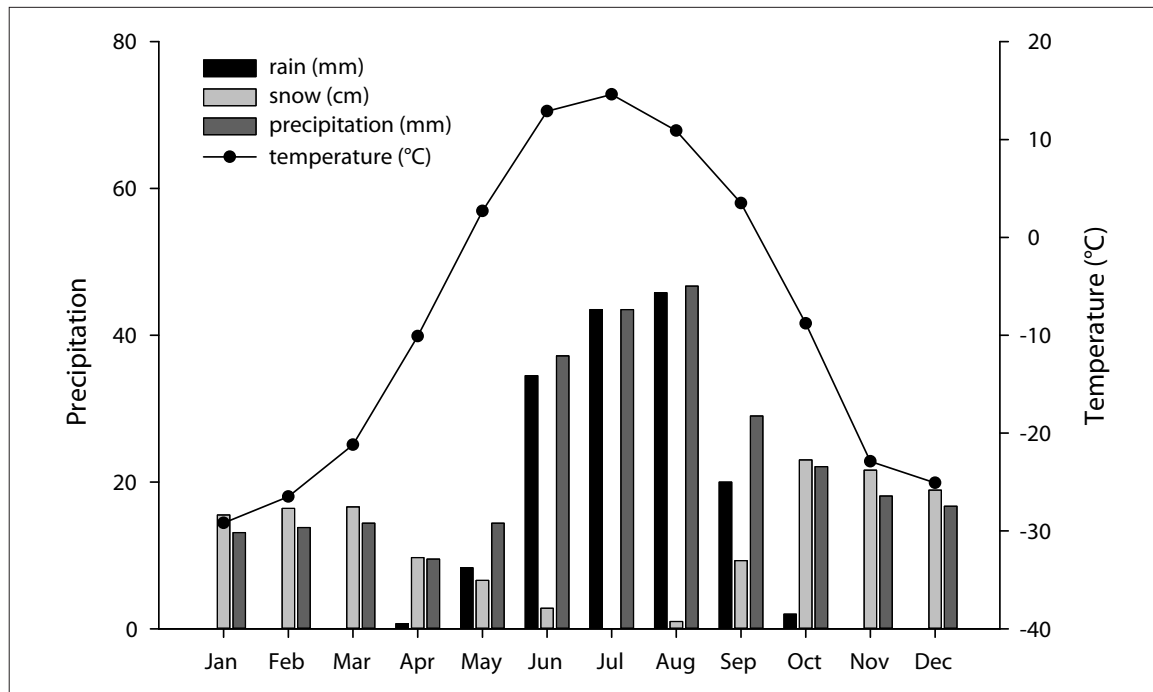


Figure 3. Climate normal (1981-2010) temperature and precipitation data for the Old Crow meteorological monitoring station (Environment Canada, 2014a). To calculate total precipitation in millimetres, snowfall was converted to snow water equivalent and summed with rainfall.

REGIONAL HYDROLOGY

Old Crow and the surrounding area are located within the Yukon River Basin, which covers 260 000 km² or 54% of Yukon (Smith et al., 2004), as well as in the subwatershed of the Porcupine River. This subwatershed is 116 000 km² in size and drains the northeastern part of the Yukon River Basin (Bradbeets et al., 2000). The Porcupine River subwatershed straddles the Yukon/Alaska border, and approximately 60 000 km² of the Porcupine River watershed falls within Yukon. In the territory, it is bounded by the Ogilvie Range to the south, the British Mountains in the north, and the Richardson Mountains in the east. The basin is primarily underlain by continuous permafrost and the major tributaries are the Old Crow, Bell, Eagle, Miner and Whitestone rivers.

The area is situated within the northern hydrologic region of the territory as defined by Janowicz (2008). The northern hydrologic region is underlain by continuous permafrost and streamflow response is characterized by a rapid increase in discharge in the late spring in response to snowmelt, with peak flows typically occurring in June. Due to the presence of continuous permafrost, peak flows in this area are generally higher than areas underlain with discontinuous or sporadic permafrost as the active layer is shallow, resulting in limited infiltration into the soil (Janowicz, 2010). Secondary peaks may occur throughout the rest of the ice-free season as a result of rainfall inputs. Annual minimum discharge occurs in March or April when groundwater inputs are low (Whitfield et al., 1993). Smaller streams in the area may have no observed flow during the latter part of the winter.

The community of Old Crow is situated on the flood plain of the Porcupine River (approximately 6 m above normal water level) and it is immediately downstream of the confluence between the Old Crow and Porcupine rivers (see Figure 1). In order to evaluate patterns in discharge, average local monthly and peak discharge were examined. The Water Survey of Canada (WSC) has maintained several gauging stations in the area over the past several decades, some of which provide real-time hydrometric data (Table 1). The Porcupine River station at Old Crow, and the Old Crow River station near the mouth have been selected for analysis due to proximity to the community.

Table 1. List of past and present Water Survey of Canada (WSC) hydrometric stations within Old Crow and the surrounding area (Water Survey of Canada, 2016). *Note that periods of record listed do not always contain complete datasets.

| Station Name | Station ID | Latitude | Longitude | Drainage (km ²) | Parameter | Period of Record* |
|---|------------|-------------|--------------|-----------------------------|--------------------------|-------------------|
| Porcupine River near international boundary | 09FD002 | 67°25'27" N | 140°53'28" W | 58 900 | streamflow and discharge | 1987-present |
| Old Crow River near the mouth | 09FC001 | 67°38'4" N | 139°41'47" W | 13 900 | streamflow and discharge | 1976-present |
| Porcupine River at Old Crow | 09FD001 | 67°33'50" N | 139°53'0" W | 55 400 | streamflow and discharge | 1961-1995 |
| Porcupine River below Old Crow River | 09FD003 | 67°34'5" N | 139°50'3" W | | water level (seasonal) | 2006-present |

At the townsite of Old Crow, the Porcupine River is about 600 m wide and occupies a broad alluvial valley of about 6-10 km in width (Jasek, 1997). Mean annual flow for the Porcupine River at Old Crow is 325 m³/s or 185 mm basin area equivalent (described in more detail below). Average winter low flows are 17 m³/s and occur in March or April, with peak flows occurring in late May and June.

Mean annual flow for the Old Crow River is 49 m³/s or 112 mm basin area equivalent. Peak flows are predominantly freshet-related, typically occurring between May 20th and June 5th. The instantaneous peak flow of record occurred in June 1977 at 1710 m³/s. Winter flows for the Old Crow River are low, with January to April mean discharge of around 1 m³/s. The record low flows for the station occurred in 1991 with mean monthly discharge <0.1 m³/s from January through April.

Both the Porcupine River and the Old Crow River hydrographs (Figures 4 and 5, respectively) show that river discharge begins to increase in April, peaks in late May or June, and decreases with secondary peaks from precipitation inputs. This pattern is typical of the northern hydrologic response zone. The peak discharge that occurs in June can be the result of ice-jam flooding or spring freshet contributions, potentially augmented by spring rainfall. The combination of all three factors can lead to very high-water levels and subsequent flooding.

Basin area equivalent is a calculation that provides information about the water balance of a river by normalizing discharge to area. As a result, it allows for comparison of discharge between basins. The basin area equivalent of the mean annual flow of the Porcupine River at Old Crow is 185 mm, whereas the Old Crow River at the mouth is 122 mm. It is speculated that the difference between these numbers can be accounted for by differences in precipitation inputs from local atmospheric conditions as well as landscape differences between the two watersheds. The Old

Crow River watershed is predominately made up of low relief wetlands which likely contribute to higher storage, slower hydrologic response and higher evaporation, contributing to comparatively lower discharge in the Old Crow River versus the Porcupine River.

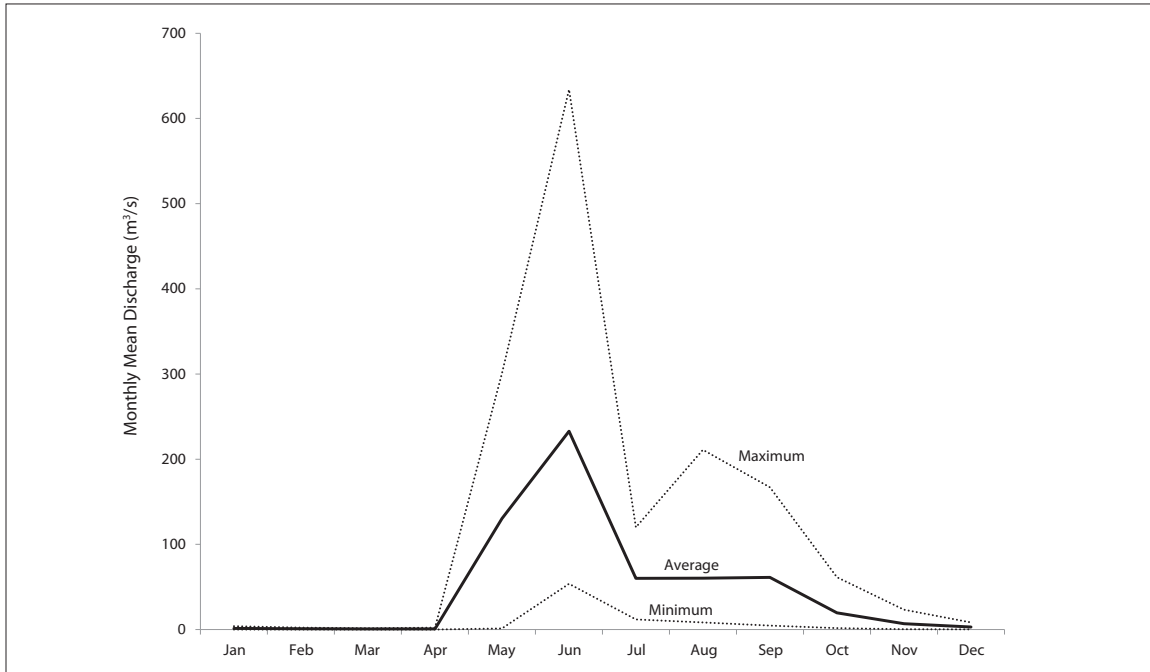


Figure 4. Porcupine River monthly mean discharge (1961 to 1995; Water Survey of Canada, 2016). Average, maximum and minimum monthly flows are shown.

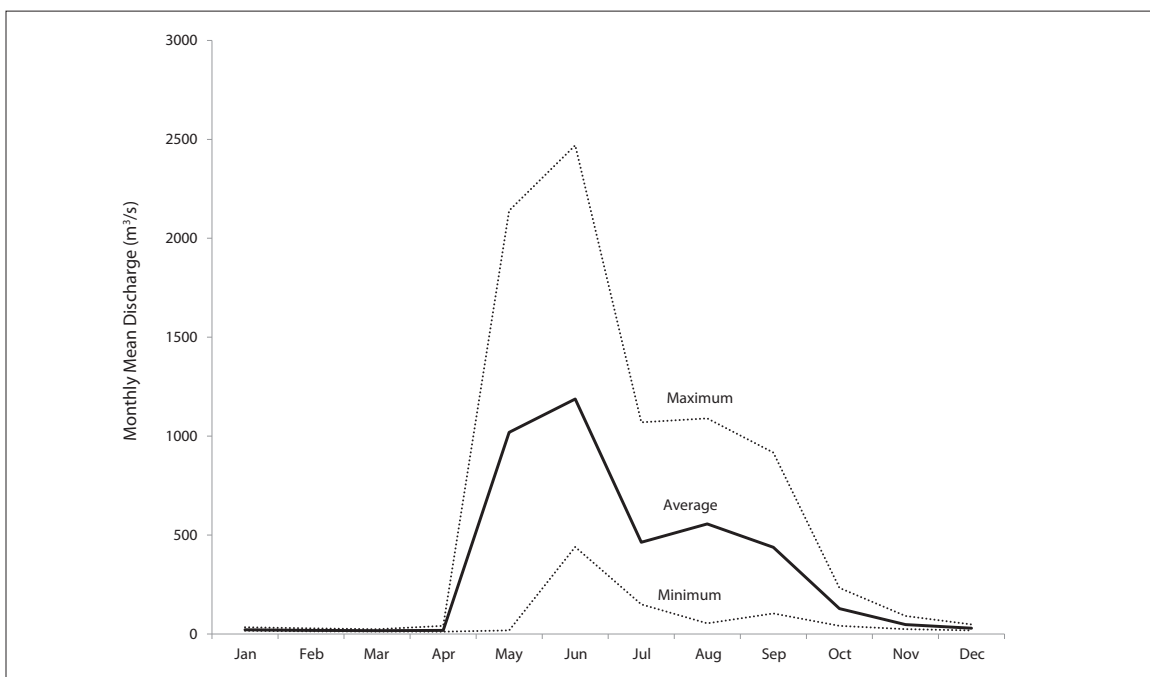


Figure 5. Old Crow River monthly mean discharge (1976-2014; Water Survey of Canada, 2016). Average, maximum and minimum monthly flows are shown.

RIVER ICE

Ice is a key component of river systems located in cold regions as it plays a regulating role in physical, biological and chemical processes of freshwater systems (Committee I, 2012). River ice plays a dominant role in controlling extreme hydrological events such as low flows and floods (Prowse et al., 2008; Committee I, 2012). These hydrological events have large environmental and economic impacts (Beltaos and Prowse, 2009). As such, it is important to understand river ice dynamics to better predict the magnitude and timing of potential flooding and low-flow events as climate changes.

In Old Crow, the river ice season is characterized by freeze-up in the autumn and break-up in the spring. Between these two events, the hydrology of the rivers remains relatively calm as flows decline and ice thickness increases. However, freeze-up timing, break-up timing, and ice jam flooding, which are all more dynamic events, are described in more detail below; additional information related to the Porcupine River are included where available.

Freeze-Up Timing

Freeze-up processes are dependent upon the heat storage gained during the open water season as well as the rate of cooling in the fall (Beltaos and Prowse, 2009; Committee I, 2012). River ice forms through the accumulation of ice lenses in a complex horizontal and vertical structure. River ice initially forms along the banks of the river. According to Committee I (2012), air temperature in the preceding weeks to months most strongly correlates with freeze-up, in comparison to all of the other meteorological variables. In general, river ice formation begins once the water temperature is around freezing (Beltaos and Prowse, 2009). Other important factors controlling freeze-up are stream channel characteristics, including width and depth, which both affect surface area-to-volume ratios.

In Yukon, freeze-up generally progresses from north to south, reflecting the latitude-temperature gradient (Janowicz, 2010). Within the northern hydrologic response zone, the timing of freeze-up is variable and dependent upon streamflow characteristics. For example, shallow, wide, slow-moving streams are likely to freeze before narrow, deep, fast-moving streams.

There are no freeze-up records available for the Porcupine River at Old Crow. In the absence of this record, examination of statistically significant summer, winter and annual air temperature trends indicate that average freeze-up dates have been and will continue to occur later, ultimately lengthening the open-water season (Janowicz, 2010).

Break-up Timing

River ice break-up occurs when the resisting forces keeping ice cover together are exceeded by the driving forces pulling ice apart (Beltaos and Prowse, 2009). The resisting forces (ice cover thickness, strength and bonding to river bed and banks) and driving forces (discharge, snowmelt inputs and rainfall) can change dramatically during the break-up period (Beltaos and Prowse, 2009). The severity of break-up is dependent upon the magnitude of change in these forces as well as meteorological conditions.

Porcupine River break-up is caused by rapid snowmelt, which usually begins in April and peaks in May. The wave of snowmelt can be sometimes augmented by precipitation, and these two forces exceed the resisting forces holding the ice cover intact (Prowse et al., 2008). Porcupine River ice break-up in the Old Crow area progresses with several break-up fronts located at key tributaries (Jasek, 1997). These key tributaries include the Bluefish River, Lord Creek, Driftwood River, Bell River and Berry Creek.

The last two decades have seen an advance in break-up dates recorded for the Porcupine River at Old Crow, based on a data record beginning in 1961. Recorded dates indicate the break-up date ranges from May 2nd to May 30th. The mean break-up date has advanced by four days, when dates from the first twenty years of record (mean break-up date = May 18) are compared to those of the last twenty years (mean break-up date = May 14; Janowicz, 2010). The advance in break-up dates is likely due to the statistically significant increases in summer, winter and annual temperatures in Old Crow (Janowicz, 2010).

It is difficult to predict how the timing of break-up will change as climate changes. However, simple approaches have relied on using temperature (melting degree days) as an indicator of the timing. Based on this approach, it is speculated that break-up dates will continue to advance for the Old Crow region as both summer and winter temperatures are projected to continue to increase.

Ice-Jam Flooding

In Yukon, numerous communities have experienced ice-jam flooding. Old Crow has flooded on a frequent basis. Within the 20th century, four major ice jam floods occurred (Janowicz, 2010). Below is a summary of the three key mechanisms that have caused flooding in the community of Old Crow in the past. Mechanisms causing flooding, as described by Jasek (1997), include:

1. **Aufeis formation at Bluefish River and Porcupine River confluence** – The Bluefish River often freezes to the bed, blocking the flow of water and forcing overflow to occur. The overflow quickly freezes and creates a large, layered ice formation. Jasek (1997) speculates that the aufeis may not actually be blocking the water, but instead creates a reach of slow moving water, and the resulting slow speed of the water is actually what allows for the development of an ice jam.

Case Study: Jasek (1997) measured the thickness of these aufeis deposits in 1994, 1995 and 1996. In 1991, when a major flood occurred and inundated the community by up to 1 m (Janowicz, 2010), the aufeis deposit was estimated to be between 3-4 m thick. It is possible that this aufeis deposit, in combination with upstream ice jamming (see point 2, below), was responsible for the high-magnitude flooding. Furthermore, in 1997, anecdotal evidence from the community indicated extensive aufeis formation and minor flooding in the community. The difference in magnitude of flooding between 1991 and 1997 can partially be accounted for by variable meteorological conditions.

2. **Flooding due to ice jam surges upstream** – Upstream ice jam surges can increase discharge downstream. This may cause flooding depending on the position of the jam, the ice jam volume, and the water level and/or rate of discharge upon jam release.

Case Study: Jasek (1997) notes that observations of the 1991 flood indicate that there was an upstream ice jam relative to Old Crow. The surge that was created upon the release of the ice jam likely contributed to the severity of flooding as this would have increased discharge and ice supply.

3. **Ice Jam Flooding due to large temperature gradient across the Porcupine River basin** – When there is a strong temperature gradient between the headwaters of a basin in the south and the downstream river reaches in the north, there can be rapid melting upstream. This can send a surge of water downstream that encounters a strong, intact ice cover. This pulse discharge, in combination with the strong ice cover, can lead to flooding behind the intact ice, or the development of a jam.

Case Study: This is what was believed to have occurred in 1989 in Old Crow. There was a large and abnormal difference in temperatures recorded in Eagle Plains compared with Old Crow. It warmed

rapidly in Eagle Plains, sending a large volume of water downstream to Old Crow where there was a strong ice cover. This ultimately led to flooding.

In summary, each of these mechanisms can cause high-water levels and possibly flooding. It is important to note that each of these mechanisms do not necessarily occur in isolation. Therefore, when these mechanisms occur in tandem, the potential for flooding, as well as its extent, can be greater.

Overall, it is difficult to speculate how projected changes in climate will affect ice-jam flooding and severity of break-up in Old Crow. This is because the impacts of climate change on ice-cover thickness and ice jams is not well understood (Beltaos and Prowse, 2009).

SNOW WATER EQUIVALENT

As part of the Yukon Snow Survey Network run by Environment Yukon, snow depth and snow water equivalent (SWE) measurements have been recorded in Old Crow since 1977. Measurements of snow depth and SWE are typically taken on March 1, April 1 and May 1 of every year. Seasonal maximum snow water equivalent is shown in Figure 6. Based on available data, there has been no significant trend in seasonal maximum SWE values in Old Crow.

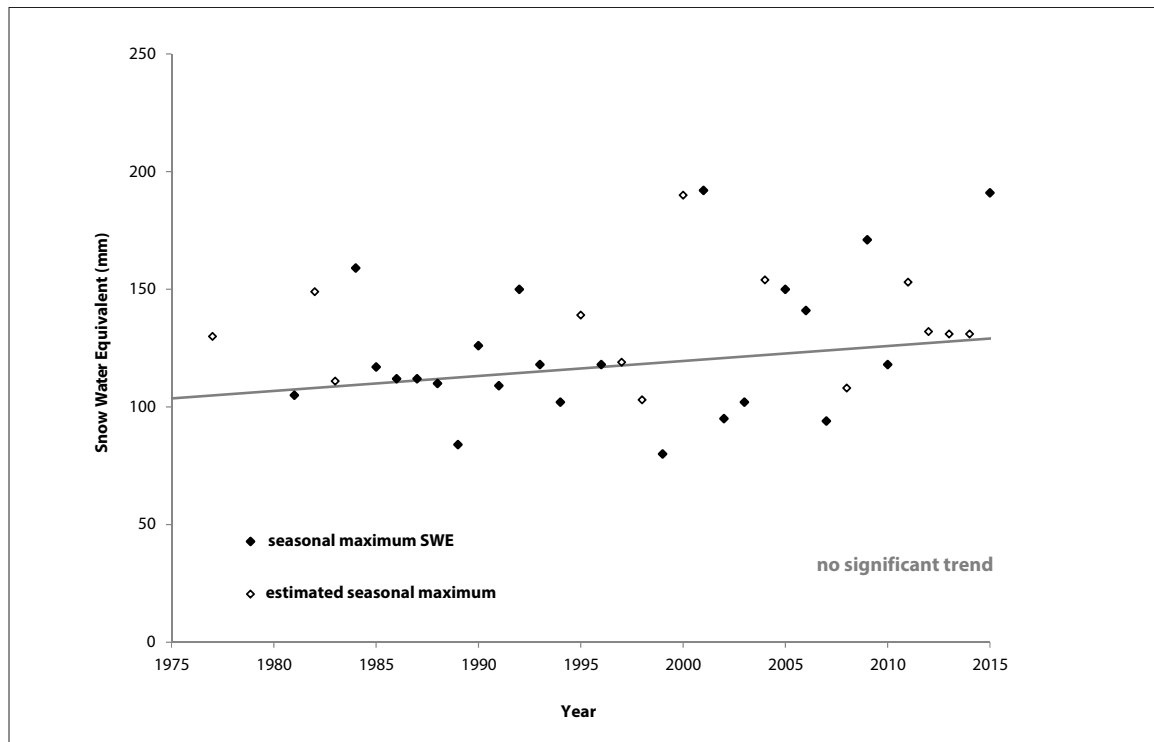


Figure 6. Seasonal maximum snow water equivalent (SWE; in mm) for the Old Crow station (1977-2015), part of the Yukon Snow Survey Network run by Environment Yukon. Note that estimated data values are shown in grey.

GROUNDWATER

Limited information regarding groundwater is available for Old Crow. No long-term records were identified as part of this project. Given that Old Crow is located on the floodplain of the Porcupine River, it is likely that flow is generally towards the river.

The community of Old Crow obtained drinking water from the Porcupine River until 1982, when two municipal wells were installed in a fractured bedrock aquifer (Gartner Lee Limited, 2003). Both wells are artesian and located within the same aquifer. When the wells were installed in 1982, the rate of artesian flow was 6.1 L/s. Well 1 is 79 m below ground surface and Well 2 is 96.6 m below ground surface (Gartner Lee Limited, 2003).

LANDSCAPE EVOLUTION

The concept of ‘landscape’ comprises both the physical elements of landforms (mountains, valleys, plateaus), water bodies (rivers, lakes, ponds), elements of the cryosphere (glaciers, permafrost), and the living parts of the landscape such as the presence and modifying pressures of plants, animals and humans. The physical and geological landscape of the map area has been conditioned by millions of years of tectonic movement, fluvial (water) erosion and deposition, the advance and retreat of glaciers, and more recently, the modifying effects of eolian (wind), colluvial (gravity), permafrost (perennially frozen ground), and human processes.

| Mya | PERIOD | EPOCH | |
|------|------------|-------------|--|
| 0.01 | QUATERNARY | HOLOCENE | <i>post-glacial era; warming to modern climate</i> |
| 2.58 | | PLEISTOCENE | <i>era of frequent glaciation in the northern hemisphere</i> |
| 5.3 | NEOGENE | PLIOCENE | |
| 23.0 | | MIOCENE | <i>era of gradual cooling, warmer than modern climates</i> |
| 33.9 | PALEOGENE | OLIGOCENE | |
| 55.8 | | EOCENE | <i>era of deposition of the youngest rocks in the Old Crow Basin</i> |
| 65.0 | | PALEOCENE | |

The study area for the Old Crow Landscape Hazards Mapping Project occupies a landscape of deeply weathered, unglaciated terrain that was part of a much larger unglaciated landmass called Beringia. Beyond the direct effects of advance and retreat of continental-scale ice sheets, the landscape surrounding Old Crow has never been ‘stripped’ by the scouring action of glaciers, and the unconsolidated sediments that comprise the surficial geology of the region extend much further into geologic history than those of glaciated regions. Surficial sediments in the map area range in age from just a few days or weeks old, to tens of millions of years old. Similarly, the consolidated bedrock of the region has a history that begins many hundreds of millions of years ago, and continues into modern time.

In discussing the evolution of the landscape in the Old Crow region, we can broadly divide the surface and bedrock geology into components that were formed prior to the epoch of frequent glacial episodes (the Neogene Period and earlier; Figure 7), those that were formed during the epoch of glacial episodes (the Pleistocene Epoch of the Quaternary Period), and those formed in the modern, post-glacial time (the Holocene Epoch of the Quaternary Period).

Figure 7. Geological timescale for the last 65 million years, during which time much of the sediment in the Old Crow Basin was deposited.

THE NEOGENE PERIOD AND EARLIER

The community of Old Crow occupies the southern edge of the Old Crow-Babbage Depression, a structural and physiographic depression encompassing the Old Crow Flats and extending north into the British Mountains. The oldest rocks in the area are quartzites that underlie Berry Hill and occur on the high ridges to the north. These are thought to be Neoproterozoic (~800 Mya) and to have been transported westward along the Porcupine shear zone – the broad fault zone that underlies the Porcupine River (Figure 8). The Porcupine shear zone brings into contact Neoproterozoic quartzite to the north with Devonian and older limestone to the south (Norris, 1985). Displacement along the Porcupine shear zone occurred mostly before intrusion of Late Devonian (~370 Mya) granites exposed mainly north of Old Crow. During Mesozoic time (between ~180-66 Mya), mountain building to the south in the Ogilvie Mountains led to development of a large marine depression into which sediments eroded from the rising mountains were deposited – first represented by fine-grained Jurassic (~180-145 Mya) shale and siltstone, succeeded by coarser-grained Cretaceous (145-66 Mya) sandstone as the sedimentary basin was filled. Mountain building continued into the Paleogene (~66-23 Mya) and led to the rise of the British Mountains to the north, and local deposition of Eocene (56-34 Mya) and Oligocene (34-23 Mya) sedimentary rocks.

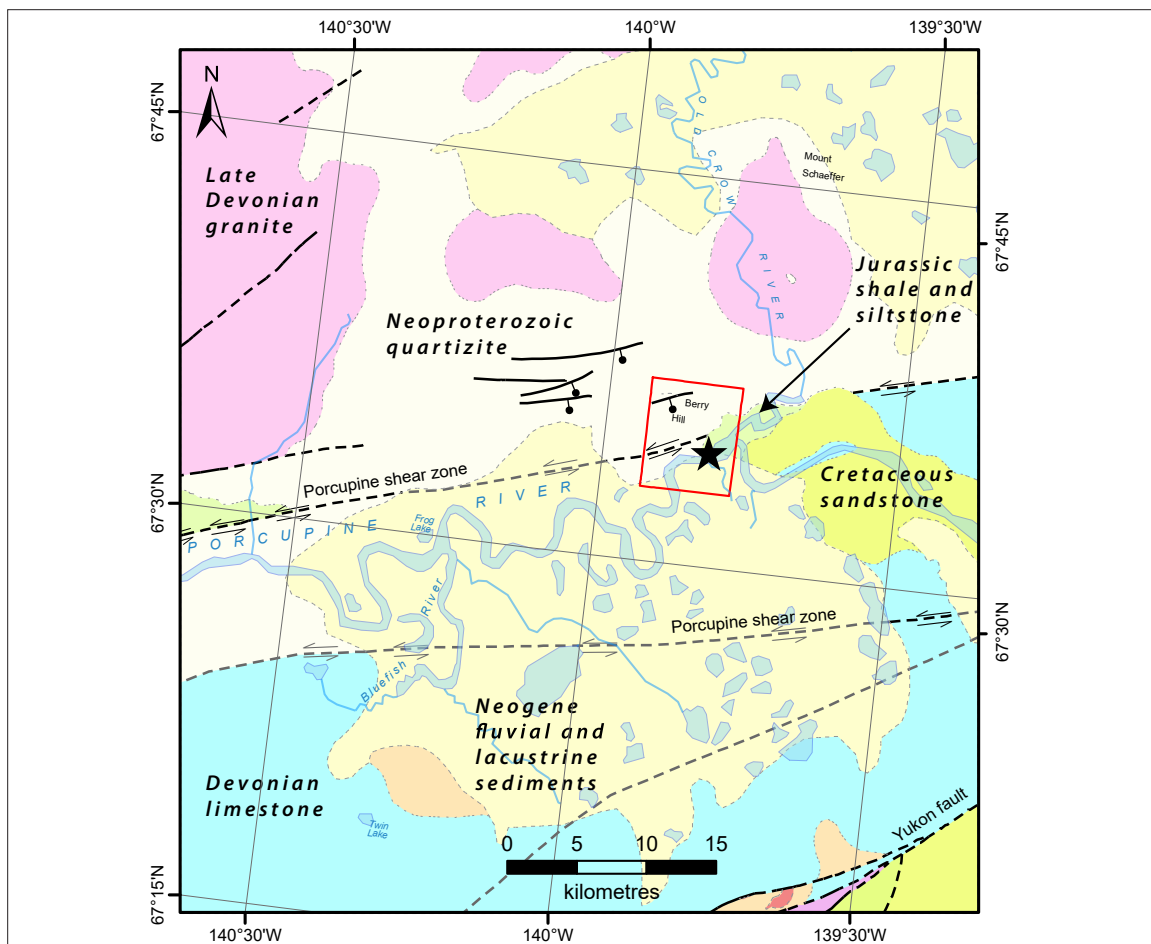


Figure 8. Bedrock geology surrounding the map area (outlined with red box). The community of Old Crow is indicated with a black star and is underlain by Neoproterozoic-aged quartzite and Jurassic-aged siltstone and shale. Light dashed lines are assumed contacts between units and heavy dashed lines are known and presumed bedrock faults (arrows indicate direction of movement if known). Geology from Colpron, 2016.

Sedimentation into the Old Crow Basin during the Neogene (~23-2.6 Mya) was dominated by shallow rivers and lakes that filled the basin with silt, sand and gravel (Figure 9). Lacustrine and fluvial sediments have been exposed by late Pleistocene fluvial incision along the Porcupine and Crow rivers and record basin sedimentation that was likely controlled by continued uplift in the surrounding mountains in conjunction with the relative subsidence of the Old Crow basin. Tephra from some of the oldest lake sediments is thought to be more than 1.2 Mya (Pearce et al., 1982), however, fossil wood, cones, and pollen from these exposures all suggest the sediments could be considerably older, and potentially extend into the early Neogene (Litchi-Federovich, 1973; Matthews et al., 1987; Schweger, 1989). Late Neogene fluvial sediments grade to considerably higher base levels than exist today and are thought to have been part of the paleo-Mackenzie River drainage prior to glacial meltwater diversions in the late Pleistocene (Duk-Rodkin and Hughes, 1995; Duk-Rodkin et al., 1996).

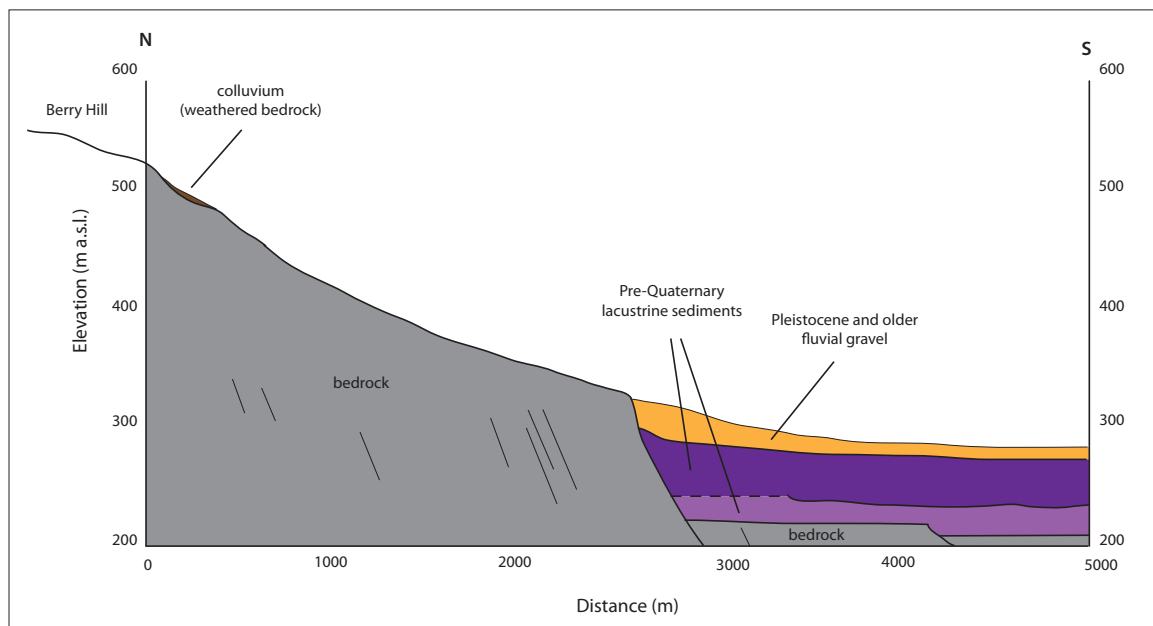


Figure 9. Idealized cross-valley profile of what the Old Crow basin might have looked like at the end of the Neogene when rivers and lakes had filled the basin with sediment.

Weathering and erosion during Neogene and earlier periods occurred under warmer and potentially wetter conditions than exist today. The enhanced chemical weathering is responsible for much of the 'subdued' appearance of the landscape including the broad, low-angle bedrock slope forming a pediment above Old Crow.

THE PLEISTOCENE EPOCH

Gradual cooling during the Neogene Period culminated in the cold, arid conditions of the Pleistocene Epoch, a time extending from 2.65 Mya until the last ice sheet receded from Yukon ~12,000 years ago. During the Pleistocene, much of North America was covered in successive ice sheets that grew from regional centres of accumulation during colder glacial periods and receded during milder interglacial periods. Neither the Laurentide Ice Sheet, which covered most of Canada east of the Rocky Mountains, nor the Cordilleran Ice Sheet, which covered most of Yukon and British Columbia, reached the study area. Instead, the Old Crow region was part of a large unglaciated landmass known as Beringia that spanned from northern Yukon to eastern Siberia. The Beringian environment was characterized by cold, dry periglacial conditions. Erosional

processes such as cryoturbation, frost shattering, frost heaving and solifluction would have been pervasive. Permafrost would have affected much of the landscape during the Pleistocene, and was likely more extensive than it is today.



Figure 10. Evidence of periglacial conditions are recorded by ice wedge casts which formed when frost cracks fill with sediment.

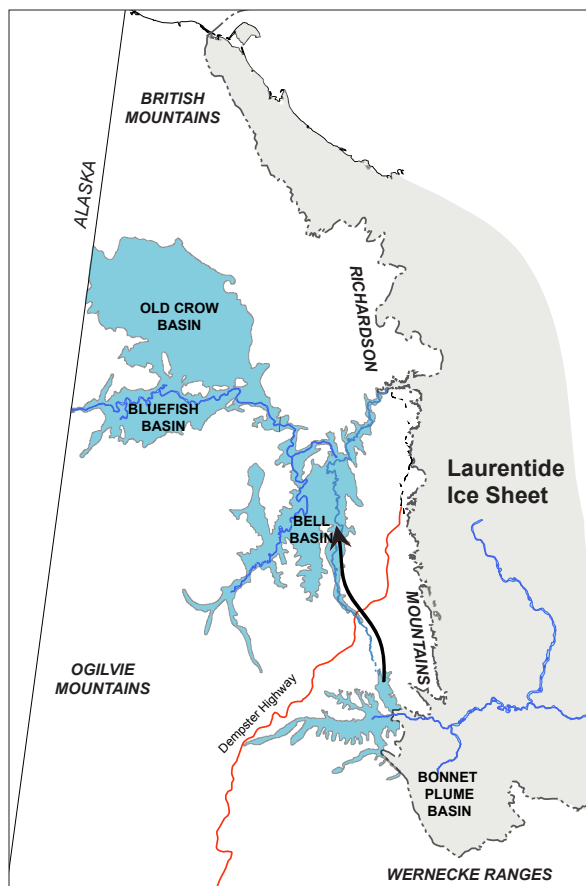


Figure 11. The maximum western advance of the Laurentide Ice Sheet is thought to have impounded easterly flowing rivers in northern Yukon and formed a large proglacial lake in the Bonnet Plume, Bell, Bluefish, and Old Crow basins.

The cold conditions of the Pleistocene Epoch are recorded in the study area by a transition from temperate to cold-climate pollen records (Lichti-Federovich, 1973; Schweger and Matthews, 1991) and preserved periglacial features such as ice wedge casts that record thermal cracking of the ground surface (Figure 10). The modern course of the Porcupine River is thought to have been established during the late Pleistocene when glacial lakes overflowed into the Old Crow Basin and cut a new western outlet to the Yukon River (Hughes, 1972; Duk-Rodkin et al., 2004). Prior to this diversion, regional streams drained eastward into the paleo-Mackenzie River. When the most extensive advance of the Laurentide Ice Sheet occurred in the late-Pleistocene, it blocked drainage through the Richardson Mountains and impounded a large glacial lake in the Old Crow, Bell, Driftwood and Bluefish basins (Figure 11; Hughes, 1972; Zazula et al., 2004). Strandlines to at least 360 m a.s.l. in the Old Crow basin mark the high stand of glacial Lake Old Crow ~15,000 to 20,000 years ago, before incision of the Ramparts of the Porcupine River drained the lake and established the modern course of the Porcupine River and its tributaries (Figure 12; Kennedy et al., 2010; Thomson and Dixon, 1983).

Deposition in the study area during the Pleistocene was dominated by colluvial and fluvial processes. Changes to the landscape during this time include the deposition of fluvial terraces along the Porcupine River, as well as blankets, aprons, and fans of colluvium (Figure 13). Thin veneers and mantles of wind-blown silt and sand (loess), were probably generated from local

stream beds and unglaciated soils (Tarnocai et al., 1985) under regional winds and strong katabatic flow from the ice sheets to the south that was ongoing throughout the Pleistocene (Froese et al., 2000; Muhs et al., 2003; Muhs and Budahn, 2006; Preece et al., 2000; Westgate et al., 1990). Slow periglacial wasting mechanisms (solifluction, slopewash) likely dominated colluvial processes throughout the Pleistocene and into the modern era. In general, colluvial deposits of weathered bedrock thicken downslope and become increasingly mixed with other surficial deposits such as loess, and high-level gravel and silt deposits.



Figure 12. Beaches of washed gravel ~10 km southeast of Old Crow mark the high stand of glacial lake Old Crow at ~360 m a.s.l.

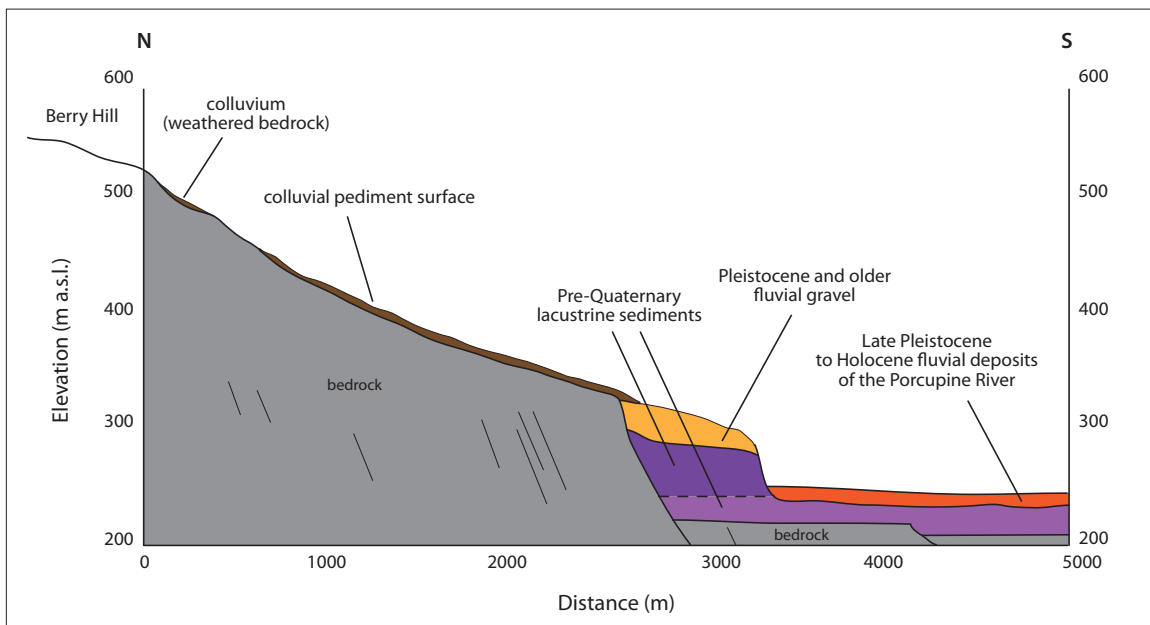


Figure 13. Idealized cross-valley profile of what the Old Crow basin might have looked like during the late Pleistocene when the reversal of the Porcupine River had incised a deep valley into older basin sediments.

THE HOLOCENE EPOCH

Holocene landscape evolution in the study area was modified by the amelioration of periglacial conditions and a gradual infilling of the Porcupine River valley margins (Figure 14). Valley-side colluvial deposits and abandonment of the high terraces along the Porcupine River resulted in the modern, broad, poorly drained valley floor (Figure 15). Landscape evolution of the Old Crow map

area continues in historic times as the result of community development on the floodplain terrace of the Porcupine River and the hillslope above.

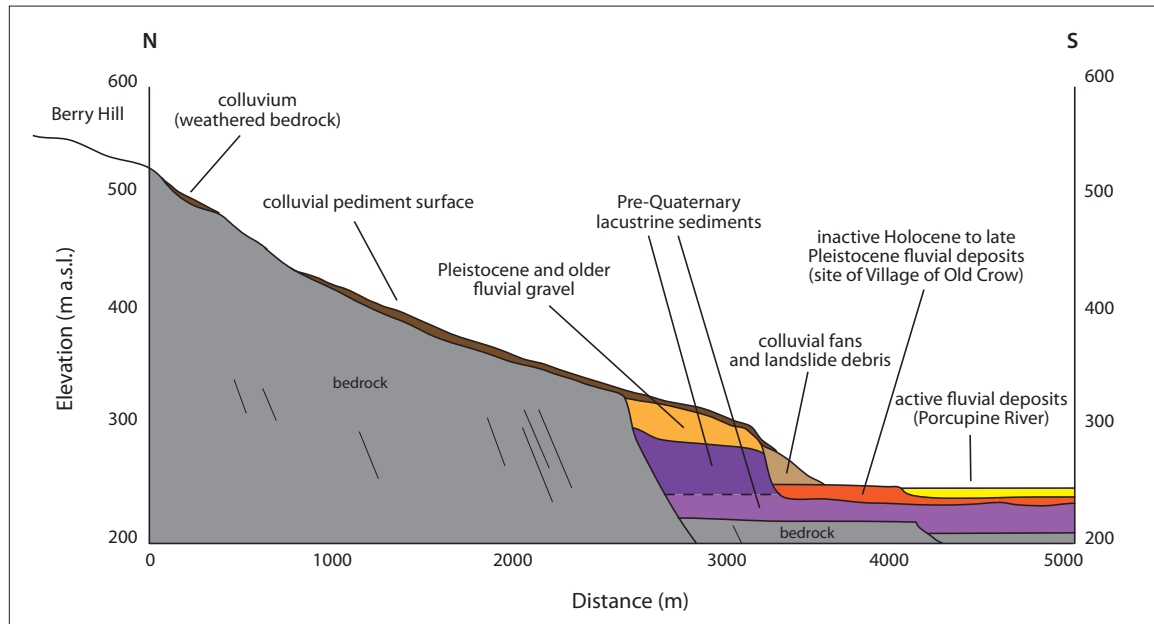


Figure 14. Idealized cross-valley profile of the modern landscape in Old Crow. Holocene changes to the landscape include development of colluvial pediment materials and valley-side colluvial aprons.



Figure 15. Holocene changes to the landscape include valley-side colluvial deposits and the growth of peat and permafrost on the valley floor. Ice-wedge polygons are visible in the foreground of this photo looking northeast toward the community of Old Crow.

SURFICIAL MATERIALS

The mapping of surficial landforms and their contained sediments is achieved primarily through air photo interpretation followed by ground truthing. While ground truthing, geologists examine riverbank exposures, road cuts, and dig small pits in order to characterize the various surficial deposits. Textural and stratigraphic information of surficial landforms is also gained through geophysical profiles of the subsurface (using Ground Penetrating Radar and Direct Current Electrical Resistivity) as well as shallow boreholes. Surficial materials are characterized based on their texture or grain size (e.g., very fine to very coarse sand); sorting (e.g., poorly sorted = inconsistent grain size); structure (e.g., layering or bedding); and the general distribution of the material.

Surficial deposits in the study area are derived from the following processes: in-situ weathering; fluvial (rivers and streams); lacustrine (lakes); colluvial (downslope movement or creep); eolian (windblown); organic processes (soil development); and anthropogenic (human activity). Detailed descriptions of the surficial materials found in the study area are also located in the map legend (see accompanying map “Surficial geology, Old Crow, Yukon”; Kennedy, 2016).

BEDROCK (R) AND WEATHERED BEDROCK (D)

Bedrock in the map area consists of Neoproterozoic (~800 Mya) and Jurassic (~180-145 Mya) clastic and carbonaceous sedimentary rocks. The Neoproterozoic Katherine Formation is characterized in North Yukon by mature, very fine-grained, thin to thick-bedded, brown, greenish grey and white orthoquartzitic sandstone with recessive intervals of shale and rare dolostone. Comprising Berry Hill and the gentle slopes below it, this distinctively white rock is the primary source for crush, rip-rap and other aggregate needs for the community of Old Crow. The Jurassic-aged Porcupine River member of the Husky Formation is in fault contact with this unit. Characterized as dark grey siltstone and shale (Norris, 1985; 1997), this unit outcrops on the west bank of the lower Crow River just above the community of Old Crow (Figure 16).

Much of the bedrock in the uplands surrounding and making up Berry Hill is mapped as ‘weathered bedrock’ (D; Figure 17). Weathered bedrock frequently forms deposits of blocks and boulders within a silty matrix that were created through frost shattering, colluviation, and chemical weathering processes. Weathered bedrock units typically contain a component of loess-derived silt and are subject to sorting and mixing from cryoturbation and other periglacial processes.

Permafrost is present in both bedrock and weathered bedrock in the map area.



Figure 16. Siltstone of the Jurassic-aged Husky Formation is visible in outcrop along the lower Crow River. Abundant fossil shell imprints are visible. Lens cap for scale.



Figure 17. Weathered bedrock is the dominant material type in the highest parts of the map area. In this photo, crushed sandstone bedrock is visible in the foreground, weathered bedrock is visible in the middle ground, and the colluvial plain of the pediment slope is visible in the far distance.

FLUVIAL DEPOSITS (F^A, F AND F>P)

Fluvial deposits are derived from modern and ancient rivers and streams and are composed of stratified beds of gravel and/or sand with sand and/or silt and/or organic materials (and rarely clay) (Howes and Kenk, 1997). Fluvial sediments mapped in the study area are predominantly those associated with floodplains, fluvial terraces and channels of the Porcupine and Old Crow rivers. Mapped fluvial materials include Pleistocene and older gravel in high-level terraces, and a large range of late-Pleistocene to Holocene-aged fluvial deposits that comprise the modern valley-

bottom floodplains, channels and terraces. Fine-grained fluvial deposits are commonly poorly drained and may be ice rich, while coarse-grained fluvial deposits are commonly well drained and ice poor. Floodplain and terrace deposits may be subject to flooding accompanied by sudden channel migration.

Late Pleistocene to Holocene-aged deposits make up the bulk of mapped fluvial materials in the study area (see surficial geology map). Of these, fluvial deposits can be active (FA) or inactive (F). Inactive Holocene fluvial deposits (F) include terraces above the modern floodplain and abandoned back-channel deposits no longer a part of the active floodplain. These deposits range from silty, sand-rich gravel channel deposits to fine-grained sand and silt overbank and back-channel materials. Inactive fluvial deposits are commonly overlain by organic materials, and where these materials occur, permafrost is usually present.

Active Holocene fluvial deposits (FA) comprise sand and gravel stream materials that are subject to regular flooding. These deposits include both coarse channel materials and fine overbank flood deposits (Figure 18). Main channel gravel deposits are moderately to well sorted, and contain clasts that are rounded and imbedded in a sandy matrix (Figure 19). Overbank deposits are represented by fine-grained sediments of silt, sand and organics that are massive (lacking structure) to thinly laminated and may contain interbeds of gravel (Figure 20). In the study area, fans, or complexes of coalesced fan-shaped landforms, are usually dominated by colluvial processes although fluvial transport does contribute to their formation. Fans typically consist of large amounts of silt, sand, and gravel colluvium derived from units of stratigraphically higher positions.



Figure 18. Both active-channel gravel deposits and back-channel depositional environments are pictured here. Abandoned meanders of the Porcupine River gradually fill with silt and sand to become poorly drained and ice-rich parts of the floodplain.



Figure 19. The active channel of the Porcupine River is characterized by moderately rounded and well-imbricated pebble and cobble-sized clasts.



Figure 20. This soil pit dug in the back-channel part of the floodplain in Old Crow (near the ski trails) has fine, silt-rich soil and a shallow active layer. At this site, the water table was encountered 45 cm below the top of the moss mat where it was perched above a ~65 cm deep permafrost table.

Pleistocene and older fluvial deposits (F>P) are mapped above elevations of ~280 m a.s.l. on the bluff above town where they are overlain by a blanket of colluvium comprising the surface of the pediment plain (Figure 21). High-level fluvial deposits in the map area range from ~10 m to 20 m thick, and are characterized by well-rounded pebble-cobble gravel with laterally and vertically discontinuous beds of massive, planar, and ripple cross-bedded sand. Gravel units range from cobble to pebble-dominated and

can be both open-work and matrix-supported (Figure 22). Discontinuous sand units are usually 2-3 m thick and poorly exposed. Where visible, sand beds contain features such as cobble lags and cut-and-fill structures that may be related to colluvial slope wash (Figure 23).



Figure 21. Pleistocene and older fluvial gravels overlain by a blanket of colluvium at the top of the escarpment above town.



Figure 22. Matrix and clast-supported facies of pebble-cobble gravel deposited above ~280 m a.s.l. on the escarpment above town.

High-level gravel deposits have a distinct clast lithology comprised of locally derived sedimentary and igneous rocks that differ significantly from valley-bottom late Pleistocene and Holocene fluvial gravel deposits, which contain far-travelled clasts derived from glaciated drainages to the east. No evidence of ice wedge casts or cryoturbation was observed, and a buried soil at one location (Figure 24) suggests the top of the high-level fluvial unit may have been a stable surface in the past. Pleistocene and older fluvial materials are interpreted as being deposited in a braided river system prior to re-routing of the Porcupine River.

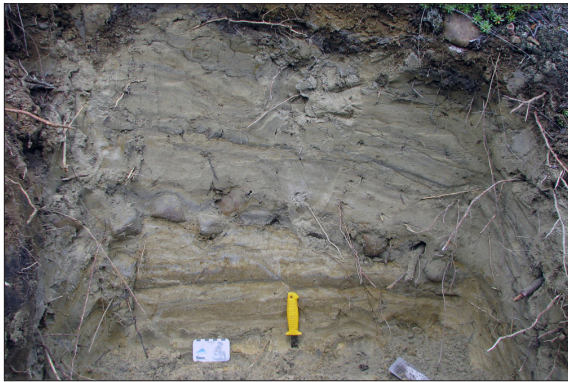


Figure 23. An exposure of a sand facies in the high-level fluvial deposits has an erosional cobble lag surface which is draped by angled sand beds that may have been deposited as slopewash.



Figure 24. Organic material (dark brown) and altered parent materials (white quartz sand) at the top of the high-level gravel where it is buried by ~5 m of diamict.

LACUSTRINE DEPOSITS (L<M; L>P)

Lacustrine deposits in the study area comprise recently deposited sediments in existing lakes on the floodplain of the modern Porcupine River (L<M), as well as extensive and thick lacustrine sediments deposited prior to the Pleistocene (L>P).

Modern lacustrine sediments (L<M) that have settled from suspension in bodies of standing water are limited to thin deposits in small bodies of still water on the floodplain of the Porcupine River. Sediments consist of stratified fine sand, silt, and clay deposited on the lake bed from suspension. Modern lacustrine sediments are likely to be thawed while covered with lake water, but can become ice rich if permafrost migrates into the sediments.

Neogene or older lacustrine sediments (L>P) are found in the lowermost half of the stratigraphy exposed on the steep bluff above the floodplain of the Porcupine River. The top of the lacustrine unit is at ~280 m a.s.l., and where visible on the Crow River, overlies bedrock near river level at ~250 m a.s.l. Sediments are finely laminated, well indurated and are composed primarily of silt with small amounts of sand (Figures 25 and 26). Neogene lacustrine sediments form a barrier to surface water drainage and may be ice rich. Ice lenses are present at the base of the active layer where it occurs in these sediments, but within the unit itself, permafrost likely occurs as porous visible or invisible ice. This unit is prone to active layer thaw detachment slides where it is exposed along the bluff above town.



Figure 25. A large exposure of lacustrine silt above the lower Crow River. One bed containing cobble-sized clasts was observed in this silt-dominated unit and is pictured here.



Figure 26. Neogene-aged lacustrine silt exposed in a pit along the escarpment above town. The unit is well indurated and friable with fracture planes commonly weathered to a rusty orange colour.

COLLUVIAL DEPOSITS (C)

Colluvial deposits are materials that have moved downslope primarily due to gravitational forces (Howes and Kenk, 1997). Deposits range from massive to moderately well-stratified, non-sorted to poorly sorted sediment, and particles may range from clay to boulder-sized. Transportation of colluvial sediment is usually not very far from the source material, therefore particles tend to be angular to sub-angular in shape; however, colluvial deposits originating from rounded materials may contain rounded clasts.

Colluvium is the dominant surficial material in the uplands of the map area (see Kennedy et al., 2016). On the gentle slopes of the pediment plain above town, periglacial processes such as solifluction, cryoturbation, and sheetwash result in the deposition of a silt-rich diamict containing angular, local bedrock clasts (Figure 27). Active layer depths control the thickness of this unit, and the periglacial processes that create it have likely only been active since the early Pleistocene or late Neogene. On steeper slopes, colluvium has been deposited by rapid mass wasting such as landslides, thaw detachments, and debris flows. These colluvial deposits incorporate various surficial materials and result in a silt-rich diamict containing well-rounded to angular clasts derived from resedimentation (Figure 28).

Colluvial aprons, blankets and hummocks mapped in the valley bottom and on lower hillslopes are typically comprised of resedimented slope materials transported by rapid or slow mass movement processes, and may also contain a component of fluvial transport and deposition. These colluvial diamicts are silt rich with mixed angular to rounded clasts and can be interbedded with organic deposits or overbank river silt close to the floodplain (Figure 29). Valley-bottom colluvial deposits are commonly ice rich with an average of 50% ice by volume (Figure 30). Colluvium is typically modified by cryoturbation to depths of 30-90 cm, resulting in a mixed profile (Smith et al., 2009).



Figure 27 (left). Silt-rich diamict is the highest stratigraphic unit on the escarpment above town and is interpreted as a colluvial deposit generated on the pediment slope above. The thickness of this unit is thought to be controlled by the depth of cryoturbation that occurs in the active layer above the permafrost table. The underlying sand unit in this photo has disturbed bedding near its contact with overlying silt, but relatively undisturbed beds below where they have been preserved by permafrost.



Figure 28 (above). Colluvium comprised of resedimented fluvial gravel can contain well-rounded clasts such as the ones pictured here.



Figure 29 (above). Coarse angular clasts and a silty matrix are typical of colluvium deposited by rapid mass movement processes. This deposit is located at the mouth of a gully.



Figure 30 (above). Dark grey ice in tan silt; deposited on a colluvial landform near Ski Chalet Road.

ORGANIC DEPOSITS (O)

Organic deposits are defined as containing at least 30% organic matter by weight and are formed by the accumulation of vegetative matter (Howes and Kenk, 1997). Organic deposits typically form in low-lying areas and valley floodplains where the ground is saturated. They may also form over inorganic materials that contain high concentrations of silt and clay or where drainage is poor due to shallow permafrost tables. Ice-rich permafrost is common in these deposits.

Organic deposits are pervasive on the landscape in the Old Crow map area and are typically poorly or very poorly decomposed. In the study area, organic materials accumulate on top of most surficial units including colluvial slopes, weathered bedrock, fluvial terraces, fans and floodplains. Accumulations of vegetative matter thicker than 1 m are mapped as organic blankets and are found in

limited areas on floodplains or shallow fluvial channels where soils are modified by near-surface permafrost. Veneers of organic material (20 to 100 cm thick) are widespread in the map area, and though not mapped, are present on most flat to gently-sloped surficial deposits (Figure 31).



Figure 31 (left). A thick organic mat (more than 20 cm) on this valley bottom site creates cold, saturated ground conditions with permafrost near surface.

EOLIAN DEPOSITS (E)

Eolian deposits are materials transported and deposited by wind. These deposits generally consist of medium to fine sand and coarse silt that is well sorted, non-compacted, and may contain internal structures such as cross-bedding or ripple laminae, or may be massive (Howes and Kenk, 1997). Eolian deposits in the study area are predominantly silt-sized quartz particles incorporated into active layer sediments and are represented by the textural symbol “z” on various units on the map.

Eolian silt deposits are found on both upland and lowland surfaces in the study area, but commonly occur in greater thicknesses along the top edge of the bluff above town (Figure 32). Enhanced colluviation and cryoturbation in the permafrost soils of Old Crow mixes loess into the underlying soil parent material. Active landforms such as fluvial channels or colluvial fans are unlikely to have noticeable accumulations of eolian deposits.



Figure 32 (left). Eolian sand and silt often accumulates in thicker deposits on ‘cliff-top’ locations like this where wind blows up exposed sediments from the steep slope below. In this photo, silt is enriched in a gravel soil.

ANTHROPOGENIC DEPOSITS (A)

Anthropogenic deposits are surface materials modified by human activities such that their original physical properties have been significantly altered (Howes and Kenk, 1997). Anthropogenic deposits in the map area include areas with significant quarried rock on the surface such as the sewage lagoon, and where aggregate used for building pads has largely replaced natural materials (Figure 33).



Figure 33. Thick aggregate building pads are an example of anthropogenic deposits in Old Crow. The airport is the biggest continuous area composed of anthropogenic materials, and much of the downtown core contains anthropogenic deposits of aggregate.

STRATIGRAPHY

Stratigraphic relationships in the map area are presented in Figures 34 and 35. Figure 35 is a schematic log from a well drilled below the village of Old Crow at the water treatment plant. The top of the log is at ground surface at ~251 m a.s.l. and the bottom of the log is at 121.9 m below the ground surface at ~129 m a.s.l. This log shows deeper stratigraphy than is visible in natural exposures in the map area, and supports the interpretation of the lowermost units in the stratigraphic profile. The water well log encounters bedrock nearly 40 m below where it occurs on the Crow River in the map area, and records evidence of a fault ~80 m below river level. Both observations support the interpretation of a rapidly subsiding bedrock surface caused by either a fault-dropped block, or a change in rock competence caused by faulting that allowed for preferential erosion in the Porcupine River valley.

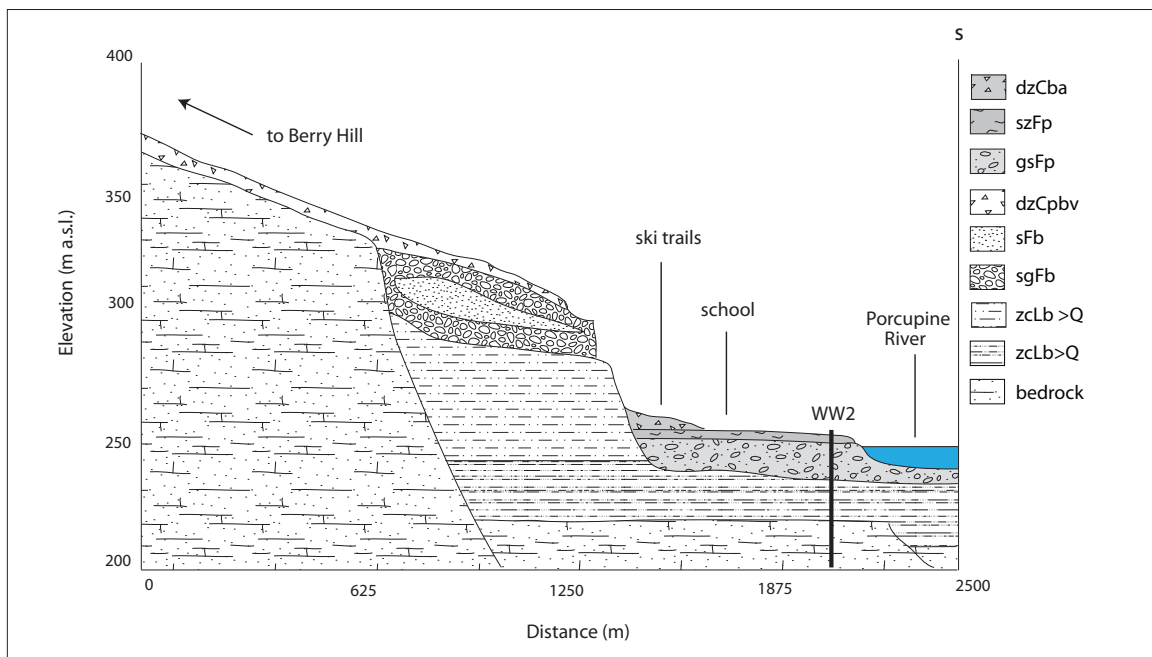


Figure 34. Idealized cross-valley profile of the map area with unit textures and landform descriptions that correspond with the surficial geology map legend. The view is to the east and the location of Figure 35 (WW2) is indicated.

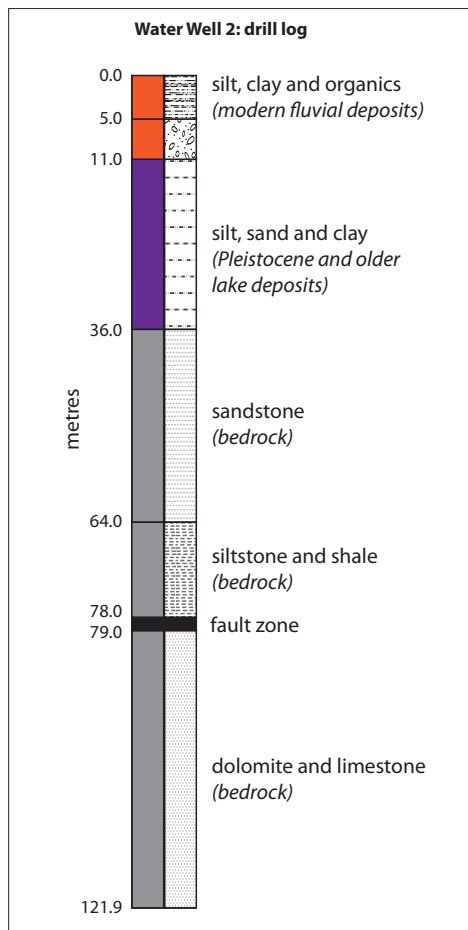


Figure 35 (left). Generalized log of well cuttings from a 122 m well beneath the community of Old Crow. Textures of materials are shown on the right side of the well, and colours on the left correlate with material types shown in Figure 34.

The lowermost stratigraphic unit in Figure 34 is a subsiding bedrock surface upon which unconsolidated basin sediments are deposited. Lacustrine sediments are interpreted to encompass at least 25 m of sediments buried beneath the modern channel of the Porcupine River. These lake deposits are also preserved above the modern river along the escarpment above Old Crow where they occur to ~280 m a.s.l. Lacustrine sediments are overlain by up to 20 m of fluvial sand and gravel deposits. These units were likely all in place before the late Pleistocene diversion of the Porcupine River that incised its modern channel ~50 m lower than the former river channel. Since the new channel was established, deposition has been in the form of colluvial blankets (both on the shallow upland pediment and along the steep flank of the escarpment), and fluvial plains and terraces. The community of Old Crow is built upon a fluvial terrace that has largely been abandoned by the modern course of the Porcupine River. Abandonment of this surface could be climatically driven, and/or related to

the ongoing incision of the Ramparts of the Porcupine as the Porcupine River keeps pace with base-level change in Alaska.

PERMAFROST

In the study region, the permafrost profile is made up of several different components which must be considered collectively to accurately characterize local permafrost conditions. These components, and comments about their relevance to the Old Crow region, are described in the following section.

FOREST COVER

The forest cover keeps the ground cool by providing shade, increasing the soil moisture (increase in heat capacity), and increasing energy diffusion before it hits the ground surface. In the winter, trees retain snow, which locally reduces snow cover on the ground that is acting as an insulating layer between the atmosphere and the ground (Brown, 1963; Brown and Péwé, 1973). Clearing of the forest cover by machinery, removing or compacting the forest litter, and forest fire usually lead to a deepening of the active layer and subsequent degradation of the upper portions of permafrost, which is commonly ice rich. When the low-lying vegetation (e.g., bryophytes, grasses) is also removed or compacted, the effects are much more pronounced.

SOIL TEXTURE

Seven different surface material types were identified in the Old Crow area based on the geotechnical characteristics of samples gathered during the permafrost-drilling program. They were classified using the Unified Soil Classification System (USCS) and are as follows: sand, silty sand, silty sand with gravel, sandy silt, sandy organic silt, silt, and peat; each is described in more detail below.

Sand

Generally, sand layers are well drained, do not contain excess ice and are not frost or thaw susceptible. However, fine and very fine sand are frost susceptible and can contain excess ice in the form of alternating ice lenses. Upon thawing, soils with excess ice will undergo thaw settlement and will be slowly drained.

Silty sand and sandy silt

Where surficial hydrologic and thermal regimes allow, coarse silt and fine sand may contain a great amount of excess ice in various forms, because these two materials present an important ice segregation potential (Konrad and Morgenstern, 1981). However, if present in an under-saturated condition, these sediments would not contain excess ice and would be mechanically stable upon thawing.

Silty sand with gravel

Because of the presence of fine-grained material, this stratigraphic class has a high ice-segregation potential. In permafrost, if saturated with water, this deposit could contain layers with ice-rich cryostructures and be affected by strong differential thaw settlement. However, if present in an unsaturated condition, these sediments would not contain excess ice and would be mechanically stable upon thawing since the water would remain in the soil porosity.

Sandy organic silt

The organic matter in sandy or silty deposits increases the water retention capacity of a soil; this may lead to the development of excess ice in permafrost, and an increase in settlement potential under a load, due to the high compaction potential of the peat.

Silt

This fine-grained material is usually highly frost susceptible. If silt is present in the active layer, and if water is available, it leads to annual frost-heave and settlement of the ground. If a silty layer occurs at, or below the permafrost table, the upper part of permafrost will be typically ice rich and mechanically unstable upon thawing. Poor drainage characterizes these permafrost-degraded areas.

Peat

Peat layers have high porosity, can retain water, and are highly compressible when thawed. In permafrost, peat is usually ice rich. When it thaws, the water is drained and the ground is susceptible to considerable settlement, especially under a load.

CONTEMPORARY PERMAFROST TEMPERATURE MODELLING

Research undertaken in southern Yukon has shown a close relationship between trends in air temperature with elevation (termed surface lapse rates) and the probability of permafrost (Bonnaventure et al., 2012). Old Crow falls within the continuous permafrost zone according to the Permafrost Map of Canada (Heginbottom et al., 1995) but this designation is based on air temperature measured at the elevation of the community and on boreholes drilled primarily on

the valley floor. Little is known about conditions at higher elevations, and work in the Dawson area has shown that the warmest locations on an annual basis are at treeline due to cold air pooling in the valley floor during winter (Lewkowicz and Bonnaventure, 2011; Lewkowicz et al., 2012). Therefore, the possibility exists that certain parts of the landscape at Old Crow might not have permafrost.

Four air and ground temperature stations were set up along a transect from the airport (~255 m a.s.l.) up to the top of one of the local mountains (~745 m a.s.l.; Figure 36). The goal was to obtain data which could be used to model the change in ground temperatures with elevation. Unfortunately, the treeline station at 460 m a.s.l. was damaged by wildlife, but data are available from three other stations for September 2014 to September 2015. Air temperatures during this 12-month period were 1.5°C above average based on a comparison between measurements reported from the airport by Environment Canada and the Old Crow 1981-2010 normals (Environment Canada, 2014a). The late winter and spring of 2015 were particularly warm, with monthly temperatures at the airport for March, April and May averaging 2.9°C, 4.0°C and 6.0°C respectively, above the long-term mean. Similar results were obtained at the climate station at the lowest elevation. Previous work in southern Yukon has shown that surface lapse rates tend to change at treeline (Lewkowicz and Bonnaventure, 2011; Lewkowicz et al., 2012). Since data from the treeline station were not available, temperatures were projected to this elevation from the trends at the two lowest stations.

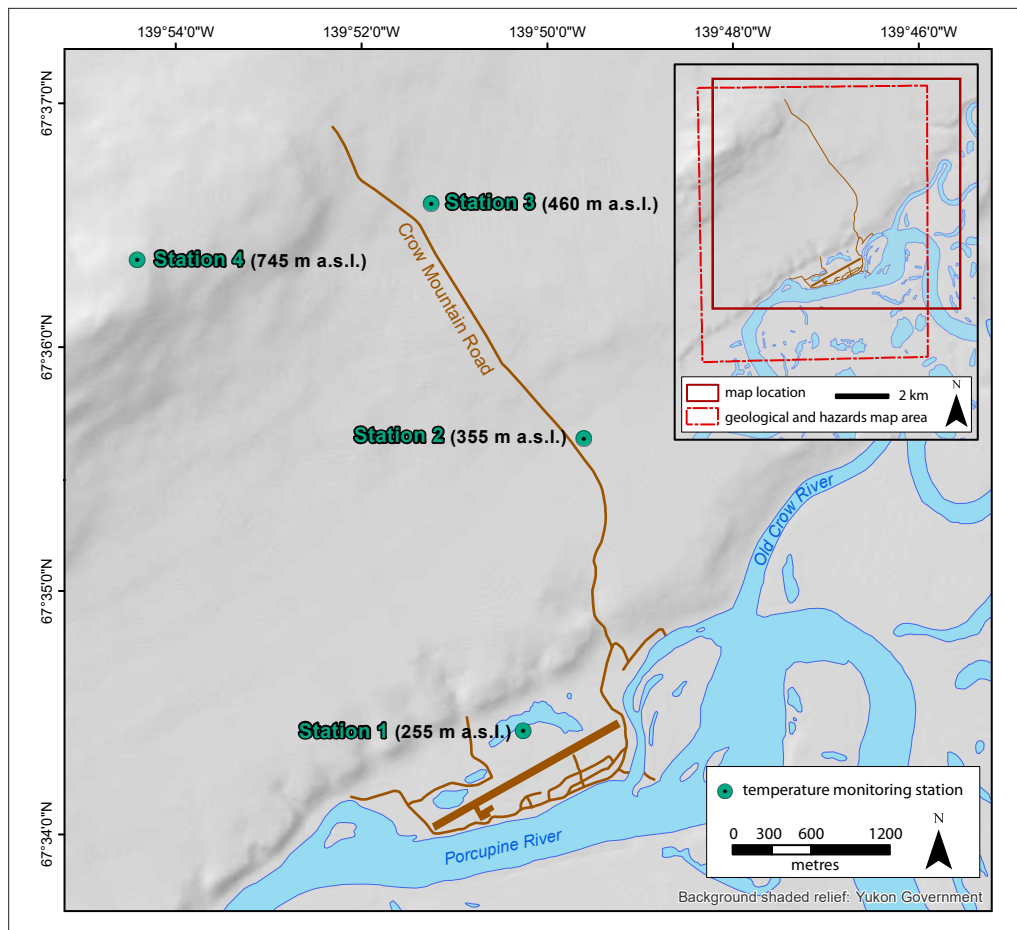


Figure 36. Location of four air and ground temperature monitoring stations installed to monitor ground temperature changes with elevation.

Monthly surface lapse rates were inverted (i.e., air temperatures became warmer with elevation) below treeline from November to May, while they were normal for the other five months (Figure 37). Above treeline, they were inverted for four months, from November to February. The results below treeline are similar to those obtained from the Dawson area except that the period of inverted lapse rates is two months longer at Old Crow. The results above treeline differ from those at Dawson where lapse rates are normal at higher elevations. For the month of January at Old Crow, the highest point was more than 10°C warmer than the community on the valley floor. On an annual basis in 2014-2015, air temperatures increased by an estimated 1.1°C from the valley floor to treeline, and then increased by a further 0.2°C to the highest station. Consequently, the highest measurement point was also the warmest location over the entire year.

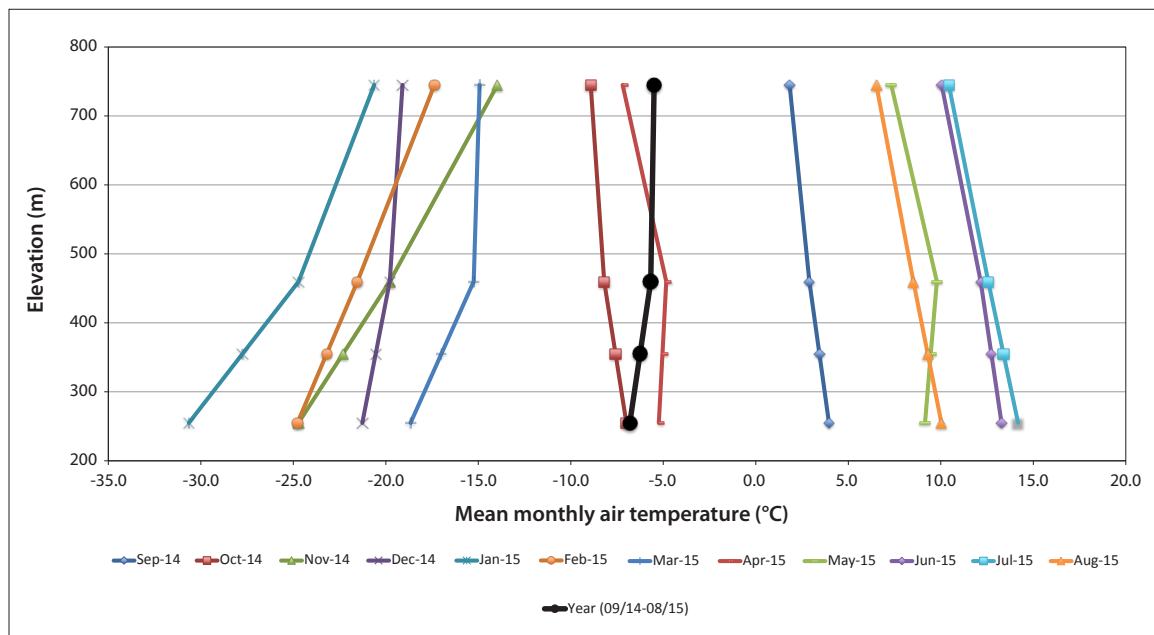


Figure 37. Monthly air temperatures measured in the Old Crow area at different elevations (2014-2015; see Figure 36 for locations). The surface lapse rate is normal if temperatures decrease with elevation (as during most of the summer) and inverted if temperatures increase with elevation (as during most of the winter). Note: values for the station at treeline (460 m a.s.l.) were estimated from the lapse rates at the two lower elevations.

Ground surface temperatures were also measured at the climate stations to determine the surface offset (the positive difference between the air and ground surface temperature; Table 2). Surface offsets are caused by shading of the ground by vegetation in summer (resulting in a cooler surface) and by insulation of the ground in winter due to the presence of snow (resulting in warmer ground surface temperatures). Surface offsets for 2014-2015 ranged from 4.7°C to 8.0°C (Table 2). Those for the two forested sites (at 255 m and 355 m a.s.l.) are larger than offsets recorded in southern Yukon and emphasize the importance of snow as an insulator in this part of the landscape. The result of these large offsets is that the stations at both 255 and 355 m a.s.l. recorded mean ground surface temperatures that exceeded 0°C for 2014-2015. If these temperatures were to persist, permafrost would be maintained at these sites only by the thermal offset (the negative change in temperature between the ground surface and the top of permafrost caused by the difference in thermal conductivities of the ground when thawed and frozen). Given that air temperatures were much higher than average in 2014-2015 and that the ERT profiles at these locations (Sites 10 and 17, described in “Case Study Sites” below) indicate permafrost that is at least 25 m thick,

it is probable that ground surface temperatures are typically below 0°C at this site, and unlike temperatures recorded during the monitoring period.

Table 2. Air and ground surface temperatures measured at Old Crow, September 2014 – August 2015.

| Site Elevation (m a.s.l.) | Mean Air Temperature (°C) | Mean Ground Surface Temperature (°C) | Surface Offset (°C) |
|---------------------------|---------------------------|--------------------------------------|---------------------|
| 255 | -6.8 | 0.9 | 7.7 |
| 355 | -6.3 | 1.7 | 8 |
| 745 | -5.5 | -0.8 | 4.7 |

Trends in permafrost temperatures with elevation can be estimated using the Temperature at the Top of Permafrost model (TTOP; Smith and Riseborough, 2002). The model calculates the temperature at the top of permafrost under equilibrium conditions using inputs of total freezing degree-days in the air, total thawing degree-days in the air, n-factors (ratios of air and ground surface temperatures), and the ratio of frozen and thawed thermal conductivities of the soil. See Appendix A for model details.

Results from TTOP modelling revealed positive mean ground surface temperatures through the forest and shrub zones, and negative values in the tundra zone (Table 3); the same pattern was measured in 2014-2015 (see Table 2). The shrub zone is defined as the area immediately above treeline to an elevation of 600 m a.s.l. and the tundra zone represents that area above the shrub zone. Modelled TTOP values range from -0.7°C to -2.4°C and the warmest part of the landscape occurs in the shrub zone above treeline, whereas the coldest temperatures were noted in the tundra zone. There is a step change predicted at the boundary between the two, resulting from a much lower nf (ratio of the ground surface freezing index to the air freezing index) for the tundra due to greater compaction of the snow and a thinner snowpack. Therefore, in spite of the fact that the uppermost climate station had the warmest mean annual air temperature (Table 2), its predicted TTOP value is much lower than those of the forested sites.

Table 3. Inputs and results of temperature at the top of permafrost (TTOP) modelling for Old Crow. See Appendix A (Approach and Methods) for unit definitions.

| Elevation (m a.s.l.) | TDD | FDD | Land Cover | Nt | Nf | Rk | MGST (°C) | TTOP (°C) |
|----------------------|--------|--------|------------|------|-----|------|-----------|-----------|
| 250 | 1330 | 4360 | forest | 0.8 | 0.2 | 0.85 | 0.53 | 0.09 |
| 300 | 1294.5 | 4227.5 | forest | 0.8 | 0.2 | 0.5 | 0.52 | -0.90 |
| 350 | 1259 | 4095 | forest | 0.8 | 0.2 | 0.5 | 0.52 | -0.86 |
| 400 | 1222 | 3955.5 | forest | 0.8 | 0.2 | 0.5 | 0.51 | -0.83 |
| 450 | 1185 | 3816 | forest | 0.8 | 0.2 | 0.5 | 0.51 | -0.79 |
| 500 | 1171.5 | 3702 | shrubs | 0.8 | 0.2 | 0.5 | 0.54 | -0.74 |
| 550 | 1158 | 3588 | shrubs | 0.8 | 0.2 | 0.5 | 0.57 | -0.70 |
| 600 | 1144.5 | 3474.5 | shrubs | 0.8 | 0.2 | 0.5 | 0.60 | -0.65 |
| 650 | 1131 | 3361 | tundra | 0.84 | 0.4 | 0.5 | -1.08 | -2.38 |
| 700 | 1117.5 | 3247 | tundra | 0.84 | 0.4 | 0.5 | -0.99 | -2.27 |
| 750 | 1104 | 3133 | tundra | 0.84 | 0.4 | 0.5 | -0.89 | -2.16 |

POTENTIAL HAZARD RISKS FOR THE OLD CROW REGION

SEISMICITY

The seismic hazard in the Old Crow area is considered low to moderate (Figure 38) and minor earthquakes do occasionally occur. Thirty earthquakes have been recorded within 100 km of Old Crow since 1985 (Natural Resources Canada, 2016), and of these, the largest was magnitude 3.9 (Figure 39). While the town is situated close to a number of large faults, they have probably not been active since the early Paleogene, over 50 million years ago. Numerous other, unmapped, inactive faults are associated with mapped faults and present a similarly small risk of earthquakes, surface ruptures, and landslides in the study area.

If a large earthquake were to occur in the Old Crow region, materials most likely to generate subsequent landslides include poorly consolidated materials on the steep slopes of the escarpment, and any recently thawed portions of ice-rich lacustrine, colluvial, and organic materials.

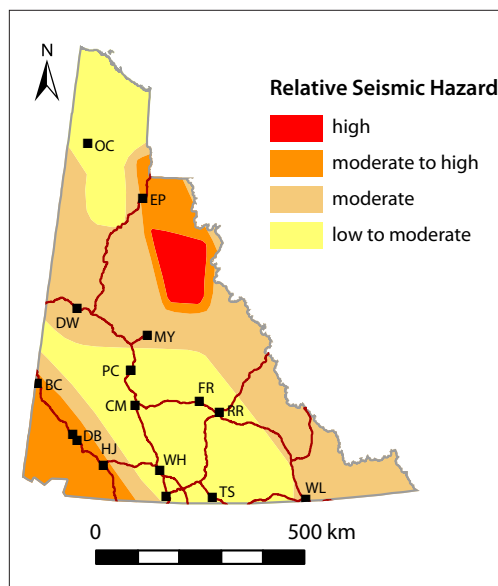


Figure 38. Simplified version of the National Building Code of Canada's 2010 seismic hazard map (for spectral acceleration at a 0.2 second period (5 cycles per second)), showing the relative likelihood of experiencing earthquakes strong enough to potentially damage some, but not all, single family (one- and two-storey) dwellings (Natural Resources Canada, 2010). Old Crow (OC) is located in the low to moderate hazard zone, where there is a less than 1% chance that significant damage will occur every 50 years.

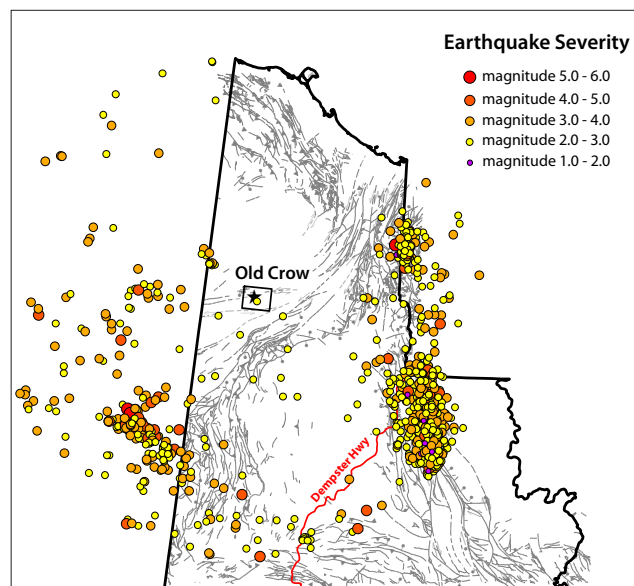


Figure 39. Recorded earthquakes from 1985 to 2016 within 250 km of the study area. Grey lines are mapped bedrock faults. All earthquakes within 100 km of Old Crow are of magnitude 4.0 or less.

MASS WASTING

Mass wasting (the downslope movement of surficial materials and/or bedrock fragments, often mixed with vegetative debris) may be restricted to very shallow surface layers, or may be deep seated and extend into thick sediments or bedrock. Mass wasting events may be rapid, occurring

in seconds to minutes, or gradually creep or rotate over years to centuries. Depending on slope geometry and sediment water content, debris may free fall, slide, rotate and/or flow. Mass wasting processes in the study area are primarily related to permafrost thaw.

LANDSLIDES

Landslides generally occur on moderate to steep slopes due to a variety of contributing and triggering factors that include: intense rainfall or snowmelt events, permafrost degradation, forest fires, river erosion, groundwater flow, earthquakes, and/or human modifications to the landscape. In many cases, several of these contributing and triggering factors act in combination.

Landslides in the Old Crow map area have been mapped through observations of mass movement on the ground (i.e., slumped material, landslide debris, tension cracks, split trees, and stretched roots; Figure 40); from historic and modern imagery of the map area (i.e., aerial photographs and satellite images); and from digital elevation models of the earth's surface. The bulk of detailed mapping was made possible by the acquisition of a one-metre or better resolution elevation surface created with a LiDAR dataset collected in 2014. The resolution of the LiDAR dataset is significantly better than other digital images and the 'bare-earth' processing (vegetation removed digitally) reveals features that are indistinguishable on the highest resolution air photos and satellite images (Figure 41).

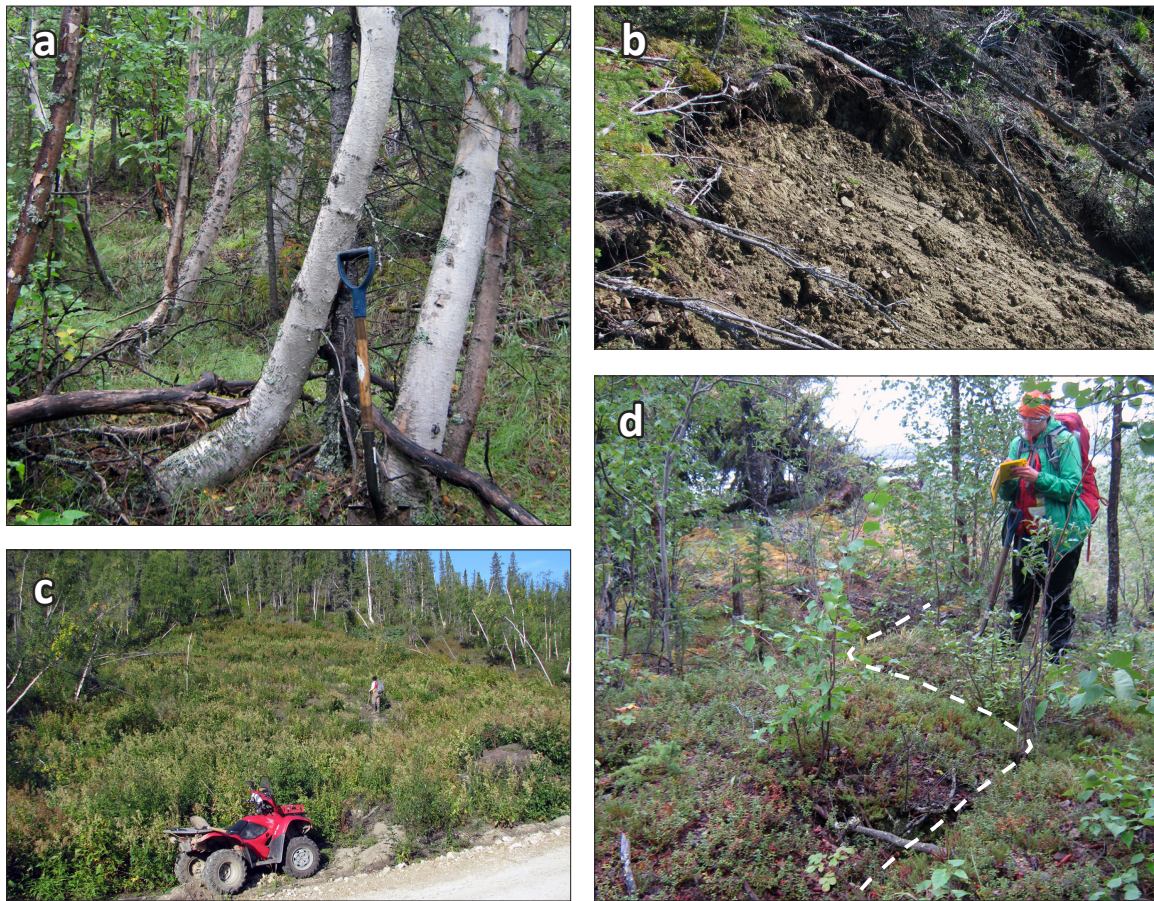


Figure 40. Examples of features that are used to map landslides and mass wasting in the study area: (a) 'trees with knees' are evidence of slow slope movement; (b) slickened surfaces and stretched roots show evidence of sliding over what was likely a frozen surface; (c) colonizing vegetation on a slope four years after an active layer detachment slide occurred; and (d) a tension crack near the top of the escarpment above town.

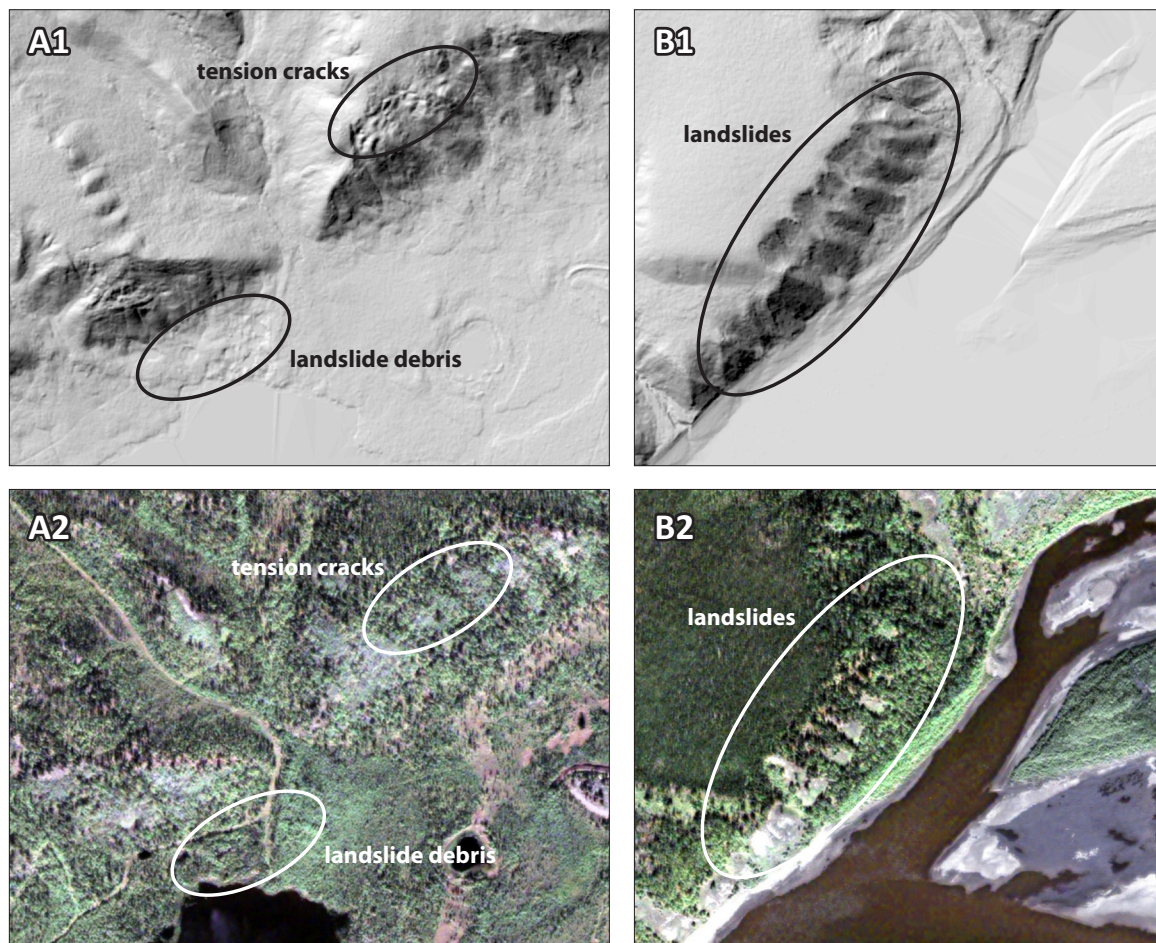


Figure 41. Hillshade images created from LiDAR data (**A1** and **B1**) show considerably more detail than high resolution satellite images (**A2** and **B2**) of the same landscape. Mass wasting features are circled on both images to show the difference in resolution with the vegetation removed from the LiDAR image.

More than 100 landslide head scarp features were mapped across the ~6 km-long escarpment above Old Crow (Figure 42). These features represent both ancient and recent mass wasting events. Landslides occur on all aspects and on both shallow and steep slopes. Mounded colluvial material at the base of the escarpment is interpreted to be landslide debris, but individual landslide deposits and paths are difficult to distinguish once they become vegetated. Some landslide features are muted, indicating they may have been caused by valley incision early in the Pleistocene and are largely relict features. Other landslide deposits are fresh looking, with clear run-out paths and debris deposits, and are known to have occurred recently. Landslide debris in the study area typically travels ~50-100 m downslope of the head scarp, but larger slides have run outs as far as 200 m from the head scarp. Landslide deposits make up 1% of the total map area (cross-hatched pattern on Figure 42), and the area at risk for landsliding accounts for ~14% of the total map area (stippled pattern on Figure 42).

DEBRIS FALLS

Landslides initiated above ~300 m a.s.l. have crescent-shaped head scarps and small debris cones close to the base of the slope (see B1 on Figure 41). These landslides are interpreted as debris falls and are relatively small and active features that release material as permafrost melts in the exposed face of the slope. Debris-fall landslides also occur where slopes are being undercut by

river erosion, by mass wasting in lower stratigraphic units, or by other natural and anthropogenic modifications that remove material from the base of the slope. Debris-fall landslides are interpreted to occur in permafrost-affected fluvial and colluvial materials, and as such, are sensitive to climatic factors such as heat and precipitation which diminish permafrost and may contribute to instability on these slopes.

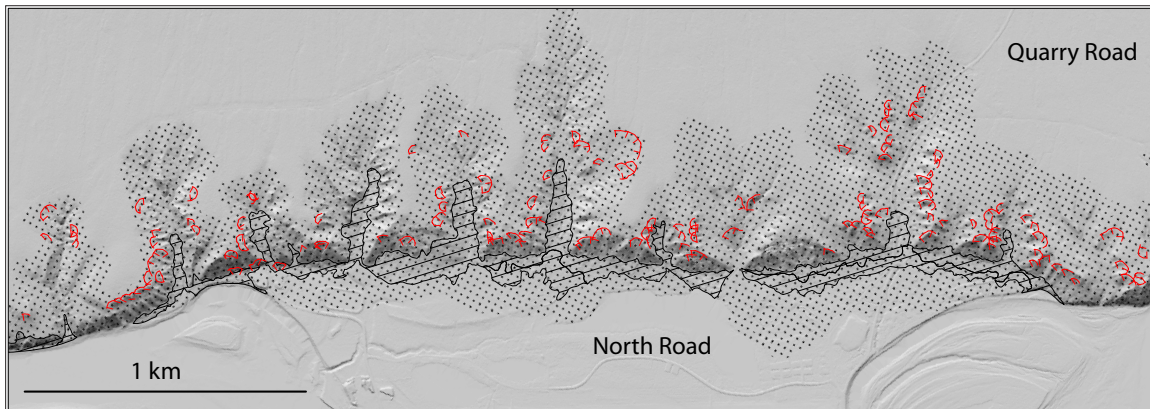


Figure 42. Distribution of landslide head scarps and landslide terrain in the map area. Red lines are mapped landslide head scarps. Cross-hatched pattern is the mapped distribution of landslide deposits. Stippled pattern indicates area affected by landsliding. Berry Hill is toward the top of the image and the Porcupine River is toward the bottom.

ACTIVE LAYER DETACHMENT

Landslides initiated below ~280 m a.s.l. are characterized by shallow translational slides, also known as active layer detachment or thaw-flow slides. These slides are characteristic of a type of fast periglacial mass wasting that occurs where the thawed or thawing portion of the active layer detaches from the underlying frozen material and moves downslope through sliding and sometimes flowing of the thawed debris. Events that cause rapid thickening of the active layer combined with high porewater pressure, such as forest fires and hot and/or wet weather, commonly trigger active-layer detachments (Lewkowicz, 1992; Lewkowicz and Harris, 2005). These landslides are likely to have head scarps characterized by linear cracks which may propagate into undisturbed materials upslope of the head scarp (i.e., tension cracks; see A1 on Figure 41). Active layer detachment slides occur when sufficient water collects at the base of the active layer to allow overlying saturated sediments to slide on a thin layer of water, ice and/or mud (Lewkowicz, 2007). As a result, these thaw detachments are most common in fine-grained soils on slopes underlain by ice-rich permafrost and in association with areas of surface water convergence such as water tracks (Kokelj and Joergenson, 2013).

Figure 43 shows stratigraphic controls on landslide generation in the study area. Neogene and older lacustrine sediments (zCLb>Q) are susceptible to thaw-detachment slides because they are fine grained (primarily silt), ice rich, and are covered in blankets of silty colluvium that can become mobilized when saturated. Ice lenses at the base of the active layer are common in this unit, and when this layer thaws rapidly it can release water into already wet soils and trigger sliding in the thawed part of the slope (Lewkowicz, 2007). Alternatively, overlying sand (sFb), gravel (sgFb), and diamict (dzCpbv) materials are more likely to be affected by debris fall mass wasting because they maintain steeper slopes, are well drained, and are less ice rich than lacustrine units. Surface water from Berry Hill drains easily through the thawed components of high-level sand and gravel deposits before saturating the poorly drained active layer soils of the lacustrine and colluvial deposits on

the lower slopes of the escarpment. Additional water added to these materials through heavy rain, or thawing of ice lenses at the base of the active layer, can cause rapid increases in pore water pressure that triggers detachment slides.

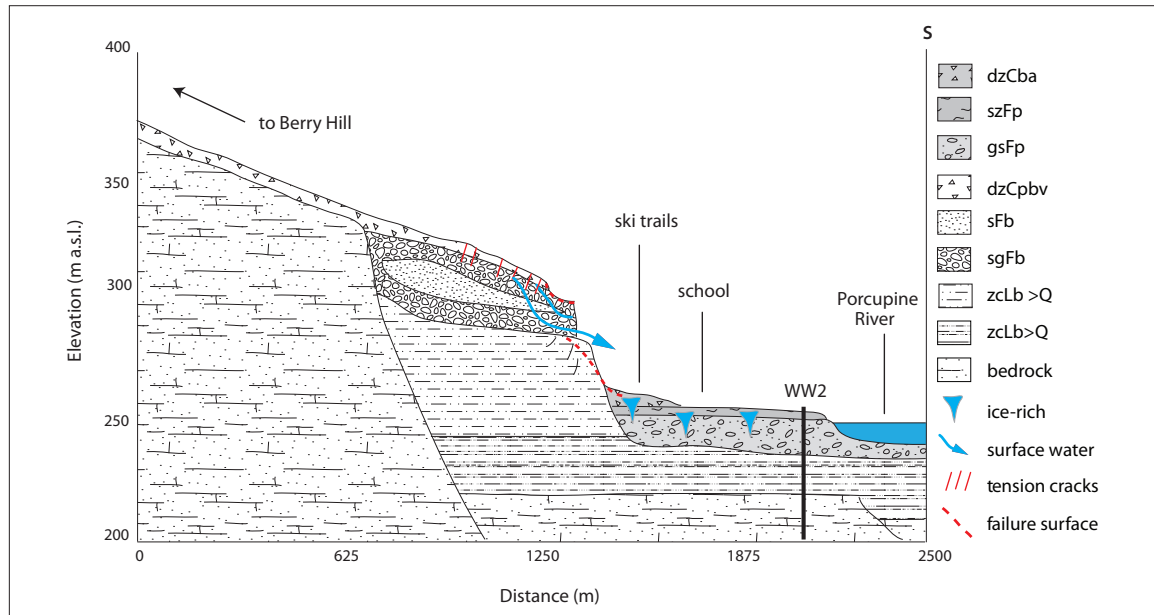


Figure 43. Idealized cross-valley profile of the map area with unit textures and landform descriptions. Landslide mechanisms are controlled by the vertical distribution of surficial materials on the escarpment behind town.

In August 2010, heavy rainfall triggered seven landslides in the community of Old Crow. Preliminary investigations found that saturated soils following a period of unusually high precipitation levels were the likely cause of the landslides (EBA, 2012). Of the seven landslides documented that year, three impacted infrastructure in the community. An active layer detachment slide beside the Quarry Road (see Figure 40c) deposited debris on the road, and within a day, two slides with combined run out paths deposited debris within 40 m of a residence (known as Rosalie’s Slide; Figure 44; EBA, 2012). The four remaining slides occurred in undeveloped parts of the community and their impact was limited to small trails. Two of the slides in the undeveloped part of the community were still active in 2015, but all the remaining slides that occurred in 2010 have since stabilized.



Figure 44. A photo taken in 2015 of bright green colonizing vegetation covering the surface of the active layer detachment slide called “Rosalie’s Slide” that occurred in August 2010.

While the Quarry Road slide occurred in a visible location and impacted a major piece of community infrastructure, it was a relatively small size with limited run out (less than 60 m). In comparison, Rosalie's slide travelled more than 200 m from the highest head scarp and almost certainly incorporated large volumes of downslope materials. This entrainment of saturated downslope material is common in active layer detachment slides, and enables large amounts of material to be mobilized even on very gentle slopes (Lewkowicz, 2007).

SLOW PERIGLACIAL WASTING

Periglacial wasting is a general term that describes cold-climate colluvial processes that are mediated by freeze-thaw and permafrost conditions (French, 1983). Periglacial wasting includes both slow processes such as solifluction, slopewash, solution, nivation, and rapid processes such as active layer detachments (described in previous section). Slopewash (modifier “-Xs” on accompanying map), and to a lesser degree solifluction, operate on upland slopes in the study area and contribute to downslope colluvial processes.

Solifluction, the slow downslope movement of saturated sediments, can be identified by distinctive slope morphology of lobes and terraces on moderate slopes, but can also occur in broad sheets on low angle slopes (French, 1983). Slopewash (also known as sheetwash), is difficult to quantify, but is a significant modifier of the landscape in the map area, particularly on the pediment slope below Berry Hill. Slopewash is characterized by unconcentrated surface wash where particles are carried downslope in an overland flow and deposited as fine unconsolidated sediment, typically at the foot of slopes as the result of the continual percolation of water downslope (French, 1983). While unlikely to cause catastrophic events, slow periglacial wasting can be a significant hazard to infrastructure built upon, or at the base of, landforms that are experiencing gradual downslope movement.

Examples of slow periglacial processes in the map area include the ‘trees with knees’ pictured in Figure 40a, and abundant tension cracks, hillslope terraces and slumps that are all evidence of the slow downward movement of the escarpment slope. It is unclear how slow periglacial processes contribute to rapid mass wasting processes, but evidence of slow slope movement may be a sign of increasing slope instability leading to larger mass wasting events.

FLOODING

There is a history of spring flooding in the Old Crow area, as outlined in “*Regional Hydrology*” (p. 13), and flooding continues to pose a hazard risk to the community. As part of a complementary Indigenous and Northern Affairs Canada-funded project in Yukon communities (http://northernadaptation.ca/sites/default/files/flood_risk_mapping.pdf), LIDAR (light imaging and ranging) imagery was captured along a swath of the Porcupine River in the vicinity of Old Crow in the summer of 2014. With this data, a high-resolution digital elevation model (DEM) of the image area was created by Yukon Government (horizontal accuracy = 50 cm, vertical accuracy = 10 cm).

Based on this DEM, project researchers developed modelled flood risk maps for the image area that depict potential flood extents based on increases in water level of the Porcupine River, simulating floods of different elevations. The models are simplistic and do not integrate hydraulic gradient, the role of secondary input sources to the Porcupine River (e.g., local creeks), or upstream or downstream propagation of flood events over time. However, given that the notable floods in the Old Crow region have been caused by ice jam events upstream of the townsite, the model is still informative, and may support planning for climate change adaptation in the context of changing hydrology.

It is important to note that any elevations within the LIDAR imagery area that fall within the elevation of each flood extent are depicted as being under water, even if they cannot be reached by floodwaters. In other words, areas behind elevated roads that may impede flood propagation are shown as being flooded, regardless of the fact that an elevated roadway may prevent water movement during a flood and prevent lower-lying areas from becoming flooded. However, the modelled flood extents are still significant, because they indicate areas that may be susceptible to flooding under substantial river level increases, or if breaches in barriers were to occur.

To examine flood risk regionally, a composite of several water level stages is presented in Figure 45. This figure illustrates the extent of flooding under water level scenarios between 241 and 246 m. It is important to note that there is some discrepancy between observed flood levels measured relative to an existing datum and the elevations measured during the LIDAR surveys. Observed minor flood levels in the Old Crow region are measured (relative to a datum) at approximately 246.4 m (R. Janowicz, pers. comm.), while LIDAR imagery shows substantial flooding of the townsite at this stage. Further surveying is required to reconcile this difference, but patterns of flooding depicted by the LIDAR imagery are nonetheless informative in the context of risk assessment.

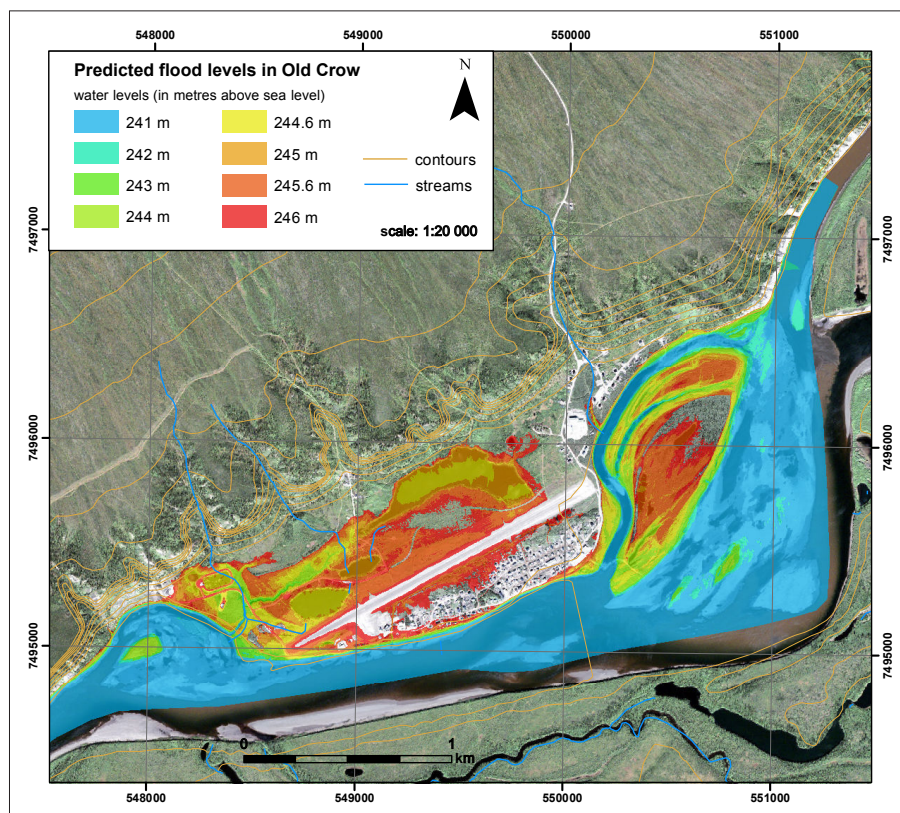


Figure 45. Modelled flood extents for the Old Crow region illustrating river levels between 241 and 246 m. Note that elevated roads and drainage ditches are not included as barriers to flooding. Model results are based on LIDAR imagery provided by the Government of Yukon.

Generally, low-water levels are present across the area of imagery between 238 and 240.5 m (not shown on Figure 45). Below 243 m, river levels remain primarily confined to normal stream channels, although by 243 m, many sand bars and small islands have been submerged. At 244 m,

the river is still primarily confined to the stream channel, although a few low-lying areas along the river's edge experience moderate water incursion, as do areas around the island at the confluence of the Old Crow and Porcupine rivers. With continued water level increases, flooding begins to leave channels and undeveloped low-lying areas, and may begin to impact infrastructure.

The area around the lagoon, at the west end of the community, is the first to be affected by modelled water level increases, as it is the most low-lying area of the community (Figure 46). Based on the LIDAR imagery, normal water levels on the Porcupine River in the vicinity of the lagoon are between 239 and 240 m. Between 241 and 243 m, rising water is contained in the main river channel, although some water begins to back up a gulch for a distance of about 250 m, towards the south end of the lagoon. At 244 m, water has pooled south of the road to the lagoon. Figure 46 shows water pooling on the northeast side of the road as well, although the road may act as a barrier to water movement. At 244.8 m, a 20-m segment of road at the west end of the runway is breached, causing flooding to extend along the north side of the runway. The lagoon itself is protected from flooding by the road and the berm surrounding it, and will not flood at this stage unless the berm is breached.

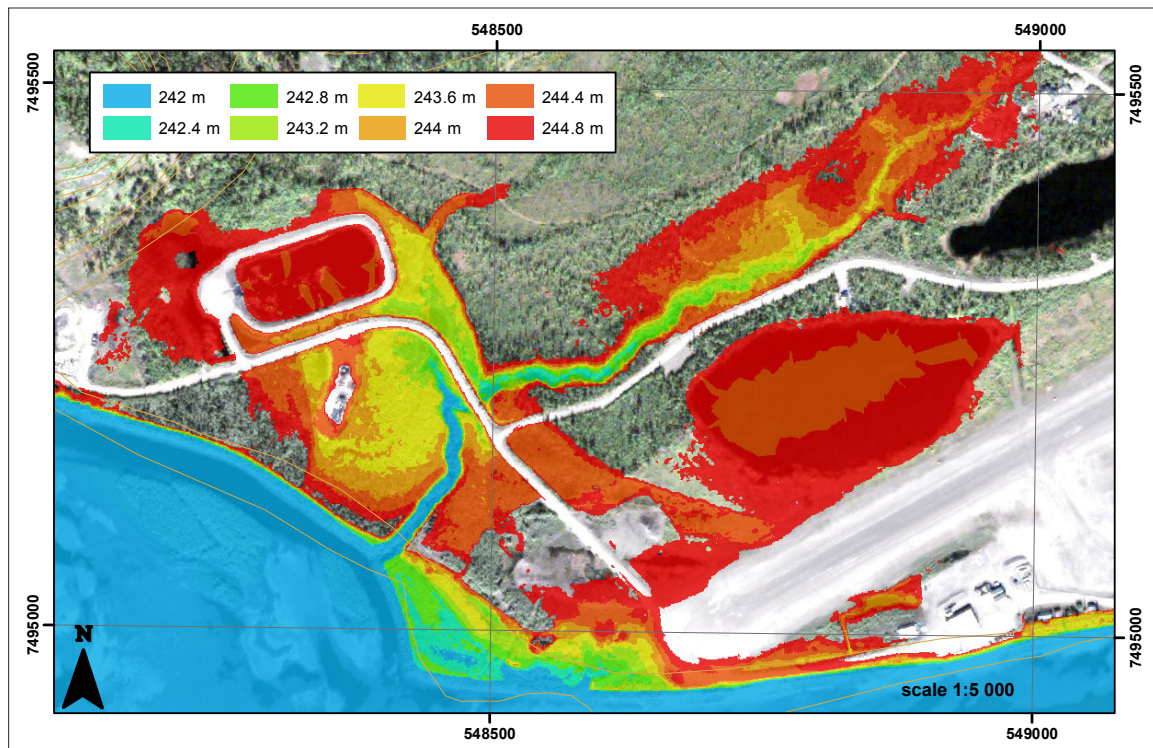


Figure 46. Close-up of modelled flood extents in the vicinity of the lagoon illustrating river levels between 242 and 244.8 m. Note that elevated roads and drainage ditches are not included as barriers to flooding. Model results are based on LIDAR imagery provided by the Government of Yukon.

In the core area of the community, flooding is minimal at all modelled stages (Figure 47). Based on the LIDAR imagery, the low-water level near the boat launch is approximately 238.5 to 239 m, while the top of the bank is 246 m. As a result, the river would have to rise approximately 7 m to overtop the bank along most of the developed portion of town. Modelling shows high water beginning to approach in the vicinity of the Northern Store at 244.8 m, although the road will act as a barrier to water movement at this stage.

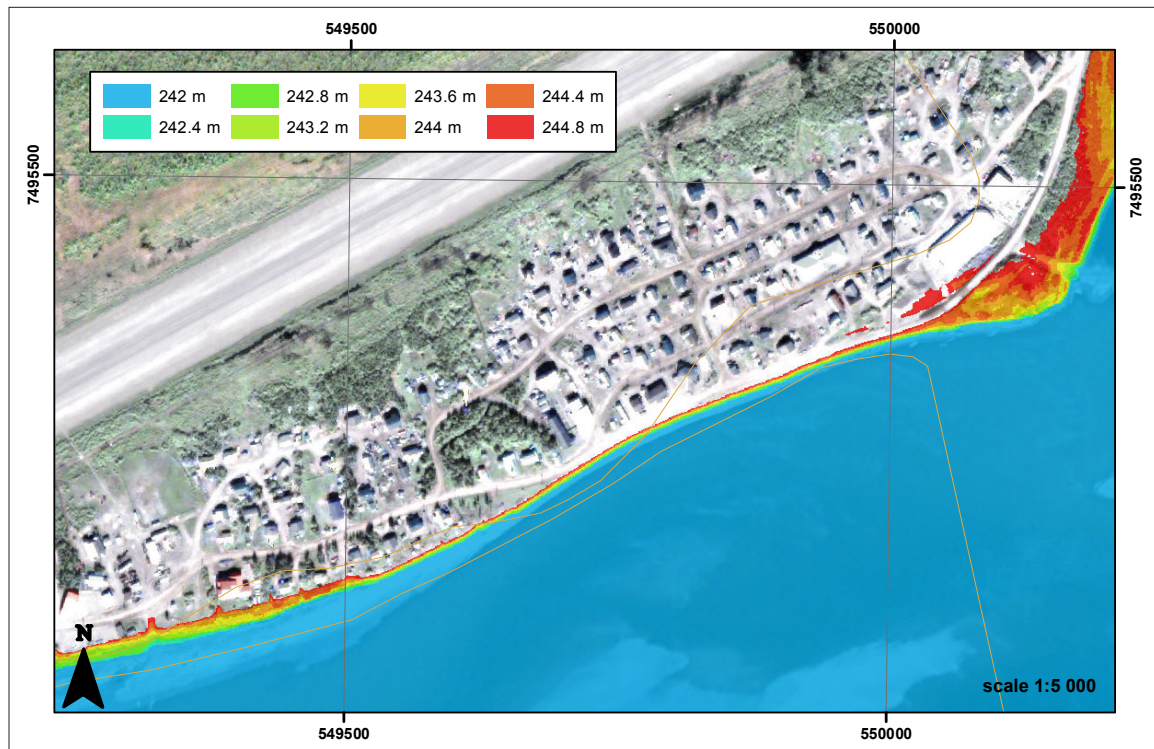


Figure 47. Close-up of modelled flood extents in the town core illustrating river levels between 242 and 244.8 m. Note that elevated roads and drainage ditches are not included as barriers to flooding. Model results are based on LIDAR imagery provided by the Government of Yukon.

As with the community core, the area around the school is also out of reach of modelled high-water events (Figure 48). The school itself is situated at 248 m of elevation (based on the LIDAR imagery), approximately 8 m above low-water levels for the Porcupine River. Water levels up to 245 m are contained within a small gulch east of the school, and flood risk to the school is non-existent.

High-water levels can impact the island located at the confluence of the Porcupine and Old Crow rivers (Figure 49). In this area, normal low-water levels appear to be between 241 and 243 m, and the main channel is approximately 100 m wide. At 243 m, the river level is high, but remains contained within the river channel. At 244 m, the island shoreline begins to flood, and an incursion of floodwater inland begins to appear. At 245 m, over 50% of the island is flooded and the main channel width has increased to approximately 200 m.

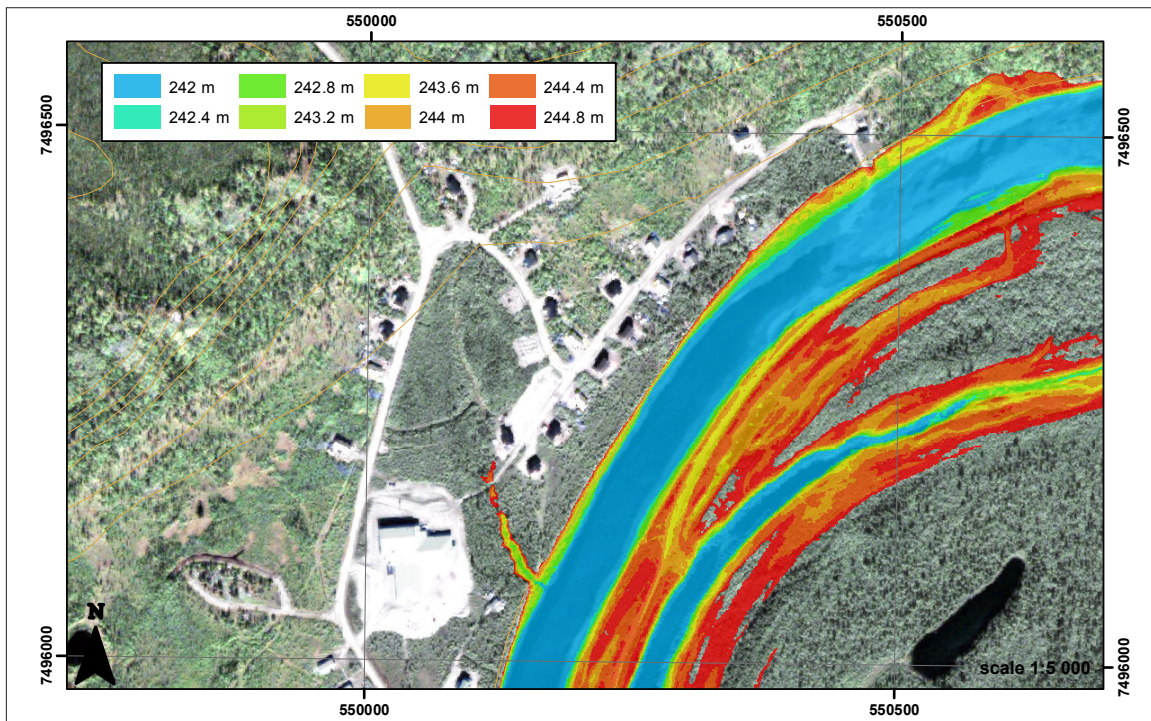


Figure 48. Close-up of modelled flood extents in the vicinity of Chief Zzeh Gittlit School illustrating river levels between 242 and 244.8 m. Note that elevated roads and drainage ditches are not included as barriers to flooding. Model results are based on LIDAR imagery provided by the Government of Yukon.

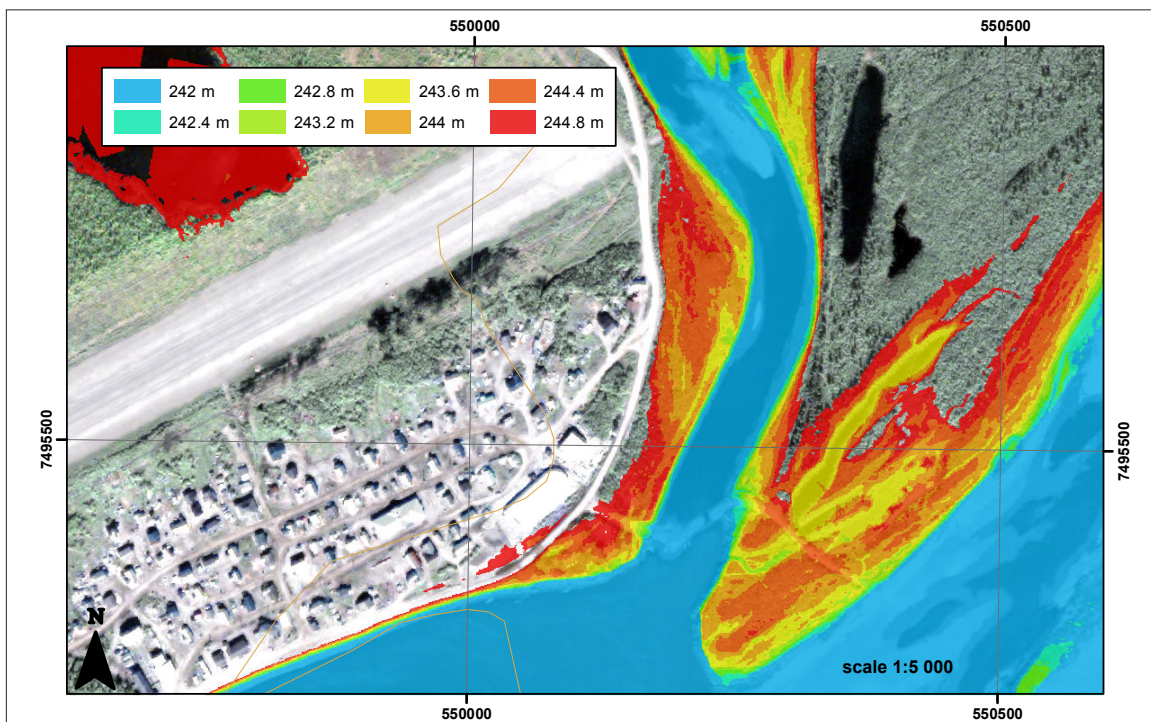


Figure 49. Close-up of modelled flood extents in the vicinity of the island at the confluence of the Porcupine and Old Crow rivers, illustrating river levels between 242 and 244.8 m. Note that elevated roads and drainage ditches are not included as barriers to flooding. Model results are based on LIDAR imagery provided by the Government of Yukon.

PERMAFROST

Hazards related to permafrost have the potential to impact several elements such as ground stability, hydrology, and infrastructure integrity. The following section provides a general description of permafrost structure and characteristics, in order to present a more comprehensive picture of the risks associated with permafrost thaw.

PERMAFROST DEVELOPMENT

In permafrost regions, the distribution of ice in surface materials or soil (i.e., cryostratigraphy) is related to the manner in which permafrost has aggraded and degraded through time. The understanding of permafrost genesis at a given site is important because permafrost structure and composition is directly related to the type of permafrost development and the distribution of ground ice. Permafrost genesis can be divided into five main types: epigenetic, syngenetic, quasi-syngenetic, para-syngenetic and polygenetic (French and Shur, 2010; O'Donnell et al., 2012). Epigenetic permafrost forms in bedrock and sediments following deposition. The ice content of epigenetic permafrost usually increases with depth, and the sediment layers in between ice features are usually ice poor and over consolidated or stiff (Stephani et al., 2010). The syngenetic growth of permafrost occurs when material is deposited at the surface while freezing is in progress. Thus, the permafrost is approximately the same age as the sediment in which it is found. The ice content of syngenetic permafrost is more likely to be uniform and ice rich throughout the soil column (Fortier and Allard, 2004; Kanevskiy et al., 2011). Quasi-syngenetic permafrost forms when the permafrost table shifts upward in response to vegetation growth at the surface, leading to the formation of an intermediate, ice-rich layer at depth. Para-syngenetic permafrost is defined by multidirectional refreezing of a talik zone (e.g., those areas of unfrozen ground under drained lakes) or a subsurface cavity. The ice content of para-syngenetic permafrost relates to the degree of saturation of the material prior to refreezing. If the permafrost has more than one origin it can be defined as polygenetic (Lunardini, 1994; French and Shur, 2010).

GEOTECHNICAL PROPERTIES

The cryostratigraphy and geotechnical properties of the ground are important characteristics as they influence permafrost dynamics and the thermal and mechanical sensitivity of frozen ground. Cryostratigraphy is defined as the study of frozen layers in the Earth's crust and is used to reconstruct the deposition history of a given site, define the type of permafrost present, determine how ice developed, and how the ice is distributed within the permafrost. It is useful to predict the rheology (rate and type of deformation) of surface and sub-surface materials in the context of permafrost thaw (French and Shur, 2010). Cryostratigraphy is defined by cryofacies (e.g., ice-rich or ice-poor sediments), which are characterized by typical cryostructures.

Cryostructures are determined by the amount and distribution of ice within the pore structure, and by ice in excess of the porosity (e.g., lenses, layers of segregated ice; French and Shur, 2010). Table 4 presents typical cryostructures that may be observed in permafrost. Layered, lenticular, and microlenticular cryostructures are present in ice-rich permafrost. They are the result of ice segregation in the sediment and are typical of fine-grained syngenetic permafrost. When permafrost thaws, the water from the melting of excess ice is drained, leading to settlement of the ground. Porous visible and porous invisible cryostructures are ice poor and result from in-situ freezing of water trapped in the soil pores with little to no migration of water to the freezing front (cryosuction) within the freezing soil. These types of cryostructures are common in coarse-grained sediments, but can also develop in fine-grained sediments that were originally ice rich, thawed, drained, and subsequently refrozen (Stephani et al., 2010). Because there is no excess ice present, no significant subsidence of the ground is expected upon thawing (Stephani et al., 2014).

Table 4. Cryostructure classification, from Stephani et al. (2014) and based on Murton and French (1994).


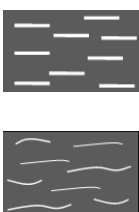







| Name | Equivalent | Description | Sediment type | Illustration* |
|-----------------------------|---|--|--|--|
| Lenticular | Lenticular ¹ | <ul style="list-style-type: none"> • lens-shaped ice in sediment • generally continuously shaped • generally horizontal (parallel to freezing front) • may be straight, wavy, inclined, interlaced • may contain air bubbles • thickness: ≥ 1 mm: <i>Syngenetic permafrost: mm to cm thick</i> <i>Epigenetic permafrost: cm to dm thick</i> <ul style="list-style-type: none"> • usually ice-rich sediment | silt to fine sand; silty clay | <p>see Fig. 3.1A</p>  |
| Microlenticular | Lenticular ^{1,2} | <ul style="list-style-type: none"> • lens-shaped ice in sediment • generally discontinuously shaped • generally horizontal (parallel to freezing front) • may be straight, wavy, inclined, interlaced • very few air bubbles • thickness: < 1 mm • usually ice-rich sediment: <i>Syngenetic permafrost: >50% by volume</i> <i>Epigenetic permafrost: 30-50% by volume</i> | silt to fine sand; peat | <p>see Fig. 3.1A</p>  |
| Layered/belt-like structure | Layered ¹ | <ul style="list-style-type: none"> • assemblage of lenticular cryostructures • thickness: centimetre to decimetre • usually ice-rich sediment | silt to fine sand; peat | <p>see Fig. 3.1C</p>  |
| Ice veins | | <ul style="list-style-type: none"> • ice-filled crack or fissure in sediment • thickness variable (millimetre to centimetre) <i>Frost crack: 1-5 mm thick</i> <i>Dilation/extension cracks: cm to dm thick</i> | all types |  |
| Reticulate | Reticulate ^{1,2} | <ul style="list-style-type: none"> • net-like cryostructure of interconnected sub-horizontal ice lenses and sub-vertical ice veins • usually ice-rich to very ice-rich sediment (~35-95% by volume) | silt to fine sand | <p>see Fig. 3.1F</p>  |
| Suspended | Suspended ¹ ; Ataxitic ² | <ul style="list-style-type: none"> • suspended aggregates in ice • usually very ice-rich sediment (up to 90-95% by volume) • common in upper part of permafrost | silt to fine sand; occasionally peat; silty clay | <p>see Fig. 3.1E</p>  |

Table 4, continued. Cryostructure classification, from Stephani et al. (2014) and based on Murton and French (1994).

| Name | Equivalent | Description | Sediment type | Illustration* |
|------------------|---|--|-------------------------------------|--|
| Crustal | Crustal ^{1,2} | <ul style="list-style-type: none"> • ice-coating around rock fragments, aggregates or wood fragments • usually partial coating, occasionally total • common just beneath permafrost table • thickness: few millimetres to centimetre-thick coating | gravel/rock fragments; diamicton | <p>see Fig. 3.1D</p>  |
| Porous visible | Ice cement ¹ ; Massive ² | <ul style="list-style-type: none"> • pore ice that is visible to the unaided eye • usually ice-poor sediment (<30% by volume) | gravel/rock fragments; diamicton | <p>see Fig. 3.1F</p>  |
| Porous invisible | Ice cement ¹ ; Massive ² | <ul style="list-style-type: none"> • pore ice not visible to the unaided eye • usually very ice-poor sediment (<10-30% by volume) | all types | <p>see Fig. 3.1F</p>  |

*Illustrations modified from Murton and French, 1994

¹ Murton and French (1994); ² Kudryavtsev (1979)

Legend: grey = sediment; dark grey = aggregate or wood fragments; white = ice.

Generally, dry or unsaturated frozen materials or soils do not present a high risk upon thawing, as the water will remain in the soil porosity or will drain away. In contrast, when a saturated soil thaws, it presents a much higher risk of settlement, mass movement, or ponding in response to poor drainage. Hazards related to the thawing of ice-rich materials or soils is affected by factors such as stratigraphy and the grain size distribution of the stratigraphic layers, as well as external factors such as slope, surface roughness, and vegetation (Stephani et al., 2014).

For thaw-settlement hazard assessments, cryostratigraphy is used to locate ice-rich and ice-poor layers, and determine the geometry and distribution of massive ice (e.g., patterns of ice wedges). Generally speaking, the presence of ice-rich deposits raises concern in terms of hazard potential. Where ice-rich deposits overlie ice-poor layers, the thaw-settlement hazard is high in the short term, and the rate of change is fast. Conversely, when ice-poor deposits overlie ice-rich sediment, the thawing of the upper layer is rapid but with minimal thaw settlement and will be followed by the slow, but constant thawing of the underlying ice-rich layer resulting in differential thaw settlement.

The grain size distribution of sediments determines the porosity and hydraulic conductivity of the ground. Coarse material (medium sand and coarser) has a high hydraulic conductivity and readily drains water as ice melts, whereas fine-grained material drains poorly once it thaws due to its low hydraulic conductivity. Furthermore, fine-grained sediments often contain excess ice (i.e., the volume of ice in excess of the total pore volume of the ground when unfrozen) and may form ice lenses or layers by ice segregation. On flat terrain, ground with excess ice will undergo severe thaw settlement; likewise, on slopes, silt and clay deposits may experience mass movement when the pore water pressure created by melting ice is high. For slope deposits, the plastic and liquid limits of the material are used to evaluate the potential of ground failure.

PERMAFROST AS A HAZARD RISK

The ground thermal regime of permafrost is influenced by climate, surface conditions, and the complex interactions of geophysical factors such as hydrography, topography, vegetation, soil texture and ground-ice content (Jorgensen and Osterkamp, 2005). As a result, variations in climate or terrain conditions (e.g., environmental changes or human interventions) can both have a great impact on permafrost stability. Higher surface temperatures, variation in snow cover depth, active-layer hydrology variations, infrastructure, and fire disturbances are good examples of changes that can play, at various scales, a major role in permafrost degradation (Stephani et al., 2014). Additionally, since it is closely linked to local factors, permafrost response to environmental change can be spatially and temporally heterogeneous and can respond differently to geomorphological processes due to different terrain conditions. Therefore, permafrost landscapes will have a dynamic response to environmental change and must be considered holistically, at diverse spatio-temporal scales.

Because permafrost stability is essentially maintained by the bonding between ice and the ground particles, when ice melts, cohesion is lost and soil stability is diminished (French, 2007). Following an increase in air temperature, the active layer is expected to deepen as the ice contained in the upper part of the permafrost (right below the bottom of the active layer) melts. If the volumetric water content of the ground is lower than the volume of soil pores, the ground is not saturated. Thawing of this type of ice-poor soil results in moderate surface settlement and is essentially due to the loss of volume upon ground ice melting and subsequent soil consolidation. If the volumetric water content of the ground is equal to, or slightly above the volume of soil pores when unfrozen, the soil is saturated. Thawing of this type of ice-rich soil results in poorly drained surface conditions, and the soil will be unable to consolidate due to the high pore-water pressure. If the volumetric water content of the ground is higher than the volume of soil pores, the ground is 'super-saturated' and contains excess ice in its frozen state. Thawing of this type of ground results in severe surface settlement, and is essentially due to the loss of volume upon ground ice melting and soil drainage (Nelson et al., 2002). In gently sloping areas, water ponding is frequent; on steep slopes, the release of water builds excess pore water pressure in the soil pores, which is conducive to rapid mass movements (e.g., slides, slumps and debris flows). When the material is coarse-grained, soil water is drained according to the hydraulic conductivity of the material and there is minimal settling or movement of the sediment. When the material is fine-grained, the drainage is slow and pore water pressure may trigger slow mass movement (e.g., solifluction). Depending on the nature of the soil material and the amount of ground ice present, significant hazards may develop. Permafrost-related hazards represent some of the principal challenges for planning and development in northern environments.

To assess permafrost stability for land planning purposes, an estimation of the maximum thaw depth that could be reached under changing climatic conditions is essential, mainly to evaluate the potential deformation that the soil may undergo in the future (Instanes, 2003). The rate and type of deformation is closely linked to the type of surficial deposits, the ground ice content and its distribution, the ground temperature, and the soil hydrological regime.

Permafrost is present the entire map area, and may be found within any of the materials described on the accompanying map. Ice-rich permafrost is common and may be present on all aspects and in moderately to well-drained materials. Near-surface permafrost within 1 m of the surface is encountered on most slopes, as well as on more level, valley-bottom sites where there is an insulating cover of organic material and/or finer textured soils. High ice contents are common especially where there is, or has been, subsurface water flow associated with large river systems, as well as surface water related to smaller drainages and fans.

Permafrost influences slope stability by strongly affecting drainage (which is restricted by the permafrost table), soil moisture (which may increase in response to rapid thaw of ground ice), and strength (through bonding of frozen soil particles).

Disturbance or clearing of the organic cover, and/or changes in surface or subsurface drainage, can cause changes to the soil thermal regime and result in thermokarst development, subsidence, and terrain destabilization.

ASSESSING CURRENT HAZARD RISKS FOR THE OLD CROW REGION

CASE STUDY SITES

To assess the risk of the hazards described above for the Old Crow region, the research team focused on several case study sites (Figure 50). Findings from case study sites were then used to assess risk on a regional scale.

The case study sites for the Old Crow area were determined in consultation with the Vuntut Gwitchin First Nation (VGFN) – they reflect areas where there are hazards-related concerns, or where future development may take place. Case study sites were also chosen to cover a variety of landscape types. Detailed investigations at each case study site is described below, and are grouped as follows: 1) the Old Crow community core; 2) North Road and vicinity; 3) the Ski Lodge and vicinity; 4) Crow Mountain Road and vicinity; and 5) Portage Trail. At each site, researchers used a combination of geophysical approaches (ERT and GPR), permafrost borehole and soil pit observations, and examined exposed surficial material where possible. (Note: not all techniques were used at every site.) Results from each case study site are described in the following section.

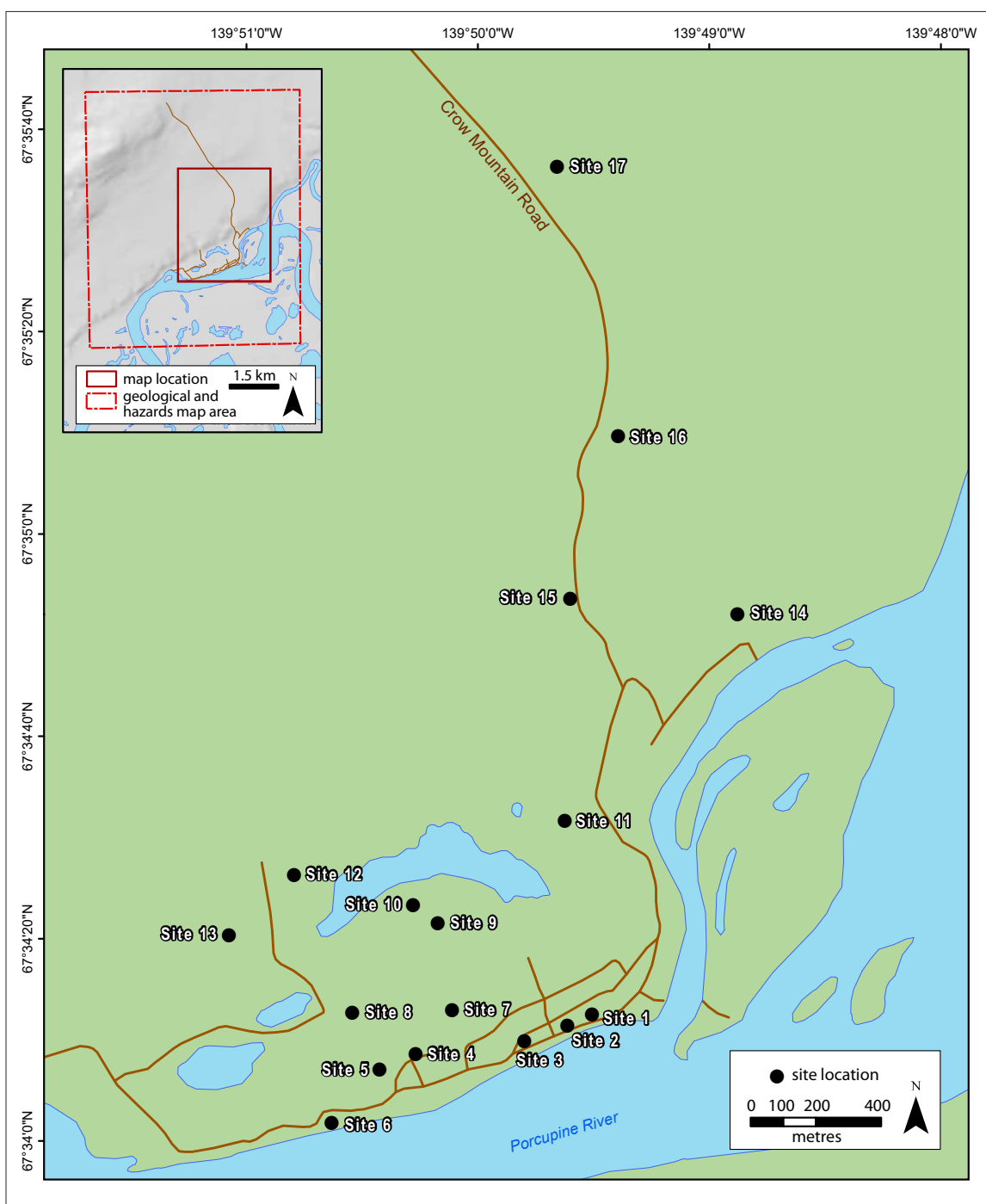


Figure 50. Overview map of case study sites in the Old Crow area. Site 18, near Portage Trail, is not included on this figure.

OLD CROW COMMUNITY CORE

The Old Crow community core encompasses sites 1-6 (Figure 50; Figure 51). Results from field investigations at each site are described below.

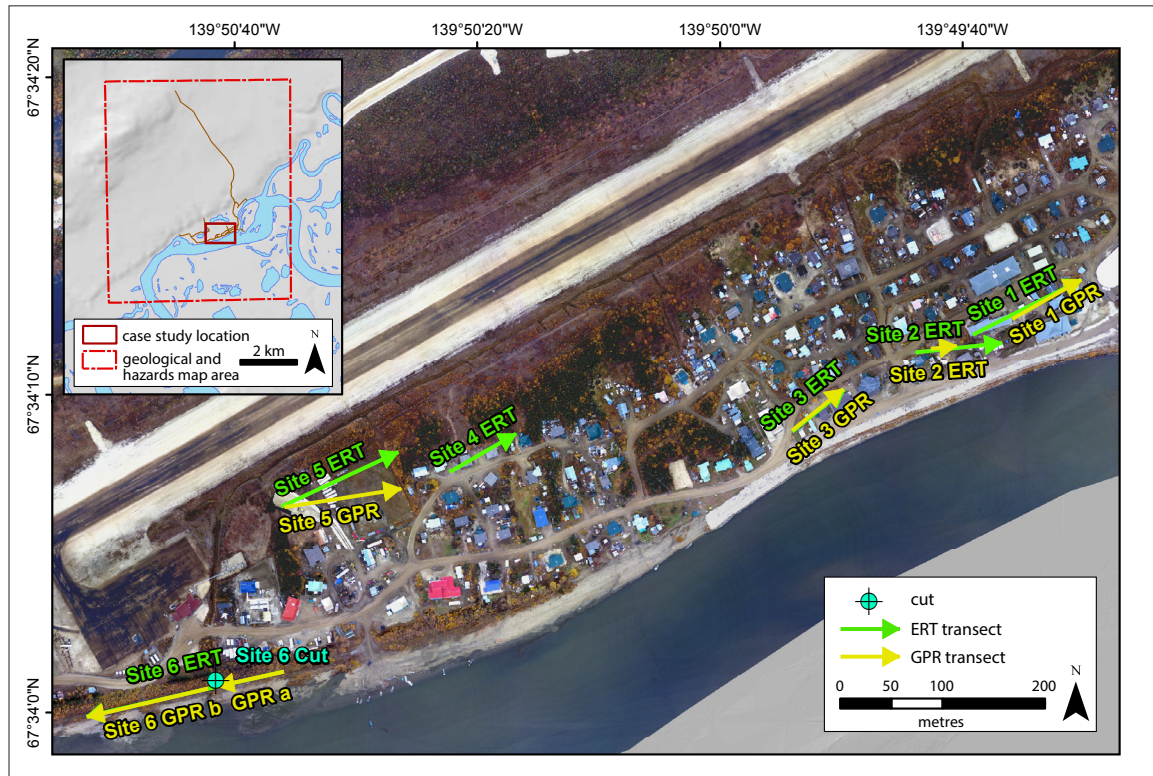


Figure 51. Overview map of case study sites 1 to 6 in the Old Crow community core area.

SITE 1

Groundcover at Site 1 was mainly composed of gravel material, used for construction of building pads for the John Tizya Centre and the arena. A 120 m-long ERT survey was run underneath the John Tizya Centre to the arena, and a GPR survey followed the same line, but its start point is located just beyond the John Tizya Centre (see Figure 51).

The ERT survey shows a high resistivity body, interpreted as permafrost, occurring across the latter two-thirds of the profile and extending to its base at 23 m (Figure 52). This body is overlain by a 1 to 3 m-thick low resistivity layer that represents seasonal thaw. The first third of the ERT profile, which was carried out beneath the John Tizya Centre, exhibits resistivities low enough to indicate unfrozen soils. This suggests that in some areas, thaw occurs to the base of this section of the profile at 8-10 m. If this interpretation is correct, a talik is present indicating that this thickness of sediment could not refreeze over the winter.

The GPR survey shows only one clear contact at a depth of about 3 m (see red line on Figure 53), corresponding approximately to the depth of the thaw front on the ERT survey. This stratigraphic contact is interpreted to represent the bottom of the active layer/top of permafrost. A pattern of convex lines are visible throughout the profile and are likely due to anthropogenic disturbances. To display this profile, a velocity of 0.08 m/ns was used and a constant gain of 100 was applied.

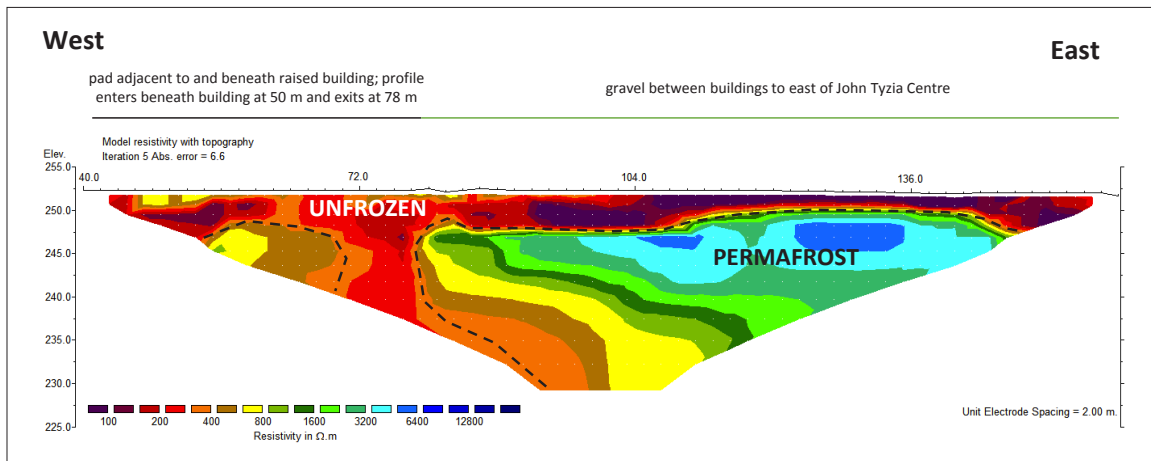


Figure 52. ERT profile for Site 1. The survey is 120 m long and has a maximum penetration depth of about 25 m. Black dashed lines outline likely areas of permafrost.

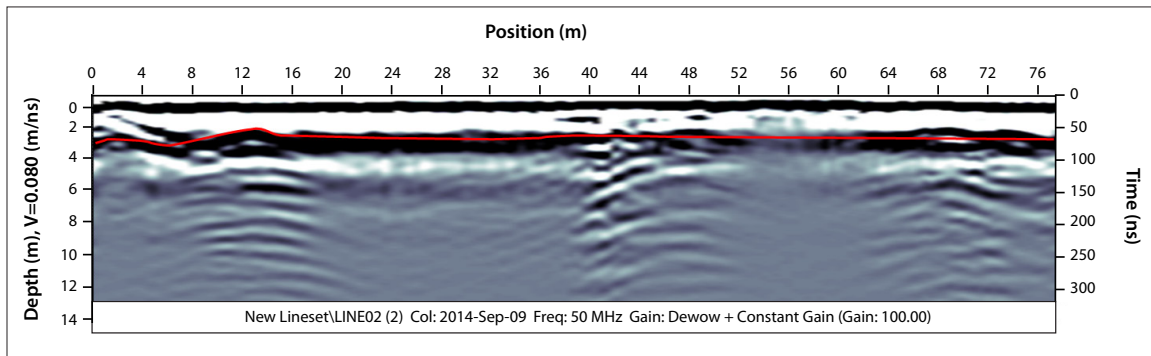


Figure 53. GPR profile for Site 1, displayed with a constant gain of 100 and a velocity of 0.08 m/ns. The red line represents the thaw front.

A second ERT survey was run directly beneath the John Tizya Centre and closer to the centre-line of the building than the first ERT profile at this site (Figure 54). This 80 m-long profile (2 m electrode spacing) shows a high-resistivity body present at depths of 4-6 m at the western end of the building and a second high-resistivity body beneath gravel outside the building at the east end of the profile. Between these two bodies, low resistivities indicate possible thaw that extends to the base of the profile at 16 m. This profile suggests that the ground was deeply, but seasonally thawed at the western end under the building, while a talik is likely at the eastern end of the profile, adjacent to a 75 cm pit associated with the building's water supply. However, this interpretation needs confirmation from ground temperature measurements as the resistivities may be reduced due to the presence of steel piles and buried cross-braces.

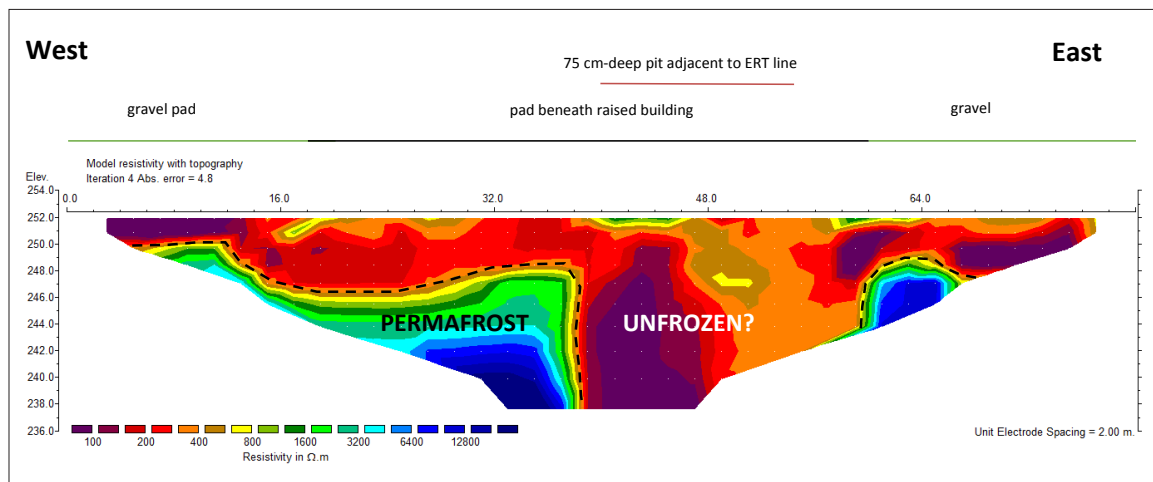


Figure 54. ERT profile for Site 1, underneath the John Tizya Centre. The survey is 80 m long and has a maximum penetration depth of about 16 m. Black dashed lines outline likely areas of permafrost.

SITE 2

Site 2 is situated in an area that was formerly occupied by a residential home that burned down in March 2014. The ground at the site was scattered with burned debris, gravel patches and garbage. A thin vegetative ground cover was composed of mosses and grasses, and some patches of taller dry grasses. ERT and GPR surveys were both run in an easterly direction over the abandoned lot southwest of the John Tizya Centre (see Figure 51 for location).

A 160 m-long ERT profile (2 m electrode spacing) crossed the abandoned lot and continued on the southern side of the John Tizya Centre adjacent to the building, and passed beneath the entry steps (Figure 55). A high-resistivity body extended to the base of the profile at 16 m and was overlain by a continuous low-resistivity layer. The contact between the two was at a depth between 2 and 4 m beneath the abandoned lot, and up to 5 m beneath the gravel pad of the John Tizya Centre. The profile is interpreted as a thawed layer over permafrost with the variable thaw depth associated with the site's disturbance history, and possibly due to the stratigraphy of the sediments. The eastern end of the profile was run parallel to the two profiles at Site 1 and shows similar apparent depths of thaw.

The GPR survey shows only one clear contact at a depth of about 3 m (see red line on Figure 56), corresponding to the depth of the thaw front on the ERT profile. This layer intercepts at least one other layer with a weaker signal, but the lack of information about the subsurface for this site does not allow for a proper interpretation of the signal. Presumably, this weaker signal corresponds to a change of material property in the stratigraphy of the active layer. To display this profile, a velocity of 0.08m/ns was used and an AGC gain (maximum gain of 500) was applied.

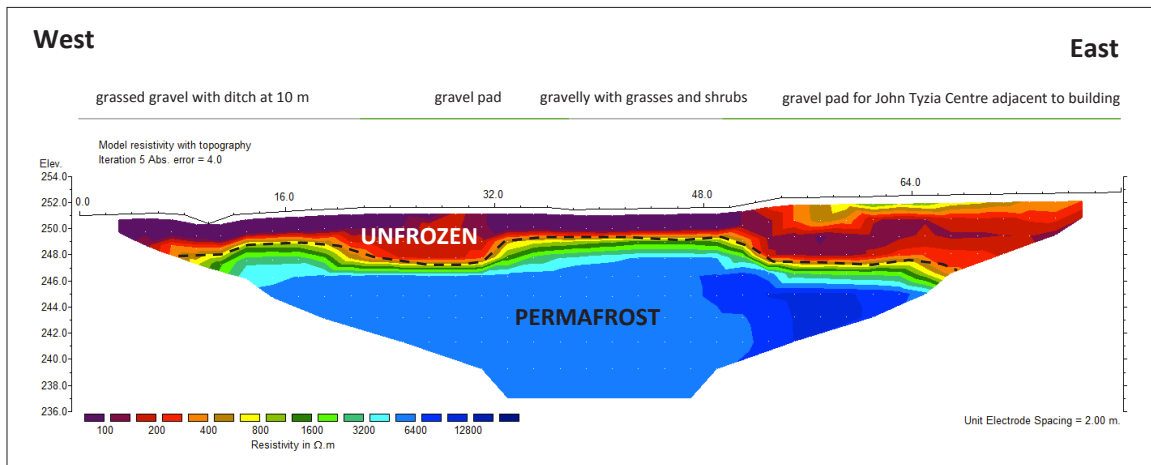


Figure 55. ERT profile for Site 2. The survey is 120 m long and has a maximum penetration depth of about 16 m. Black dashed lines outline likely areas of permafrost.

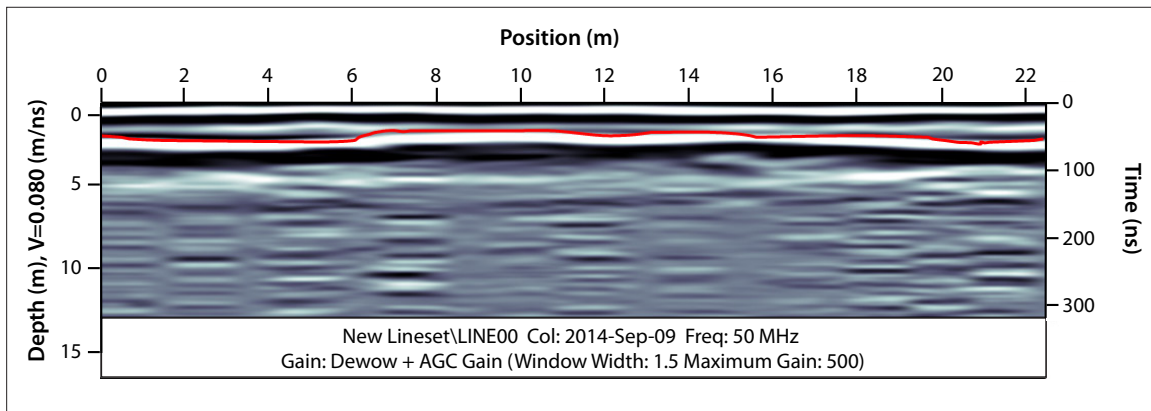


Figure 56. GPR profile for Site 2, displayed with an AGC gain (maximum gain of 500) and a velocity of 0.08 m/ns. The red line represents the thaw front.

SITE 3

This site is the location of a proposed multiplex. GPR and ERT surveys were run along the north side of the former Northern Store (see Figure 51 for location). The first part of both surveys was conducted on grass-covered gravel, while the remaining part of the surveys crossed exposed gravel pads.

The 76 m-long ERT profile (2 m electrode spacing) reveals a near-surface, low-resistivity layer of variable thickness overlying moderate to high-resistivity materials that extend to the base of the profile (Figure 57). The profile is interpreted as follows: deep seasonal thaw (about 2 m) in the vegetated areas at the western end of the profile, and deeper seasonal thaw or taliks (up to 4 m) beneath the unvegetated gravel pad. Permafrost extends to the base of the profile at 13 m. The central part of the profile has an area of lower resistivities that likely represent terrain near the thawing point but still frozen. The dry gravel pad creates some higher, near-surface resistivities in the eastern half of the profile. A pre-existing borehole drilled approximately 32 m along the profile showed 2.8 m of thaw over ice-poor sediments of sand with silt and gravel (R. Trimble, pers. comm.). The lesser amount of thaw in the borehole compared to the ERT profile suggests that the post-processing of the ERT profile may exaggerate the depth of the thaw front.

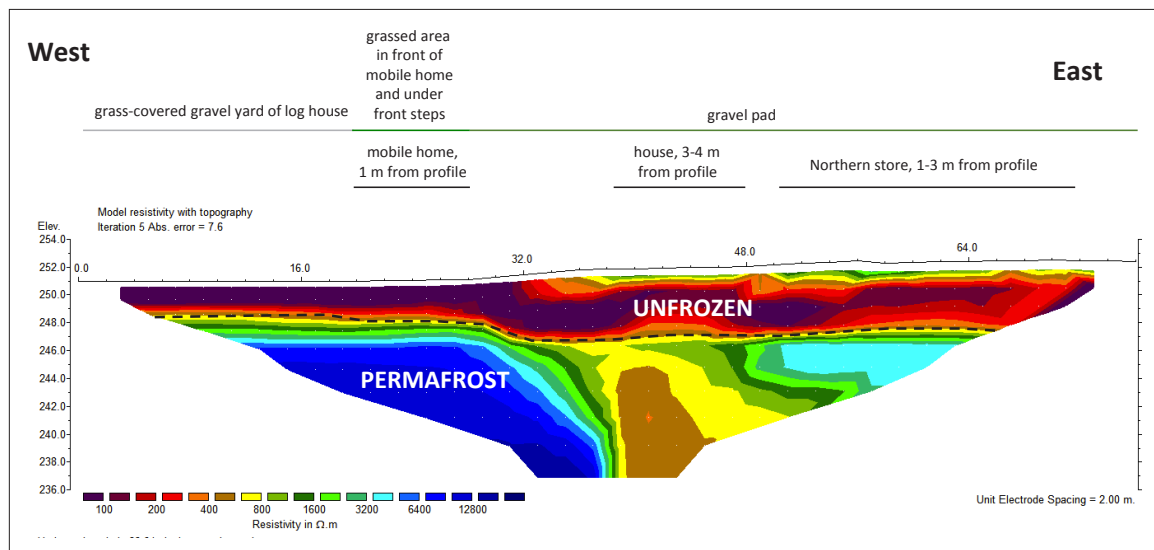


Figure 57. ERT profile for Site 3. The survey is 76 m long and has a maximum penetration depth of about 13 m. Black dashed lines outline likely areas of permafrost.

The GPR survey shows a strong contact at a depth of about 2.5 m (see red line on Figure 58), which could correspond to the thaw front in the active layer. Another strong reflector appears at a depth of about 5 m (see green line on Figure 58), which likely corresponds to a major stratigraphic change. However, the lack of information about the subsurface for this site does not allow for a clear interpretation of the signal. To display this profile, a velocity of 0.08m/ns was used and an AGC gain (maximum gain of 500) was applied.

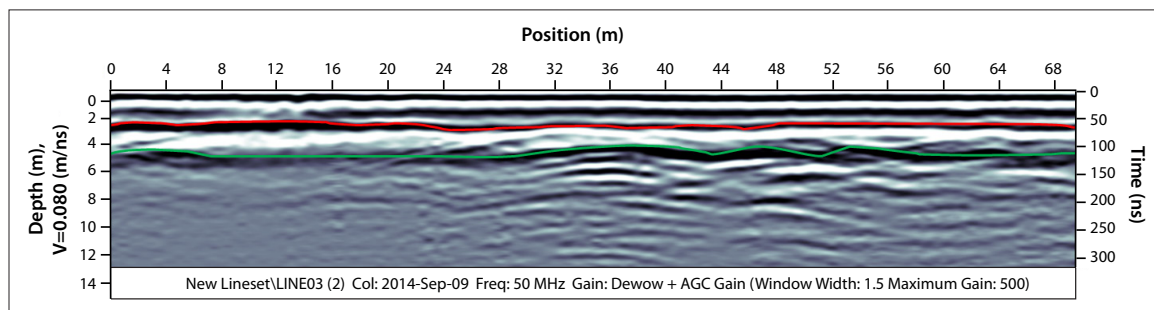


Figure 58. GPR profile for Site 3, displayed with an AGC gain (maximum gain of 500) and a velocity of 0.08 m/ns. The red and green lines represent cryostratigraphic contacts.

SITE 4

Site 4 is located east of the tank farm where there are two abandoned log homes (see Figure 51 for location). An ERT survey was run under the two log buildings. The survey was conducted mainly on the gravel pads and crossed a shallow ditch at its eastern end (Figure 59). The 76 m-long ERT survey revealed a continuous low-resistivity layer 4-5 m thick overlying high-resistivity material that extends to the base of the profile at a depth of 13 m. The profile is interpreted as having a subsurface of deep seasonal thaw, or a supra-permafrost talik that overlies permafrost. The substantial thaw of the permafrost is clearly linked to the structural damage evident in the log homes and it is therefore assumed that the soil that has thawed contained excess ice.

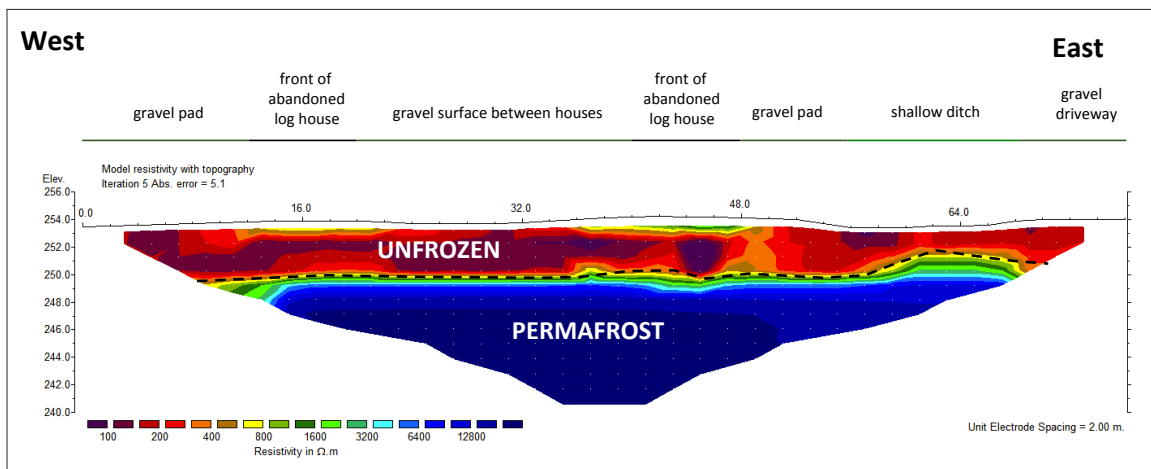


Figure 59. ERT profile for Site 4. The survey is 76 m long and has a maximum penetration depth of about 13 m. Black dashed lines outline likely areas of permafrost.

SITE 5

Site 5 is located at the new tank farm (see Figure 51 for location). Here, GPR and ERT surveys were run in an eastward direction, beginning a few metres from the airport fence, through the former playground and between the oil tanks, and ending at another fence in the baseball field. No fill materials were present at the time of the investigations, and groundcover consisted solely of grass.

The ERT survey was 114 m long with 2 m electrode spacing. The ERT survey produced a profile with a uniform low-resistivity layer overlying materials of high resistivity extending to the base of the profile at a depth of 20 m (Figure 60). The profile is interpreted as having a subsurface with a deeply thawed active layer that overlies permafrost. The slightly lower resistivities at the western end of the transect indicate that this part of the profile may be slightly warmer, giving rise to higher unfrozen moisture contents and more electrically conductive soils.

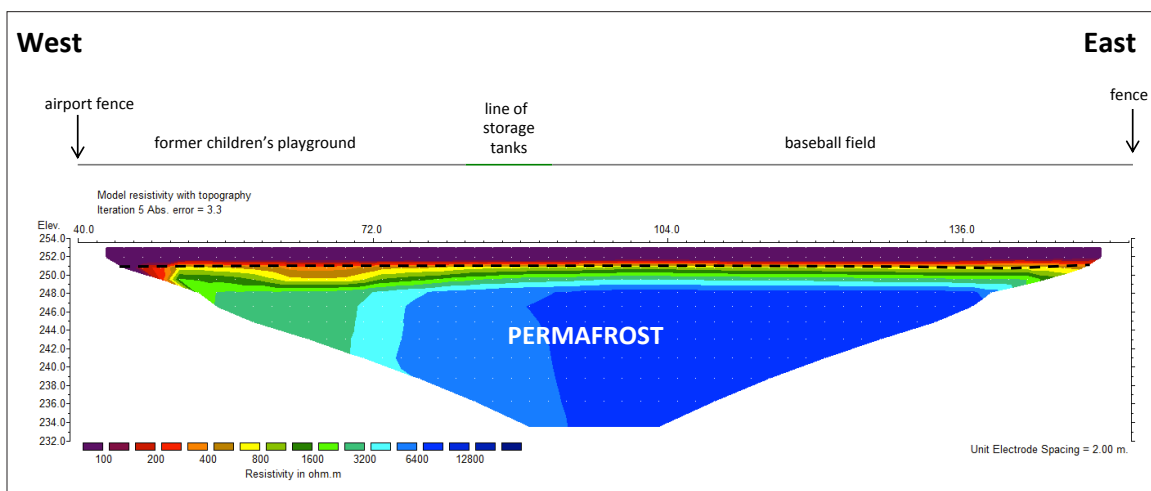


Figure 60. ERT profile for Site 5. The survey is 114 m long and has a maximum penetration depth of about 20 m. Black dashed lines outline likely areas of permafrost.

The GPR survey shows only one clear contact at a depth of about 2.5 m (see red line on Figure 61). This is interpreted as the thaw front in the active layer, and corresponds to the depth of the thaw front on the ERT profile. Vertical artifacts are visible along the profile and are due to metal pipes and fences at surface. There is no indication of any changes to stratigraphy in the first 5 m. To display this profile, a velocity of 0.07 m/ns was used and an AGC gain (maximum gain of 500) was applied.

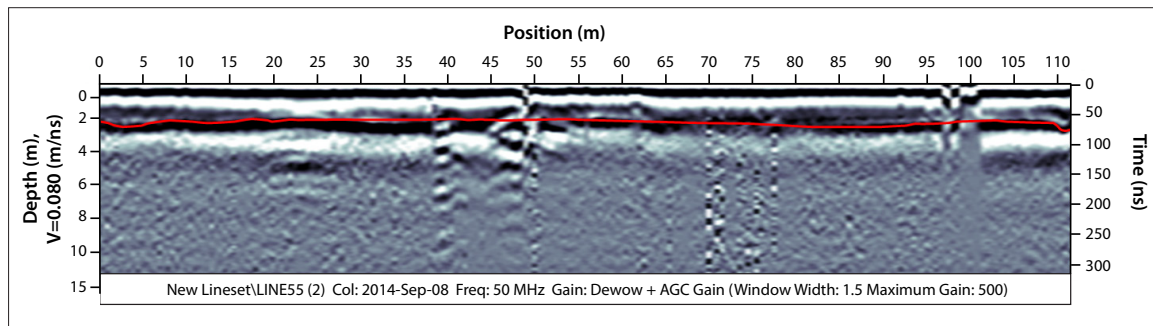


Figure 61. GPR profile for Site 5, displayed with an AGC gain (maximum gain of 500) and a velocity of 0.07 m/ns. The red line represents the thaw front.

SITE 6

Site 6 is located at the southwestern edge of the community, on the upper part of the north bank of the Porcupine River (see Figure 51 for location). One 200 m-long ERT transect was conducted in an east to west direction along the shore, and across a small gully (~6 m wide at its widest part). A two-section GPR transect was run along the same line as the ERT survey; however, the two GPR surveys are separated by the gully (see *GPR a* and *b* on Figure 51). The transects followed a narrow discontinuous path with a gentle slope to the south. Where the profiles crossed the gully, centimetre-wide tension cracks were visible on either side. The ground was covered with moss, grasses, scattered branches and pebble to cobble, subrounded gravel. Willow and alder shrubs were abundant along most of the pathway, reaching up to 2 m on the south side, and up to 4 m on the north side. A 220 cm-high exposure in the gully was investigated about 10 m inland from the stream outlet (see Site 6 cut on Figure 46). The site is situated on overbank deposits, composed of stratified layers of silty sand and subrounded gravel.

The ERT profile shows a 1 to 2 m-thick, low-resistivity layer overlying a layer with moderate to high resistivities that extends to a depth of 10-15 m (Figure 62). A second low-resistivity layer is present below ~15 m and extends to the base of the profile at a depth of 25 m. The higher resistivity layer is penetrated by low resistivities centred at 72 m along the profile, and is associated with the gully mentioned above. The profile is interpreted as follows: a thin active layer overlying permafrost whose base is at 10-15 m. The permafrost is penetrated by a talik beneath the gully that connects the surface and subsurface hydrological systems. The thin permafrost is likely the result of the combined effects of coarse, near-surface materials, the absence of an organic mat, enhanced snow accumulation around shrubs, and warming by the river when water levels are higher in the spring and early summer.

Both GPR profiles show a strong reflector at a depth of about 2 m. It is interpreted as the thaw front, and can also be observed on the ERT profile (see red line on Figure 63). Another reflector emerges over this layer in the last third of the profile (see upper green line on Figure 63). The reflector located at a depth of about 5.5 m is considered a multiple. A last reflector appears in the

last 15 m of the profile, at a depth of about 10 m (see lower green line on Figure 63). To display this profile, a velocity of 0.1 m/ns was used and an AGC gain (maximum gain of 500) was applied.

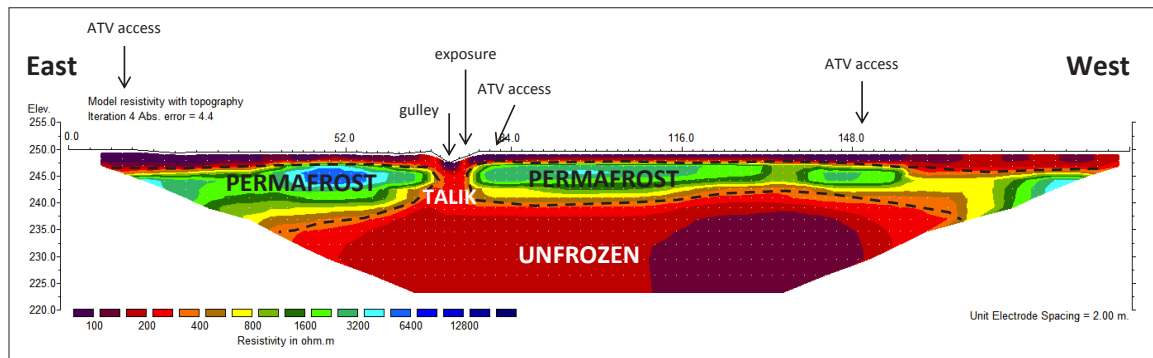


Figure 62. ERT profile for Site 6. The survey is 200 m long and has a maximum penetration depth of about 25 m. Black dashed lines outline likely areas of permafrost.

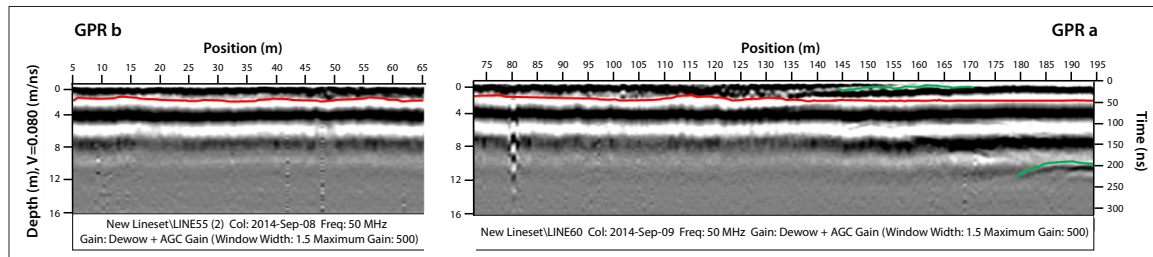


Figure 63. GPR profiles for Site 6, displayed with an AGC gain (maximum gain of 500) and a velocity of 0.1 m/ns. GPR survey **a** is shown on the right and survey **b** is on the left. The red lines represent the thaw front and the green lines represent a stratigraphic contact.

NORTH ROAD AND VICINITY

North Road and vicinity contains Sites 7 through 11 (see Figures 50 and 64). At the time of the field investigations, there was active development in the area – Sites 9 and 10 are located at a site of new pads for home construction, whereas Site 11 is a proposed location for another residential home. Sites 7 and 8 are located on the south and north sides of the runway, respectively. Results from field investigations at each site are described below.

SITE 7

Site 7 is located halfway along the airport runway, 3 m south of the fence bordering the runway. It is mainly covered with tall grasses, sedge tussocks and small scattered willow shrubs 1-2 m high (*Salix sp.*). GPR and ERT surveys were conducted along the same trajectory, running in a southwesterly direction on flat terrain. A borehole (Site 7 BH) was also drilled 60 m along the survey lines (see Figure 64).

At Site 7, the borehole consisted of an overbank deposit comprising sandy organic silt, silty sand, and coarse sand. Finer material was moderate to ice rich (down to about 2 m), and ice poor in the coarser material (below 2 m). The permafrost table was encountered at a depth of 65 cm, under silty organic deposits. The permafrost was mainly composed of organic sandy silt (65 to 196 cm deep) overlying a sandy deposit with lesser amounts of gravel (196 to 253 cm deep). The borehole was drilled to a depth of 270 cm, at which point the presence of gravel prevented further coring.

The sandy silt unit was composed of a lenticular cryostructure with ice volume content between 15 and 20%. At a depth of 141 cm, in ice-rich permafrost, thaw settlement and consolidation test results exhibited 52% total settlement under a stress load of 25 kPa (theoretical value for this material type = 39%), and 58% total settlement under a stress load of 150 kPa. Deeper, in the ice-poor permafrost where the material was coarser, thaw settlement and consolidation test results revealed 19% total settlement under a stress load of 25 kPa (theoretical value for this material type = 15%), and 38% total settlement under a stress load of 150 kPa. The complete borehole log for this site is shown in Appendix B.

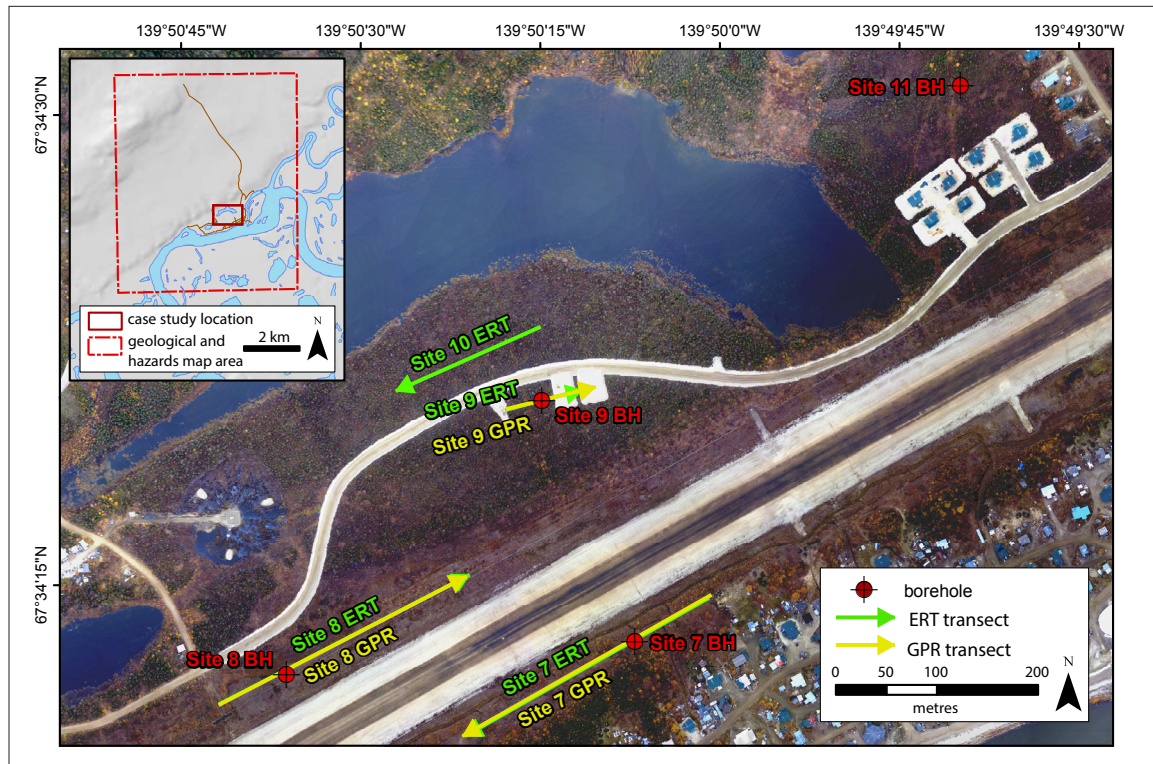


Figure 64. Overview map of the study sites in the vicinity of North Road.

The ERT survey (2 m minimum electrode spacing) shows a complex pattern of low, moderate and high resistivities (Figure 65). A continuous low resistivity layer near surface is evident across the entire profile and corresponds to the active layer. The depth of thaw at the time of the survey in mid-August 2014, averaged 65 cm, having a range between 42 and 82 cm; however, at a ditch containing shallow water, the depth of thaw exceeded 120 cm. The higher resistivity layer beneath is interpreted as permafrost. The variable resistivities present are interpreted as being associated with variations in both stratigraphy and temperature. A talik, possibly connected to the active layer, appears to be present at 58 m along the profile; other isolated low-resistivity zones are apparent at 28 m, 168 m and 246 m along the profile and may represent intra-permafrost taliks. The permafrost varies in thickness from less than 5 m (e.g., at 136 m along the profile) to more than 25 m (e.g., at 154 m along the profile). If the inferences regarding ground freezing conditions are correct, the taliks may be associated with surface drainage (as is observed at the ditch at 56-58 m along the profile), snow accumulation around shrubs, and possibly groundwater connections within and through the permafrost.

An irregular layer at a depth of 25 to 100 cm can be seen on the GPR profile, and is interpreted as the thaw front (see red line on Figure 66). Just below this contact, another strong reflection is visible at a depth that oscillates between 1 and 2.5 m which corresponds to the contact with the sand layer observed in borehole Site 7 BH (see uppermost green line in Figure 61). A third contact is visible at a depth of about 4 m (see lowermost green line in Figure 61) and is believed to represent a gravel layer based on the known stratigraphy in the area (i.e., overbank deposits) and corresponds well with a more resistive layer as is observed in the ERT profile. The lowest contact, at a depth of about 8 m, is considered to be a multiple. To display this profile, a velocity of 0.09 m/ns was used and an AGC gain (maximum gain of 500) was applied.

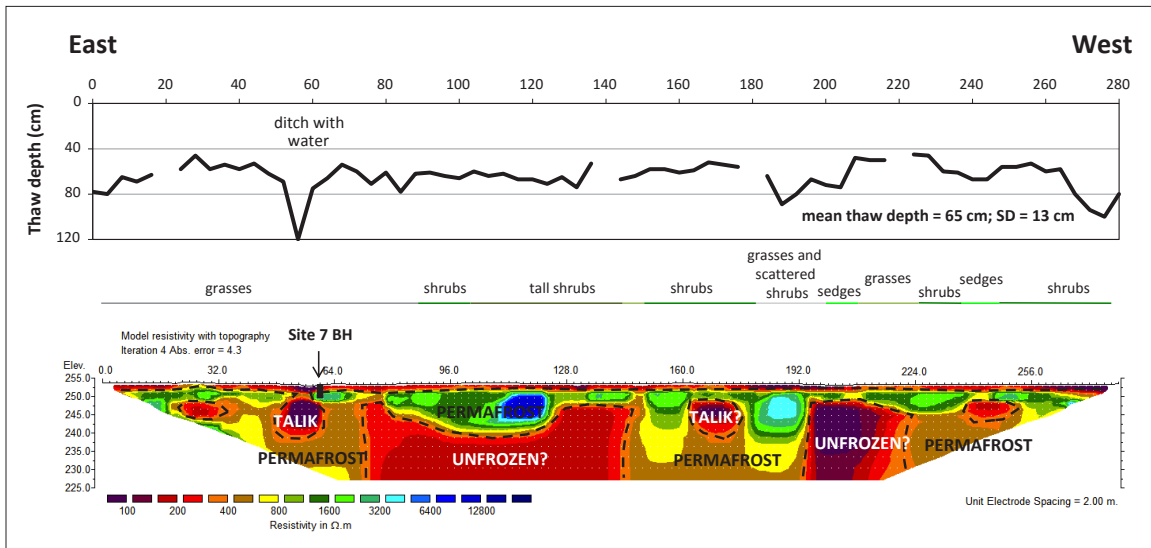


Figure 65. ERT profile for Site 7. The survey is 280 m long and has a maximum penetration depth of about 25 m. Black dashed lines outline likely areas of permafrost. SD = standard deviation.

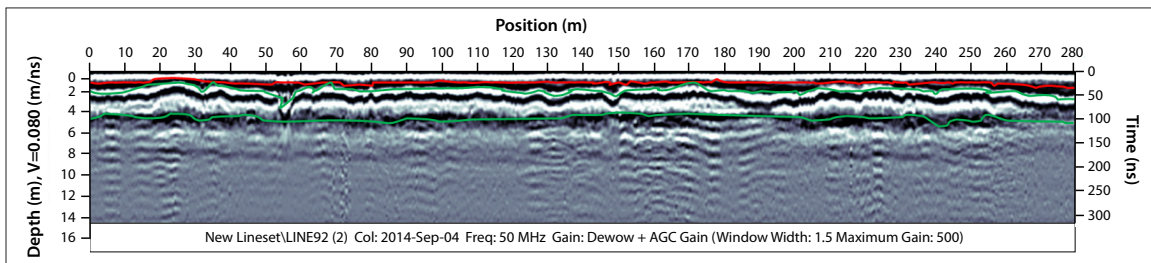


Figure 66. GPR profile for Site 7, displayed with an AGC gain (maximum gain of 500) and a velocity of 0.09 m/ns. The red line represents the thaw front and the green lines represent stratigraphic contacts.

SITE 8

Site 8 is located on the north side of the airport runway. This site consisted mainly of a flat, open field with shallow standing water and sedges; slightly higher and drier areas had grasses and minor willow shrubs up to 1 m high. The shrubs were more abundant in the last third of the transect. ERT and GPR surveys (280 m long and overlapping) were run in a northeasterly direction a few metres from the fence that surrounds the airport. A 406 cm-deep borehole (Site 8 BH) was drilled at ~90 m along the survey lines, where the active layer was saturated with water (see Figure 64 for location).

Borehole material (Site 8 BH) consisted of overbank deposits, which were moderate to ice rich in the first 130 cm, and ice poor below this depth. The permafrost table was encountered at a depth of 32 cm. The permafrost stratigraphy was composed of layers of ice-rich, microlenticular sandy silt, overlying layers of porous visible and invisible silty organic sand. Ice content was at its highest at the top of the permafrost having values of 69% by volume. Below, in coarser deposits, the volumetric ice content dropped considerably to values ranging from 24 to 36%. At a depth of 114 cm, in ice-rich permafrost, thaw settlement and consolidation test results exhibited 45% total settlement under a stress load of 25 kPa, and 48% total settlement under a stress load of 150 kPa. Deeper, in coarser sand deposits, thaw settlement and consolidation test results revealed 15% total settlement under a stress load of 25 kPa, and 19% total settlement under a stress load of 150 kPa. The complete borehole log for this site is shown in Appendix B.

The ERT survey is somewhat similar to that documented at Site 7 on the other side of the airstrip, that is, displaying a thin, quasi-continuous low-resistivity layer near surface that overlies a more resistive layer extending to depths of 4 m to >25 m (Figure 67). The latter exhibits considerable variation in modelled values with discrete zones exceeding 5 kilo-ohm m, alternating laterally with values of less than 1 kilo-ohm m. Resistivities remain moderate to high down to the base of the profile at a depth of 25 m and end at 160 m along the profile; from this point onward, the basal resistivities are much lower. Thaw depths were about one-third shallower than at Site 7, averaging 47 cm, with a range of 35 to 82 cm. Interpretation of the resistivity profile reveals permafrost more than 25 m thick up to 166 m along the profile, at which point it thins to 5-10 m. This change may correspond to a slight rise in the ground surface at 178 m and the presence of shrubs which would affect snow accumulation, resulting in ground warming and thinning of the permafrost. In contrast, areas containing shallow standing water (marked with a W on Figure 67) did not have a major impact on the observed resistivities.

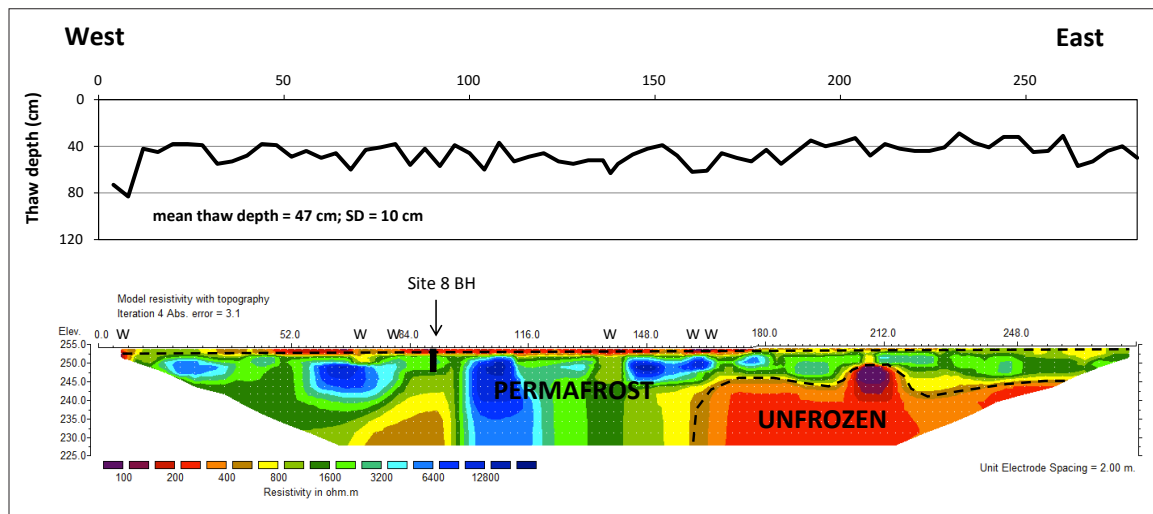


Figure 67. ERT profile for Site 8. The survey is 280 m long and has a maximum penetration depth of about 25 m. Black dashed lines outline likely areas of permafrost. W = areas of standing water; SD = standard deviation.

A shallow reflector is visible at a depth of about 30 cm on the GPR profile, corresponding to the thaw front (see red line on Figure 68). Another reflector is observed at a depth of about 3 m (see green line on Figure 68). According to the borehole data, the lowermost reflector corresponds to a contact with coarse sand and small pebbles; this also correlates to a more resistive layer shown

on the ERT profile. The reflector seen at a depth of about 8 m is considered a multiple. To display this profile, a velocity of 0.09 m/ns was used and an AGC gain (maximum gain of 200) was applied.

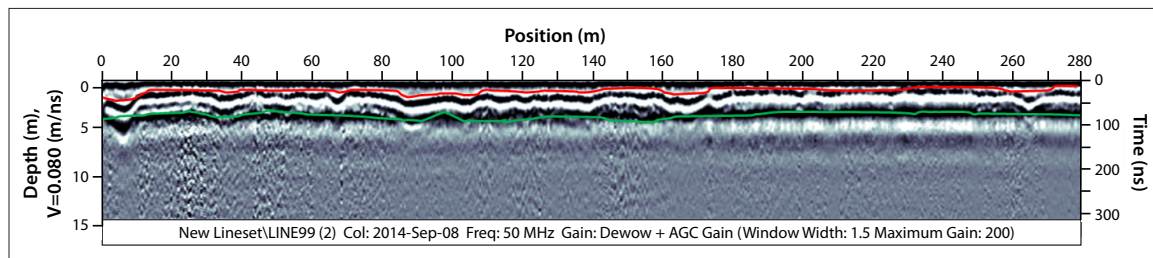


Figure 68. GPR profile for Site 8, displayed with an AGC gain (maximum gain of 200) and a velocity of 0.09 m/ns. The red line represents the thaw front and the green line represents a stratigraphic contact.

SITE 9

At the time of field investigations, a lot was being developed at the location of Site 9. ERT and GPR surveys at this site were conducted in an eastward direction, beginning at the end of a gravel pad, and running through an undisturbed forest of stunted black spruce up to 5 m high (*Picea mariana*). Both surveys then crossed a second gravel pad; the ERT survey was completed in undisturbed terrain at the end of this second gravel pad, while the GPR survey continued to approximately halfway across the second gravel pad. A borehole (Site 9 BH) was drilled ~50 m along the surveys in relatively undisturbed terrain (see Figure 64 for locations). Undisturbed groundcover consisted of a thick organic mat with peat (averaging 10 cm in thickness), and small shrubs up to 15 cm in height (*Vaccinium oxycoccos* and *Rhododendron groenlandicum*).

Borehole material consisted of overbank deposits. The material was moderate to ice rich in the first 130 cm, and ice poor to the bottom of the borehole. The permafrost table was encountered at a depth of 32 cm. Permafrost stratigraphy consisted of layers of ice-rich, microlenticular, silty organic sand and sandy silt, overlying layers of porous visible and invisible silty sand and sand. Ice content was at its highest at the top of the permafrost with values of 75% by volume (38% contained excess ice). Below, in coarser deposits, the volumetric ice content values dropped to values ranging from 39 to 49% (3 to 6% contained excess ice). At a depth of 114 cm, in ice-rich permafrost, thaw settlement and consolidation test results exhibited 35% total settlement under a stress load of 25 kPa (theoretical value for this material type = 28%), and 44% total settlement under a stress load of 150 kPa. Deeper, in dryer and ice-poor permafrost, thaw settlement and consolidation test results revealed 41% total settlement under a stress load of 25 kPa (theoretical value for this material = 12%), and 53% total settlement under a stress load of 150 kPa. The complete borehole log is shown in Appendix B.

The 80 m-long ERT survey (electrode spacing 2 m) exhibits an area of lower resistivities near surface underlain by a zone of higher resistivities that extends to the base of the profile at 15 m (Figure 69). Most of the near-surface layer exhibits modelled values in excess of 1 kilo-ohm m which would normally indicate soils that are frozen. This is because the thawed layer averaged only 36 cm in thickness (range: 26-50 cm), preventing accurate modelling during the ERT inversion process. The gravel pad, which was certainly thawed at the time of the survey, also exhibits relatively high resistivities since dry, coarse materials are poor conductors of electricity.

When examining the GPR profile, an uppermost reflector is visible at a depth of about 50 cm in that part of the GPR survey that was run through the forested area (from 0 to 42 m along the survey line); this reflector corresponds to the thaw front (see red line on Figure 70). Another

reflector is displayed at a depth of about 2 m (see green line on Figure 70). According to the borehole data, this second reflector likely corresponds to a sand layer. The lowermost reflector displayed at a depth of about 6 m is considered a multiple. To display this profile, a velocity of 0.09 m/ns was used and a constant gain of 50 was applied.

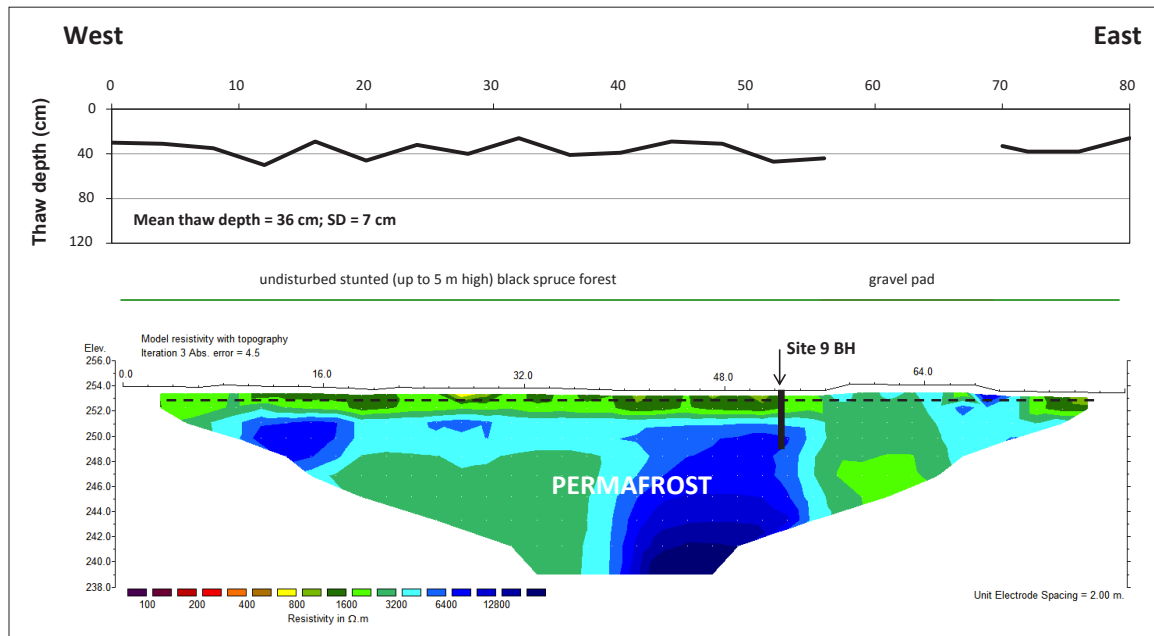


Figure 69. ERT profile for Site 9. The survey is 80 m long and has a maximum penetration depth of about 15 m. Black dashed lines outline likely areas of permafrost. SD = standard deviation.

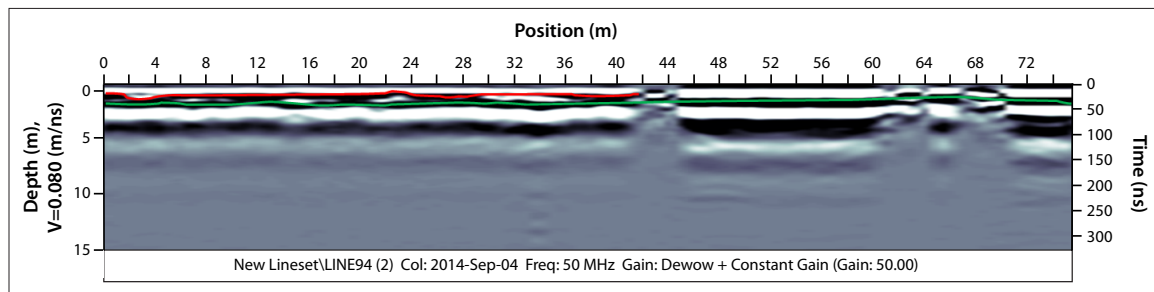


Figure 70. GPR profile for Site 9, displayed with a constant gain of 50 and a velocity of 0.09 m/ns. The red line represents the thaw front and the green line represents a stratigraphic contact.

SITE 10

At Site 10, a 160 m-long ERT survey (electrode spacing 2 m) was run through terrain comparable to that of Site 9, north of a recently constructed road (see Figure 64). The survey reveals a layer with lower resistivities near surface, underlain by a zone of higher resistivities that extends to the base of the profile at 25 m (Figure 71). Most of the near-surface layer exhibits modelled values in excess of 1 kilo-ohm m which would normally indicate soils that are frozen. However, because the thawed layer averaged only 36 cm in thickness (range: 26-50 cm), this prevented accurate modelling during the ERT inversion process. The gravel pad, which was most certainly thawed at the time of the survey, also shows relatively high resistivities because dry coarse materials are poor conductors of electricity.

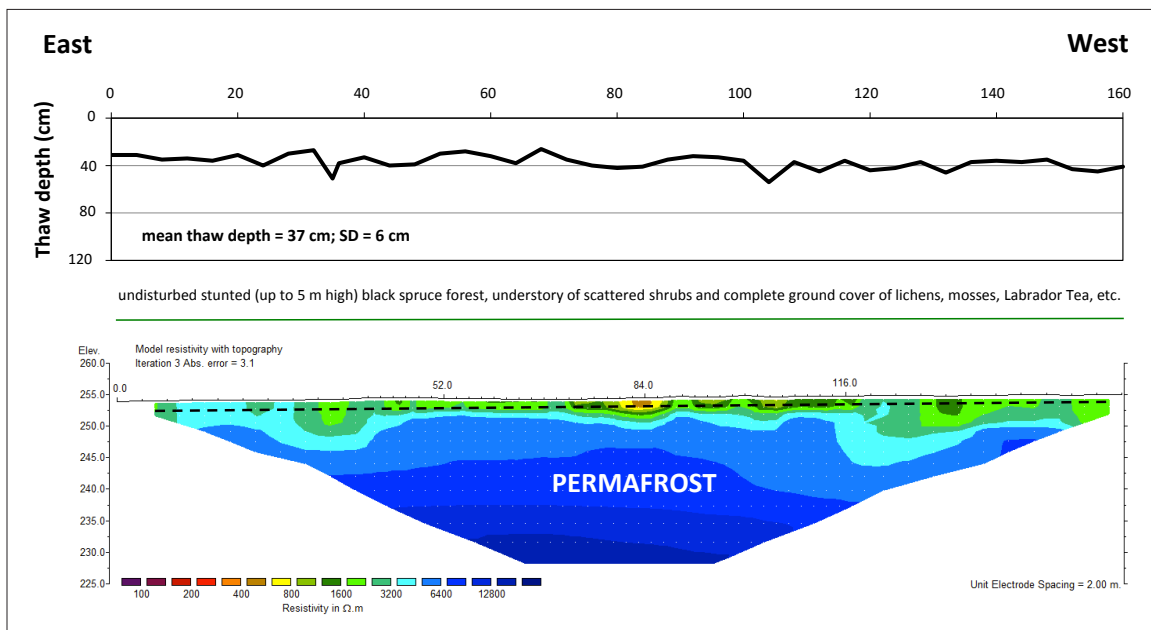


Figure 71. ERT profile for Site 10. The survey is 160 m long and has a maximum penetration depth of about 25 m. Black dashed lines outline likely areas of permafrost. SD = standard deviation.

SITE 11

Site 11 is the location of a future residential development (see Figure 64). To characterize permafrost at this site, a 497 cm-deep borehole (Site 11 BH) was drilled 4 m north of the gravel pads. The surroundings consisted of an open black spruce forest with trees 3-5 m high (*Picea mariana*) with lesser amounts of birch trees up to 5 m high (*Betula glandulosa*), shrubs and bushes reaching up to 1.5 m in height (*Salix* and *Alnus*), and hummocks up to 50 cm high. Ground cover was composed of moss, lichen and small bushes less than 50 cm in height (*Rhododendron groenlandicum*, *Vaccinium oxycoccos*). The permafrost table was encountered directly under the organic cover at a depth of 35 cm. Borehole data revealed a permafrost stratigraphy consisting of layers of lenticular and microlenticular organic silty sand. The deposits became coarser with depth; occasional roots and branches were noted. Excess ice contents were higher towards the top of the permafrost and values ranged from 37 to 50% by volume. Lower down, in the dryer, coarser sediments, the volumetric ice content values dropped to 10%. The complete borehole log is shown in Appendix B.

SKI LODGE AND VICINITY

The area surrounding the ski lodge is characterized by an undisturbed forest of black spruce and birch (up to 6 m high), with an understory of scattered shrubs averaging 1 m in height (*Salix*, *Alnus* and *Betula*); ground cover consists of lichens, *Sphagnum* mosses, and small shrubs less than 50 cm high (*Rhododendron groenlandicum* and *Vaccinium oxycoccos*). This area of investigation includes sites 12 and 13 (see Figures 50 and 72).

SITE 12

At Site 12, a 160 m-long ERT transect was run eastward and a GPR survey directly overlapped the first 53 m of this survey. Additionally, two boreholes ('Site 12 BH a' and 'Site 12 BH b') were drilled at this site (see Figure 72).

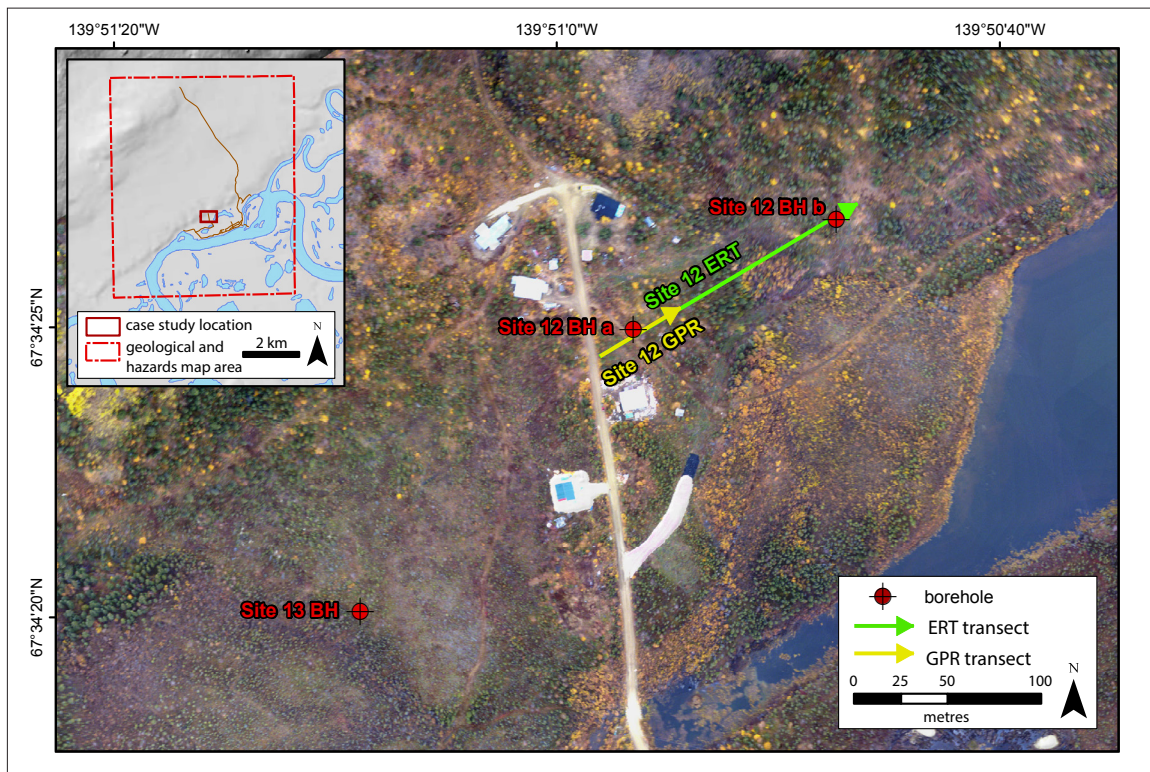


Figure 72. Overview map of study sites in the vicinity of the ski lodge.

Site 12 BH a was drilled near the beginning of the geophysical survey lines (southwest end of the transect) to a depth of 94 cm. The permafrost table was documented at a depth of 64 cm; subsurface sediments were composed of sandy silt (to a depth of 65 cm) overlying a layer of gravel with subrounded clasts up to 10 cm in diameter. The gravel layer prevented any further drilling beyond about 90 cm (see Appendix B).

Borehole Site 12 BH b was drilled at the 150 m-mark along the ERT survey, to a depth of 308 cm. The site had been recently cleared at the time of drilling, however tree stumps still remained. The permafrost table was encountered at a depth of 45 cm. The permafrost consisted of interlaced layers of microlenticular and lenticular cryostructure with sand, overlying layers of porous visible and invisible silty sand. Multiple layers of ice-rich microlenticular cryostructure were observed between 113 and 171 cm. At the bottom of the borehole (308 cm), layers of sand and fine gravel were identified. Volumetric ice content was at its highest within the first metre in sandy silt with values ranging from 49-70% by volume. Further down in the borehole, in sandy and gravelly deposits, the volumetric ice content values dropped to 34%. At a depth of 116 cm, where volumetric ice content results were the highest, thaw settlement and consolidation test results revealed 44% total settlement under a stress load of 25 kPa (theoretical value for this material type = 34%), and 47% under a stress load of 150 kPa. Deeper, in layers containing coarser material, thaw settlement and consolidation tests resulted in 38% total settlement under a stress load of 25 kPa (theoretical value for this material type = 23%), and 42% under a stress load of 150 kPa. The complete borehole log is shown in Appendix B.

The ERT survey at Site 12 shows a two-layered system comprising a low-resistivity, thawed layer, overlying permafrost with a higher resistivity that extends to the base of the profile at 25 m (Figure 73). The near-surface thawed layer was of variable thickness, ranging from 33 cm to >120 cm (the length of the probe). Deeper thaw and lower resistivities are evident from 44 m to

110 m along the profile where active and inactive alluvial fan deposits were noted. At this location, three small channels containing flowing water were present and the vegetation consisted of very dense alder shrubs. The ERT survey suggests that thaw depths below the active alluvial fan deposits may be 2 m or more. The resistivities beneath these areas are noticeably higher than on either side at the same depth suggesting that the permafrost has been warmed by the surface drainage. Furthermore, differences in snow characteristics within the dense alder shrubs have likely contributed to warming of underlying permafrost. However, the thaw does not appear to be deep enough to constitute a talik, even beneath the active fan channels.

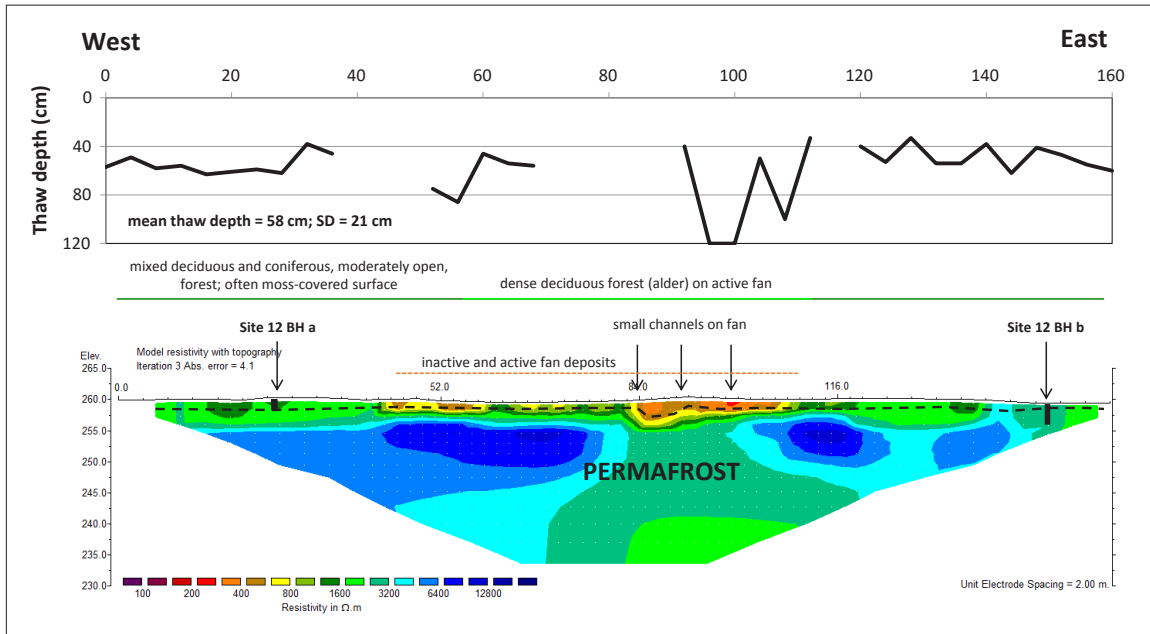


Figure 73. ERT profile for Site 12. The survey is 160 m long and has a maximum penetration depth of about 25 m. Black dashed lines outline likely areas of permafrost. SD = standard deviation.

Several reflectors are visible on the GPR profile at Site 12. An upper reflector occurs at a depth of about 50 cm, corresponding to the thaw front (see red line on Figure 74). Another reflector is located at a depth between 2 and 2.5 m, and may correspond to a gravel layer (see green line on Figure 74). A lowermost reflector occurs at a depth of about 6 m and may indicate a stratigraphic change; however, since no change in resistivity is visible on the ERT profile at that depth, it likely represents an artifact. To display this profile, a velocity of 0.08 m/ns was used and an AGC gain (maximum gain of 200) was applied.

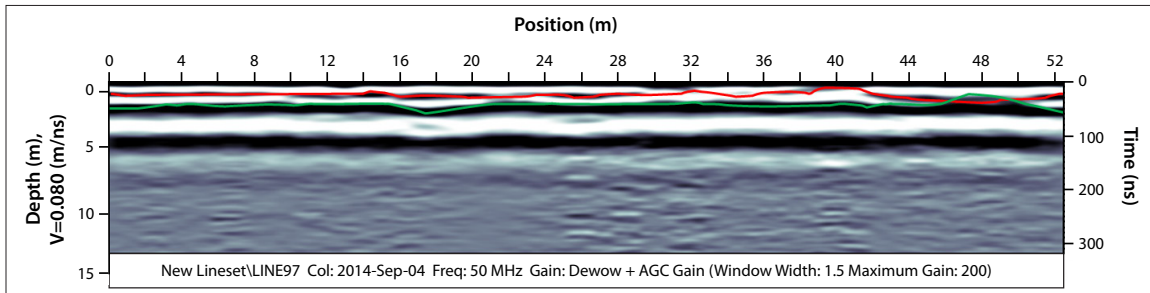


Figure 74. GPR profile for Site 12, displayed with an AGC gain (maximum gain of 200) and a velocity of 0.08 m/ns. The red line represents the thaw front and the green line represents a stratigraphic contact.

SITE 13

A third borehole (Site 13 BH) was drilled on the west side of the road, just west of a ski trail (see Figure 72). The borehole was drilled to a depth of 448 cm, at which point the extractor rod got stuck, preventing further coring. The permafrost table was encountered at a depth of 50 cm. Permafrost stratigraphy consisted of a succession of lenticular and microlenticular sandy silt and minor black, organic interlayers. The deposits were coarser with depth and contained occasional roots and branches. Excess ice contents were higher towards the top of the permafrost with values ranging from 51 to 55% by volume. At these depths, the ratio of silt to sand was significantly higher. The complete borehole log is shown in Appendix B.

CROW MOUNTAIN ROAD AND VICINITY

This area contains investigative Sites 14-17, and makes up a large portion of the land north of the community of Old Crow, including the Crow Mountain Road (Figure 75).

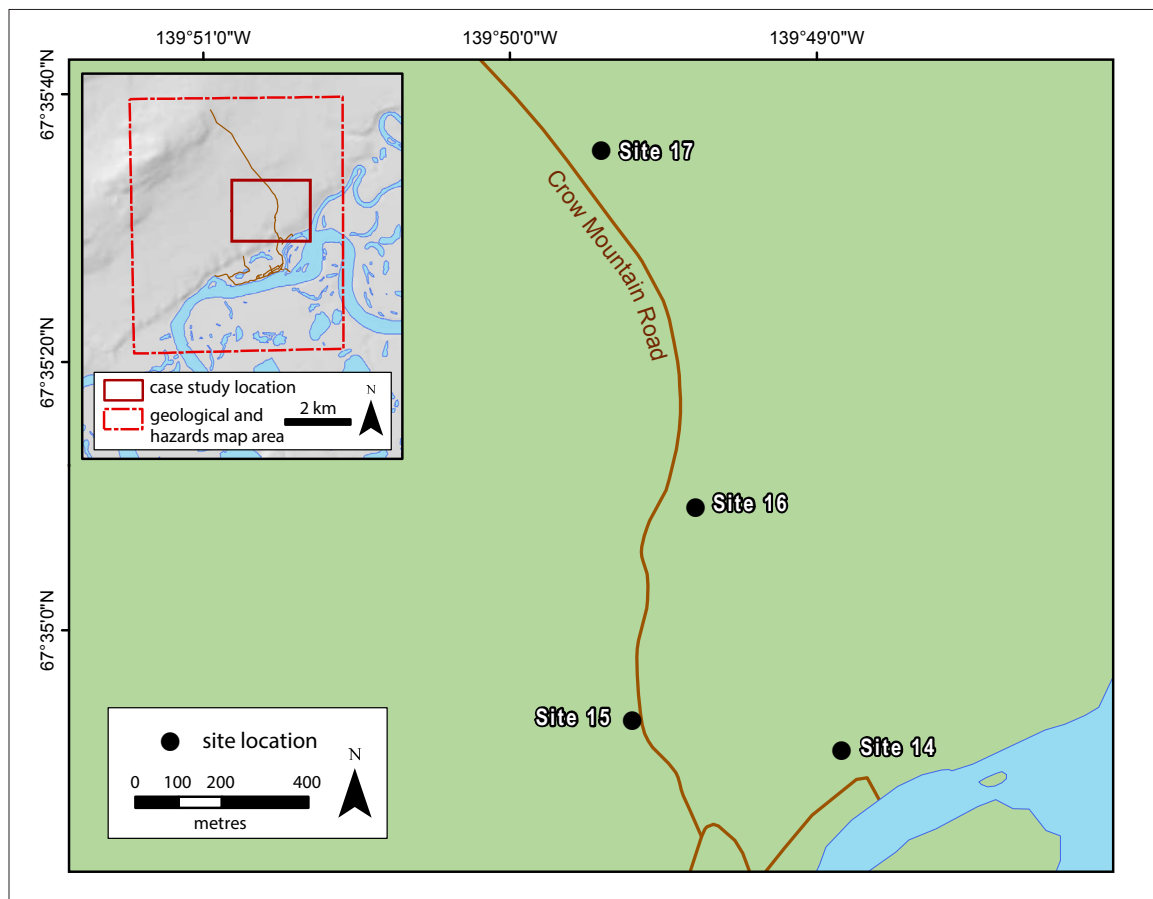


Figure 75. Overview map of study sites in the Crow Mountain Road and vicinity.

SITE 14

Site 14, at the eastern edge of the community, is characterized by a large scar left by a landslide that occurred in 2010 (Figure 76). The undisturbed vegetation above the landslide is composed of a mature forest of black spruce and birch up to 10 m tall, with a ground cover of moss and lichen. The landslide scar is partially colonized by early succession grasses and shrubs. To investigate permafrost conditions along the landslide profile, a 160 m-long ERT survey (2 m minimum

electrode spacing) was run upslope across the road, the landslide toe, and part of the landslide track. A second ERT survey (80 m long; electrode spacing 2 m) was run in the upper part of the scar zone and into undisturbed terrain.

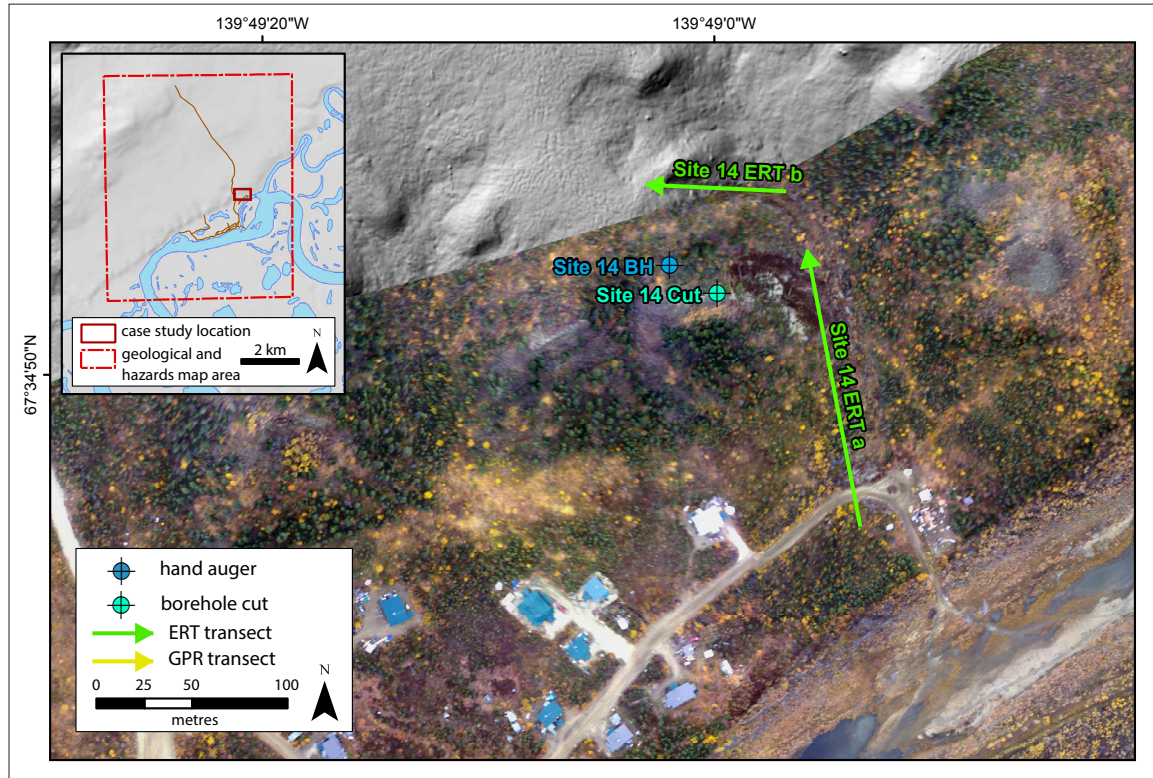


Figure 76. Overview map of field investigation locations at Site 14.

The ERT survey in the lower part of the landslide covered the accumulation zone, as well as a portion of the landslide track which had been subject to stream erosion following slope failure (Figure 77). Because the landslide track was not straight, the end of the ERT survey (from 140 m to 160 m) intersected the side of the landslide and extended into adjacent terrain that was essentially undisturbed apart from the presence of tension cracks. The ERT profile shows a sharp contact and strong contrast between a near-surface, low-resistivity layer and an underlying, very high resistivity layer. Frost probing was carried out in several locations on the landslide and more than half of these locations exceeded 120 cm without encountering the frost table. The small patch of undisturbed forest at the end of the survey, in contrast, exhibited thaw depths of 49–64 cm. The low-resistivity layer clearly represents a thawed layer with an apparent thickness of up to 3 m in the toe and accumulation zone of the landslide. The very high resistivities show that permafrost beneath remains cold and possibly ice rich. The only exception to this pattern is from 130 m to 150 m along the profile where low resistivities are apparent beneath the 5 to 7-m thick layer of frozen ground. This area is tentatively interpreted as an unfrozen layer beneath the base of the permafrost.

The second ERT survey began in the centre of the headscarp and extended upslope into the undisturbed terrain (Figure 78). Almost all of the thaw depths within that part of the scar with new colonizing vegetation exceeded 120 cm, whereas thaw depths in the undisturbed part of the slope ranged from 33 to 57 cm. The ERT profile depicts an upper low-resistivity layer within the

scar, overlying a high-resistivity body with a second lower resistivity layer beneath. This pattern continues beneath the upper, undisturbed portion of the slope, although the near-surface layer exhibits moderate resistivities. Beneath the scar zone, interpretation of the profile reveals a relatively thick thawed layer overlying permafrost. In the upper part of the slope, there exists a relatively thin thawed layer over permafrost. The low resistivities near the base of the profile indicate that the permafrost may be only about 10 m thick which corresponds with the upper part of the ERT profile from the survey undertaken on the toe of the landslide (see Figure 77).

In the undisturbed area above the landslide, probing with a hand auger (Site 14 BH) was completed to a depth of 97 cm, where the frost table was reached. A cut (Site 14 Cut) 147 cm high was investigated in the headscarp and was composed mainly of sandy silt. A pit was dug at the bottom of the cut and the frost table was encountered at a depth of 118 cm. A layer of pure ice was found at the top of the frost table, or the thaw front.

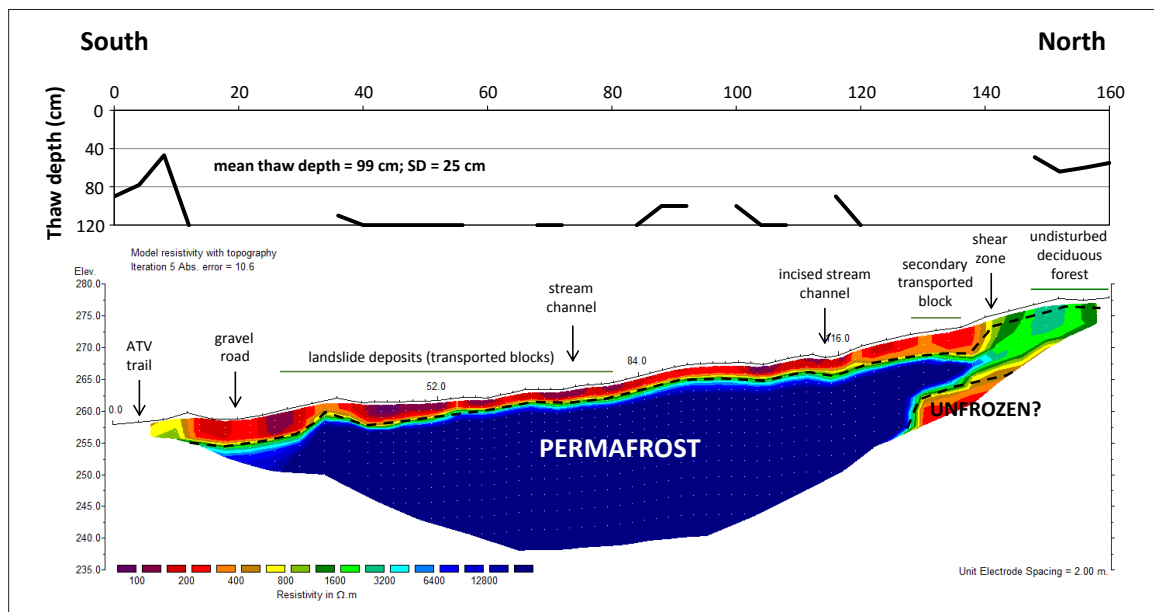


Figure 77. ERT profile for Site 14, extending along the track to the toe of a 2010 landslide. The survey is 160 m long and has a maximum penetration depth of about 25 m. Black dashed lines outline likely areas of permafrost. SD = standard deviation.

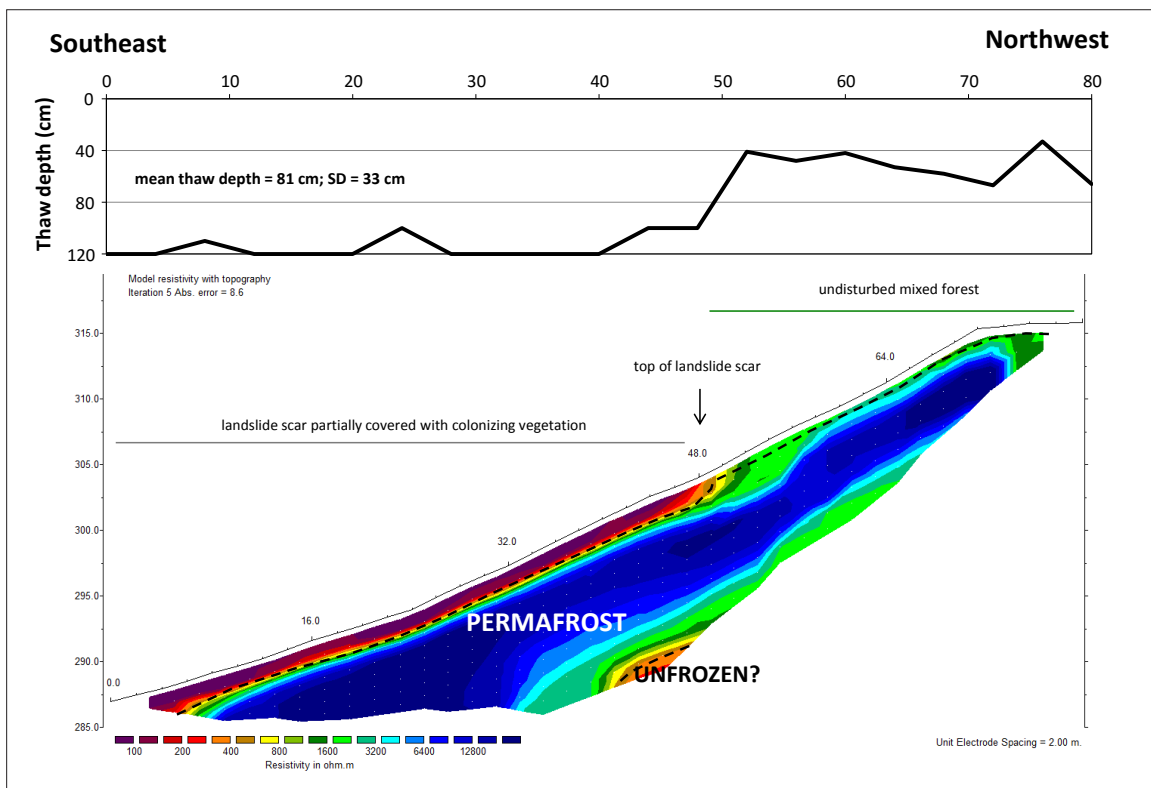


Figure 78. ERT profile for Site 14, extending across the upper part of the landslide scar zone and undisturbed terrain. The survey is 80 m long and has a maximum penetration depth of about 16 m. Black dashed lines outline likely areas of permafrost. SD = standard deviation.

SITE 15

At Site 15, a borehole was drilled (Site 15 BH) on the west side of Crow Mountain Road, at the foot a landslide scar (Figure 79). The site is situated on a gentle, south-facing slope with a mixed forest of black spruce (1-8 m high) and birch. Ground cover consisted of rotting tree trunks and other forest litter, along with moss, lichen, tall grasses, spruce seedlings and small shrubs (*Rhododendron groenlandicum*, *Vaccinium oxycoccos*). The active layer was composed of layers of brown silty sand and grey sandy silt containing minor amounts of subrounded clasts (1-5 cm in diameter). The permafrost table was encountered at a depth of 50 cm. Permafrost consisted of a very ice-rich, suspended cryostructure in sandy silt deposits. The borehole was drilled to a depth of 140 cm, at which point the presence of coarse gravel, prevented further coring. Excess ice contents ranged from 26 to 34% by volume. The complete borehole log is shown in Appendix B.

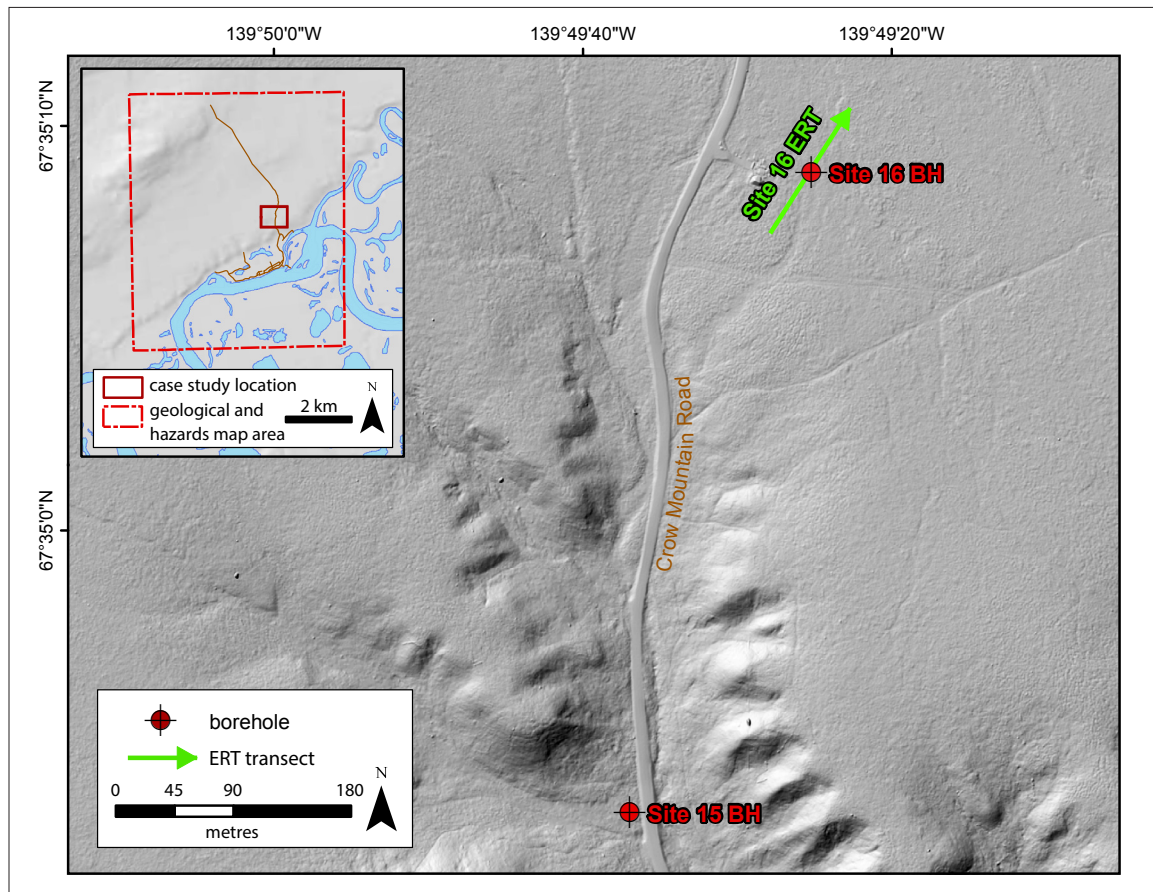


Figure 79. Overview of field investigation locations at Sites 15 and 16.

SITE 16

Site 16 is located on the east side of Crow Mountain Road (Figure 79), behind a house that was under construction at the time of field investigations. Vegetation at the site included shrubs (*Salix*, *Alnus*, *Betula*, *Rhododendron groenlandicum*) ranging from 50 cm to 1 m in height and a ground cover of moss, lichen, tall grass patches, and small shrubs less than 50 cm high (*Rhododendron groenlandicum*, *Vaccinium oxycoccos*).

A borehole (Site 16 BH) was drilled at this site. The active layer was composed of grey, silty sediment containing slightly decomposed organic matter. The permafrost table was encountered at a depth of 47 cm. Permafrost was composed of a very ice-rich sandy silt with lenticular and microlenticular cryostructure. High percentages of pebbles and cobbles (12 and 27%, respectively) were documented throughout the samples. The borehole was drilled to a depth of 225 cm, at which point the presence of coarse gravel prevented further coring. Excess ice contents were highest in the uppermost metre of the borehole, with values ranging from 16 to 58% by volume. Excess ice contents dropped significantly at the bottom of the borehole (11%), where the permafrost was dryer and had higher concentration of coarse gravel. The complete borehole log is shown in Appendix B.

SITE 17

Site 17 is located north of Site 16 and east of Crow Mountain Road (Figure 80). ERT and GPR surveys were run in a northeast direction; the surveys were run parallel and began 20 m east

of the road. The surveys were carried out through a mature, open forest of black spruce (up to 6 m high), with an understory of lichen, grass, shrubs (*Rhododendron groenlandicum*, *Vaccinium oxycoccos*), spruce seedlings and a ground cover of relatively thick moss (13 cm).

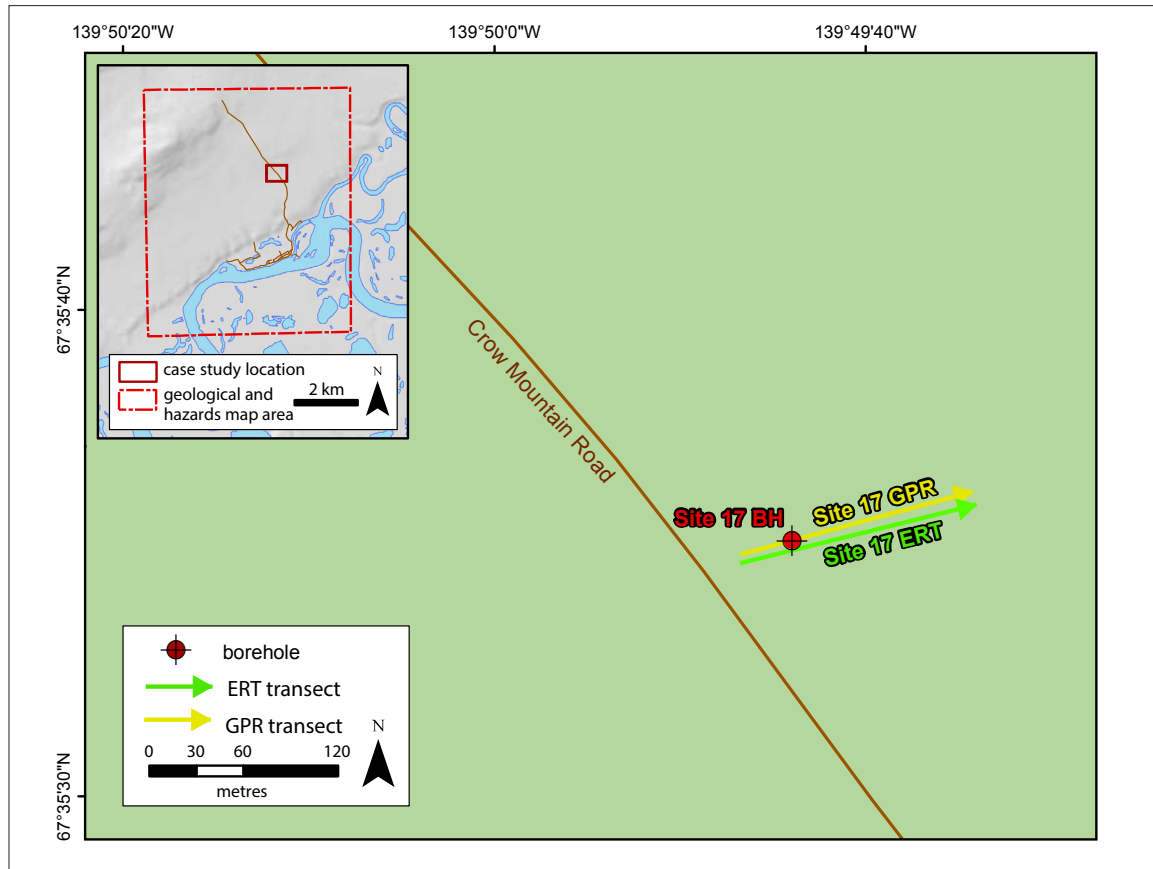


Figure 80. Overview of field investigation locations at site 17.

A borehole (Site 17 BH) was drilled to a depth of 294 cm, 38 m along the ERT transect. The permafrost table was encountered at a depth of 48 cm. The first metre below the permafrost table was composed of ice-rich sandy silt. Below this was a deposit of very ice-rich gravel in a sandy to silty matrix; this unit continued to the end of the borehole in a coarsening-downward sequence. At the base of the borehole, samples contained high concentrations of coarse material (49% cobbles). Ice volumetric content was at its highest within the first metre below the frost table, due to the high concentration of sandy silt; values ranged from 49-55% by volume (15 to 35% contained excess ice). Below, in sandy and gravelly deposits, the volumetric ice content values ranged from 23-52% (3 to 29% contained excess ice). At a depth of 105 cm, where volumetric ice content was the highest, thaw settlement and consolidation test results revealed 44% total settlement under a stress load of 25 kPa (theoretical value for this material type = 40%), and 48% under a stress load of 150 kPa. Deeper, in layers containing coarser material, thaw settlement and consolidation tests resulted in 15% total settlement under a stress load of 25 kPa (theoretical value = 5%), and 44% under a stress load of 150 kPa. The complete borehole log is shown in Appendix B.

The ERT profile from Site 17 shows a continuous, near-surface, low-resistivity layer underlain by higher resistivities that extend to the base of the profile at 25 m (Figure 81). The near-surface layer includes values that are indicative of unfrozen material. This layer thickens slightly at

approximately 120 m along the profile, a point that coincides with a depression at ground surface from an ATV/snowmobile trail. Depth to thaw ranged from 40 cm to 94 cm with an average of 64 cm. The permafrost is characterized by an upper layer of high resistivities (extending to depths of 8-10 m) underlain by moderate resistivities. The change in resistivity likely corresponds to a cryostratigraphic change from higher to lower ice contents.

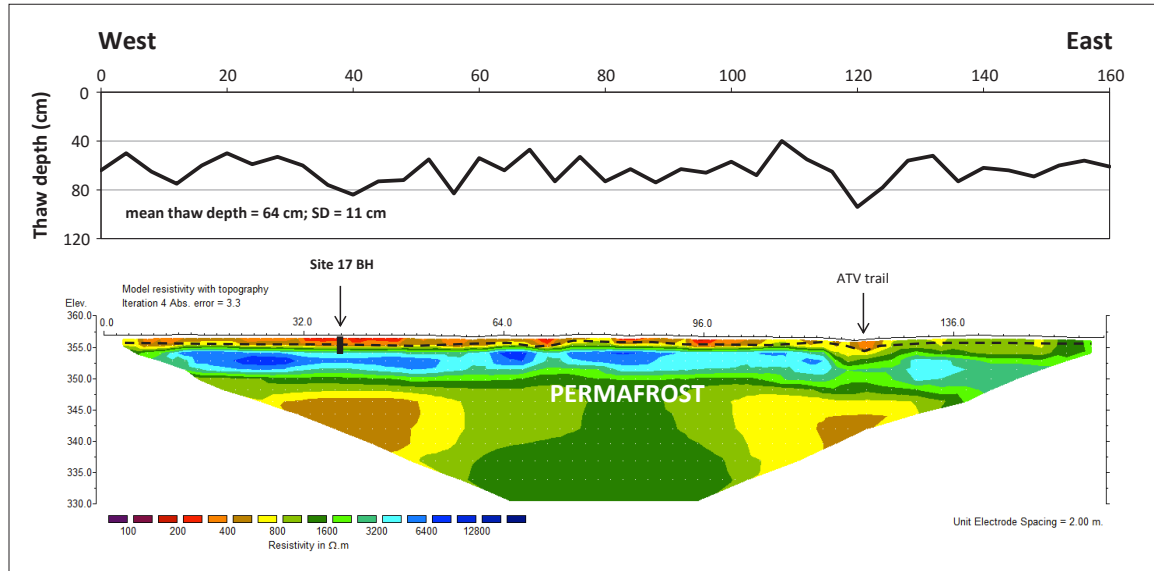


Figure 81. ERT profile for Site 17. The survey is 160 m long and has a maximum penetration depth of about 25 m. Black dashed lines outline likely areas of permafrost. SD = standard deviation.

The GPR profile at Site 17 depicts an irregular, strong reflector at a depth of about 50 cm, corresponding to the thaw front (see red line on Figure 82). A second strong reflector is located at a depth of 3 m and is interpreted as a stratigraphic contact with a gravel unit (see green line on Figure 82). This reflector also corresponds well with a clear change observed in the ERT profile. A vertical artifact located at about 78 m along the profile corresponds to the location of a meteorological station with buried thermistor cables. To display this profile, a velocity of 0.09 m/ns was used and an AGC gain (maximum gain of 200) was applied.

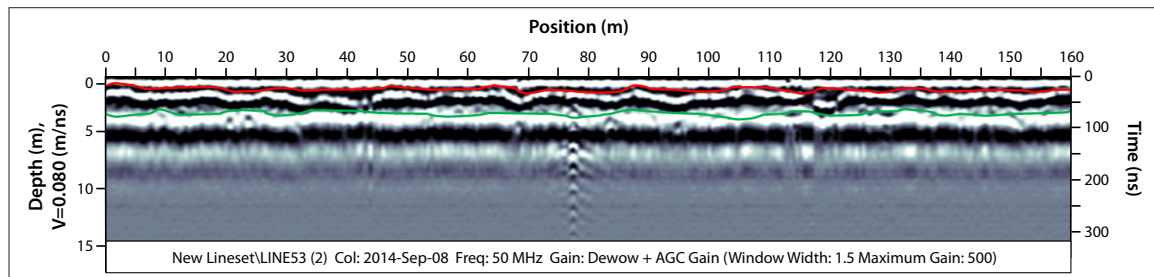


Figure 82. GPR profile for Site 17, displayed with an AGC gain (maximum gain of 200) and a velocity of 0.09 m/ns. The red line represents the thaw front and the green line represents a stratigraphic contact.

PORTAGE TRAIL

SITE 18

Site 18 is located 3 km downstream of Old Crow, approximately 600 m west of the bank of the Porcupine River (Figure 83). A 561 cm-deep borehole (Site 18 BH) was drilled through saturated, hummocky terrain. Ground cover consisted of moss, lichen, tall grasses and small shrubs (*Rhododendron groenlandicum* and *Vaccinium oxycoccos*). Also present were taller bushes (up to 1 m high) of *Betula*, *Salix* and *Alnus*, and isolated black spruce (*Picea mariana*) 1 to 4 m high.

Adjacent to the borehole, a Campbell Scientific meteorological station (CR1000, Wind Speed and Direction, Radiation, T-109 Air Temperature) was installed. The borehole was instrumented with a custom-made 11 channel thermistor string (measuring ground temperatures at depths of 0, 0.25, 0.5, 1, 1.5, 2, 2.5, 3, 4, 5, and 5.60 m), which was then connected to the meteorological station data logger.

In the borehole, the permafrost table was encountered at a depth of 35 cm, directly beneath the mossy ground cover. Permafrost stratigraphy consisted of interlaced layers of ice-rich, lenticular silty organic sand (from 101 to 258 cm), overlying layers of reticulate and suspended sandy organic silt (from 296 to 373 cm), and porous invisible coarse sand with gravel (from 394 to 561 cm). Pockets of porous invisible sandy organic silt were observed at the top of the permafrost from 70 to 101 cm, and deeper in the borehole from 258 to 296 cm. The silty sand with gravel deposits at the bottom of the borehole were very dry and ice poor, and had an average of 9% excess ice content, compared to 31% for the silty organic sand deposits near the top of the permafrost. Thick ice lenses (up to 3 cm) were observed in the sandy organic silt deposit in the middle of the borehole. Grain size analysis and ice content results are shown in Appendix B.

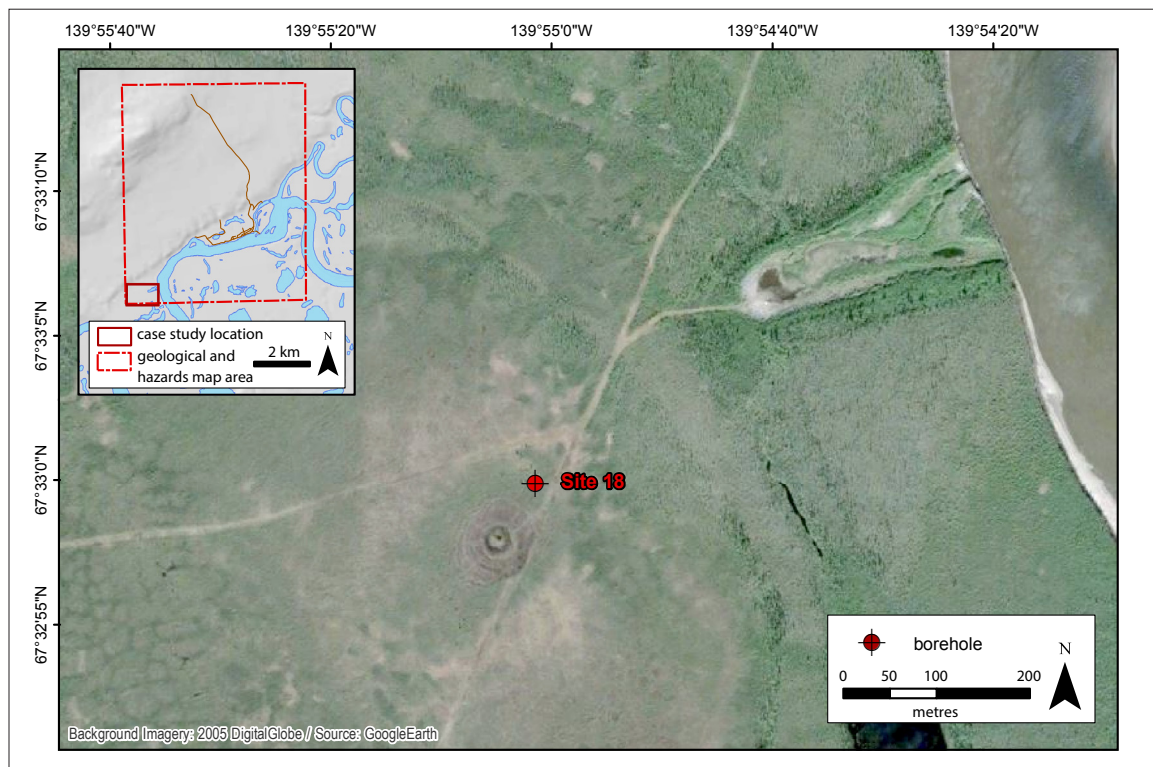


Figure 83. Location of borehole at Site 18 and meteorological station installed near Portage Trail.

HAZARD RISKS IN A CHANGING CLIMATE

PROJECTED CLIMATE CHANGE FOR THE OLD CROW REGION

Climate projection summaries are included for the Old Crow region in order to prepare for potential future changes in response to projected shifts in climate. Predicting future climate change around the globe has become a critical component in climate change science and adaptation. Scientists use a variety of Global Climate Models in combination with discrete scenarios in order to make a range of projections for numerous climate variables (e.g., temperature and precipitation). It is important to note, however, that due to uncertainty associated with climate models and natural variability in climate systems, climate projections are useful for examining trends over time rather than precise values at specific points in time.

GLOBAL CLIMATE MODELS

Global Climate Models (GCMs) – also referred to as Atmosphere-Ocean General Circulation Models – are mathematical representations of atmospheric and oceanic circulation in the world. There are several types of GCMs; however, three-dimensional global atmosphere and ocean models are most commonly used to generate future climate projections. GCMs are complex mathematical models that incorporate a wide range of climate variables including radiation, energy transfer by winds, cloud formation, evaporation and precipitation of water, and transport of heat by ocean currents (CCRUN, 2011). The model calculations are based on a complex grid system that covers the globe in both a horizontal and vertical dimension on the order of 200-500 km. Data for each grid box is input into the model equations to solve for atmosphere, land surface and oceans (CCRUN, 2011).

CLIMATE CHANGE SCENARIOS

In order to generate future climate projections, the Intergovernmental Panel on Climate Change – the leading international body for the assessment of climate change – developed several scenarios that outline a range of possible emission futures. In its fifth Assessment Report (AR5), the IPCC refers to these scenarios as Representative Concentration Pathways (RCP; IPCC, 2014). Each RCP is extrapolated to the year 2100, and represents a different future climate scenario based on an assumption about socioeconomic responses to climate change. The RCPs are labelled according to the radiative forcing values relative to pre-industrial values, and are referred to as RCP 2.6, RCP 4.5, RCP 6.0, and RCP 8.5. Each RCP scenario is summarized below (based on information provided by the Scenarios Network for Arctic and Alaska Planning (SNAP, 2016)):

- RCP 2.6: greenhouse gas emissions peak between 2010 and 2020 and then decline substantially. This is an unrealistic scenario and is not included in this report.
- RCP 4.5: greenhouse gas emissions peak around 2040 and then decline, and radiative forcing is stabilized shortly after 2100. This is considered a ‘low’ scenario.
- RCP 6.0: greenhouse gas emissions peak around 2080 and then decline, and radiative forcing is stabilized shortly after 2100. This is considered a ‘medium’ scenario.
- RCP 8.5: greenhouse gas emissions continue to rise throughout the 21st century. This is considered a ‘high’ scenario.

Projections based on RCP 4.5, 6.0 and 8.5 were regionally downscaled for the Old Crow region using PRISM as a baseline (see SNAP, 2016 for more details), and are summarized below.

Every RCP scenario projects temperature increases in all modelled decades (Figure 84). Temperature increases between 1.2°C and 3.1°C in January, and 0.8°C and 1.3°C in July, are projected to take place between the modelled historical period (1961-1990) and the current decade (2010-2019; Table 5), which is consistent with observations of on-going temperature change in the region. All projection models result in greater increases in temperature in winter than in summer; furthermore, there is a relatively steady increase in temperature regardless of projection and its associated socioeconomic scenario. By the decade 2090-2099, projections suggest temperature increases between 4.6°C and 7.9°C in January, and 2.1°C and 3.5°C in July (compared with the current decade, 2010-2019). Such temperature increases are likely to have profound effects on biophysical systems in the region, including hydrology, vegetation, permafrost and wildlife. Local observational data from the region identifies on-going concerns related to climate impacts on low-water levels in rivers and lakes, thawing permafrost, and changing wildlife abundance (Wolfe et al., 2011), which are very likely to be exacerbated by continued increases in temperature.

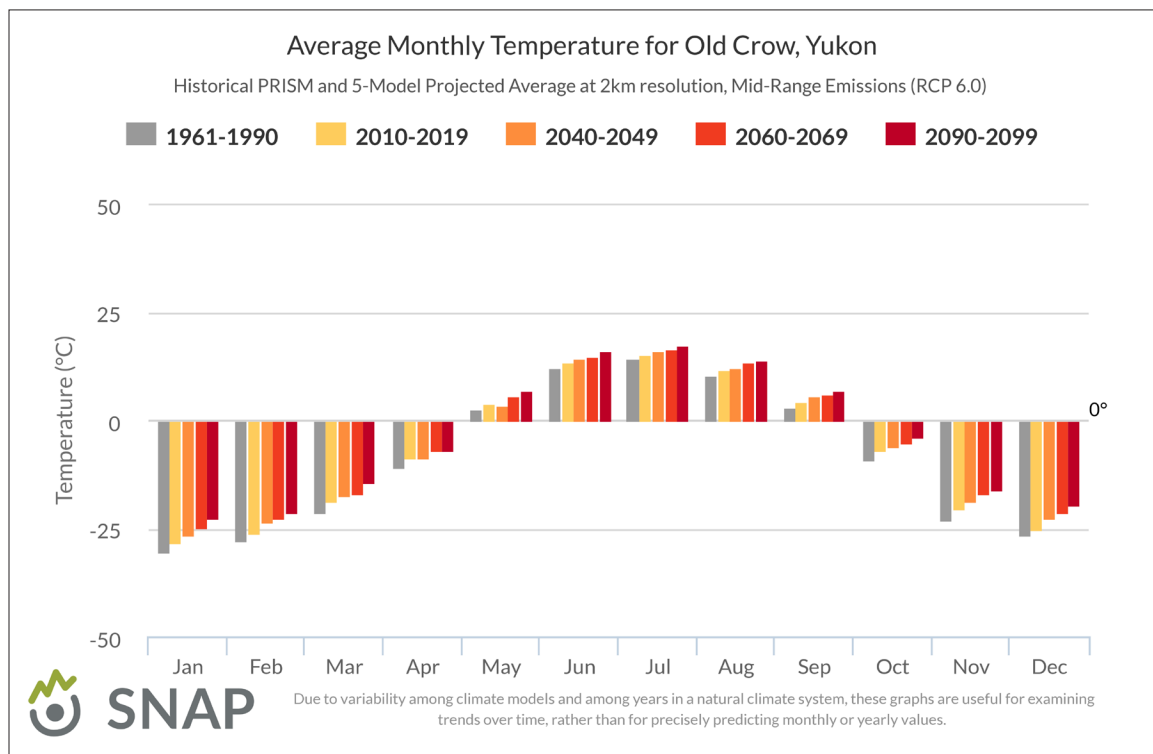


Figure 84. Summary showing historical and projected average monthly temperatures for Old Crow using historical PRISM data and the Intergovernmental Panel on Climate Change's Representative Concentration Pathway (RCP) scenario 6.0, downscaled to a 2 km resolution (see SNAP, 2016 for details). RCP 6.0 is shown here as a medium-range projection of potential temperature increases in a changing climate.

Table 5. Summary of projected increases in temperature for historical and future decades, based on data from SNAP (2016). Values in brackets indicate changes in temperature between the current (2010-2019) and projected decade.

| | Temperature (°C) | | | | |
|-----------------|------------------|-----------|-------------|-------------|-------------|
| | 1961-1990 | 2010-2019 | 2040-2049 | 2060-2069 | 2090-2099 |
| RCP 4.5 January | -33.8 | -32.6 | -28.5 (4.1) | -28.4 (4.2) | -28 (4.6) |
| RCP 6.0 January | -33.8 | -31.6 | -29.8 (1.8) | -28.1 (3.5) | -25.9 (5.7) |
| RCP 8.5 January | -33.8 | -30.7 | -27.9 (2.8) | -25.9 (4.8) | -22.8 (7.9) |
| RCP 4.5 July | 13.8 | 14.6 | 15.9 (1.3) | 16.2 (1.6) | 16.8 (2.2) |
| RCP 6.0 July | 13.8 | 15 | 15.7 (0.7) | 16.4 (1.4) | 17.1 (2.1) |
| RCP 8.5 July | 13.8 | 15.1 | 16.8 (1.7) | 17.5 (2.4) | 18.6 (3.5) |

As with temperature projections, RCP scenarios for precipitation also show increasing precipitation throughout most scenarios, regardless of scenario or decade modelled (Figure 85). However, projected precipitation values between the modelled historical period (1961-1990) and the current decade (2010-2019; Table 6) do not show notable increases for January; in fact, the RCP 4.5 scenario shows a decrease in precipitation over the period of -1 mm, while the highest scenario (RCP 8.5) shows a modest increase of 1 mm. However, all scenarios show increases in July precipitation over the period noted above, with highest increases under the RCP 4.5 scenario (+8 mm). Between the current decade (2010-2019) and 2090-2099, January precipitation is projected to increase between 1 and 2 mm, while July precipitation is expected to increase between 2 and 10 mm. Wetter summers may increase open-water flood risk, vegetation patterns, and active layer detachments like those that have already taken place near Old Crow (e.g., Rosalie's slide).

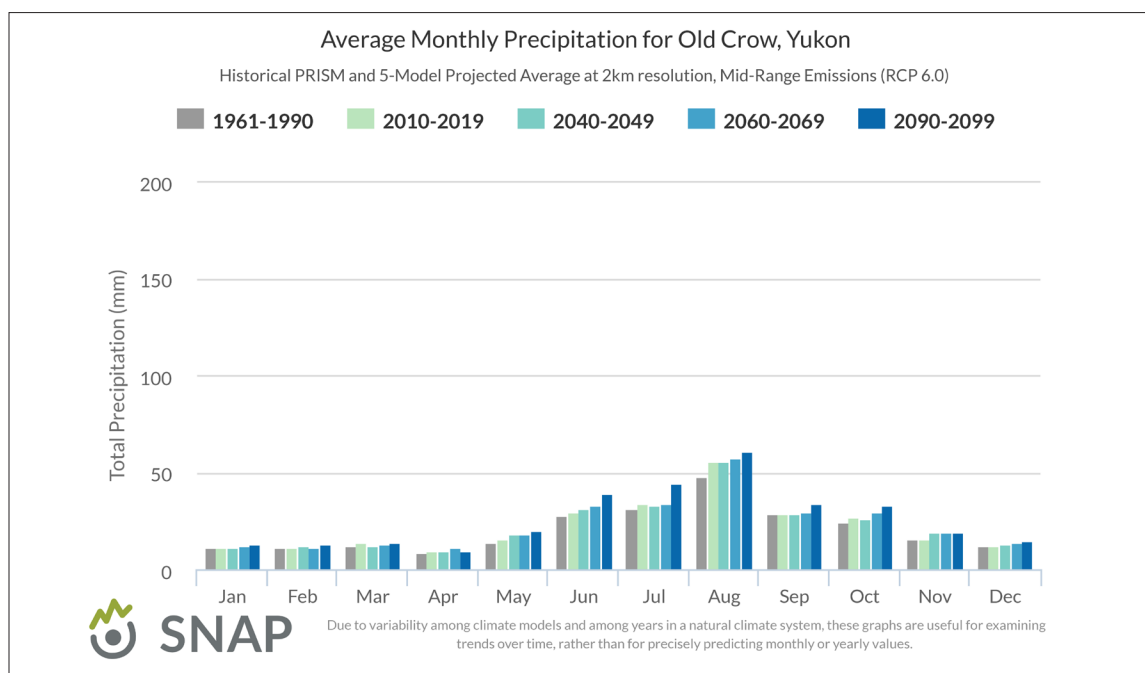


Figure 85. Summary showing historical and projected average monthly precipitation for Old Crow using historical PRISM data and the Intergovernmental Panel on Climate Change's Representative Concentration Pathway (RCP) scenario 6.0, downscaled to a 2 km resolution (see SNAP, 2016 for details). RCP 6.0 is shown here as a medium-range projection of potential precipitation change in a changing climate.

Table 6. Summary of projected changes in precipitation for historical and future decades, based on data from SNAP (2016). Values in brackets indicate changes in precipitation between the current (2010-2019) and projected decade.

| | Precipitation (mm) | | | | |
|-----------------|--------------------|-----------|-----------|-----------|-----------|
| | 1961-1990 | 2010-2019 | 2040-2049 | 2060-2069 | 2090-2099 |
| RCP 4.5 January | 11 | 10 | 13 (3) | 14 (4) | 12 (2) |
| RCP 6.0 January | 11 | 11 | 11 (0) | 12 (1) | 13 (2) |
| RCP 8.5 January | 11 | 12 | 12 (0) | 13 (1) | 13 (1) |
| RCP 4.5 July | 31 | 39 | 40 (1) | 39 (0) | 41 (2) |
| RCP 6.0 July | 31 | 34 | 33 (-1) | 34 (0) | 44 (10) |
| RCP 8.5 July | 31 | 36 | 36 (0) | 46 (10) | 45 (9) |

IMPLICATIONS OF CLIMATE CHANGE FOR HAZARDS IN THE OLD CROW REGION

Under the projected climate scenarios presented in this report, risks associated with surficial materials are variable and primarily related to the effects of changing soil moisture and surface runoff on terrain stability. In general, terrain stability declines with increased soil moisture and/or surface runoff, both of which can be caused by thawing of ice-rich permafrost, and changing hydrological regimes (including streamflow, flooding, groundwater flow, seasonal precipitation patterns and extreme snowmelt and rainfall events).

Changes in permafrost strongly affect surface and groundwater drainage and can cause near-surface soils to become either wetter or drier depending on site conditions. In ice-rich permafrost, active layer thickening may increase soil moisture and decrease slope stability, whereas in ice-poor permafrost, deepening of the active layer may actually improve local drainage capacity and increase surface slope stability. Increases in regional moisture delivery could also raise stream levels which, in turn, may enhance incision or aggradation rates, and erosion on stream banks. Changes in the amount or seasonal timing of precipitation, snowmelt and sediment supply may also increase stream channel instability and migration, undercutting and oversteepening of cutbanks and initiation of landslides.

The ‘temperature at the top of permafrost-modelling’ (TTOP) described above (see *Contemporary Permafrost Temperature Modelling*, p. 34) suggests that the permafrost in Old Crow is more vulnerable to thaw than might be expected given the community’s location in the continuous permafrost zone. For example, if a site’s organic material is stripped, the ratio of thawed to frozen thermal conductivity of the ground will increase. If this reaches 0.85 at the elevation of the airport, the temperature at the top of permafrost becomes greater than 0°C. This explains results such as the talik development around the abandoned log homes at Site 4, as well as the thin permafrost at Site 6 indicating TTOP values close to 0°C along the bank of the Porcupine River.

In terms of climate change, the measured thawing and freezing factors in the forest zone indicate that one thawing degree-day increase in summer has four times the warming impact of one less freezing-degree day in winter. Global climate models for arctic regions predict the reverse, with much more warming in winter than in summer. The impact of this winter warming on permafrost, however, will be greatly buffered by the snow cover.

Extreme rainfall and heating events will also trigger landslides by rapidly saturating soils, especially in areas where groundwater can accumulate, such as in gullies or depressions, or where drainage is limited by shallow permafrost or impermeable lacustrine sediments. Changes to existing drainage

patterns in ways that concentrate water into channels will have detrimental impacts on slope stability along the Old Crow escarpment. In particular, road building in the existing gullies could result in increased slope instability in the overall gully system and threaten homes on the fans at the mouths of the gullies.

Flooding is an ongoing concern in the study area. With climate change, the intensities and frequency of this flooding will likely be less predictable. In addition, thermokarst development and channel migration may also pose significant hazards to any future development in the valley-bottoms. The projected degradation of near-surface permafrost will increase the hazard associated with periglacial processes, including active layer detachment slides, sheetwash and thermokarst erosion.

INTEGRATING RISK IN A LANDSCAPE HAZARDS MAP FOR THE OLD CROW REGION

Landscape hazards for the Old Crow study area are modelled using a Geographic Information System (GIS) to generate an integrated risk ranking for each landscape 'unit' (defined by 30 m² pixels). Input data for the model include the following datasets: slope angle (steepness); slope aspect (directionality); and surface materials (derived from geological maps).

Attributes of the individual datasets are classified on a 1-10 scale of potential risk, where one represents a low risk of landscape hazard and ten represents a high risk of landscape hazard. High-risk landscape units include steep or unstable slopes, low-lying areas subject to flooding or inundation by water, and landscape units with a high likelihood of being affected by ice-rich or thaw-unstable permafrost. Low-risk areas are predicted to have favourable conditions for landscape development and include areas with well-drained soils, gentle or moderate slopes, and a low likelihood of containing ice-rich or thaw-unstable permafrost. However, additional site-specific geotechnical investigations are still necessary before development, even in low-risk areas.

INPUT DATA

Slope angle

Slope rankings are summarized in Table 7, and are based on the values recommended by the British Columbia Terrain Classification System (Howes and Kenk, 1997). Steep slopes were ranked the highest value possible (10), followed by moderately steep slopes (8), moderate slopes (6), gentle slopes (3), and flat to gentle slopes (1). Slope angles were computed and assigned rankings using a digital elevation model with a pixel resolution of 30 m² (30 m DEM). Figure 86 depicts ranked risks associated with slope angle for the study area.

Table 7. Hazard risk rankings associated with different slope angles for the Old Crow region.

| Description of Surface | Slope Percentage | Slope Degree | Classified Value |
|---------------------------|------------------|--------------|------------------|
| flat to gently undulating | 0-5 | 0-3 | 1 |
| gentle slope | 6-27 | 4-15 | 3 |
| moderate slope | 28-49 | 16-26 | 6 |
| moderately steep slope | 50-70 | 27-35 | 8 |
| steep slope | >70 | >35 | 10 |

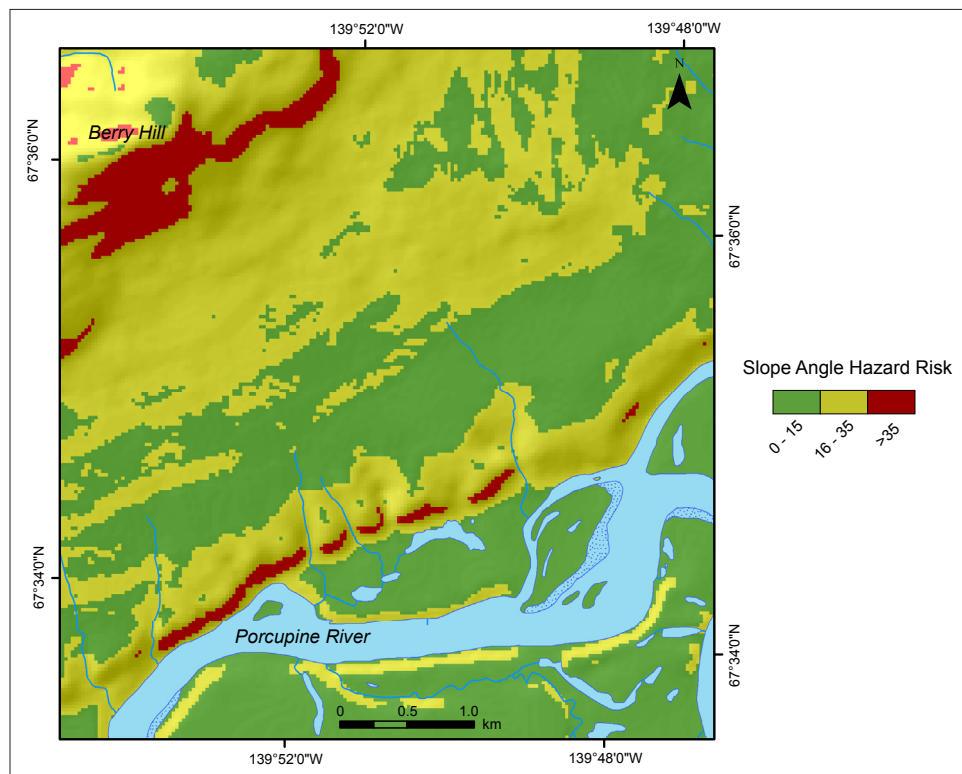


Figure 86. Hazard risk associated with slope angle for the Old Crow region.

Slope aspect

Aspect rankings were developed by identifying warmer slopes that are more susceptible to permafrost thaw (Table 8). While permafrost is prevalent throughout the study region and therefore all slopes in the study area contain permafrost, colder aspects (north, northwest, northeast and east) receive the least solar radiation and are therefore more likely to have colder, less thaw-sensitive permafrost compared with warmer aspects. In contrast, warmer aspects (south, west, and southwest) receive the most sunlight and are likely more susceptible to permafrost thaw than colder aspects. Figure 87 depicts ranked risks associated with slope aspect for the study area.

Table 8. Hazard risk rankings associated with different slope aspects for the Old Crow region.

| Slope Direction | Slope Orientation (degrees) | Classified Value |
|-----------------|-----------------------------|------------------|
| flat | no slope (0) | 1 |
| northwest | 295-340 | 2 |
| northeast | 25-70 | 2 |
| north | 340-25 | 2 |
| east | 70-115 | 2 |
| southeast | 115-160 | 6 |
| west | 250-295 | 8 |
| southwest | 205-250 | 10 |
| south | 160-205 | 10 |

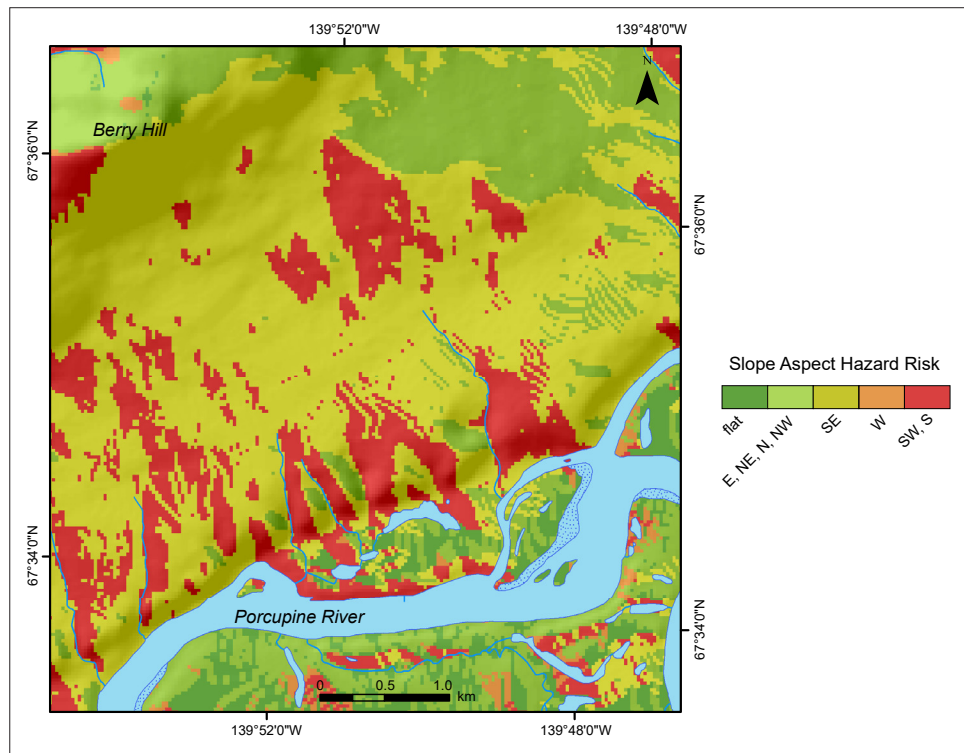


Figure 87. Hazard risk associated with slope aspect for the Old Crow region.

Surficial materials

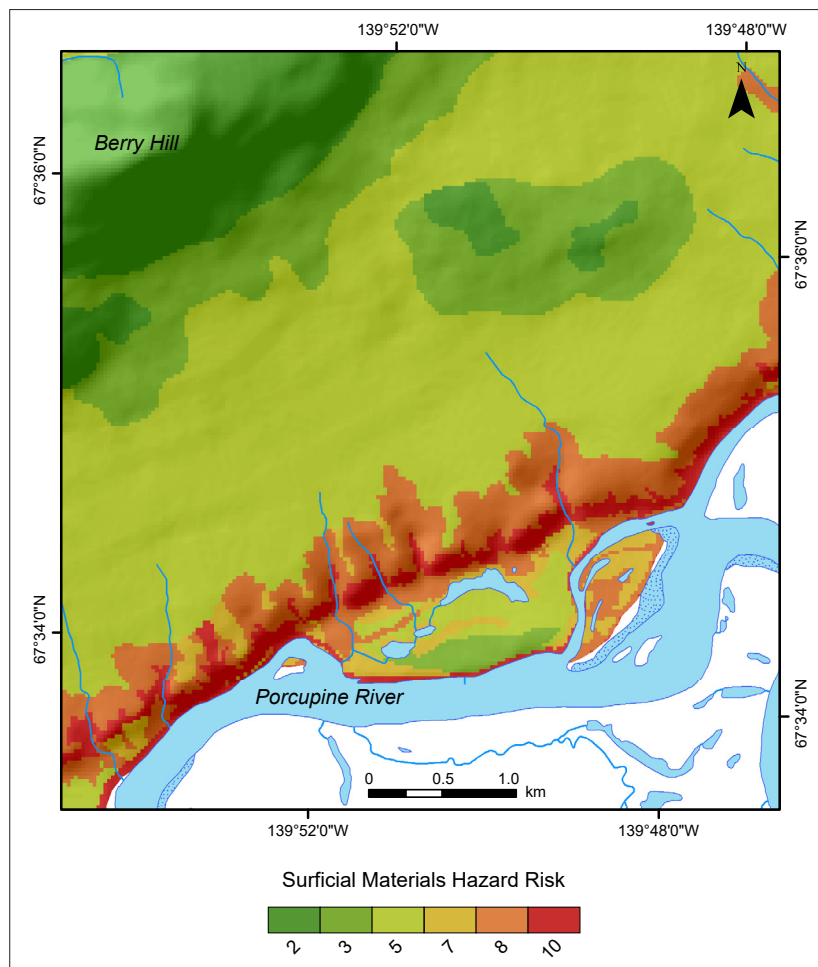
Hazard risk rankings associated with surficial materials were determined based on a combination of material textures (e.g., fine or coarse-grained), material composition, landform shape (e.g., potential for drainage), landform location (e.g., slope position), and geological processes acting on the materials (e.g., permafrost, seasonal or regular inundation by water, mass movement processes); these are summarized in Table 9. In general, any geological units that were modified by landslides, thermokarst, ice-wedge polygons, or inundation were ranked at the highest level (9). Poorly drained, fine-grained materials in valley-bottom positions were also ranked at high levels (7-9). Field investigations suggest that these units are often ice rich and sometimes have notable thaw settlement potential. Most hillslope and colluvial materials, where ice content of permafrost can be highly variable, were ranked at intermediate levels (4-7). The lowest ranked (least risk) geological units include coarse fluvial terrace landforms above the floodplain, and weathered bedrock and coarse-grained (rubble) colluvium overlying bedrock (1-3). Figure 88 depicts ranked risks associated with surficial materials for the study area.

Table 9. Hazard risk rankings associated with different surficial materials for the Old Crow region.

| Geological Process and Materials | Classified Value |
|----------------------------------|------------------|
| landslides | 10 |
| tension cracks | 10 |
| thermokarst | 10 |
| ice-wedge polygons | 10 |
| inundation (flooding) | 10 |
| active floodplain | 9 |

Table 9, continued. Hazard risk rankings associated with different surficial materials for the Old Crow region.

| Geological Process and Materials | Classified Value |
|---|------------------|
| lacustrine materials | 7 |
| gully erosion | 7 |
| colluvial materials and landforms | 7 |
| permafrost | 5 |
| fine-grained fluvial materials | 5 |
| coarse-grained fluvial materials | 3 |
| periglacial processes and bedrock materials | 3 |

**Figure 88.** Hazard risk associated with surficial materials for the Old Crow region.

MODELLING

The model process used to generate cumulative hazard risk rankings for the study area is depicted in Figure 89. Each of the input datasets described above was assigned a unique weighting in the model to describe the degree to which they control cumulative landscape risk. For this model, slope angle (the steepness of the landscape) was given a weighting of 25%. Slope aspect (the degree to which the landscape is exposed to sunlight) was given a weighting of 15%. Surface

materials have a significant impact on landscape stability, and integrate permafrost and flood characteristics. As a result, this input was given a weighting of 60%.

To calculate cumulative hazard risk for the study area, the weightings for each input layer were combined as follows:

$$\text{Cumulative Ranking} = 0.25(\text{slope angle}) + 0.15(\text{slope aspect}) + 0.6(\text{surface materials})$$

Combining the individual rankings of each input raster, multiplied by their unique weighting, results in a cumulative hazard ranking for the landscape ranging from 1 (low) to 8 (high). The cumulative rankings were reclassified into four categories (low, moderate, moderately high, and high) that represent potential hazard due to permafrost, slope stability, and flooding in the map area (Table 10). The model represents current conditions, and does not integrate any potential changes to landscape stability associated with a changing climate.

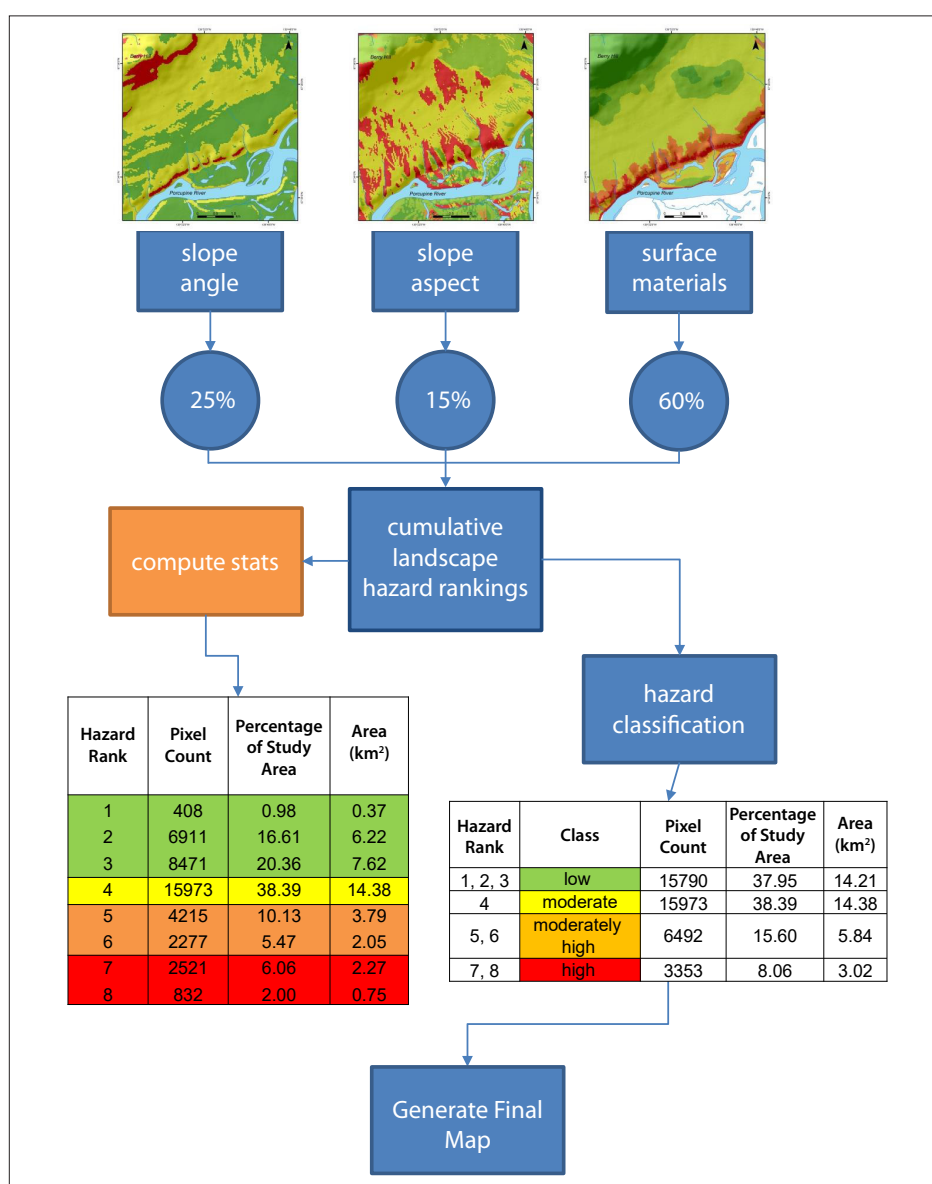






Figure 89. Flowchart illustrating the process used to create the cumulative hazard risk map out of model input parameters for the Old Crow region.

Table 10. Hazard risk categories assigned to cumulative risk rankings for the Old Crow region. Cumulative hazard risk rankings refer to the combined risks of slope aspect, slope angle and surficial material risk.

| Hazard Risk | Cumulative Hazard Risk Ranking |
|-----------------|--------------------------------|
| low | 0, 1, 2, 3, 4 |
| moderate | 5 |
| moderately high | 6 |
| high | 7, 8, 9 |

HAZARD RISK RANKINGS FOR THE OLD CROW REGION

Based on the modelling exercise described above, the study region was classified into four colour-coded categories representing hazard risk. These categories are characterized as follows:

-  **Low-Risk** terrain in the Old Crow area is characterized by flat to gently sloped terrain comprised of well-drained gravel or weathered bedrock surface materials. Low-risk terrain contains permafrost that may be ice rich, but it is less likely to be affected by flooding and mass movement than more hazardous terrain in the map area.
-  **Moderate-Risk** terrain in the Old Crow area is characterized by gentle to moderate slopes with moderate to poor drainage. Moderate-risk terrain is found on the pediment slopes of Berry Hill, as well as on poorly drained parts of the fluvial terrace near the North Road and school subdivisions. Moderate-risk terrain contains finer grained material compared with material found in low-risk terrain, and is almost always affected by permafrost with high potential for thaw settlement.
-  **Moderately High-Risk** terrain in the Old Crow area is characterized by moderate to steep slopes with all slope aspects. Moderately high-risk terrain is found on the steep escarpment above town, and in areas subject to regular flooding. Moderately high-risk terrain contains permafrost and is subject to landslides related to poor slope drainage and permafrost thaw. The difference between moderate and moderately high-risk terrain in the study area is largely related to landslide susceptibility.
-  **High-Risk** terrain in the Old Crow area is characterized by steep slopes and warm aspects (i.e., west and south facing). It is characterized by an increased risk of landslides. High-risk terrain in the study area occurs in areas with documented landslide debris, paths, or features of slow mass movement such as tension cracks. High-risk terrain contains both permafrost and fine-grained surficial materials on steep to very steep slopes that can easily generate landslides with significant run-out distances.

The hazard map for the Old Crow study area is comprised of 41,608 individually classified 30 m² pixels in a total map area of 37.4 km². Of these, 38% (14.2 km²) are classified as low-risk terrain, 48% (18.2 km²) are classified as moderate-risk terrain, 6% (2 km²) are classified as moderately high-risk terrain, and 8% (3 km²) are classified as high-risk terrain. Results are summarized in Table 11. A subset of the hazard map is included in Figure 90, and the full map (Landscape Hazards Risk Old Crow, Yukon; Kennedy, 2016) accompanies this report.

Table 11. Statistics summarizing cumulative hazard risk rankings by category and area for the Old Crow region.

| Hazard Rank | Class | Pixel Count | Percentage of Study Area | Area (km ²) |
|-------------|-----------------|-------------|--------------------------|-------------------------|
| 1, 2, 3 | Low | 15790 | 37.95 | 14.21 |
| 4 | Moderate | 15973 | 38.39 | 14.38 |
| 5, 6 | Moderately High | 6492 | 15.60 | 5.84 |
| 7, 8 | High | 3353 | 8.06 | 3.02 |

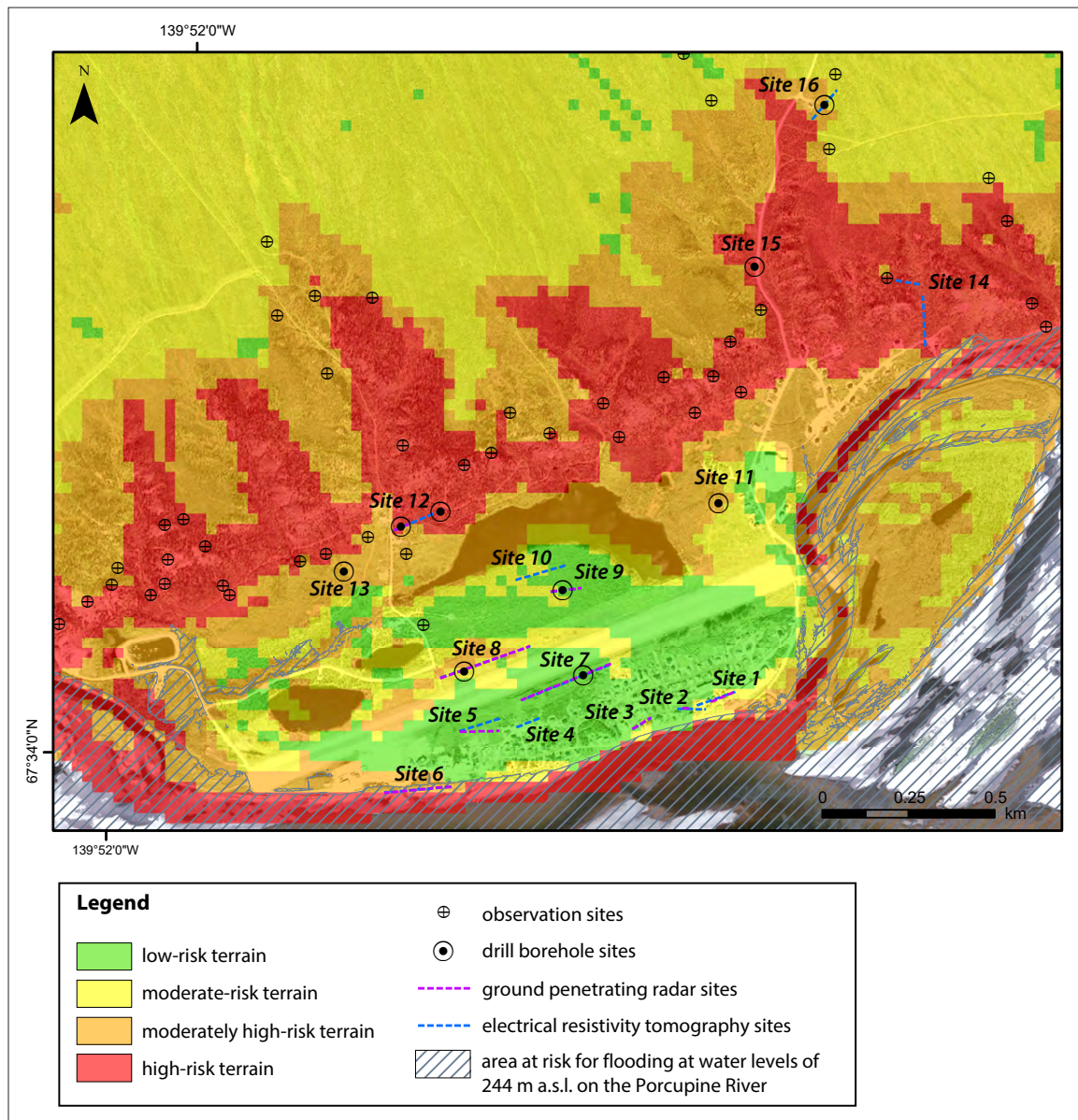


Figure 90. Map depicting a subset of the mapped hazard risk rankings for the Old Crow region. A complete version of this map, covering the entire study area, is included in the map pocket at the back of this report, and is available online at yukoncollege.yk.ca/research.

Hazard risks in the region align with site-specific findings. Much of the Old Crow community core is ranked as having a low hazard risk. Risks associated with surficial materials are low, given that most of the area is situated on a fluvial terrace, and slope angle and aspect are also ranked as low risk. Furthermore, the community core is generally above the floodplain of the Porcupine River, so flood risk is low. The area is underlain by continuous permafrost, and the coarse material making up the fluvial terrace is usually not frost-sensitive. Permafrost cores from the area were relatively ice poor for the first few metres, and the seasonal thaw depth appears to be relatively deep (1-4 m). Taliks (areas of permanently thawed ground under the seasonally thawed layer but above permafrost) have developed in many locations. While this indicates that permafrost in the community core is sensitive to thaw upon disturbance, existing taliks are likely to be fairly stable and not advancing rapidly, and may therefore represent relatively low risk. This area may be suitable for development (e.g., by infill on existing unused pads), if it is done in such a way as to mitigate additional future thaw (see Appendix C for details).

Hazard risk is also generally low along the North Road and vicinity, although there are some moderate and moderately high-risk areas that are generally associated with zones where standing water was present in historical air photos. As with the community core, risks associated with surficial geology, slope angle and slope aspect are low throughout most of the area. Given the distance from the river, flood risk is also relatively low to all but the most extreme floods (e.g., 245.6-246 m). In most areas in the vicinity of the North Road, the seasonal thaw depth was less than 1 m (and sometimes less than 50 cm), and ice content of sediments was generally moderate to ice rich, overlying ice-poor materials. Taliks were identified in this area, and are typically associated with surface drainage, snow accumulation, and potential groundwater connections within and through permafrost. As with the community core, the presence of taliks here indicates the sensitivity of permafrost to thaw. However, surface materials are finer grained compared with those areas of the community that are closer to the river, and there are fewer localities that have been developed, resulting in less time for the establishment of deep taliks. Consequently, development in this area should integrate thaw mitigation techniques (see Appendix C), and the continued development of taliks under building pads should be anticipated. On-going monitoring of permafrost temperatures under the pad at site 9 will be useful in identifying possible permafrost thaw associated with pad construction.

Hazard risk in the vicinity of the ski lodge is moderately high to high. This is due to the presence of steep, often west and south-facing slopes where landslide risk is high. Numerous tension cracks were noted in the slopes north of the ski lodge, and persist along the bluff bordering the community. Nearby surface features indicate evidence of past landslides, some which are quite recent such as Rosalie's slide. This terrain is composed of fine-grained material with ice-rich permafrost, and local surface drainage features appear to have warmed shallow permafrost. Ice content and thaw settlement potential in sites at the base of slopes (e.g., Sites 12 and 13) were relatively high, and, as with other areas, the potential for permafrost thaw with disturbance is notably high. While this area is unlikely to be flooded during even the highest flood events, water movement downslope can trigger landslides with significant run-out distances. For example, extreme rainfall events have been associated with past slide activity in the area; increased frequency of extreme events as a result of a changing climate (IPCC, 2014) may exacerbate hazards in this region. Development in this area should be minimized as much as possible, and care should be taken to ensure any development that does take place is situated out of landslide run-out zones.

Hazard risk in the Crow Mountain Road area and vicinity is variable, and generally decreases with elevation and proximity to the top of Crow Mountain. As with the area in the vicinity of the ski lodge, much of the terrain along the bluff on the southern, lower part of the road is classified as moderately high or high risk. This is due to the presence of steep slopes, documented landslide

activity, the presence of tension cracks, and the occurrence of permafrost which is commonly ice rich. As described above, hazard risk in this area can be exacerbated by water movement downslope, and development should be minimized or avoided. It is also important to note that quad trails in gullies increase erosion, and may exacerbate permafrost thaw associated with drainage and disturbance.

Hazard risk generally declines with elevation up the Crow Mountain Road. North of Site 16, hazard risk becomes moderate. Slope angle and aspect both present moderate risk (although some areas of high risk associated with south and southwest-facing slopes are manifest in this area). Surficial material hazard risk is also moderate, as a result of the presence of a distributed pattern of drainage and surface sheetflow. Hazard risk continues to decline with elevation where there is more bedrock exposure, and permafrost in bedrock is typically ice poor. Low-risk terrain along Crow Mountain Road may be suitable for development, and development on moderate risk terrain should be done in such a way as to mitigate permafrost thaw and preserve natural drainage patterns (e.g., linear infrastructure should not be situated perpendicular to drainage).

LIMITATIONS

The Old Crow hazards map is meant to be used as a preliminary assessment of potential ground conditions in the study area, and does not replace detailed on-site investigations. Cumulative hazard rankings are highly dependent on rankings assigned to surface material units, and both the boundaries of the units and the materials assigned to those units are highly subjective and based on limited field checking conducted during surficial geological mapping studies.

Additionally, flood hazard mapping was not incorporated into the hazard model and flood potential is based on geological units mapped as active floodplains or as being subject to periodic inundation. These units likely represent areas that are subject to regular annual or decadal flooding, but are unlikely to represent the highest and most catastrophic floods with lower recurrence intervals.

Finally, the resolution of this map is limited by the 30 m² pixel size used to calculate slope and aspect, and the 1:10 000-scale mapping used to identify surficial materials and landforms. Local variations in all model inputs should be expected, and will be more pronounced for surface materials.

It is important to note that cumulative hazard rankings are based on general observations of surface materials, drainage, slope angle, vegetation and the presence of permafrost landforms, as well as subsurface information provided by ERT and GPR profiles, drilling and probing of permafrost, and textural analyses of surficial and borehole samples. This has resulted in a projected risk ranking that will require geotechnical and/or engineering analyses to quantify.

The hazards map for the Old Crow region is presented in Figure 90, as well as in a larger print version in the back pocket of this report.

GENERATING ACTION FROM SCIENCE

The knowledge and data generated by the Old Crow hazards mapping project can be used to inform planning and policy development and establish a baseline from which future science can be generated. It is the hope of the authors that the information contained herein informs planning and decision-making processes in the Old Crow area.

This project has contributed to the assessment of vulnerability for the Old Crow area. In particular, this project has characterized the local landscape and assessed local hazards, while advancing our understanding of potential climate change impacts in the region. This information may serve as a

basis for evaluating how community infrastructure, security and well-being may be influenced by climate variability, and how the community might take action to respond. By integrating variability into decision-making through multiple scenarios, robust and responsive adaptation strategies can be developed. In this way, the science of hazards assessment is an important foundation from which to build action.

BLANK PAGE

REFERENCES

- Belatos, S. and Prowse, T., 2009. River-ice hydrology in a shrinking cryosphere. *Hydrological Processes*, vol. 23, p. 122-144.
- Bonnaventure, P.P., Lewkowicz, A.G., Kremer, M. and Sawada, M., 2012. A regional permafrost probability model for the southern Yukon and northern British Columbia, Canada. *Permafrost and Periglacial Processes*, vol. 23, p. 52-68, doi:10.1002/ppp.1733.
- Bradberts, T.P., Wang, B. and Meade, R.H., 2000. Environmental and Hydrologic Overview of the Yukon River Basin, Alaska and Canada. US Geological Survey, Water Resources Investigations Report 99-4204, 106 p.
- Brown, R.J.E., 1963. Influence of vegetation on permafrost. First International Conference on Permafrost, Lafayette, PA, November 1963.
- Brown, R.J.E. and Péwé, T.L., 1973. Distribution of permafrost in North America and its relationship to the environment: A review, 1963-1973. Second International Conference on Permafrost, Yakutsk, USSR, July 1973.
- Brown, J., Ferrians, Jr., O.J., Heginbottom, J.A. and Melnikov, E.S. (eds.), 1997. Circum-Arctic map of permafrost and ground-ice conditions. Washington, DC: US Geological Survey in Cooperation with the Circum-Pacific Council for Energy and Mineral Resources, Circum-Pacific Map Series CP-45, scale 1:10 000 000, 1 sheet.
- Colpron, M. (compiler), 2016. Update of the Yukon bedrock geology map. Yukon Geological Survey, http://www.geology.gov.yk.ca/update_yukon_bedrock_geology_map.html.
- Committee, I., 2012. River and lake ice in the Arctic. [<http://www.eoearth.org/view/article/155762>]. Accessed February, 2016.
- Consortium for Climate Risk in the Urban Northeast (CCRUN), 2011. What methods do scientists use to make projections about future climate change and its impacts? CCRUN, Fact Sheet #4, Columbia University, New York, NY, 3 p. [http://ccrun.org/ccrun_files/attached_files/FactSheet4.pdf]. Accessed September, 2014.
- Duk-Rodkin, A., Barendregt, R.W., Froese, D.G., Weber, F., Enkin, R., Smith, I.R., Zazula, G.D., Waters, P., Klassen, R., 2004. Timing and extent of late Plio-Pleistocene glaciations in north-western Canada and east-central Alaska. *In*: J. Ehlers and P.L. Gibbard (eds.), *Quaternary Glaciations – Extent and Chronology, Part II*, p. 313-342.
- Duk-Rodkin, A., Barendregt, R.W., Tarnocai, C. and Phillips, F.M., 1996. Late Tertiary to Late Quaternary record in the Mackenzie Mountains, Northwest Territories, Canada: stratigraphy, paleomagnetism, and chlorine-36. *Canadian Journal of Earth Sciences*, vol. 33, p. 875-895.
- Duk-Rodkin, A. and Hughes, O.L., 1995. Quaternary geology of the northeastern part of the central Mackenzie Valley Corridor, District of Mackenzie, Northwest Territories. *Geological Survey of Canada Bulletin*, 458, 45 p.
- EBA Engineering Consultants Ltd., 2012. Old Crow landslide assessment, impacts and recommendations. EBA Engineering Consultants Ltd., Whitehorse, Yukon. Unpublished report prepared for Vuntut Gwitchin Government, EBA File W14101482, 41 p.
- Environment Canada, 2014a. Historical Climate Data. Environment Canada, Ottawa, Ontario. [http://climate.weather.gc.ca/index_e.html]. Accessed December, 2015.

- Environment Canada, 2014b. Climate Trends and Variations. Environment Canada, Ottawa, Ontario. [<http://ec.gc.ca/adsc-cmda/default.asp?lang=En&n=F3D25729-1>]. Accessed December, 2015.
- Fortier, D. and Allard, M., 2004. Late Holocene syngenetic ice-wedge polygons development, Bylot Island, Canadian Arctic Archipelago. *Canadian Journal of Earth Sciences*, vol. 41, p. 997-1012.
- Fred, J. (compiler), 2014. First Nations Community Profile: Vuntut Gwitchin First Nation-Community of Old Crow. Government of Yukon and Statistics Canada Training Program, Whitehorse, Yukon, 18 p.
- French, H.M., 1983. *The Periglacial Environment*. Longman Group Limited, London, 309 p.
- French, H., 2007. *The Periglacial Environment*, 3rd edition. John Wiley and Sons, West Sussex, England, 478 p.
- French, H. and Shur, Y., 2010. The principles of cryostratigraphy. *Earth Science Reviews*, vol. 101, p. 190-206.
- Froese, D.G., Barendregt, R.W., Enkin, R.J. and Baker, J., 2000. Paleomagnetic evidence for multiple late Pliocene-early Pleistocene glaciations in the Klondike area, Yukon Territory. *Canadian Journal of Earth Sciences*, vol. 37, 863-867.
- Gartner Lee Limited, 2003. Yukon Groundwater and Ground Source Heat Potential Inventory. Prepared for Energy Solutions Centre Inc., Report #GLL 22-680.
- Government of the Vuntut Gwitchin First Nation, 2015. [<http://www.vgfn.ca/index.php>]. Accessed November, 2015.
- Hauck, C., Isaksen, K., Vonder Mühll, D. and Sollid, J.L., 2004. Geophysical surveys designed to delineate the altitudinal limit of mountain permafrost: an example from Jotunheimen, Norway. *Permafrost and Periglacial Processes*, vol. 15, p. 191-205. DOI:10.1002/ppp.493.
- Heginbottom, J.A., Dubreuil, M.A. and Harker, P.T., 1995. Permafrost Map of Canada. *In: The National Atlas of Canada*, 5th Edition, (1978-1995), published by Natural Resources Canada, sheet MRC 4177, 1: 7 500 000 scale.
- Hilbich, C., Hauck, C., Hoelzle, M., Scherler, M., Schudel, L., Voelksch, I., Vonder Muehll, D. and Mausbacher, R., 2008. Monitoring mountain permafrost evolution using electrical resistivity tomography: a 7-year study of seasonal, annual, and long-term variations at Schilthorn, Swiss Alps. *Journal of Geophysical Research-Earth Surface*, vol. 113, F01S90. DOI:10.1029/2007JF000799.
- Hilbich, C., Marescot, L., Hauck, C., Loke, M.H. and Mausbacher, R., 2009. Applicability of electrical resistivity tomography monitoring to coarse blocky and ice-rich permafrost landforms. *Permafrost and Periglacial Processes*, vol. 20, p. 269-284. DOI:10.1002/ppp.652.
- Howes, D.E. and Ken, E., 1997. *Terrain Classification System for British Columbia (Version 2)*. Recreational Fisheries Branch, Ministry of Environment and Surveys and Resource Mapping Branch, Ministry of Crown Lands, Province of British Columbia, Victoria, BC, 102 p.
- Hughes, O.L., 1972. Surficial geology of northern Yukon Territory and northwestern District of Mackenzie, Northwest Territories. Paper 69-36, Geological Survey of Canada, Department of Energy, Mines and Resources, 11 p.

- Huntington, H. and Weller, G., 2005. Chapter 1: An Introduction to the Arctic Climate Impact Assessment. *In: Arctic Climate Impact Assessment Scientific Report*, C. Symo, L. Arris and B. Heal (eds.), Cambridge University Press, p. 1-20.
- Instanes, A., 2003. Climate change and possible impacts on Arctic infrastructure. *Proceedings of the Eighth International Conference on Permafrost*, Zurich, Switzerland, June 2003, p. 461-466.
- IPCC, 2014. *Climate Change 2014: Synthesis Report. Contribution of Working Groups I, II and III to the Fifth Assessment Report of the Intergovernmental Panel on Climate Change* [Core Writing Team, R.K. Pachauri and L.A. Meyer (eds.)]. IPCC, Geneva, Switzerland, 151 p.
- Janowicz, R., 2008. Apparent recent trends in hydrologic response in permafrost regions of northwest Canada. *Hydrology Research*, vol. 39, p. 267-275.
- Janowicz, R., 2010. Observed trends in the river ice regimes of northwest Canada. *Hydrology Research*, vol. 41, p. 462-470.
- Jasek, M.J., 1997. Ice Jam Flood Mechanisms on the Porcupine River at Old Crow, Yukon Territory. *The 9th Workshop on River Ice*. Fredericton, New Brunswick, p. 351-370.
- Jorgenson, M.T. and Osterkamp, T.E., 2005. Response of boreal ecosystems to varying modes of permafrost degradation. *Canadian Journal of Forest Research*, vol. 35, p. 2100-2111.
- Kanevskiy, M.Z., Shur, Y., Fortier, D., Jorgenson, M.T. and Stephani, E., 2011. Cryostratigraphy of late Pleistocene syngenetic permafrost (yedoma) in northern Alaska, Itkilik exposure. *Quaternary Research*, vol. 75, p. 584-596. DOI: 10.1016/j.yqres.2010.12.003.
- Kennedy, K.E., 2016. *Surficial geology, Old Crow, Yukon; parts of NTS 116O /12*. Yukon Geological Survey, Energy, Mines and Resources, Government of Yukon, Open File 2016-16, 1:10 000 scale.
- Kennedy, K.E., Froese, D.G., Zazula, G.D. and Lauriol, B., 2010. Last Glacial Maximum age for the northwest Laurentide maximum from the Eagle River spillway and delta complex, northern Yukon. *Quaternary Science Reviews*, vol. 29, p. 1288-1300.
- Kneisel, C., Hauck, C. and Vonder Mühl, D., 2000. Permafrost below the timberline confirmed and characterized by geoelectrical resistivity measurements, Bever Valley, eastern Swiss Alps. *Permafrost and Periglacial Processes*, vol. 11, p. 295-304. DOI:10.1002/1099-1530(200012)11:4<295::AID-PPP353>3.0.CO;2-L.
- Kneisel, C., Hauck, C., Fortier, R. and Moorman, B., 2008. Advances in geophysical methods for permafrost investigations. *Permafrost and Periglacial Processes*, vol. 19, p. 157-178.
- Kokelj, S.V. and Joergenson, M.T., 2013. Advances in thermokarst research. *Permafrost and Periglacial Processes*, vol. 24, p. 108-119.
- Konrad, J.-M. and Morgenstern, N.R., 1981. The segregation potential of a freezing soil. *Canadian Geotechnical Journal*, vol. 18, p. 482-491.
- Lewkowicz, A.G., 1992. Factors influencing the distribution and initiation of active-layer detachment slides on Ellesmere Island, Arctic Canada. *Periglacial Geomorphology*, John Wiley and Sons (eds.), p. 223-250.
- Lewkowicz, A.G., 2007. Dynamics of active-layer detachment failures, Fosheim Peninsula, Ellesmere Island, Nunuvut, Canada. *Permafrost and Periglacial Processes*, vol. 18, p. 89-103.

- Lewkowicz, A.G. and Bonnaventure, P.P., 2011. Equivalent elevation: a method to incorporate variable lapse rates into mountain permafrost modeling. *Permafrost and Periglacial Processes*, vol. 22, p. 153-162. DOI: 10.1002/ppp.720, 2011.
- Lewkowicz, A.G., Bonnaventure, P.P., Smith, S.L. and Kuntz, Z., 2012. Spatial and thermal characteristics of mountain permafrost, Northwest Canada. *Geografiska Annaler*, vol. 94, issue 2, p. 195-213. DOI: 10.1111/j.1468-0459.2012.00462.x.
- Lewkowicz, A.G. and Harris, C., 2005. Frequency and magnitude of active-layer detachment failures in discontinuous and continuous permafrost, northern Canada. *Permafrost and Periglacial Processes*, vol. 16, p. 115-130.
- Lorimer & Associated, 2005. Old Crow. Yukon Government Community Services, Sports and Recreation Branch. Old Crow, Yukon, 13 p.
- Lunardini, V.J., 1994. Heterogenetic and syngenetic growth of permafrost. Ground Freezing '94, Proceedings of the Seventh International Symposium on Ground Freezing, Nancy, France, p. 361-373.
- Matthews, J.V., Harington, C.R., Hughes, O.L., Morlan, R.E., Rutter, N.W., Schweger, C.E., Tarnocai, C., 1987. Stop 28: Schaeffer Mountain Lookout and Old Crow Basin Stratigraphy/Paleontology. *In*: S.R. Morison and C.A.S. Smith (eds.), XIIth INQUA Congress Field Excursions A20a and A20b Research in Yukon, p. 75-83.
- Moses, M., 2015. Old Crow. The Canadian Encyclopedia, Toronto, Ontario. [<http://www.thecanadianencyclopedia.ca/en/article/old-crow/>]. Accessed November, 2015.
- Muhs, D.R., Ager, T.A., Bettis, E.A., III, McGeehin, J., Been, J.M., Begét, J.E., Pavich, M.J., Stafford, T.W., Jr. and Stevens, D.A.S.P., 2003. Stratigraphy and paleoclimatic significance of late Quaternary loess-paleosol sequences of the last interglacial-glacial cycle in central Alaska. *Quaternary Science Reviews*, vol. 22, p. 1947-1986.
- Muhs, D.R. and Budahn, J.R., 2006. Geochemical evidence for the origin of late Quaternary loess in central Alaska. *Canadian Journal of Earth Science*, vol. 43, p. 323-337.
- Murton, J.B. and French, H.M., 1994. Cryostructures in permafrost, Tuktoyaktuk coastlands, western arctic Canada. *Canadian Journal of Earth Sciences*, vol. 31, no. 4, p. 737-747.
- Natural Resources Canada, 2016. Earthquakes Canada. [<http://www.earthquakescanada.nrcan.gc.ca/>]. Accessed January 2016.
- Nelson, F.E., Anisimov, O.A. and Shiklomanov, N.I., 2002. Climate change and hazard zonation in the circum-Arctic permafrost regions. *Natural Hazards*, vol. 26, p. 203-225.
- Norris, D.K., 1985. Geology of the northern Yukon and northwestern District of Mackenzie. Geological Survey of Canada, map 1581A, scale 1:500 000.
- Norris, D.K. (ed.), 1997. Geology and mineral hydrocarbon potential of northern Yukon Territory and northwest District of Mackenzie. Geological Survey of Canada, Bulletin 422, 401 p.
- Noson, L., 2002. Hazard Mapping and Risk Assessment. *In*: Regional Workshop on Best Practices in Disaster Mitigation, Bali, Indonesia, September 24-26, 2002; Asian Disaster Preparedness Center (ADPAC), p. 69-94.
- O'Donnell, J.A., Jorgenson, M.T., Harden, J.W., McGuire, A.D., Kanevskiy, M.Z. and Wickland, K.P., 2012. The effects of permafrost thaw on soil hydrologic, thermal and carbon dynamics in an Alaskan peatland. *Ecosystems*, vol. 15, p. 213-229.

- Pearce, G.W., Westgate, J.A. and Robertson, S., 1982. Magnetic reversal history of Pleistocene sediments at Old Crow, northwestern Yukon Territory. *Canadian Journal of Earth Sciences*, vol. 19, p. 919-929.
- Porcupine Caribou Management Board, 2002. Unit Two: The Value of Caribou. Video Series Teacher's Manuals, Whitehorse, Yukon, 57 p.
- Preece, S.J., Westgate, J.A., Alloway, B.V. and Milner, M.W., 2000. Characterization, identity and distribution and source of late Cenozoic tephra beds in the Klondike district, Yukon. *Canadian Journal of Earth Sciences*, vol. 37, p. 983-996.
- Prowse, T.D., Bonsal, B.R., Duguay, C.R., Hessen, D.O. and Vuglinsky, V.S., 2008. River and Lake Ice. *Global Outlook for Ice and Snow*. United Nations. [http://www.unep.org/geo/geo_ice/]. Accessed February, 2016.
- Schweger, C.E., 1989. The Old Crow and Bluefish Basin, Northern Yukon: Development of the Quaternary History. *In*: D.L. Carter, T.D. Hamilton and J.P. Galloway (eds.), *Late Cenozoic History of the Interior Basins of Alaska and the Yukon*, US Geological Survey Circular, vol. 1026, p. 30-33.
- Schweger, C.E. and Matthews, J.V., Jr., 1991. The last (Koy-Yukon) interglaciation in the Yukon: Comparisons with Holocene and interstadial pollen records. *Quaternary International*, vol. 10-12, p. 85-94.
- Sherry, E.E. and Myers, H.M., 2002. Traditional environmental knowledge in practice. *Society and Natural Resources*, vol. 15, p. 345-358.
- Smith, C.A.S., Meikle, J.C. and Roots, C.F. (eds), 2004. *Ecoregions of the Yukon Territory: Biophysical Properties of Yukon Landscapes*. PARC Technical Bulletin No. 04-01, Summerland, British Columbia, Agriculture and Agri-Food Canada, 313 p.
- Smith, M.W. and Riseborough, D.W., 2002. Climate and the limits of permafrost: a zonal analysis. *Permafrost and Periglacial Processes*, vol. 13, p. 1-15.
- Smith, C.A.S., Sanborn, P.T., Bond, J.D. and Frank, G., 2009. Genesis of Turbic Cryosols on north-facing slopes in a dissected, unglaciated landscape, west-central Yukon Territory. *Canadian Journal of Soil Science*, vol. 89, p. 611-622.
- SNAP (Scenarios Network for Alaska and Arctic Planning, University of Alaska), 2016. Community Charts. [https://www.snap.uaf.edu/sites/all/modules/snap_community_charts/charts.php]. Accessed March 2016.
- Statistics Canada, 2013. National Household Survey (NHS) Profile: Old Crow, Yukon, 2011. Government of Canada, Ottawa, Ontario. [<http://sewp.gov.yk.ca/region?regionId=YK.OC>]. Accessed November, 2015.
- Stephani, E., Fortier, D. and Shur, Y., 2010. Applications of cryofacies approach to frozen ground engineering – Case study of a road test site along the Alaska Highway (Beaver Creek, Yukon, Canada). *GEO2010: 63rd Canadian Geotechnical Conference and 6th Canadian Permafrost Conference*, Calgary, AB, Canada.
- Stephani, E., Fortier, D., Shur, Y., Fortier, R., Doré, G. and Walsh, R., 2014. A geosystems approach to permafrost investigations for engineering applications, an example from a road stabilization experiment, Beaver Creek, Yukon, Canada. *Cold Region Science and Technology*, vol. 100, p. 20-35.

- Tarnocai, C., Smith, C.A.S. and Hughes, O.L., 1985. Soil development on Quaternary deposits of various ages in central Yukon Territory. In *Current Research, Part A*, Geological Survey of Canada, Paper 85-1A, p. 229-238.
- Thornson, R.M. and Dixon, E.J., 1983. Alluvial history of the Porcupine River, Alaska; role of glacial-lake overflow from Northwest Canada. *Geological Society of America Bulletin*, vol. 94, no. 5, p. 576-589.
- Water Survey of Canada, 2016. Wateroffice. Environment and Climate Change Canada. [<http://wateroffice.ec.gc.ca/>]. Accessed February, 2016.
- Westgate, J.A., Stemper, B.A. and Péwé, T.L., 1990. A 3 m.y. record of Pliocene-Pleistocene loess in interior Alaska. *Geology*, vol. 18, p. 858-861.
- Whitfield, P.H., Whitley, W.G. and Wade, N.L., 1993. Chemistry of winter low flows in the Yukon Territory. In: T.D. Prowse (ed.), *Proceedings of the Workshop on Environmental Aspects of River Ice*, NHRI Symposium Series 12. Environment Canada, Saskatoon, SK, p. 217-234.
- Wolfe, B.B., Humphries, M.M., Pisaric, M.F.J., Balasubramaniam, A.M., Burn, C.R., Chan, L., Cooley, D., Froese, D.G., Graupe, S., Hall, R.I., Porter, T.J., Roy-Leveillé, P., Turner, K.W., Wesche, S.D. and Williams, M., 2011. Environmental Change and Traditional Land Use of the Old Crow Flats in Northern Canada: An IPY Opportunity to Meet the Challenges of the New Northern Research Paradigm. *Arctic*, vol. 64, no. 1, p. 127-135.
- Yukon Bureau of Statistics, 2015. Population Report: March 2015. Government of Yukon, Executive Council Office, Whitehorse, Yukon, 8 p.
- Yukon College, 2012. Old Crow Alice Frost Community Campus. [https://www.yukoncollege.yk.ca/about/campuses/old_crow_alice_frost_community_campus] Accessed December, 2015.
- Yukon Community Profiles, 2015. Old Crow. [<http://www.yukoncommunities.yk.ca/old-crow>] Accessed November, 2015.
- Zazula, G.D., Duk-Rodkin, A., Schweger, C.E. and Morlan, R.E., 2004. Late Pleistocene chronology of glacial Lake Old Crow and the north-west margin of the Laurentide Ice Sheet. In: J. Ehlers and P.L. Gibbard (eds.), *Quaternary Glaciations – Extent and Chronology, Part II*, p. 347-362.
- Zazula, G. and Froese, D., 2013. Ice Age Old Crow: Yukon's Ancient History from North of the Arctic Circle. Government of Yukon, Whitehorse, YT, 44 p.

APPENDIX A - APPROACH AND METHODS

SURFICIAL GEOLOGY

Surficial geology is the study of unconsolidated material (i.e., the surficial material that overlies bedrock) on the Earth's surface, including all sediments and soils. These sediments may be deposited through a variety of different processes including glacial (deposited directly out of glacial ice); glaciofluvial (formed by glacial rivers and streams); colluvial (deposited on or at the base of hillslopes by gravity); fluvial (river and stream deposits); lacustrine (lake deposits); eolian (wind deposits); and organic (accumulation of vegetative matter). Additionally, organic deposits can accumulate over bedrock or unconsolidated material, particularly in depressions.

Surficial geology mapping involves a combination of aerial photograph interpretation and field work. The maps provide information on the physical properties and characteristics (e.g., texture or grain size) of the surface sediments, the morphology (shape) of the landforms produced, and the genesis or origin of the landforms (the past climate and environment in which the landform was produced), and identifies any geomorphological processes that may have significantly modified those materials (e.g., landslides, gullying, or permafrost). In the process of mapping the surficial geology, the distribution of permafrost is also captured, making these maps an essential part of the hazards assessment process.

Surficial geological field mapping was completed for the study area at a scale of 1:10 000 during the summers of 2014 and 2015 (Kennedy, 2016). Previous mapping of surficial geology within the study area includes 1:125 000-scale regional mapping (Hughes et al., 1973), as well as an unpublished report documenting landslide hazards in the community (EBA Engineering Consultants Ltd., 2012).

Remote predictive mapping was completed using 1:40 000-scale 2002 digital monochrome aerial photographs with PurView/ArcGIS softcopy viewing software. LiDAR data acquired by the Government of Yukon in 2014 for part of the map area was also used to create a one-metre hillshade for detailed mapping where available. Historic geological features in the map area, many of which have been subsequently obscured by anthropogenic development in the community, were mapped from monochrome and colour digital aerial photographs dating from 1951 (~1:70 000-scale), 1962 (1:40 000-scale), 1973 (1:12 000-scale) and 1988 (1:12 000-scale). Historic photos were also viewed and mapped using PurView/ArcGIS softcopy viewing software.

Field checking of units was completed by documenting anthropogenic and natural exposures of surficial materials, and by digging soil pits (up to ~1 m deep) in a broad range of surface sediments and landforms. Other new data incorporated includes geophysical profiles of the subsurface (using ground-penetrating radar (GPR) and direct current electrical resistivity (ERT)), and new shallow boreholes. Previously acquired subsurface geological data was made available from borehole, test pits, and water well logs provided by EBA Engineering Consultants Ltd. (R. Trimble, Tetra Tech EBA, pers. comm., 2010).

PERMAFROST

TEMPERATURE AT TOP OF PERMAFROST MODELLING

Trends in permafrost temperatures with elevation were estimated using the Temperature at the Top of Permafrost (TTOP) model (Smith and Riseborough, 2002). The model calculates the temperature at the top of permafrost under equilibrium conditions using inputs of total freezing degree-days in the air, total thawing degree-days in the air, n-factors (ratios of air and ground

surface temperatures), and the ratio of frozen and thawed thermal conductivities of the soil:
Where:

$$TTOP = (rk \cdot n_t \cdot TDD_a - n_f \cdot FDD_a) / P \quad [1]$$

TTOP is the temperature at the top of permafrost;

rk is the ratio of thawed to frozen thermal conductivity of the ground;

TDD_a is the air thawing index (degree-days);

FDD_a is the air freezing index (degree-days);

n_t is the thawing n-factor (ratio of the ground surface thawing index to the air thawing index);

n_f is the freezing n-factor (ratio of the ground surface freezing index to the air freezing index); and

P is the annual period (365 days).

The inputs needed for equation [1] were developed as follows:

1. rk was assumed to be 0.5 which is representative of organic soils.
2. Values of TDD_a and FDD_a were calculated for the three operational weather stations for 2014-2015, and for the 1981-2010 long-term climate normals at Old Crow airport (Environment Canada, 2014a). The rates of change with elevation for TDD_a and FDD_a were calculated using the measured data for 2014-2015. These TDD_a/FDD_a lapse rates were then applied to the long-term average values from the Old Crow airport and projected up to treeline using the lapse rate for the two lowest stations, and above treeline using one projected value, and the actual value for the highest station. Values of TDD_a and FDD_a were then calculated for a range of elevations from 250 to 750 m a.s.l.
3. n_t and n_f employed the surface lapse rates measured and inferred for the area and the long-term Old Crow climate normals (Environment Canada, 2014a). The n-factors were obtained for forest and tundra from the measured data at the three operational weather stations for 2014-2015. The shrub zone, which occurs immediately above treeline and extends to an elevation of 600 m a.s.l., was assumed to have the same n_t and n_f as the forest, based on measurements elsewhere in Yukon (Lewkowitz et al., 2012).

GROUND-PENETRATING RADAR

Ground-penetrating radar (GPR) is a non-invasive method used to identify subsurface features such as stratigraphic boundaries, permafrost, and other anomalies using electromagnetic fields. For this project, GPR was used to gain a two-dimensional image below the ground surface. The GPR system used for field investigations was a Pulse Ekkopro system with 50 MHz antennas, with a maximum penetration depth of 8 m. The antennas were moved manually with a separation of 2 m and a step size of 0.5 m. The penetration speed used for this system depended on ground type and was between 0.07 and 0.1 m/ns (determined by CMP analysis and validated with the cryostratigraphic boundaries observed in core samples). The GPR transects typically ran parallel to, or directly overlapped the electrical resistivity tomographic profiles and passed right over borehole sites; this enabled a comparison of the results from the three techniques and allowed verification of the findings.

Post collection data processing was conducted using Ekko_Project 2 and EKKO_View software and was applied to all of the profiles. Processing of the GPR data included the following: the correction of the initial pulse to time-zero to ensure that the first reflection is at ground surface, and the subsequent reflections are from below the ground surface; correction of the penetration depth with a common midpoint method or with borehole information; and the application of dewow, lowpass, vertical and horizontal filters to remove unwanted low frequencies, as well as horizontal and vertical noise. The profiles were visualized either with a constant gain or with an automatic gain control (AGC), which enhances the spatial continuity of reflection events, but does not preserve the relative signal strength. Overall, the processing procedures were employed to reduce signal attenuation with depth, as well as improve the continuity of stratigraphic reflections and the signal-to-noise ratio.

ELECTRICAL RESISTIVITY

Electrical Resistivity Tomography (ERT) profiling is a geophysical technique that measures variations in the ability of the ground to conduct electricity along a transect, producing a two-dimensional image of changes in electrical conductance. In permafrost areas, variations in conductance relate mainly to the changes in frozen versus thawed ground, because water and ice serve as good and poor conductors of electricity, respectively.

ERT profiling has been used extensively to investigate mountain permafrost in Europe (e.g., Kneisel et al., 2000, 2008; Hauck et al., 2004; Hilbich et al., 2008, 2009) and is growing in importance in North America as a technique for permafrost investigations in both mountains and lowlands (e.g., Lewkowicz et al., 2011; Miceli, 2012). ERT is regarded as one of the best methods to examine changes in frozen ground conditions over short distances, such as in areas underlain by discontinuous permafrost.

Many ERT profiles show very clear distinctions relating to frozen ground conditions which can be correlated to surface changes in drainage, vegetation cover, or land use (Lewkowicz et al., 2011). However, like all geophysical techniques, confidence in the interpretation increases where complementary information is available; this may include data from borehole logs, observations of natural exposures, ground temperature measurements, probing of the active layer, or other geophysical techniques such as ground penetrating radar.

There is a major difference in the resistivity of water and ice, but there is not always a sharp line between the phase of water in soil pores (frozen or unfrozen) at temperatures above and below 0°C. Instead, percentages of unfrozen moisture gradually increase in the pores of frozen soils (especially in fine-grained soils such as silts and clays) as their temperatures approach 0°C. Consequently, the difference in the electrical resistivity of frozen and unfrozen soils can be gradational rather than sharp (Lewkowicz et al., 2011). In addition, because there can be differences in the porewater salinity and in the conductance of the soil minerals, it is not possible to identify a single universal threshold resistivity value below which soils are definitely unfrozen and above which soils are definitely frozen. However, given the scale of the case study sites examined in this project, a threshold value unique to each case study site was determined based on site characteristics and other ground-truthing approaches (e.g., permafrost drilling). This value is typically between 300 and 800 ohm m in the southern Yukon (Lewkowicz et al., 2011), but it depends on the local ground temperatures and stratigraphy. The value used for most of the ERT profiles in this report is 400 ohm m which generally coincided with a gradient in resistivity indicative of phase change.

The ERT profiling included in this report was undertaken in September 2015, when the active layer (i.e., depth from ground surface to the top of permafrost) was at its thickest. The equipment used was an ABEM Terrameter LS profiling system with the electrode array (stainless steel pins) inserted

into the ground in a Wenner configuration. The electricity entering the ground builds up an image of its resistivity along a profile whose depth depends on the spread of the array of electrodes (25 m for an array 160 m in length, and 8 m for a 40-m array). The penetration depth remains at 25 m, even if surveys longer than 160 m are created using a roll-along technique. Fifteen ERT profiles were completed.

Each ERT site was described in terms of vegetation and other salient features. UTM coordinates (relative to the WGS 84 datum) were taken using a hand-held Garmin Etrex Vista GPS. Relative variations in elevation along the individual profiles were measured in the field using an abney level and are expected to have accuracies of ± 1 m.

Resistivity profiles were topographically corrected using the abney level surveys. The actual elevations shown on the surveys are approximate. Measured resistivity data were processed with RES2DINV software (Loke and Barker, 1996) using a robust inversion that can respond to the rapid transitions and high contrasts in resistivity (Loke et al., 2003) that occur between frozen and unfrozen ground. A reversed colour scheme was used to portray the profiles so that blue represents high resistivities (generally indicative of frozen soils) and red represents low resistivities (ice-poor or unfrozen soils). All the resistivity profiles use the same scale to allow for inter-site comparison.

There is no single model that fits the observed resistivities. Instead the modelled results converge by iteration with the measured values. The choice of when to stop iteration in the RES2DINV software is made by the operator. Too few iterations leads to large Root Mean Square (RMS) errors (i.e., the model does not fit the measurements). Too many iterations can result in model 'over-fit' in which the broad patterns are lost. Analyses for this study were stopped after the 4th iteration as RMS errors were all very low (less than 5%) by that point. The profiles are presented with a linear depth scale and no vertical exaggeration. ERT profiles were interpreted in conjunction with the results of frost probing along the profiles, GPR surveys, field descriptions of vegetation cover at the site, borehole and laboratory analyses undertaken by the research team, and surficial mapping.

DRILLING AND SAMPLE COLLECTION

The drilling program was carried out in September 2014 and September 2015. The objective was to core and collect permafrost samples from predetermined study sites. These sites were selected in advance through a desktop interpretation based on available maps, aerial photos, satellite images and consultation with community members. The drilling and coring operations required the use of two different drills to account for changes in subsurface conditions: one core-drill (a custom GÖLZ™ portable core-drill system), and one hand auger.

The GÖLZ™ portable core-drill system (Figure A1) is a light hand drill with a high rotation speed (600 rpm) that can be controlled by two people, and is therefore used with minimal impact on the environment. Stainless steel rods measuring 1 m in length and 4.5 cm in diameter, and a core barrel 40 cm long and 10 cm in diameter were used, making it possible to drill up to 5 m into unconsolidated, fine to medium-grained material (sand to clay). A core catcher was used to extract the frozen core out of the borehole, which allows for continuous undisturbed permafrost sampling.

The hand auger is used to sample the thawed active layer; it has a 10.2 cm-diameter sampling core barrel, and three 1 m-long extension rods (Figure A2). It is ideal for sampling near-surface, fine-grained, unfrozen soil (e.g., clay, silt, sand and fine gravel containing pebbles with a maximum diameter of 25 mm).



Figure A1. Photograph of the GÖLZTM portable core-drill system used for permafrost coring.

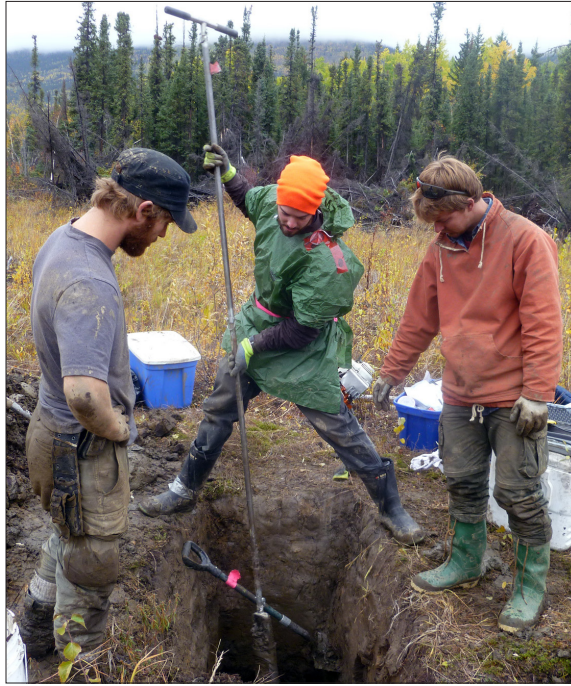


Figure A2. Photograph of the hand auger, used for permafrost coring.

Using a combination of these drills, boreholes were drilled along ERT and GPR profiles in representative areas (e.g., forested areas, open fields) or in an area belonging to a particular surficial geology unit. For each borehole, the same sampling and drilling procedures were followed. The site was first described (e.g., hydrology, vegetation type and density, and topography), photos were taken, and locations were recorded using a handheld GPS. The boreholes were initiated using a hand auger if the ground was soft or an auger drill if the ground was gravelly or compact. As soon as the permafrost table was reached, the GÖLZ™ portable core-drill system was used.

A sample of every unfrozen layer was collected from each borehole. Each sample was photographed and described in situ (e.g., soil type, soil moisture, presence or absence of organic matter, any particularities). The sample was identified with the borehole name and depth and put in sealed poly bags for laboratory analyses. Frozen samples were also collected and described on site (Figure A3). Each core was cleaned to remove the drilling mud and photographed.

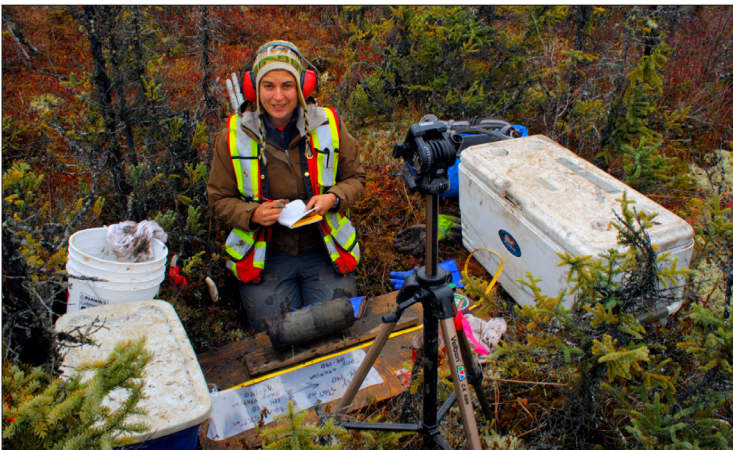


Figure A3. Photograph of the setup used for in-field core descriptions.

GEOTECHNICAL ANALYSIS OF PERMAFROST

Laboratory analyses were carried out to measure geotechnical properties of active layer and permafrost samples, and additional tests were conducted to evaluate the mechanical behavior of the permafrost upon thawing. Both soil grain characteristics and ice characteristics were evaluated. To evaluate soil grain characteristics, a grain-size analysis was performed on every sample. Additionally, plasticity index, remolded bulk density, porosity, specific gravity and thaw settlement potential were calculated for representative samples. To evaluate ice characteristics in permafrost samples, the cryostructure, volumetric ice content, gravimetric ice content and settlement potential were quantified. These methods are described below.

GRAIN-SIZE ANALYSIS

Sieve and hydrometer analysis of grain size were performed following a specifically modified American Standard and Testing Method protocol (ASTM D422-63, 2000). The sieves typically used were 4, 2, 1, 0.5, 0.25, 0.125 and 0.063 mm. A hydrometer test was performed on samples with enough fine-grained material, or on specific samples. A 40-g subsample was passed through 0.25 mm openings, and after sedimentation started, readings were taken after 0.25, 0.50, 0.75, 1, 1.5, 2, 5, 15, 30, 60, 120, 180, 300 and 1440 minutes. A total of 56 analyses were completed.

SPECIFIC GRAVITY

Specific gravity (the ratio of a solid's grain density to the density of water) was systematically measured for every sample collected, and followed the American Standard and Testing Method (ASTM D854-10, 2000). The results were used to compute the porosity of the soil (see below) for 6 types of soils.

CRYOSTRUCTURE

Cryostructure (the geometry of the ice in the permafrost) depends on water availability, as well as the soil's ice-segregation potential and the time of freezing, resulting in the development of ice structures in the soil matrix. Information such as soil genesis, climate conditions at the time of freezing, permafrost development history, and ground vulnerability when permafrost degrades can be interpreted from cryostructure, cryofacies analysis, and general cryostratigraphy.

The cryostructure of the core samples was described in situ during the drilling process, using a standard terminology (Stephani et al., 2010; Murton and French, 1994). The classification was validated with the visual analysis of high-resolution photos taken of each sample in the field.

CONSOLIDATION TESTING

Compaction and consolidation testing were carried out at Laval University. They were measured by thawing a soil sample and measuring the associated total settlement. A load was then applied vertically (stress) on a confined and drained sample to simulate the influence of weight from an embankment, or a building on consolidation. The total settlement was the sum of two distinct processes: 1) the compaction associated with the water phase change, resulting in a significant decrease in volume, especially when excess ice is present; and 2) the consolidation of the soil under the applied stress following the expulsion of water out of the pore structure and the rearrangement of soil particles. In general, compaction is more prevalent for samples with excess ice (e.g., segregated ice lenses), whereas consolidation is common in samples with interstitial ice (e.g., unsaturated to saturated soils).

During testing, an initial vertical stress of 25 kPa (corresponding to the approximate weight of a thawed active layer) was applied to frozen samples. Using two thermal baths to control the upper and lower temperatures, the permafrost samples were thawed from above by applying heat with

a temperature of $2^{\circ}\text{C} \pm 1^{\circ}\text{C}$. Ultimately, the temperature of both thermal baths was increased to ensure complete thawing of the sample. After complete thawing, when there was no more vertical deformation, the stress was increased to 150 kPa for a minimum period of 24 hours in order to simulate the weight of an embankment or a medium-sized building. By proceeding in near oedometric conditions, it was possible to estimate the index of final voids (e_t) when thawing and consolidation of the grains were completed (at a given applied force). By also determining the index of initial voids in the frozen state (e_f – calculated using the frozen density and water content), it was possible to obtain a total settlement value under different forces for the same sample.

To assess the total settlement (s), the sum of the thaw settlement (s_t) and the subsequent consolidation of the soil (s_c) were calculated by using:

$$s = s_t + s_c \quad [2]$$

When the thickness of the original frozen soil layer (H_f) is subject to effective stress (σ'), the components of the total settlement are expressed using:

$$s_t = A_0 H_f \quad [3]$$

$$s_c = m_v \sigma' H_f \quad [4]$$

The thawing compaction parameter (A_0) is expressed as a percentage and represents the relationship between void ratio in frozen (e_f) and thawed (e_t) states which is summarized by using:

$$A_0 = \frac{e_f - e_t}{1 + e_f} \quad [5]$$

The volume change coefficient (m_v) is defined as a volume changing unit added by an effective stress unit. When the effective stress increases from σ' to σ'_0 and the void ratio decreases from e_t to e , this coefficient is expressed using:

$$m_v = \frac{1}{1 + e_t} \cdot \left(\frac{e_t - e}{\sigma' - \sigma'_0} \right) \quad [6]$$

In order to determine the total settlement following the thawing of permafrost under loads imposed by buildings or transportation infrastructure, A_0 and m_v values must be determined from consolidation tests on representative soil samples. Once these values are determined, the total compaction of partially or completely thawed frozen soil layers is determined by using:

$$s = \sum_{i=1}^n A_{0,i} H_i + \sum_{i=1}^n m_{v,i} H_i \sigma'_i \quad [7]$$

BULK DENSITY

Bulk density and voids in aggregate (ρ_b ; the ratio of a dried soil's mass, including its porosity, to its volume (g/cm^3)) were calculated following American Standard and Testing Method protocol (ASTM C29 – 09, 2000). Values were generated by weighing a 45- cm^3 beaker filled with compacted

sediment and subtracting the empty beaker weight. The sediment weight was then divided by the beaker's volume using:

$$\rho_s = \frac{(M_{S+B} - M_B)}{V_B} \quad [8]$$

where M_{S+B} is the weight of the beaker full of compacted sediment, M_B is the weight of the empty beaker, and V_B is the beaker's internal volume.

GRAVIMETRIC ICE CONTENT

Ice content was calculated using:

$$u_I = \frac{(M_I)}{(M_S)} \quad [9]$$

where M_I is the ice weight (measured as weight loss after drying (g)) and M_S is dry soil weight (g). Results are expressed as percentages (dimensionless).

VOLUMETRIC ICE CONTENT

Ice volume was measured using a water displacement method. The frozen sample was weighed and lowered into a four-inch diameter PVC tube filled with 1.5 L of water. Water was then extracted from the tube until the initial water level (1.5 L) was achieved. The amount of water displaced was measured using a 250 mL graduated cylinder with a precision of ± 2 mL. The sample was then removed from the tube, placed in a clean tin tray, and dried completely in a drying oven at 60°C. The dry sample was then weighed, crushed using a mortar and pestle, vacuum sealed in a clear plastic bag, and labelled according to the borehole and sample increment. The volumes of the vacuum-sealed dry samples were measured using the same methods as the frozen cores, and the volume of the vacuum bags was subtracted from the measurement to obtain a dry sample volume. Assuming the density of ice to be 1.09 cm³/g, the volumetric ice content was calculated using:

$$IVC_{(\%)} = \left(\frac{W_c \times 1.09}{V_{tot}} \right) \times 100 \quad [10]$$

where W_c is the water mass content and V_{tot} is the total (frozen) core volume. Results are expressed as percentages.

For the consolidation test samples, the volume has been measured using Glycol displacement. This allowed the samples to remain under 0°C and avoid the use of vacuum sealed bag.

VOLUMETRIC EXCESS ICE CONTENT

The volume of excess ice content was calculated using:

$$V_{tot} - V_{sed} = V_{ice} \quad [11]$$

where V_{tot} is the total frozen core volume and V_{sed} is the dry soil volume. The volumetric excess ice content (V_{ice}) is then divided by the total frozen core volume (V_{tot}) and expressed as a percentage (fundamentally meaning cm³/cm³). This method is valid for mineral soils only.

PLASTICITY INDEX

The plasticity index (*PI*; the range of water content where the soil has a plastic behaviour) was measured according to the American Standard and Testing method (ASTM D4318-00, 2000) using:

$$PI = LL - PL \quad [12]$$

where *LL* is the liquid limit and *PL* is the plastic limit.

The *LL* was calculated using the multipoint liquid limit (ASTM method A; ASTM D4318-00, 2000) which requires one of the trials to be between 25 to 35 blows, one closure between 20 and 30 blows, and one trial with a closure requiring 15 to 25 blows. The *PL* was calculated using the *Hand Method* which consists of rolling the mass between the palm or fingers and the ground-glass plate with sufficient pressure to roll the mass into a thread of uniform diameter throughout its length. The thread is further deformed on each stroke so that its diameter reaches 3.2 mm (1/8 in).

BOREHOLE LOGS

A log for each borehole was created using the *Rockware Log Plot* software. Borehole logs include GPS coordinates; the pictures of core samples; the stratigraphy of the sediment; the depth to the water table, to the frozen table in the active layer, and to the permafrost table; the ice structure (cryostructure); the grain size ratio; the loss on ignition ratio; the frozen bulk density; the gravimetric water content; the volumetric ice content; the volumetric excess ice content; and the thaw-settlement potential (see Appendix B for all borehole log descriptions and data).

REFERENCES

- ASTM Standard C29 – 09, 2000. Standard Test Method Bulk Density (“Unit Weight”) and Voids in Aggregate. West Conshohocken, PA, ASTM International.
- ASTM Standard D422 – 63, 2000. Standard Test Method for Particle-Size Analysis of Soils. West Conshohocken, PA, ASTM International.
- ASTM Standard D854 – 10, 2000. Standard Test Methods for Specific Gravity of Soil Solids by Water Pycnometer. West Conshohocken, PA, ASTM International.
- ASTM Standard D4318 – 00, 2000. Standard Test Methods for Liquid Limit, Plastic Limit, and Plasticity Index of Soils. West Conshohocken, PA, ASTM International.
- EBA Engineering Consultants Ltd., 2012. Old Crow landslide assessment, impacts and recommendations. EBA Engineering Consultants Ltd., Whitehorse, Yukon. Unpublished report prepared for Vuntut Gwitchin Government, EBA File W14101482, 41 p.
- Environment Canada, 2014a. Historical Climate Data. Environment Canada, Ottawa, Ontario. [http://climate.weather.gc.ca/index_e.html]. Accessed December, 2015.
- Hauck, C., Isaksen, K., Vonder Mühll, D. and Sollid, J.L., 2004. Geophysical surveys designed to delineate the altitudinal limit of mountain permafrost: An example from Jotunheimen, Norway. *Permafrost and Periglacial Processes*, vol. 15, p. 191-205, doi:10.1002/ppp.493.
- Hilbich, C., Hauck, C., Hoelzle, M., Scherler, M., Schudel, L., Voelksch, I., Vonder Muehll, D. and Maüsbacher, R., 2008. Monitoring mountain permafrost evolution using electrical resistivity tomography: A 7-year study of seasonal, annual, and long-term variations at Schilthorn, Swiss Alps. *Journal of Geophysical Research-Earth Surface*, vol. 113, doi:10.1029/2007JF000799.

- Hilbich, C., Marescot, L., Hauck, C., Loke, M.H. and Mausbacher, R., 2009. Applicability of electrical resistivity tomography monitoring to coarse blocky and ice-rich permafrost landforms. *Permafrost and Periglacial Processes*, vol. 20, p. 269-284, doi:10.1002/ppp.652.
- Hughes, O.L., Pilon, J., Veillette, J.J., Zoltai, S.C., and Pettapiece, W.W., 1973. Three surficial geology and geomorphology maps of Trial river, Bell river, Old Crow map-areas, Mackenzie Valley and northern Yukon Territory. Geological Survey of Canada, Open File 167, 1 sheet. doi:10.4095/129201
- Kennedy, K.E., 2016. Surficial geology, Old Crow, Yukon; parts of NTS 116O/12. Yukon Geological Survey, Energy, Mines and Resources, Government of Yukon, Open File 2016-16, 1:10 000 scale.
- Kneisel, C., Hauck, C. and Vonder Mühll, D., 2000. Permafrost below the timberline confirmed and characterized by geoelectrical resistivity measurements, Bever Valley, eastern Swiss Alps. *Permafrost and Periglacial Processes*, vol. 11, p. 295-304, doi:10.1002/1099-1530(200012)11:4<295::AID-PPP353>3.0.CO;2-L.
- Kneisel, C., Hauck, C., Fortier, R. and Moorman, B., 2008. Advances in geophysical methods for permafrost investigations. *Permafrost and Periglacial Processes*, vol. 19, p. 157-178.
- Lewkowicz, A. G., Bonnaventure, P. P., Smith, S. L. and Kuntz, Z., 2012. Spatial and thermal characteristics of mountain permafrost, Northwest Canada, *Geografiska Annaler*, vol. 94, p. 195–213, doi:10.1111/j.1468-0459.2012.00462.x.
- Lewkowicz, A. G., Etzelmüller, B.E. and Smith, S.L., 2011. Characteristics of discontinuous permafrost from ground temperature measurements and electrical resistivity tomography, southern Yukon, Canada. *Permafrost and Periglacial Processes*, vol. 22, p. 320-342.
- Loke, M.H. and Barker, R.D., 1996. Rapid leastsquares inversion of apparent resistivity pseudosections using a quasi-Newton method. *Geophysical Prospecting*, vol. 44, p. 131-152, doi:10.1111/j.1365-2478.1996.tb00142.x
- Loke, M.H., Acworth, I. and Dahlin, T., 2003. A comparison of smooth and blocky inversion methods in 2D electrical imaging surveys. *Exploration Geophysics*, vol. 34, p. 182-187.
- Miceli, C., 2012. Seasonal cycling in electrical resistivities at ten thin permafrost sites, southern Yukon and northern British Columbia. Unpublished MSc thesis, Department of Geography, University of Ottawa, ON, 201 p.
- Murton, J.B. and French, H.M., 1994. Cryostructures in permafrost, Tuktoyaktuk coastlands, western arctic Canada. *Canadian Journal of Earth Sciences*, vol. 31, no. 4, p. 737-747.
- Smith, M.W. and Riseborough, D.W., 2002. Climate and the limits of permafrost: a zonal analysis. *Permafrost and Periglacial Processes*, vol. 13, p. 1-15.
- Stephani, E., Fortier, D. and Shur, Y., 2010. Applications of cryofacies approach to frozen ground engineering – Case study of a road test site along the Alaska Highway (Beaver Creek, Yukon, Canada). GEO2010: 63rd Canadian Geotechnical Conference and 6th Canadian Permafrost Conference, Calgary, Canada.

APPENDIX B - BOREHOLE LOGS

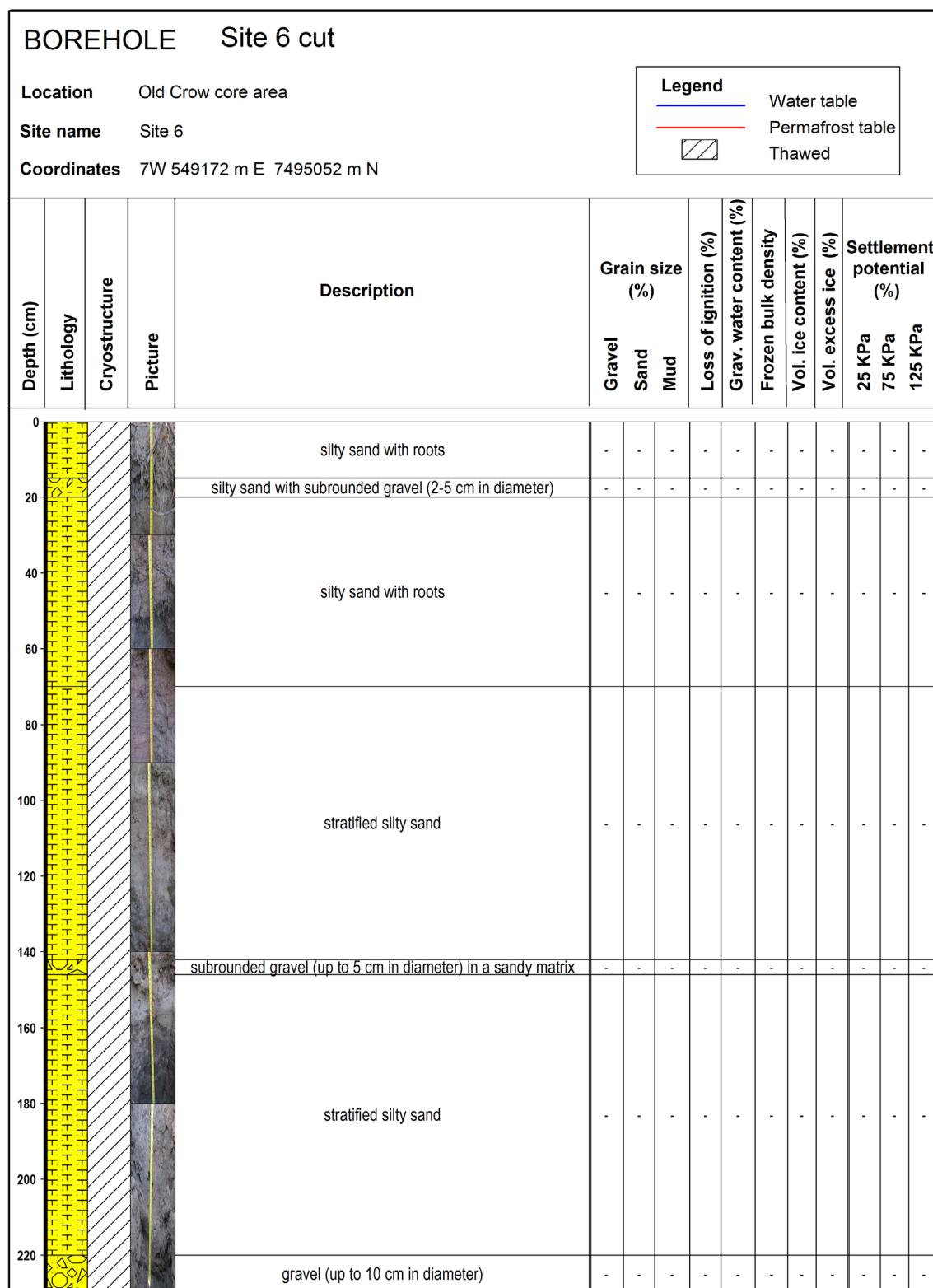


Figure B1. Borehole log for borehole Site 6 cut, from the Old Crow Community Core case study site (see Figure 51 in the main body of this report for location).

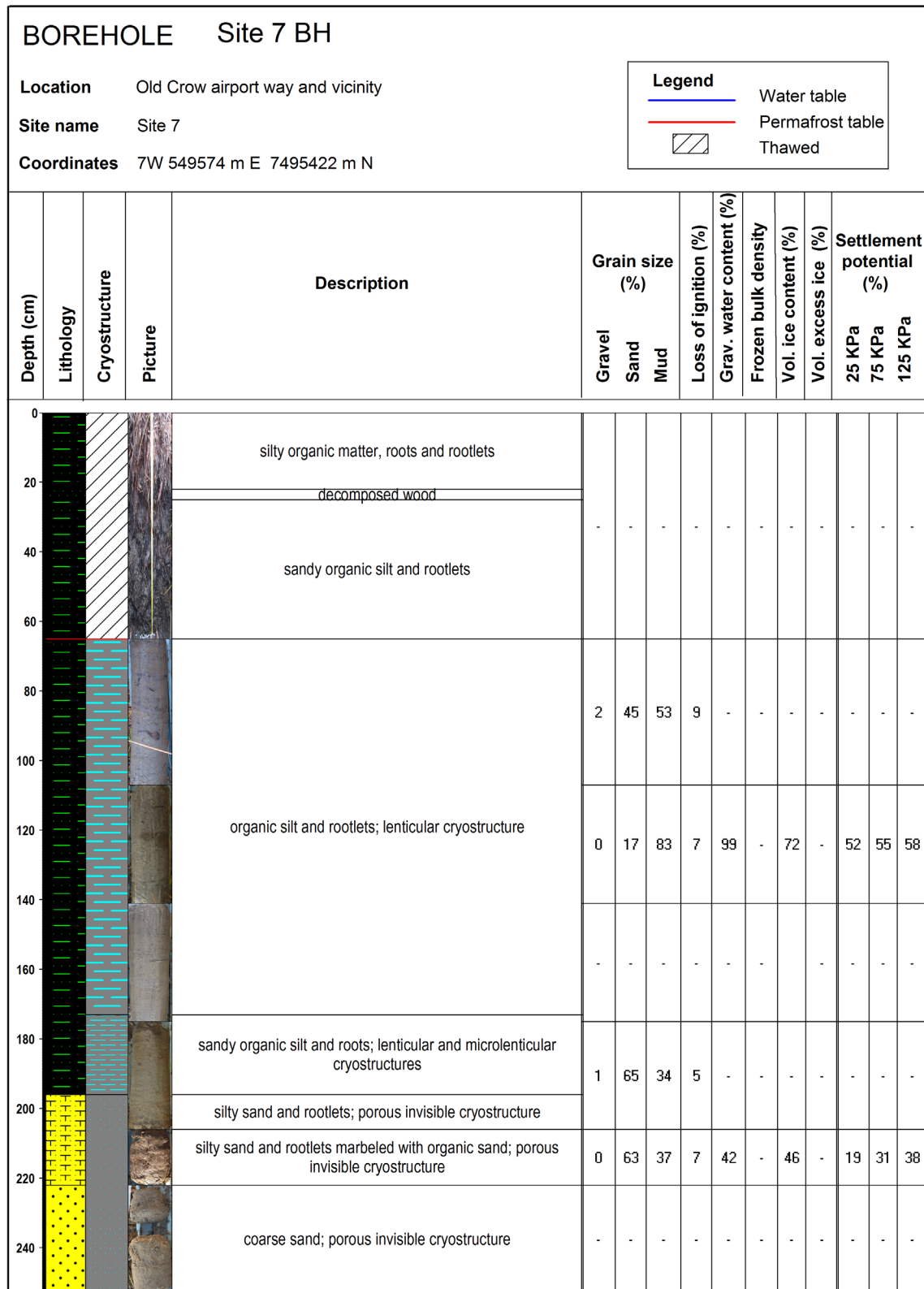


Figure B2. Borehole log for borehole Site 7 BH, from the North Road and Vicinity case study site (see Figure 64 in the main body of this report for location).

| BOREHOLE Site 8 BH | | | | | | | | | | | | | | | |
|---|-----------|-----------------------------------|---------|---|----------------|------|-----|----------------------|-------------------------|---------------------|----------------------|---------------------|--------------------------|--------|---------|
| Location | | Old Crow airport way and vicinity | | | | | | | | | | | | | |
| Site name | | Site 8 | | | | | | | | | | | | | |
| Coordinates | | 7W 549232 m E 7495384 m N | | | | | | | | | | | | | |
| <div><div>Legend</div><div><div></div>Water table</div><div><div></div>Permafrost table</div><div><div></div>Thawed</div></div> | | | | | | | | | | | | | | | |
| Depth (cm) | Lithology | Cryostructure | Picture | Description | Grain size (%) | | | Loss of ignition (%) | Grav. water content (%) | Frozen bulk density | Vol. ice content (%) | Vol. excess ice (%) | Settlement potential (%) | | |
| | | | | | Gravel | Sand | Mud | | | | | | 25 KPa | 75 KPa | 125 KPa |
| 0 | | | | slightly decomposed fibric peat | - | - | - | - | - | - | - | - | - | - | - |
| 20 | | | | moderately decomposed fibric organic matter | - | - | - | - | - | - | - | - | - | - | - |
| 40 | | | | silt with one big gravel (7 cm in diameter) and roots; lenticular cryostructure | - | - | - | - | 95 | 1,31 | 69 | 41 | - | - | - |
| 60 | | | | silt with roots; reticulate cryostructure | - | - | - | - | - | - | - | - | - | - | - |
| 80 | | | | silt with rootlets; microlenticular cryostructure | - | - | - | - | - | - | - | - | - | - | - |
| 100 | | | | silt; porous invisible cryostructure | 0 | 21 | 79 | 7 | 102 | - | 78 | - | 45 | 46 | 48 |
| 120 | | | | silt with rootlets; microlenticular cryostructure | - | - | - | - | 62 | 1,59 | 58 | 10 | - | - | - |
| 140 | | | | fine sand with roots; porous invisible cryostructure | - | - | - | - | 38 | 1,31 | 39 | 22 | - | - | - |
| 160 | | | | grey sand marbled with dark sand and rootlets; porous invisible cryostructure | - | - | - | - | 45 | 1,48 | 50 | 9 | - | - | - |
| 180 | | | | pale grey sand marbled with dark silty sand and some roots; porous invisible to visible cryostructure | - | - | - | - | - | - | - | - | - | - | - |
| 200 | | | | brown coarse sand; porous invisible cryostructure | - | - | - | - | 24 | 1,71 | 36 | 7 | - | - | - |
| 220 | | | | sorted sand and pebbles; porous invisible cryostructure | 2 | 73 | 25 | 1 | 16 | 1,79 | 27 | 1 | 15 | 18 | 19 |
| 240 | | | | black lens with pebbles; porous invisible cryostructure | - | - | - | - | 14 | 1,8 | 25 | - | - | - | - |
| 260 | | | | sorted and oriented sand and pebbles (up to 2 cm in diameter); porous invisible cryostructure | - | - | - | - | - | - | - | - | - | - | - |
| 280 | | | | coarse sand to fine pebbles; porous invisible cryostructure | - | - | - | - | - | - | - | - | - | - | - |
| 300 | | | | coarse sand; porous invisible cryostructure | - | - | - | - | 20 | 1,49 | 27 | - | - | - | - |
| 320 | | | | | - | - | - | - | - | - | - | - | - | - | - |
| 340 | | | | | - | - | - | - | - | - | - | - | - | - | - |
| 360 | | | | | - | - | - | - | - | - | - | - | - | - | - |
| 380 | | | | | - | - | - | - | - | - | - | - | - | - | - |
| 400 | | | | | - | - | - | - | - | - | - | - | - | - | - |

Figure B3. Borehole log for borehole Site 8 BH, from the North Road and Vicinity case study site (see Figure 64 in the main body of this report for location).

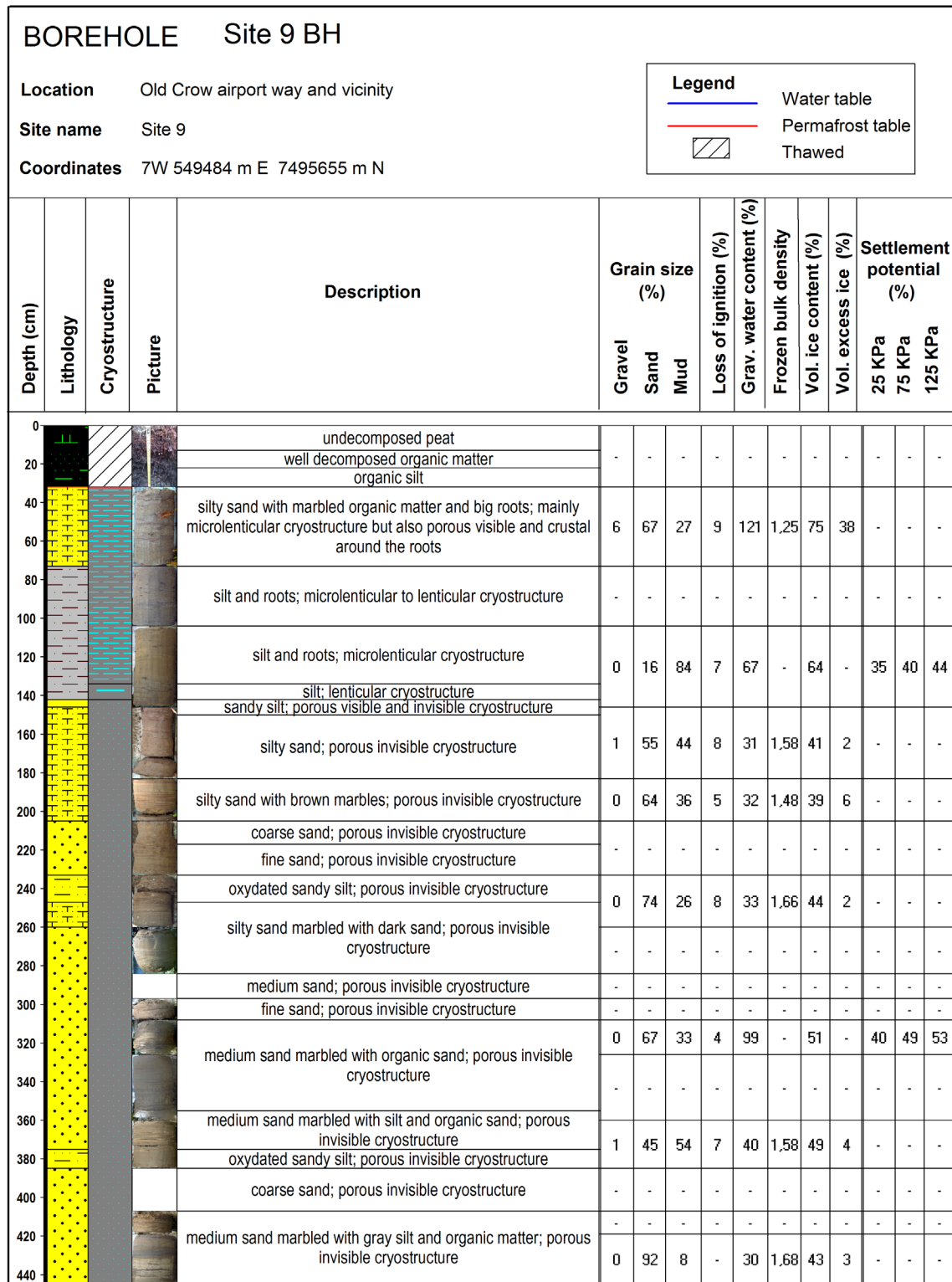


Figure B4. Borehole log for borehole Site 9 BH, from the North Road and Vicinity case study site (see Figure 64 in the main body of this report for location).

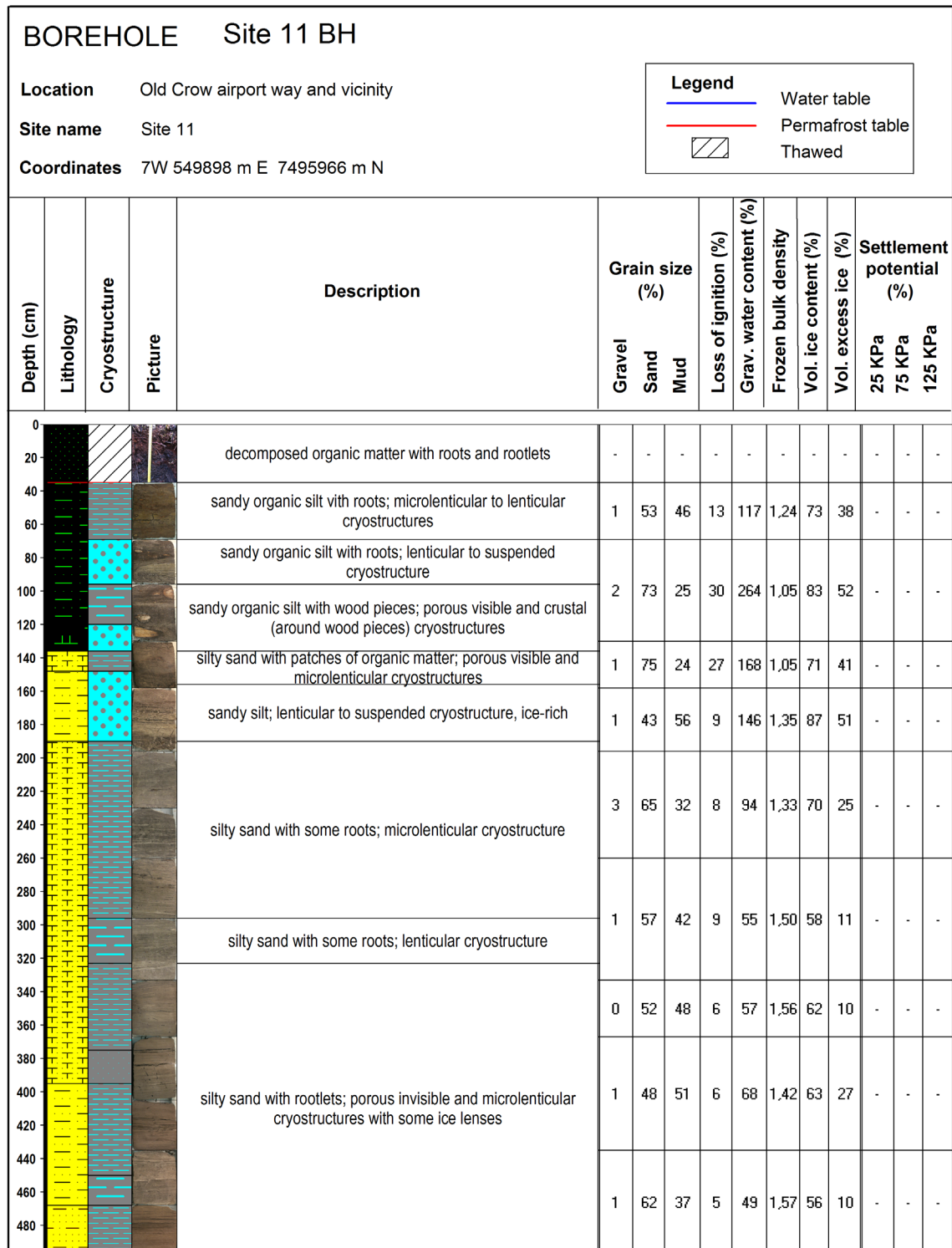


Figure B5. Borehole log for borehole Site 11 BH, from the North Road and Vicinity case study site (see Figure 64 in the main body of this report for location).

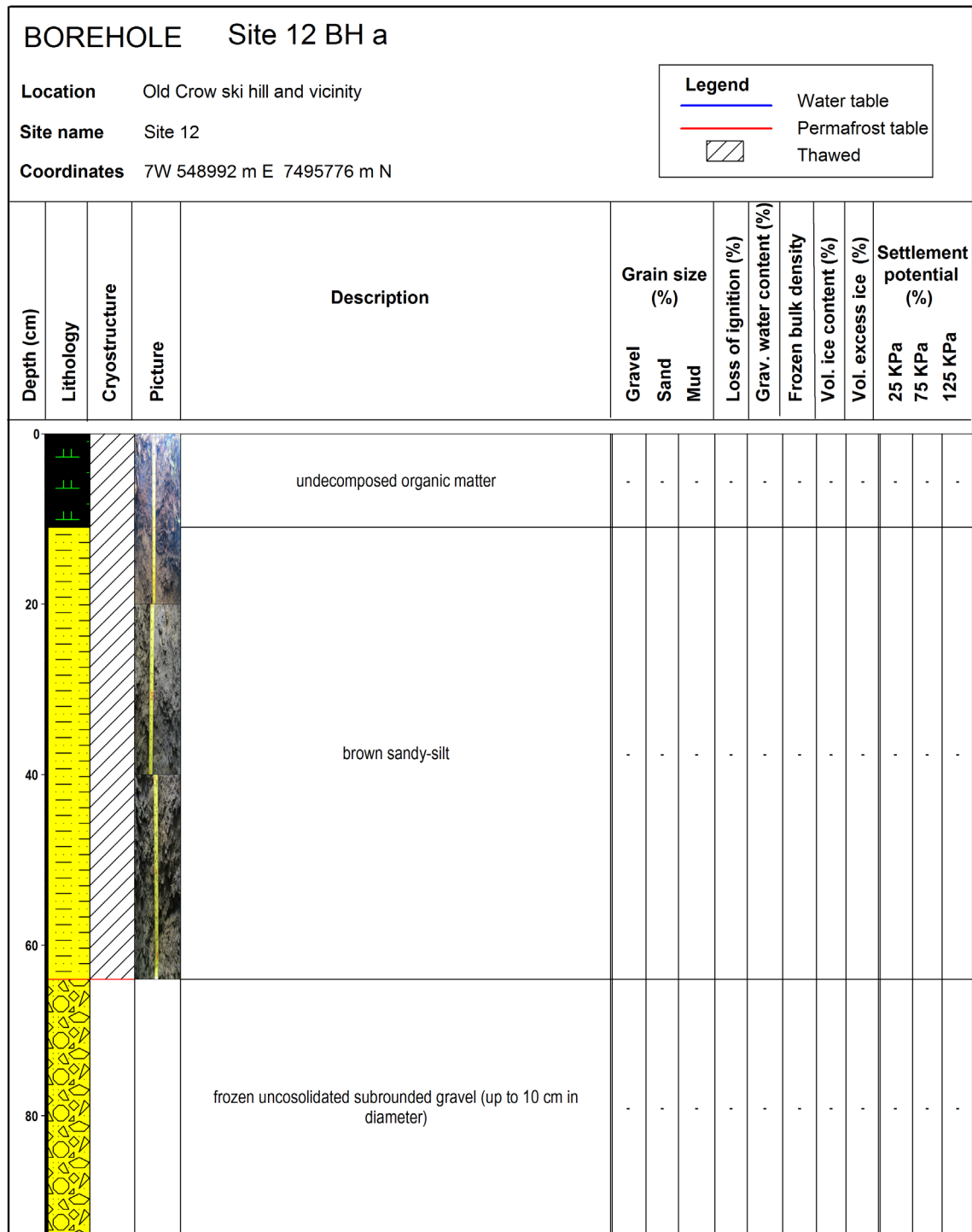


Figure B6. Borehole log for borehole Site 12 BH a, from the Ski Lodge and Vicinity case study site (see Figure 72 in the main body of this report for location).

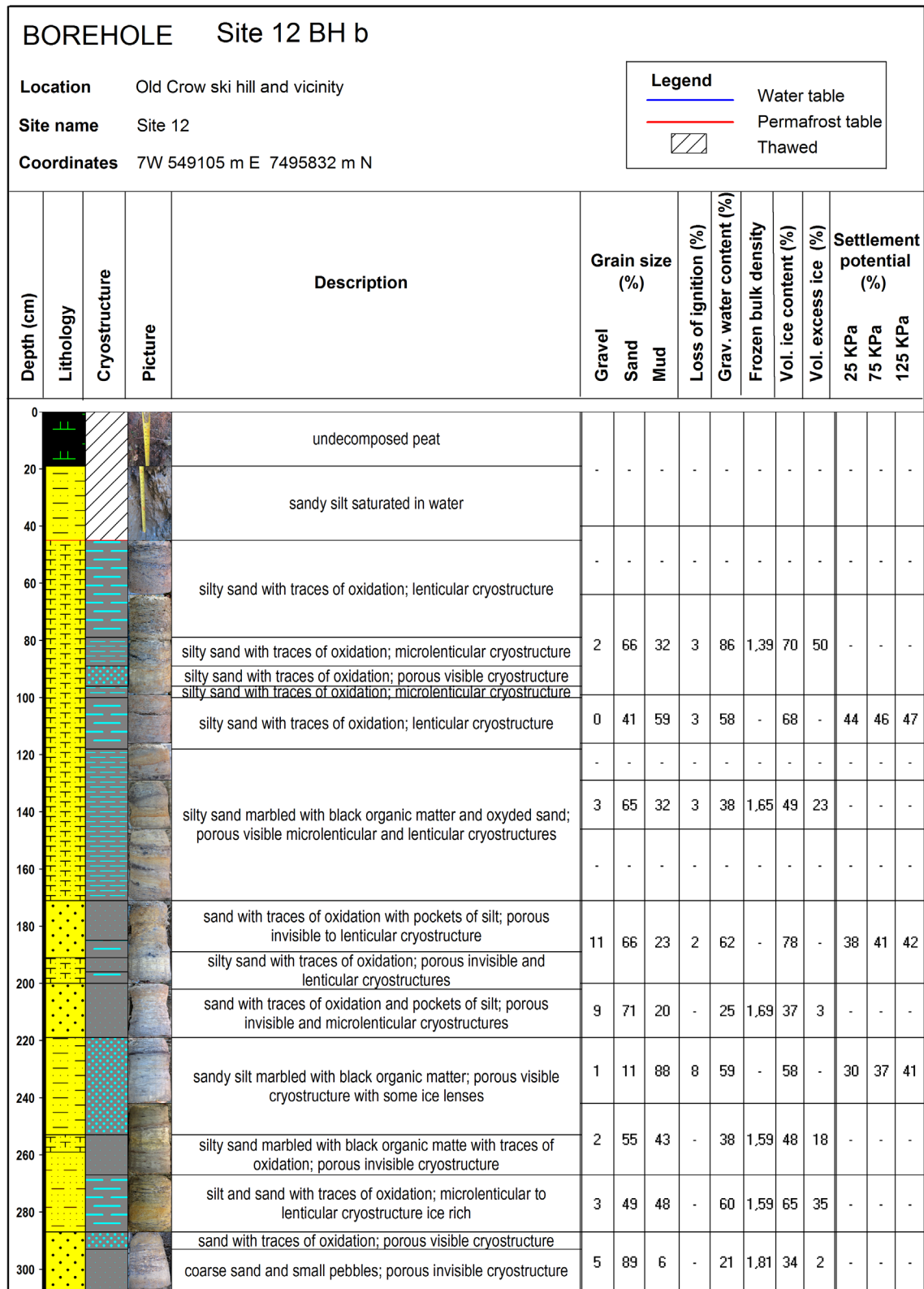


Figure B7. Borehole log for borehole Site 12 BH b, from the Ski Lodge and Vicinity case study site (see Figure 72 in the main body of this report for location).

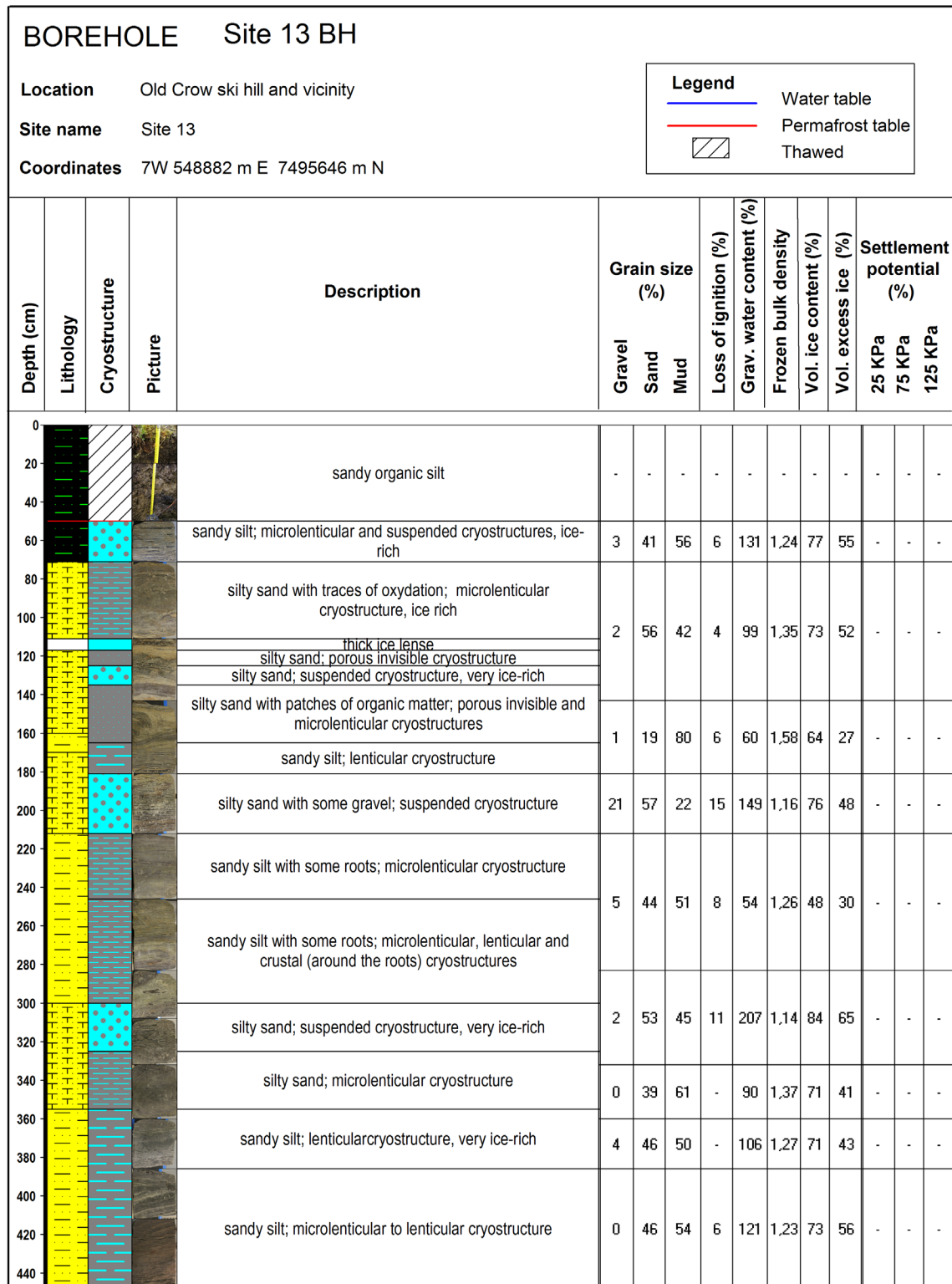


Figure B8. Borehole log for borehole Site 13 BH, from the Ski Lodge and Vicinity case study site (see Figure 72 in the main body of this report for location).

| BOREHOLE Site 15 BH | | | | | | | | | | | | | | | |
|--------------------------|-----------|--|---------|--|----------------|------|-----|----------------------|-------------------------|---------------------|----------------------|---|--------------------------|--------|---------|
| Location | | Old Crow benchlands, pediment and Crow Mountain road | | | | | | | | | | <div>Legend</div> <div><div></div>Water table</div> <div><div></div>Permafrost table</div> <div><div></div>Thawed</div> | | | |
| Site name | | Site 15 | | | | | | | | | | | | | |
| Coordinates | | 7W 549909 m E 7496660 m N | | | | | | | | | | | | | |
| Depth (cm) | Lithology | Cryostructure | Picture | Description | Grain size (%) | | | Loss of ignition (%) | Grav. water content (%) | Frozen bulk density | Vol. ice content (%) | Vol. excess ice (%) | Settlement potential (%) | | |
| | | | | | Gravel | Sand | Mud | | | | | | 25 KPa | 75 KPa | 125 KPa |
| 0 | | | | non-decomposed to well decomposed organic matter | | | | | | | | | | | |
| 20 | | | | brown silty sand mixed with organic matter and subrounded gravel (1-5cm in diameter) | - | - | - | - | - | - | - | - | - | - | - |
| 40 | | | | brown silty sand with subrounded gravel (1-5cm in diameter) | | | | | | | | | | | |
| 60 | | | | grey sandy silt with subrounded gravel (1-5cm in diameter) | 9 | 61 | 30 | 5 | - | - | - | - | - | - | - |
| 80 | | | | silty sand with gravel; reticulate to suspended cryostructure, ice-rich | 13 | 64 | 23 | 2 | 54 | 1,52 | 58 | 34 | - | - | - |
| 100 | | | | | | | | | | | | | | | |
| 120 | | | | cobbles in a sandy silty matrix with some gravel; suspended cryostructure | 56 | 33 | 11 | 3 | 34 | 1,66 | 46 | 27 | - | - | - |
| 140 | | | | cobbles in a sandy silty matrix; porous invisible cryostructure | | | | | | | | | | | |

Figure B9. Borehole log for borehole Site 15 BH, from the Crow Mountain Road and Vicinity case study site (see Figure 79 in the main body of this report for location).

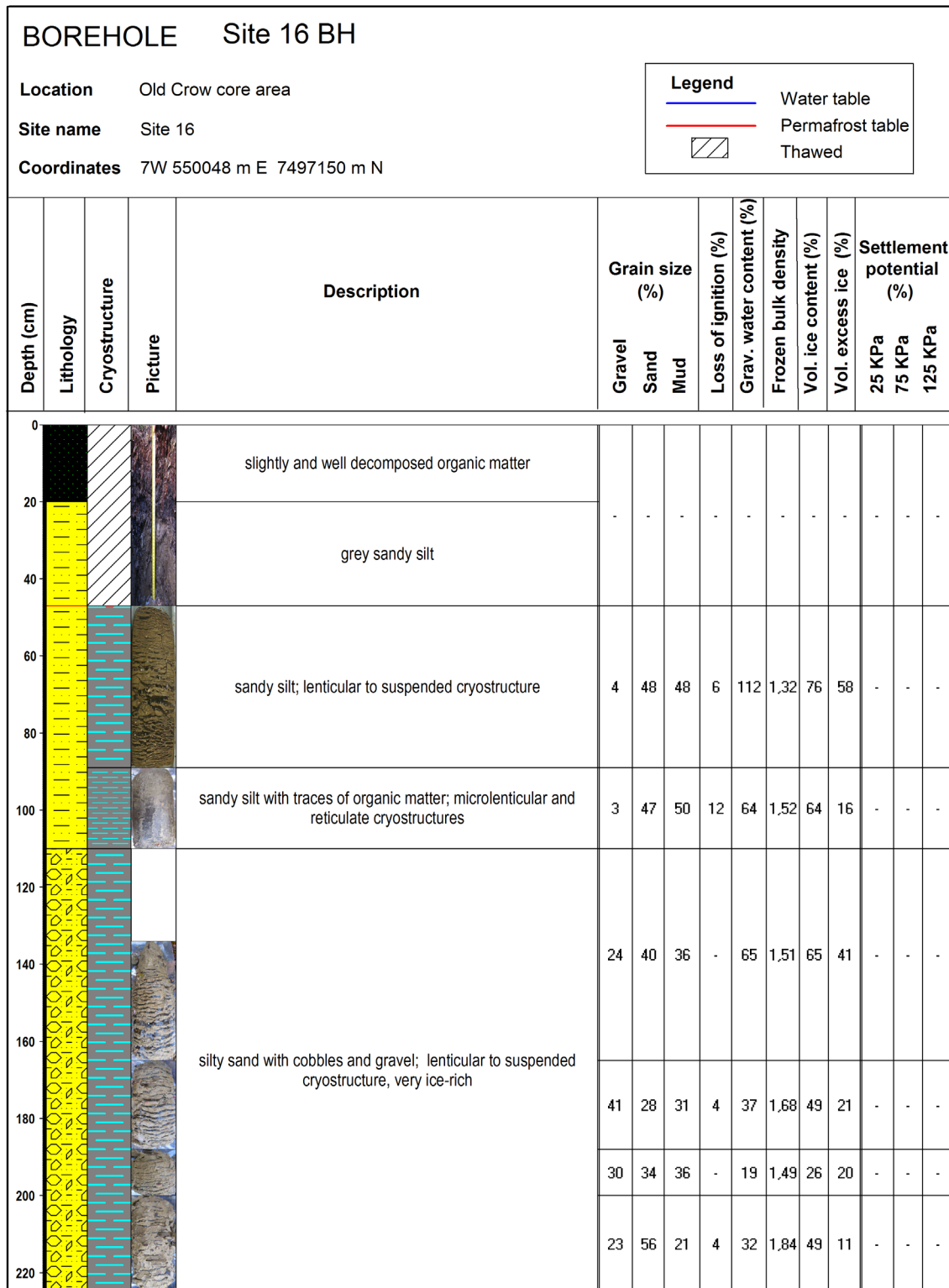


Figure B10. Borehole log for borehole Site 16 BH, from the Crow Mountain Road and Vicinity case study site (see Figure 79 in the main body of this report for location).

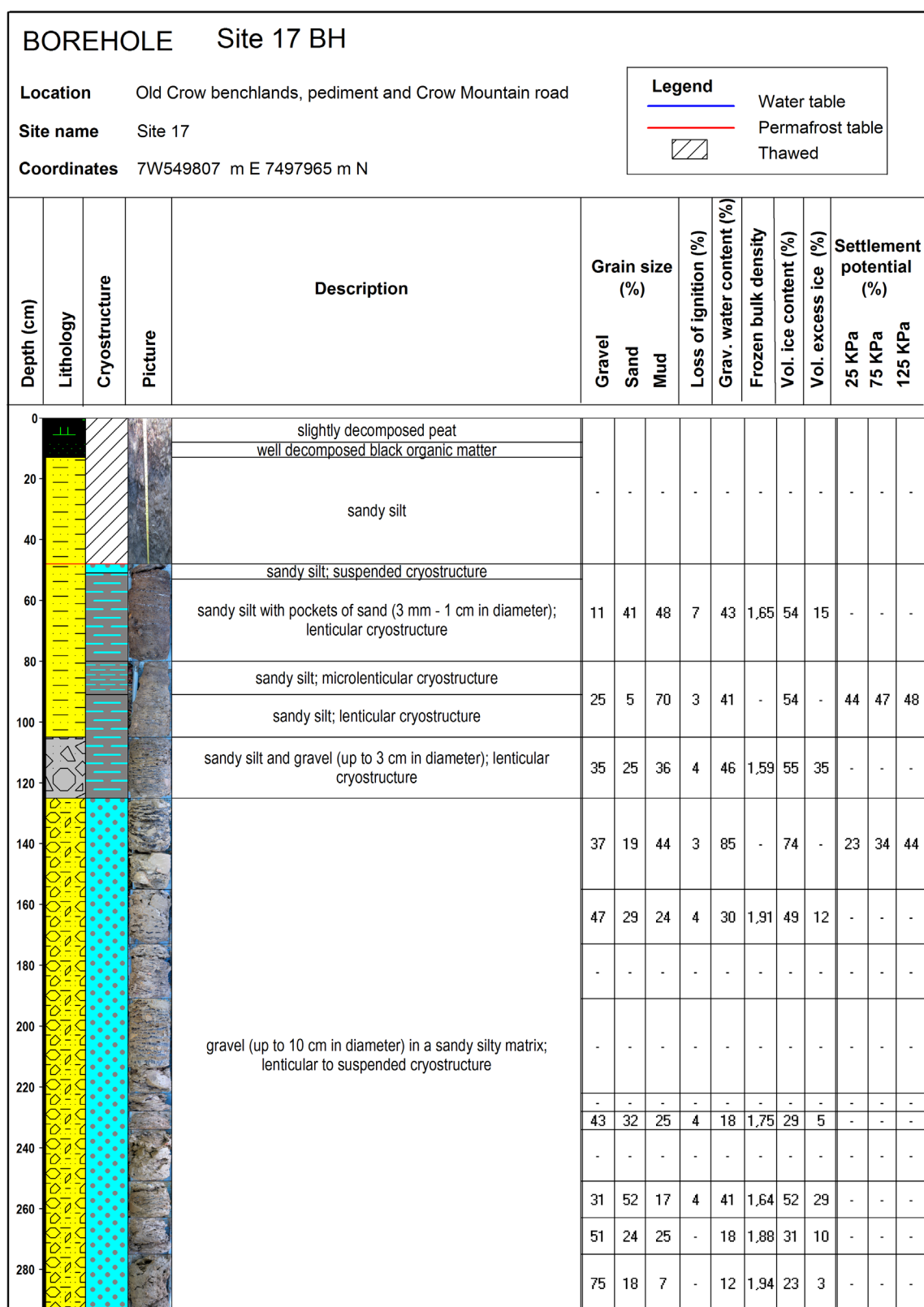


Figure B11. Borehole log for borehole Site 17 BH, from the Crow Mountain Road and Vicinity case study site (see Figure 80 in the main body of this report for location).

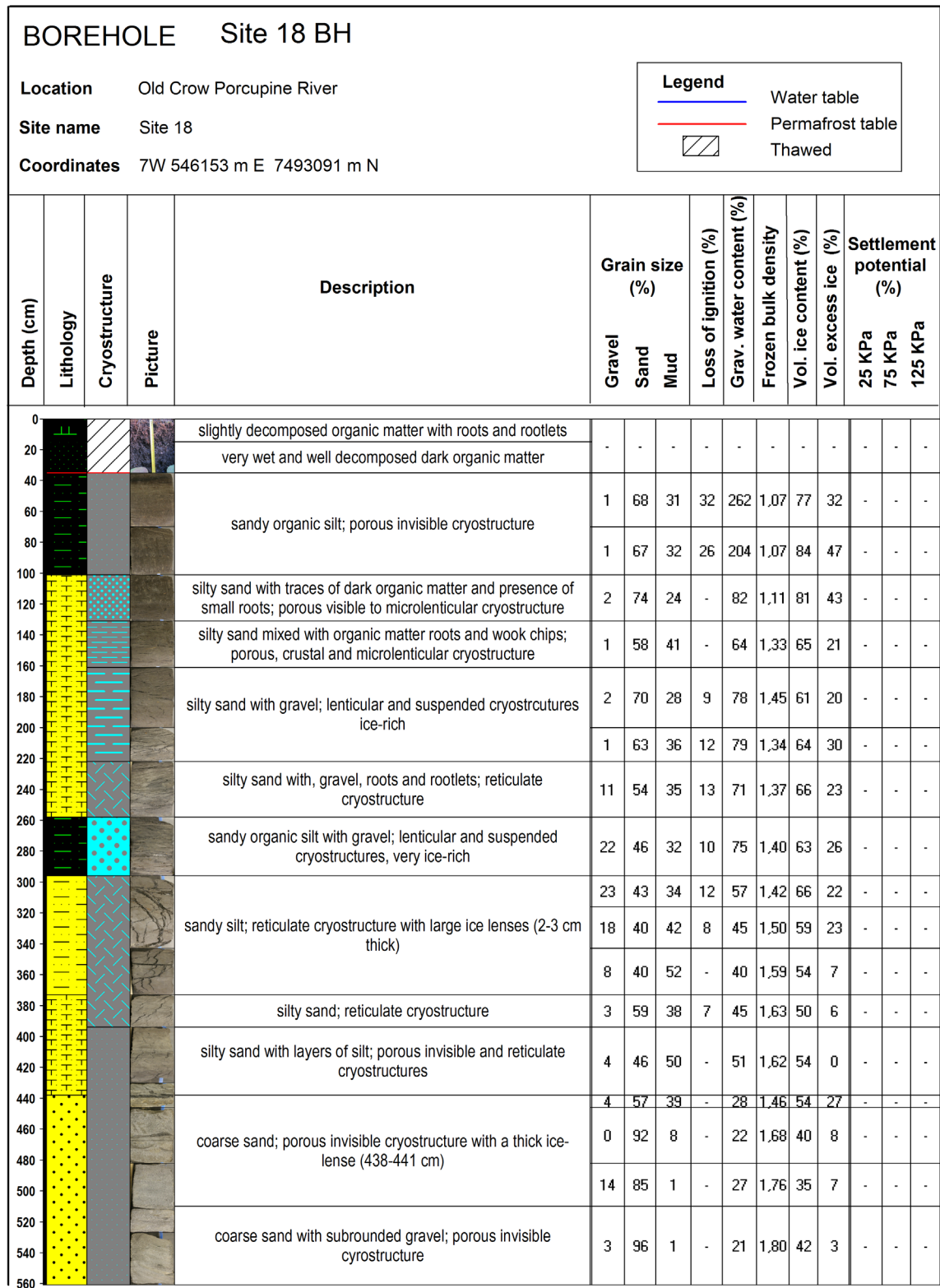


Figure B12. Borehole log for borehole Site 18 BH, from the Portage Trail case study site (see Figure 83 in the main body of this report for location).

APPENDIX C - SAFE HOME CONSTRUCTION ON PERMAFROST

Prepared by

Julie Malenfant-Lepage (M.A., Eng.) and Benoit Loranger (Jr. Eng.)

Northern Climate ExChange, Yukon Research Centre, Yukon College

TABLE OF CONTENTS

| | |
|--|-----|
| INTRODUCTION | 122 |
| CONSTRUCTION ON PERMAFROST | 122 |
| Problems Related to House Construction on Permafrost | 123 |
| Types of Surface Materials and the Thawing Processes | 124 |
| SITE INVESTIGATION | 125 |
| Preliminary Observations | 126 |
| Frost Probing | 126 |
| Drilling | 126 |
| Geophysics | 126 |
| FOUNDATIONS IN PERMAFROST | 127 |
| Construction Data Requirements | 127 |
| Foundation Types | 128 |
| <i>Surface gravel pads</i> | 128 |
| <i>Insulation</i> | 129 |
| <i>Screw-jack foundations</i> | 130 |
| <i>Timber-block foundations</i> | 131 |
| <i>Space-frame foundations</i> | 131 |
| <i>Pile foundations</i> | 131 |
| <i>Foundations with heat exchangers</i> | 133 |
| BASIC PRINCIPLES TO MAINTAIN PERMAFROST | 134 |
| Drainage | 134 |
| Ventilation | 135 |
| Shading | 135 |
| Heat Extraction | 135 |
| Monitoring | 135 |
| CONCLUSIONS AND RECOMMENDATIONS | 135 |
| REFERENCES | 136 |

INTRODUCTION

Construction in permafrost environments requires a good understanding of the nature of permafrost as well as the surficial geology. There are several principles and techniques for building on permafrost that have been proven efficient in various parts of northern Canada and Alaska. This report aims to briefly present the different approaches applied in construction of new buildings. In some ways, it can be considered as an introductory guide for basic principles, design and construction on permafrost. It is important to note, however, that this report is not prepared as an engineering design text and should not be used as such.

This report on safe home construction in permafrost environments will provide an overview of building construction on permafrost including issues related to house construction on permafrost, types of surface materials and thawing processes, preliminary investigation procedures, construction data requirements, types of foundations built in northern regions, basic principles to maintain permafrost under existent structures, and finally, recommendations that should be followed throughout the construction process.

CONSTRUCTION ON PERMAFROST

The best advice that could be given to an individual or to a contractor is to avoid building on permafrost terrain. If possible, it is always better to find a new site than to face the extra expense and maintenance involved in construction on permafrost. However, in many regions where permafrost is extensive (e.g., in northern Canada, including the Yukon) or where other factors preclude construction on non-permafrost terrain, this advice is sometimes impossible to follow. Building directly on bedrock is a good practice and should be done whenever possible (Figure C1).



Figure C1. Houses in Ilulissat, western Greenland, built directly on bedrock.

In areas underlain by continuous permafrost, permafrost is one of the major controlling factors in design parameters. As a result, it is important to design and build in a way that will preserve the underlying permafrost. Stability and lifetime of the infrastructure depend directly on the success of this endeavour.

Areas that are underlain by discontinuous permafrost offer the greatest engineering challenge since it is very difficult to determine exactly where there is underlying permafrost as it may change on a very local scale. Despite the high costs associated with the analysis of a potential construction site by drilling, these analyses will never confidently ensure the presence or absence of permafrost. If the site is located in a thaw-stable area, more conventional and less expensive construction techniques can be used without risk of destabilizing the ground. However, if the site is located in an area of ice-rich soil, which is considered thaw-unstable, standard structural foundations may thaw the underlying permafrost and potentially lead to an eventual failure of the structure. It is sometimes possible to remove or thaw permafrost on a site before starting construction, but this is a process that is rarely performed. The choice of a good structural foundation design and good mitigation techniques will help preserve permafrost, as well as respect a budget, which is the main challenge in regions underlain by discontinuous permafrost (Permafrost Technology Foundation, 2000).

PROBLEMS RELATED TO HOUSE CONSTRUCTION ON PERMAFROST

The most significant impact to permafrost usually occurs immediately beneath the house as heat is conducted downwards into the soil foundation. If a heated building is directly placed on permafrost, it will warm the ground throughout the entire year (Figure C2). However, if the building is not in contact with the ground surface, as is commonly found in northern communities, thawing is still possible due to the following: obstructed water drainage, insulation of ground by snow piling, and wind obstruction beneath the house. Furthermore, impacts from site preparation and infrastructure construction such as vegetation clearance, surface grading, and removal or compression of the organic layer, can increase heat intake by the ground surface. These ground disturbances usually result in an increase of ground temperatures, deepening of the thaw depth, and subsequent thaw settlement. In most cases, it will take several years for permafrost temperatures to reach a new equilibrium following construction.

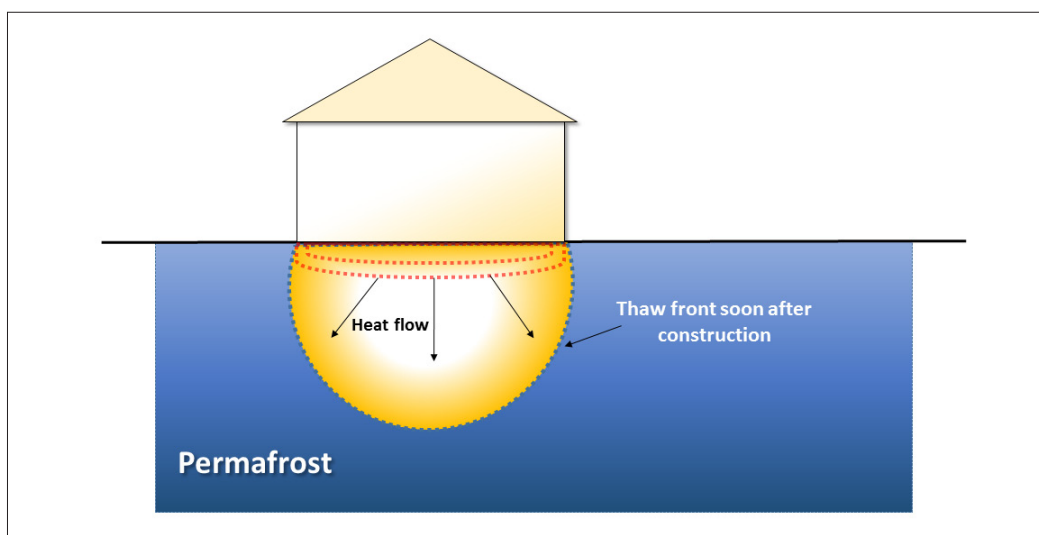


Figure C2. Cross section displaying the evolution of permafrost degradation under house construction. Based on Barriault (2012).

Foundation failure does not normally occur in a short period of time. Sudden collapse is extremely rare in the context of permafrost and is more likely associated with thermal erosion by water. The

time it takes for heat generated by a building to diffuse into the underlying permafrost depends on permafrost type, as well as factors such as the thickness of the active layer (i.e., layer of soil that thaws and freezes annually), the soil type, the temperature of the permafrost, the presence of water in the soil, and the amplitude of temperature change at the surface. However, once the process of warming is initiated, thawing of the soil is irreversible.

If buildings are left unattended, soil degradation can end up affecting the structure and will lead to the formation of cracks and bindings on doors, walls and ceilings (Figure C3). Tilted floors can also be associated with permafrost-related problems. Eventually, a building can become non-functional and even condemned. Damage associated with permafrost degradation should therefore be monitored and repaired as soon as possible to ensure viability of the structure. Monitoring can also be used to collect relevant data that would be useful in assessing permafrost-related damage. It is by far more cost effective to initiate repairs at the first signs of permafrost-related failures.



Figure C3. Examples of unmaintained buildings in Pyramiden, Svalbard, displaying cracks and uneven settlement in response to permafrost thaw.

TYPES OF SURFACE MATERIALS AND THE THAWING PROCESSES

In permafrost regions, coarse, granular surface material (sand and gravel) and rocks without ice inclusions are typically the best material on which to construct a foundation. Upon thawing, these materials are stable and have good bearing capacity. Bearing capacity refers to the load a surface material can safely withstand, without significant compaction or settlement. Foundation design in such materials should follow the current practice of moderate temperature regions.

Conversely, fine-grained surface materials, which are often ice rich, have low permeability and tend to be oversaturated after thawing. Pore-pressure generated during thawing may result in a significant loss of stiffness (bearing capacity) and volume (Figure C4). For fine-grained deposits, foundation design in permafrost poses several challenges when attempting to control differential settlement of the materials that leads to the deformation of structures. The bearing capacity of fine-grained materials is largely a function of the amount and temperature of ground ice present.

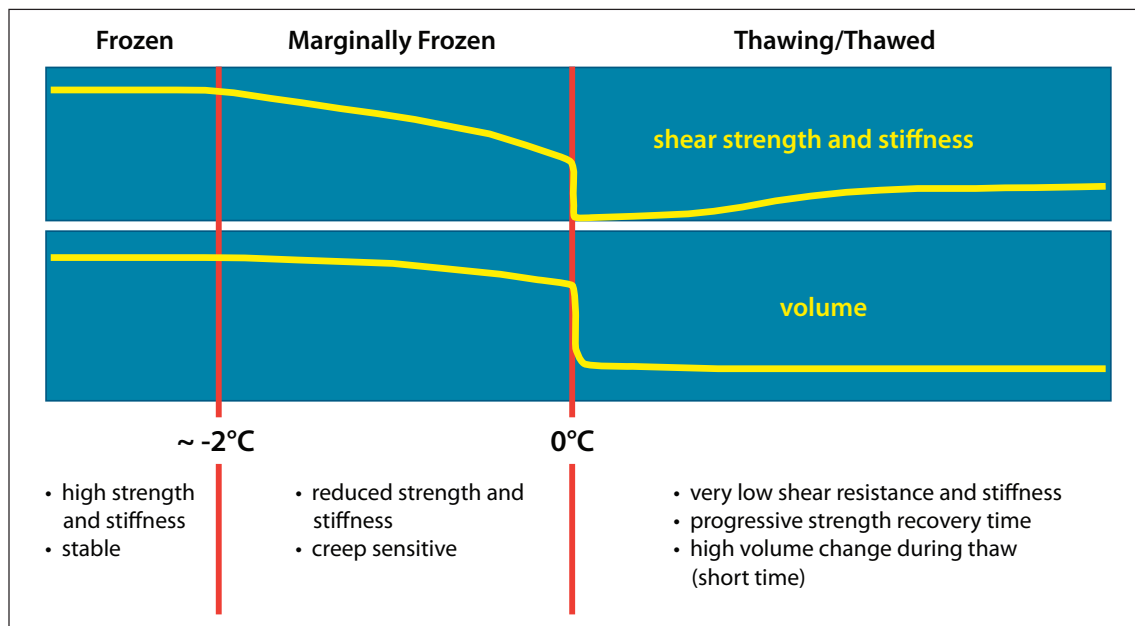


Figure C4. Mechanical properties of frozen ground undergoing thaw (Doré, 2011).

As the amount of ground ice commonly varies across a construction site in zones of discontinuous permafrost, bearing capacity may differ within a foundation, causing different portions of the structure to experience settlement at different rates. Furthermore, since ice-rich deposits consolidate and discharge excess water as they thaw, variably distributed ground ice can result in the settlement of specific areas of the ground, causing distortion in the structure above. Therefore, these types of surface materials do not offer good support for construction of buildings (Canadian Standard Association (CSA), 2010).

It is also important to note that permafrost with a temperature between -2°C and 0°C is marginally frozen (i.e., considered to be 'warm permafrost') and may not appear to be warming rapidly. At this temperature, a significant amount of heat transfer is mainly used to melt ground ice instead of warming the surface materials. Consequently, the strength of permafrost under the structure will be reduced significantly as the ground ice melts even if the temperature of the sediments remains below 0°C (see Figure C4). Moreover, several problems of creeping related to thick gravel pads and heavy structures are commonly associated with warm permafrost. Creep is related to slow ice deformation within the ground under a constant load. Ice then reacts as a malleable material and tends to flow laterally, away from the load source.

In summary, fine deposits of silt and clay are more likely to be problematic because of their frost susceptibility. Well-drained materials such as sand and gravel will be more stable; however, it is important to note that many sandy and gravelly deposits may contain a significant amount of fines that could pose a threat to the integrity of a structure. Frost susceptibility appears when approximately 10% of the mass of the surface deposit is composed of material with a fine grain size, i.e., $80\ \mu\text{m}$. If in doubt, it is best to seek advice from a geotechnical engineer.

SITE INVESTIGATION

The objectives of the site investigation are to identify terrain units, determine relevant surface material properties, and identify areas of thaw-sensitive or unstable deposits. The type of building

and its lifespan define the quantity and complexity of information necessary. The following section provides the current practices used during the site investigation.

PRELIMINARY OBSERVATIONS

The first step is an attentive observation of all permafrost-related features that could be present at the site. Features such as frost mounds, cracks, depressions and uneven terrain are typical characteristics of a permafrost landscape. Therefore, it is important to pay close attention to terrain morphology and topography since these are indicators of underlying permafrost conditions.

FROST PROBING

When the top of the permafrost is shallow and the active layer is relatively soft, frost probing is an effective method for locating depth to permafrost (Figure C5). This technique uses a steel rod with a handle, which is pushed into the ground manually until the top of the permafrost is reached. With this method, shallow permafrost can easily be detected, and its depth measured. Frost probing is inexpensive, fast and very useful for preliminary site investigations.



Figure C5. Frost-probing to determine depth to permafrost.



Figure C6. Example of ice-rich permafrost core from the Beaver Creek area, Yukon.

DRILLING

The most effective way to determine ground ice conditions at a potential site is to drill boreholes and collect samples of permafrost for geotechnical analysis (Figure C6). This provides specific information about soil characteristics and conditions at the subsurface at a particular location. A good borehole log will provide information at varying depths, including the thickness of the active layer, the soil or rock types, the ice content, the depth and characteristics of permafrost, the presence of massive ice bodies, and in some cases, the depth to bedrock.

The information derived from multiple boreholes in a given area can be extrapolated to obtain a spatial representation of subsurface conditions. It is very important to drill deep enough to obtain the appropriate information for each project. Generally speaking, the larger the building, the deeper the drilling must be. Permafrost drilling requires trained personnel with proper equipment adapted to site conditions.

GEOPHYSICS

If a larger area is being surveyed, complementary geophysical approaches like electrical resistivity tomography (ERT) and ground penetrating radar (GPR) surveys should be considered. Both applications work by sending signals into the ground and measuring the rate or strength of their return, and using those results to map subsurface conditions.

Geophysical surveys can be applied to help extrapolate information between boreholes. It is particularly useful for determining the thickness and extent of permafrost bodies, and zones of unfrozen ground within permafrost (Figure C7 a,b). ERT and GPR are applied for different detection purposes and professional geophysicists will select the most appropriate technique for the site. Geophysical surveys have the advantage of covering a relatively large area in a short period of time. Furthermore, ERT and/or GPR surveys are a cost-effective way to minimize the number of boreholes that need to be completed at any given site. The results obtained by drilling, coupled with geophysical surveys allow for a more comprehensive analysis of the subsurface conditions of the entire site.

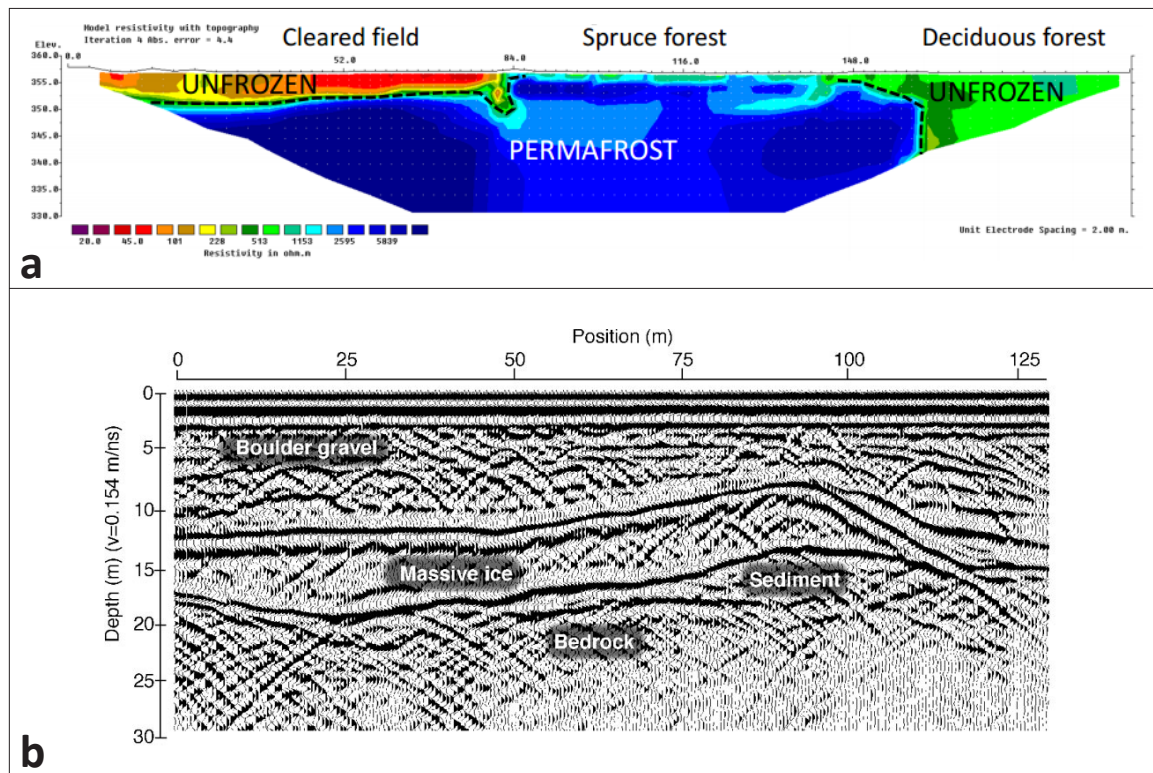


Figure C7. (a) ERT profile from the Klondike Valley, Yukon (Lewkowicz et al., 2014). **(b)** GPR profile along an ice-cored esker near Carat Lake, Northwest Territories (Moorman et al., 2007).

FOUNDATIONS IN PERMAFROST

Robust foundations for infrastructure in permafrost areas are critical for long-term building stability. General data requirements and the most common types of foundations are presented below.

CONSTRUCTION DATA REQUIREMENTS

The following list indicates principal information requirements related to construction and foundation design (Andersland and Ladanyi, 2004). This list is for large-scale projects and only needs to be fully applied in those cases. However, some elements are essential in the selection of the right type of foundation, such as the amount and temperature of ground ice, as well as the active layer thickness. It is good practice to gather as much information as possible about a site prior to construction.

1. Site data:
 - a. location
 - b. climate
 - c. physiography and geology
 - d. subsurface materials and their characteristics
 - e. thermal regime
 - f. hydrology and drainage
 - g. materials and construction
 - h. transportation facilities and access
 - i. construction cost factors
 - j. Availability of :
 - i. labor, skills, and knowledge
 - ii. construction equipment
 - iii. support facilities and equipment
2. Design policies, general criteria, and cost limitations
3. Technology (state of the art)
4. Facility technical data
 - a. size and design life (e.g., permanent versus temporary)
 - b. foundation loading
 - c. thermal conditions
 - d. movement and distortion

FOUNDATION TYPES

Good foundation construction in the North is essential to assure a full service life of a structure. Proper foundation design will be the difference between a safe, stable structure with relatively low maintenance costs, and one with constant stability problems leading to a shorter lifespan. The selection of a foundation type will generally depend on the soil behaviour upon thawing. Foundations built on permafrost can be divided into three main categories: 1) surface pads; 2) deep foundations, and; 3) foundations with heat exchangers.

SURFACE GRAVEL PADS

Construction on a surface pad to preserve the temperature of the underlying permafrost is common in northern Canada. According to Allard et al. (2010), houses built on properly designed, compacted, granular foundations should not undergo significant thaw settlement because the adjustment of the thermal profile to the new geometry leads to a rise of the permafrost into the gravel pad (Figure C8 a,b). The active layer then becomes limited to the non-frost sensitive foundation, which ensures stability over cycles of freezing and thawing. Gravel pads are frequently used with insulant panels and techniques that allow airflow beneath the building.

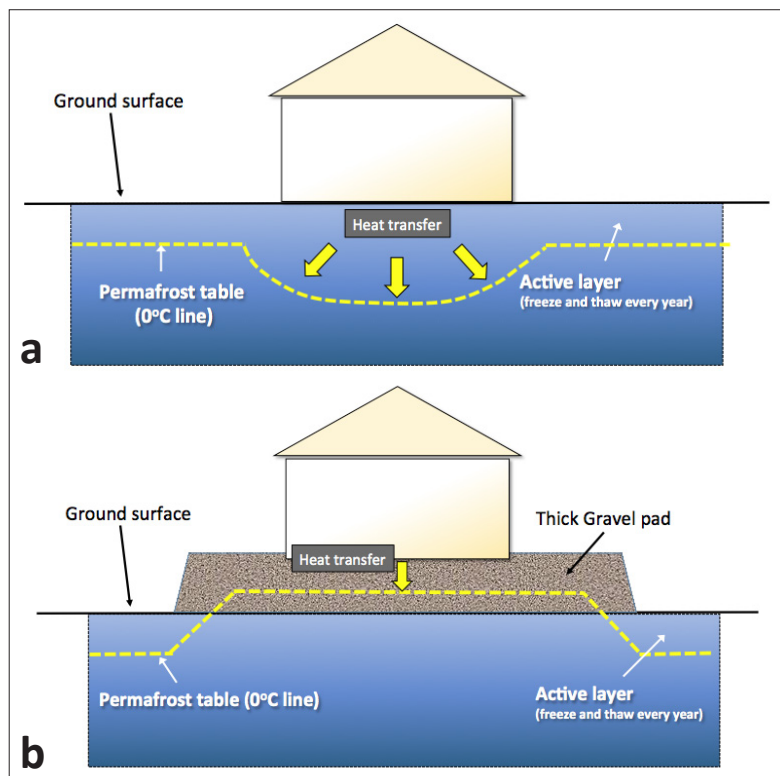


Figure C8. Schematics demonstrating the theoretical position of the permafrost table underneath (a) a building built directly on the ground, and (b) a building built on a gravel pad.

INSULATION

Structures may be built directly on insulating material (Figure C9). Insulation will slow the rate at which heat enters the ground, but it does not eliminate heat exchange. It is possible to add enough layers of insulation to establish a new thermal balance between heat input from the area around the building and winter cooling, but this procedure is almost never performed due to the high cost. Insulation is commonly applied along with a gravel pad.

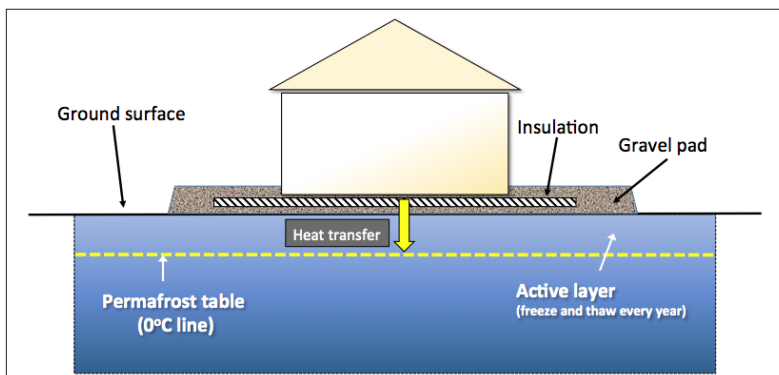


Figure C9. Basic insulation-pad foundation design (modified from CSA, 2010).

Several types of insulation can be considered in the construction of an unheated foundation. An insulated layer that is intended to be in contact with the soil must be able to withstand deterioration of its thermal properties and physical shape in the presence of soil moisture, soil chemicals, physical loading and other outside forces (Permafrost Technology Foundation, 2000).

SCREW-JACK FOUNDATIONS

In the 1980s, the Société d'Habitation du Québec developed a concept for house foundations to preserve permafrost. It involved buildings that are constructed on adjustable metal jacks over a compacted granular foundation (Figure C10). The granular foundation is laid directly on the ground surface without the removal of the vegetation cover. To date, this construction technique has been proven very effective for preserving permafrost (Gravel, 2012). The foundation must raise the building high enough to promote uninhibited air circulation beneath the building. It allows the wind to flow freely under the building, mainly to avoid snow accumulation that could increase the soil temperature (by insulation) under the foundation. Under these conditions, a snow bank will form approximately six metres away from the dwelling's foundation. It is important that nothing be stored in the space between the floor and the ground surface so as to not interfere with the free air circulation during the winter months. The winter airflow allows for the extraction of heat from the ground beneath the building, and helps preserve permafrost. Sufficient insulation should be placed under the floor of the structure so the energy loss from the bottom of the building is minimized and the floor inside the building is comfortable for residents.

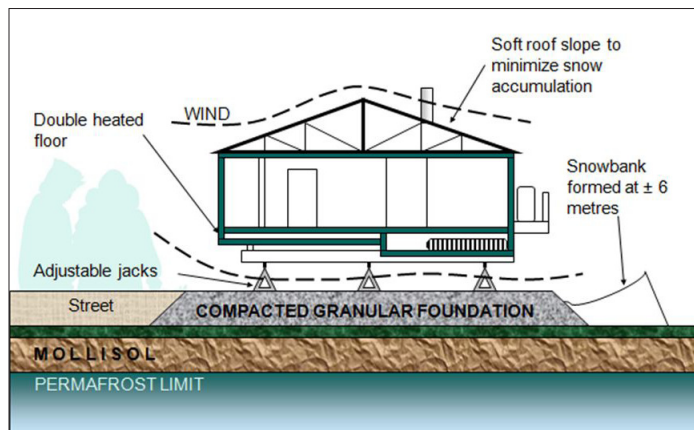


Figure C10. Conceptual design of a screw-jack foundation on a compact granular foundation (Gravel, 2012).

Once or twice a year, maintenance of a building on jacks needs to be performed in order to preserve the building's stability. During the maintenance process, screws in the middle of the jacks are used to raise or lower the height of the building (Figure C11). For a small, single-family house, it is common to use about nine adjustable jacks which can withstand nearly 35 000 kg each (Gravel, 2012). It is important to ensure that the slope of the terrain around the building allows for adequate drainage of surface water away from the structure.



Figure C11. Examples of adjustable-jack foundations from Gravel (2012) and CSA (2010).

TIMBER-BLOCK FOUNDATIONS

Timber-block foundations (Figure C12) work on the same principle as the screw-jack technique. However, screw jacks are not always easily obtainable and it can be more convenient to use timber blocks. Timber blocks are normally screwed together to ensure lateral stability. Timber blocks are commonly sited directly on natural ground (without a gravel pad).



Figure C12. Example of a timber-block foundation used in Nunavut (Government of Nunavut, 2013).

Maintenance operations are almost the same as for screw-jack foundations, described above; however, the operator must use a hydraulic jack to lift the load of the building before shimming the timber blocks. Maintenance for this style of foundation is therefore more labour intensive than for screw-jack foundations.

SPACE-FRAME FOUNDATIONS

Another surface foundation that has proven successful in permafrost regions is the rigid, three-dimensional, truss-type foundation (Figure C13). This is a commercially available, pre-manufactured foundation that consists of metal tube members flattened on each end and connected by metal node pieces at the top and bottom to form approximately one metre-square cells. It is custom-made to fit the building, and is assembled directly on-site on a compacted, granular foundation.

A screw at each structural node is used to level the building in the event of permafrost thaw underneath the building. These types of foundations are quite expensive, and are used mainly for service buildings and large, public infrastructure.



Figure C13. Examples of space-frame foundations in Nunavut (Barriault, 2012).

PILE FOUNDATIONS

In the far North, the majority of public and private dwellings, as well as commercial buildings, are built on steel piles. Piles are long steel pipes driven into the ground to stabilize buildings into the permafrost or bedrock (Figure C14). This type of foundation requires little to no gravel, which can be a very expensive resource to procure and transport to northern communities. The

use of steel piles also allows for construction on harsher and steeper terrain compared with conventional foundations. The steel piles are also more resilient to climate change compared to other foundation types when they are placed directly on bedrock.



Figure C14. Example a steel-pile foundation in Nunavik (Gravel, 2012).

There are two principal pile types currently in use in the Canadian North: 1) adfreeze piles (driven and slurry), and 2) rock-socketed piles. Their design and applications are fundamentally different. Adfreeze piles are commonly installed where permafrost extends to substantial depths without encountering bedrock. These piles rely on the bond with the surrounding ground for their load-bearing capacity. They can be driven directly into the ground, or a drill hole can be fixed to accommodate the pile. Slurry is then used to fill the empty space between the soil and the pile. For this application, the ground can be ice rich, but should be below -3°C , or colder if the soil is saline (CSA, 2010).

Rock-socketed piles are used where bedrock occurs within a practical depth below the surface. These piles are designed to transfer the full load of a structure to the underlying bedrock. In Nunavut, rock-socketed piles are commonly used. Adfreeze piles have been either discontinued or are being driven deeper due to a deepening of the active layer (Barriault, 2012).

In response to ground warming, if the active layer deepens, foundation systems that rely on piles may experience increased frost heaving (Figure C15). This frost heaving occurs when a small part of each pile's surface is frozen to the surrounding soil year-round, while a larger part of the pile's surface is exposed to the lifting force exerted through soil expansion when the water in the active layer re-freezes in the autumn and winter (CSA, 2010). If piles are used in a frost-sensitive soil and cannot be placed directly on bedrock, the piles must be equipped with anti-lift shafts to prevent the exertion of a vertical force by seasonal frost, which can distort the building's structure. Various methods can prevent frost heaving when using pile jacking and a competent engineer should be consulted if this method is being considered.



Figure C15. Examples of pile jacking in Nunavut (Barriault, 2012).



Figure C16. Example of thermosyphons, a foundation system that requires a significant amount of expertise to design, install, maintain and monitor (CSA, 2014).

FOUNDATIONS WITH HEAT EXCHANGERS

Foundations enhanced with heat exchangers are now widespread in Canada's North. They are generally used where heated crawl spaces and warm first floors at finished grade are required. For such structures, systems are built to intercept heat that would otherwise flow into the ground and affect the underlying permafrost. Thermosyphons are the most widely used heat exchangers (Figure C16). Two-phase thermosyphons work passively during the winter to extract heat from the ground and preserve permafrost (Figure C17 a,b,c). When designs using thermosyphons are being considered, detailed geothermal analyses are required. The inclusion of climate warming in the design process requires careful consideration of the conditions of the site chosen for the design, particularly in winter when low temperatures drive heat removal (CSA, 2010). Due to their high cost, thermosyphons are mainly placed in strategic locations next to high-risk service buildings, bridges or pipelines.

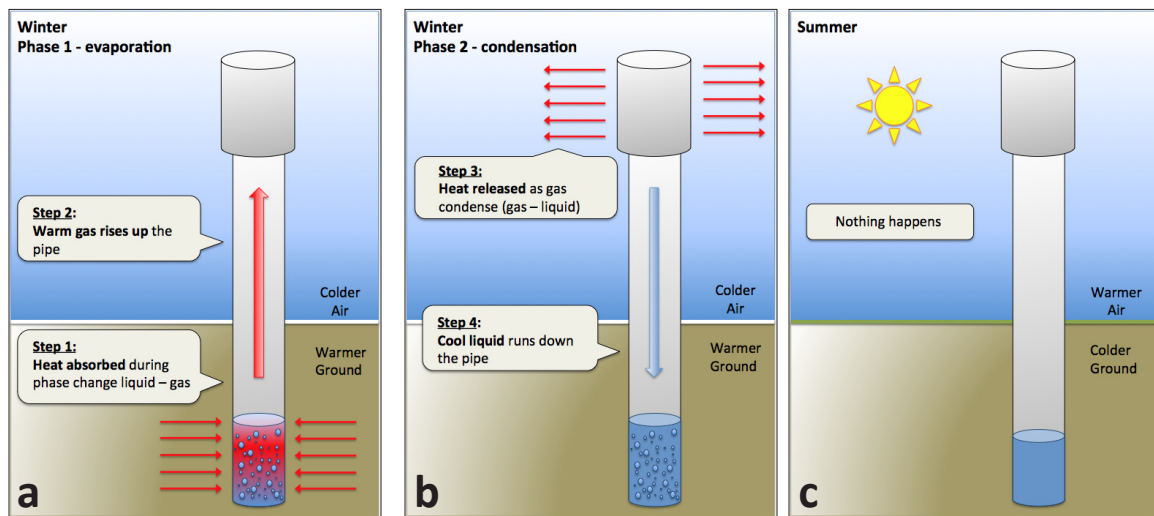


Figure C17. Schematic demonstrating (a) and (b) a winter two-phase thermosyphon cycle, as well as (c) the non-operative state during summer.

BASIC PRINCIPLES TO MAINTAIN PERMAFROST

Once construction of a building is finished, it is essential to maintain the permafrost beneath and around it. Basic elements to consider are outlined below. For more detail, please refer to the Canadian Standards Council (CSA, 2014 and 2013).

DRAINAGE

Because water transfers heat to the ground and can negatively impact permafrost, ditches should not be excavated in permafrost. Proper surface drainage to avoid water ponding beneath or next to the building is very important (Figure C18), especially with regards to spring meltwater (which can result in a high volume of flow during a short period of time). Slopes of approximately 4% are considered sufficient to drain any water at least 4 m (and preferably 6 m) from a building. Any terrain modification that could alter water paths should be carefully considered.



Figure C18. Example of water ponding around a foundation built on permafrost (Government of Nunavut, 2013). Water ponding can have a negative impact on permafrost thermal regimes.

VENTILATION

Winter airflow under buildings extracts considerable heat from the ground and thereby keeps the ground frozen. Air space should be at minimum 0.5-1 m to allow free circulation. Nothing should be stored beneath the building, in order to avoid restricting ventilation. Furthermore, snow should be managed such that it does not reduce ventilation and insulate the ground near the building. Frequent snow clearing may be required.

SHADING

In some cases, vegetation cover or a sun shade may be put in place to shade the ground surface. As mentioned above, it is important to not interfere with airflow or to enhance snow accumulation near the building. Natural vegetation and trees that exist prior to construction should not be disturbed in order to promote shading.

HEAT EXTRACTION

Active heat extraction systems like thermosyphons may be installed if required. These are described in more detail above.

MONITORING

The effectiveness of measures used to preserve permafrost should be monitored to ensure performance is maintained. Ground temperature should also be monitored to detect changes to the ground thermal regime that may affect permafrost – the temperature regime can be a powerful forecasting tool. For example, thermistor cables may be inserted along a pile if drilling is used during the construction phase.

CONCLUSIONS AND RECOMMENDATIONS

Construction in regions underlain by permafrost is a process that requires many steps, including preliminary site investigation, drilling, data analysis, as well as the appropriate choice of foundation design, construction and maintenance. In summary, several recommendations related to building on permafrost can be made:

- Foundations need to be adapted to local permafrost and landscape conditions.
- The organic layer should not be removed before construction.
- The best available geotechnical measures and techniques should be applied for all construction.
- A geotechnical investigation should be completed before construction.
- Compacted granular foundations should be built at least two years in advance of construction to allow the rise of the permafrost table and the stabilization of the soil (Allard et al., 2010).

The permafrost thermal regime should be considered in the design-phase of construction while at the same time integrating the anticipated effects of climate warming in northern Canada.

It may also be appropriate, in some areas, to develop a municipal program with appropriate regulations to ensure yearly maintenance of houses and infrastructure (Allard et al., 2010).

It must be reiterated that this guide does not replace the necessary engineering design needed for building on permafrost. It is important to consult permafrost experts in order to get appropriate advice at the preliminary investigation stages, as well as through the construction and maintenance phases. Additionally, for detailed guidance with respect to roads and permafrost, the *“Guidelines for Development and Management of Transportation Infrastructure in Permafrost Regions”* should be consulted (McGregor et al., 2010).

REFERENCES

- Allard, M., L'Hérault, E., Gybérien, T. and Barrette, C., 2010. Impact des changements climatiques sur la problématique de la fonte du pergélisol au village de Salluit (Nunavik). Rapport final, Centre for Northern Studies, Université Laval, Quebec City, QC, 69 p.
- Andersland, O.B. and Ladanyi, B., 2004. Frozen Ground Engineering, 2nd Edition. Wiley, Hoboken, NJ, 384 p.
- Barriault, A., 2012. Climatic Adaptations to Construction in Nunavut. Nunavut Housing Corporation, Northern Forum, April 18 2012, Quebec City, QC.
- Canadian Standards Association (CSA), 2014. Standards Council of Canada Approves New National Standard to Help Address the Effect of Climate Change on Canada's North. [<https://www.scc.ca/en/news-events/news/2014/standards-council-canada-approves-new-national-standard-help-address-effects-climate-change-canadas>]. Accessed February, 2015.
- Canadian Standards Association (CSA), 2010. Technical guide: Infrastructure in permafrost: A guideline for climate change adaptation, 1st edition. Canadian Standards Association Publication, 112 p.
- Canadian Standards Association (CSA), 2013. Moderating the Effects of Permafrost Degradation on Building Foundations. Document S501 Draft Standard No. 3, 42 p.
- Doré, G. 2011, Advanced Seminar on Permafrost Engineering Applied to Transportation Infrastructure, lecture notes, Yukon College, Whitehorse.
- Government of Nunavut, 2013. A Homeowner's Guide to Permafrost in Nunavut: Keep Your House on Solid Ground. Government of Nunavut, 28 p.
- Gravel, J.-F., 2012. Impact of climate change on habitat development in Nunavik (Société d'habitation du Québec). Northern Forum, Quebec City, QC.
- Lewkowicz, A., Miceli, M., Duguay, M., Bevington, A., 2014. Electrical Resistivity Tomography (ERT) as an Essential Tool to Investigate Sites in Discontinuous Permafrost. University of Ottawa. EUCOP, June 18-21 2014.
- Moorman, B.J., Robinson, S.D. and Burgess, M.M., 2007. Imaging Periglacial Conditions with Ground-Penetrating Radar. University of Calgary, Alberta, Canada. 17 p.
- Permafrost Technology Foundation, 2000. Design Manual for New Foundations on Permafrost. Permafrost Technology Foundation publications, 94 p.
- McGregor, R., Hayley, D., Wilkins, D., Hoeve, E., Grozic, E., Roujanski, V., Jansen, A. and Doré, G., 2010. Guidelines for Development and Management of Transportation Infrastructure in Permafrost Regions. Transportation Association of Canada, Ottawa, ON, 177 p.